RCA

Photomultiplier Manual

Theory Design Application

Technical Series PT-61

$2.50 Optional Price

RCA

Photomultiplier Manual

The purpose of this Manual is to help designers and users of electro-optical equipment using modern photomultiplier tubes achieve a better understanding of these devices. The Manual includes information on the construction and theory of operation of photomultipliers together with discussions of photomultiplier characteristics and the methods used to measure these characteristics. Information on typical applications is given along with basic data dealing with the measurement of light and radiant energy, noise statistics, spectral matching factors, and other topics as shown in the Table of Contents. Finally, a data section is included that gives typical characteristics of RCA photomultipliers.

RCA | Electronic Components | Harrison, N.J. 07029

Printed in U.S.A. 9/70

Contents

Introduction	3
Photoemission and Secondary Emission	5
Principles of Photomultiplier Design	19
Basic Performance Characteristics	30
Statistical Fluctuation and Noise	56
Application of Photomultipliers	77
Voltage-Divider Considerations	103
Photometric Units and Photometric-to-Radiant Conversion	112
Radiant Energy and Sources	119
Spectral Response and Source-Detector Matching	127
Technical Data	134
Outlines	161
Basing Diagrams	174
Index	183

Introduction

PHOTOMULTIPLIERS are extremely versatile photosensitive devices that are widely used to detect and measure radiant energy in the ultraviolet, visible, and near-infrared regions of the electromagnetic spectrum. In most of this range, photomultipliers are the most "sensitive" detectors of radiant energy available. The basic reason for this superior sensitivity is the use of secondary-emission amplification which makes it possible for photomultipliers to approach "ideal" device performance limited only by photoemission statistics. Other outstanding characteristics of photomultipliers include a choice of photosensitive areas from a fraction of a square centimeter to hundreds of square centimeters, internal amplifications ranging from 10 to as much as 10^9 in some types, extremely fast time response with rise times as short as a fraction of a nanosecond, and output signal levels that are compatible with auxiliary electronic equipment without need for additional signal amplification.

Photomultipliers are used with scintillators and Cerenkov radiators for the detection and measurement of X-rays, gamma rays, and energetic particles, and find wide usage in nuclear research, industrial controls, and space exploration. The availability of many different types of lasers has opened up many new fields of application for photomultipliers in Raman spectroscopy, laser ranging, precision measurements, and communications. Photomultipliers are used in video playback equipment for home entertainment, and in the audio-visual educational field; optical character-recognition equipment utilizes photomultipliers for computer processing of financial statements.

The history of the development of the photomultiplier is an interesting one. The use of secondary emission as a means for signal amplification was proposed as early as 1919.[1] The active development of photomultipliers was begun approximately 35 years ago by combining a photoemitter and one or more stages of secondary-electron-emission amplification in one vacuum envelope. In 1935, Iams and Salzberg [2] of RCA described a single-stage photomultiplier which had a secondary-emission amplification of 6; in 1940, Rajchman and Snyder [3] of RCA described a 9-stage electrostatically focused photomultiplier that served as a prototype design for a family of types that are still used throughout the world today. Other forms of photomultipliers were developed in the late 1930's, and with the sharp increase in research in atomic energy and nuclear physics, much progress in photomultiplier development was made in the 1940's and 1950's. The rapid growth of electro-optics in the 1960's further advanced the development of photomultipliers. The ad-

vent of the bialkali photocathode and more recently the Extended Red Multi-Alkali (ERMA) photocathode provided further improvements. Very recently, advances in solid-state theory and semiconductor-materials research have opened new vistas in the development of photomultipliers having performance capabilities that were literally impossible only a few years ago.

REFERENCES

1. J. Slepian, U. S. Patent 1,450.-265, April 3, 1923 (Filed 1919).
2. H. Iams and B. Salzberg, "The Secondary-Emission Phototube," *Proc. IRE, Vol. 23,* pp. 55–64 (1935).
3. J. A. Rajchman and R. L. Snyder, "An Electrostatically-Focused Multiplier Phototube," *Electronics, Vol. 13,* p. 20 (1940).
4. P. T. Farnsworth, "An Electron Multiplier," *Electronics, Vol. 7,* pp. 242–243 (1934).
5. V. Zworykin, G. Morton, and L. Malter, "The Secondary-Emission Multiplier—A New Electronic Device," *Proc. IRE, Vol. 24,* pp. 351–375 (1936).
6. G. Weiss, "On Secondary-Electron Multipliers," *Z. f. Techn. Physik, Vol. 17,* No. 12, pp. 623–629 (1936).
7. W. Kluge, O. Beyer, and H. Steyskal, "Photocells with Secondary-Emission Amplification," *Z. f. Techn. Physik, Vol. 18,* No. 8, pp. 219–228 (1937).
8. J. R. Pierce, "Electron-Multiplier Design," *Bell Lab. Record, Vol. 16,* pp. 305–309 (1938).
9. V. K. Zworykin and J. A. Rajchman, "The Electrostatic Electron Multiplier," *Proc. IRE, Vol. 27,* pp. 558–566 (1939).
10. C. C. Larson and H. Salinger, "Photocell Multiplier Tubes," *Rev. Sci. Instr., Vol. 11,* pp. 226–229 (1940).
11. R. C. Winans and J. R. Pierce, "Operation of Electrostatic Photomultipliers," *Rev. Sci. Instr., Vol. 12,* pp. 269–277 (1941).
12. R. W. Engstrom, "Multiplier Phototube Characteristics; Application to Low Light Levels," *J. O. S. A., Vol. 37,* No. 6, pp. 421–431 (1947).

Photoemission and Secondary Emission

THIS section covers the means by which radiant energy is converted into electrical energy in a photomultiplier tube.

Photomultipliers convert incident radiation in the visible, infrared, and ultraviolet regions into electrical signals by use of the phenomenon of photoemission and then amplify the signals by means of secondary emission.

A basic component arrangement of a typical modern photomultiplier is shown in Fig. 1. Radiant energy enters the evacuated enclosure through a "window" which has a semitrans-

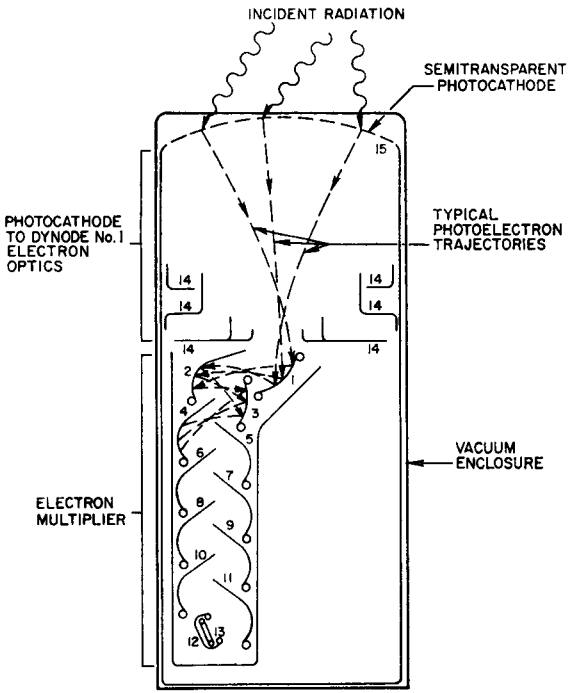

Fig. 1 — Schematic of typical photomultiplier showing some electron trajectories.

parent photocathode deposited upon its inner surface. The photocathode emits photoelectrons by the process of photoemission, i.e., by the interaction of the incident radiant energy with electrons in the photocathode material. Photoelectrons from all parts of the photocathode are accelerated by an electric field so as to strike a small area on the first dynode. Secondary electrons resulting from the process of secondary emission (i.e., from the impact of the photoelectrons on the first dynode) are accelerated toward the second dynode by an electric field between dynodes No. 1 and No. 2 and impinge on the second dynode. The impact of the secondary electrons on dynode No. 2 results in the release of more secondary electrons which are then accelerated toward dynode No. 3. This process is repeated until the electrons leaving the last dynode are collected by the anode and leave the photomultiplier as the output signal. If, on the average, 4 secondary electrons are liberated at each dynode for each electron striking that dynode, the current amplification for a 12-stage photomultiplier is 4^{12}, or approximately 17 million. Thus, the liberation of a single photoelectron at the photocathode results in 17 million electrons being collected at the anode. Because this pulse has a time duration of approximately 5 nanoseconds, the anode current is approximately 1 milliampere at the peak of the anode-current pulse.

PHOTOEMISSION AND PHOTOCATHODES

Photoemission is a process in which electrons are liberated from the surface of a material by the interaction of photons of radiant energy with the material.[1] The energy of a photon E_p is given by

$$E_p = h\nu = \frac{hc}{\lambda} \qquad (1)$$

where ν is the frequency of the incident radiation, λ is the wavelength of the incident radiation, h is Planck's quantum of action, and c is the velocity of light. Substitution of the numerical values of these constants from Appendix A provides the following relation:

$$E_p = \frac{1239.5}{\lambda} \qquad (2)$$

where E_p is in electron-volts and λ is in nanometers. Thus, photons of visible light which are in the wavelength range from 400 to 700 nanometers have energies ranging from 3.1 to 1.8 electron-volts.

Fundamentals of Photoemission

An ideal photocathode has a quantum efficiency of 100 per cent; i.e., every incident photon releases one photoelectron from the material into the vacuum. All practical photoemitters have quantum efficiences below 100 per cent. To obtain a qualitative understanding of the variations in quantum efficiency for different materials and for different wavelengths or photon energies, it is useful to consider photoemission as a process involving three steps: (1) absorption of a photon resulting in the transfer of energy from photon to electron, (2) motion of the electron toward the material-vacuum interface, and (3) escape of the electron over the potential barrier at the surface into the vacuum.

Energy losses occur in each of these steps. In the first step, only the absorbed portion of the incident light is effective and thus losses by transmission and reflection reduce the quantum efficiency. In the second step, the photoelectrons may

lose energy by collision with other electrons (electron scattering) or with the lattice (phonon scattering). Finally, the potential barrier at the surface (called the work function in metals) prevents the escape of some electrons.

The energy losses described vary from material to material, but a major difference between metallic and semiconducting materials makes separate consideration of each of these two groups useful. In metals, a large fraction of the incident visible light is reflected and thus lost to the photoemission process. Further losses occur as the photoelectrons rapidly lose energy in collisions with the large number of free electrons in the metal through electron-electron scattering. As a result, the escape depth, the distance from the surface from which electrons can reach the surface with sufficient energy to overcome the surface barrier, is small, and is typically a few nanometers. Finally, the work function of most metals is greater than three electron-volts, so that visible photons which have energies less than three electron-volts are prevented from producing electron emission. Only a few metals, particularly the alkali ones, have work-function values low enough to make them sensitive to visible light. Because of the large energy losses in absorption of the photon and in the motion of the photoelectron toward the vacuum (the first and second steps described above), even the alkali metals exhibit very low quantum efficiency in the visible region, usually below 0.1 per cent (one electron per 1000 incident photons). As expected, higher quantum efficiencies are obtained with higher photon energies. For 12-electron-volt photons, quantum yields as high as 10 per cent have been reported.

The concept of the energy-band models that describe semiconductor photoemitters is illustrated in its simplest form in Fig. 2. Electrons can have energy values only within well defined energy bands which are separated by forbidden-band gaps.

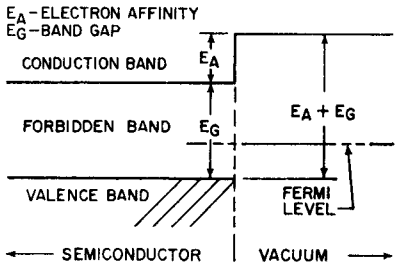

Fig. 2 — Simplified semiconductor energy-band model.

At 0°K, the electrons of highest energy are in the so-called valence band and are separated from the empty conduction band by the band-gap energy E_G. The probability that a given energy level may be occupied by an electron is described by Fermi-Dirac statistics and depends primarily on the difference in energy between the level under consideration and a reference level called the "Fermi level." As a first approximation, it may be said that any energy levels which are below the Fermi level will be filled with electrons, and any levels which are above the Fermi level will be empty. At temperatures higher than 0°K, some electrons in the valence band have sufficient energy to be raised to the conduction band, and these electrons, as well as the holes in the valence band created by the loss of electrons, produce electrical conductivity. Because the number of electrons raised to the conduction band increases with temperature, the conductivity of semiconductors also increases with temperature. Light can be absorbed by valence-band electrons only if the photon energy of the light is at least

equal to the band-gap energy E_G. If, as a result of light absorption, electrons are raised from the valence band into the conduction band, photoconductivity is achieved. For photoemission, an electron in the conduction band must have energy greater than the electron affinity E_A. The additional energy E_A is needed to overcome the forces that bind the electron to the solid, or, in other words, to convert a "free" electron within the material into a free electron in the vacuum. Thus, in terms of the model of Fig. 2, radiant energy can convert an electron into an internal photoelectron (photoconductivity) if the photon energy exceeds E_G and into an external photoelectron (photoemission) if the photon energy exceeds $(E_G + E_A)$. As a result, photons with total energies E_p less than $(E_G + E_A)$ cannot produce photoemission.

The following statements can therefore be made concerning photoemission in semiconductors. First, light absorption is efficient if the photon energy exceeds E_G. Second, energy loss by electron-electron scattering is low because very few free electrons are present; thus, energy loss by phonon scattering is the predominant loss mechanism. The escape depth in semiconductors is therefore much greater than in metals, typically of the order of tens of nanometers. Third, the threshold wavelength, which is determined by the work function in metals, is given by the value of $(E_G + E_A)$ in semiconductors. Synthesis of materials with values of $(E_G + E_A)$ below 2 electron-volts has demonstrated that threshold wavelengths longer than those of any metal can be obtained in a semiconductor. Semiconductors, therefore, are superior to metals in all three steps of the photoemissive process: they absorb a much higher fraction of the incident light, photoelectrons can escape from a greater distance from the vacuum interface, and the threshold wavelengths can be made longer than those of a metal. Thus, it is not surprising that all photoemitters of practical importance are semiconducting materials.

In recent years, remarkable improvements in the photoemission from semiconductors have been obtained through deliberate modification of the energy-band structure. The approach has been to reduce the electron affinity, E_A, and thus to permit the escape of electrons which have been excited into the conduction band at greater depths within the material. Indeed, if the electron affinity is made **less** than zero (the vacuum level lower than the bottom of the conduction band, a condition described as "negative electron affinity" and illustrated in Fig. 3), the escape depth may be as much as 100 times greater than for the normal material. The escape depth of a photoelectron is limited by the energy loss suffered in phonon scattering. Within a certain period of time, of the order of 10^{-12} second, the electron energy drops from a level above the vacuum level to the bottom of the conduction band from which it is not able to escape into the vacuum. On the other hand, the electron can stay in the conduction

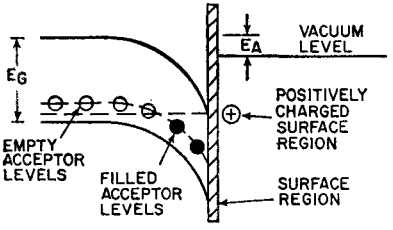

Fig. 3 — Semiconductor energy-band model showing negative electron affinity.

band in the order of 10^{-10} second without further loss of energy, i.e., without dropping into the valence band. If the vacuum level is below the bottom of the conduction band, the electron will be in an energy state from which it can escape into the vacuum for a period of time that is approximately 100 times longer than if an energy above the bottom of the conduction band is required for escape, as in the materials represented by Fig. 2. Therefore, a material conforming to the conditions of Fig. 3 has a greatly increased escape depth. Under such circumstances, the photosensitivity is significantly enhanced. Substantial response is observed even for photons with energies close to that of the band gap where the absorption is weak. Efficient photoemission in this case results only because of the greater escape depth.

The reduction of the electron affinity is accomplished through two steps. First, the semiconductor is made strongly p-type by the addition of the proper "doping" agent. For example, if gallium arsenide is the host material, zinc may be incorporated into the crystal lattice to a concentration of perhaps 1,000 parts per million. The zinc produces isolated energy states within the forbidden gap, near the top of the valence band, which are normally empty, but which will accept electrons under the proper circumstances. The p-doped material has its Fermi level near the top of the valence band. The second step is to apply to a semiconductor a surface film of an electropositive material such as cesium. Each cesium atom becomes ionized through loss of an electron to a p-type energy level near the surface of the semiconductor, and is held to the surface by electrostatic attraction.

The changes which result in the energy-band structure are two-fold. In the first place, the acceptance of electrons by the p-type impurity levels is accompanied by a downward bending of the energy bands. This bending can be understood by observing that a filled state must be, in general, below the Fermi level; the whole structure near the surface is bent downward to accomplish this result. In the second place, the potential difference between the charged electropositive layer (cesium) and the body charge (filled zinc levels) results in a further depression of the vacuum level as a result of a dipole moment right at the surface.

Another way to describe the reduction of the electron affinity is to consider the surface of the semiconductor as a capacitor. The charge on one side of the capacitor is represented by the surface layer of cesium ions; the other charge is represented by the region of filled acceptor levels. The reduction in the electron affinity is exactly equal to the potential difference developed across the capacitor.

In a more rigorous analysis, the amount by which the energy bands are bent is found to be approximately equal to the band-gap, and the vacuum level is lowered until the absorption level of the electropositive material is essentially at the top of the valence band.

Measurements of Photocathode Sensitivity

There are various ways of specifying the sensitivity of a photocathode. For many purposes, a knowledge of the response of the photocathode to particular wavelengths or equivalent energies of radiation is necessary. Sometimes it is convenient to have

a single number to describe the response of the photocathode to some standard broad-band source, such as a tungsten lamp.

Variation in photocathode sensitivity over the range of wavelengths to which the photocathode material is sensitive is usually described by means of a spectral-response curve such as the one shown in Fig. 4. The abscissa may represent the wavelength in nanometers or angstroms, or the photon energy in electron-volts. The values can be converted from one scale to the other by use of Eq. 1.

The ordinate can also be expressed in many ways. The most common scale is amperes per incident watt, as shown; a second common scale is that of quantum efficiency, the average numbers of photoelectrons emitted per incident photon.

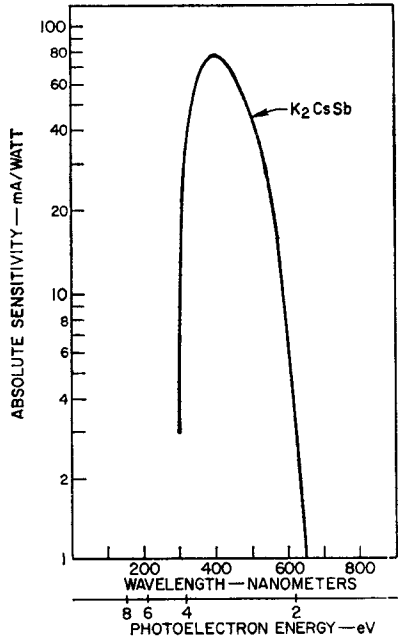

Fig. 4 — Typical spectral-response curve for a bialkali photocathode with a 008 lime-glass window.

It should be noted that the spectral response of photoemitters is modified by the window material. Therefore, the short-wavelength limit of the spectral response is generally a characteristic of the window rather than of the photocathode.

A common practice is to specify the response of the device to the incident flux from a tungsten lamp with a lime-glass window operating at a color temperature of 2854°K. The units of measurement are most frequently amperes per lumen. Sometimes sensitivity is expressed in terms of photocurrent and the total incident radiant power from the lamp on the photocathode window. This sensitivity is commonly stated in amperes per watt. It is the general practice to give sensitivity measurements in terms of incident flux. For some purposes, such as the study of photoemission phenomena, it may be useful to specify the sensitivity in terms of absorbed flux.

Opaque and Semitransparent Photocathodes

The photocathode consists of a material that emits electrons when exposed to radiant energy. There are two types of photocathodes. In one, the opaque photocathode, the light is incident on a thick photoemissive material and the electrons are emitted from the same side as that struck by the radiant energy. In the second type, the semitransparent photocathode, the photoemissive material is deposited on a transparent medium so that the electrons are emitted from the side of the photocathode opposite the incident radiation.

Because of the limited escape depth of photoelectrons, the thickness of the semitransparent photocathode film is critical. If the film

is too thick, much of the incident radiant energy is absorbed at a distance from the vacuum interface greater than the escape depth; if the film is too thin, much of the incident radiant energy is lost by transmission. Because radiant-energy absorption varies with wavelength, as shown in Fig. 5, the spectral response of a semitransparent photocathode can be controlled to some extent by control of its thickness. With increasing thickness, for example for alkali antimonides, blue response decreases and red response increases because of the difference in absorption coefficients.

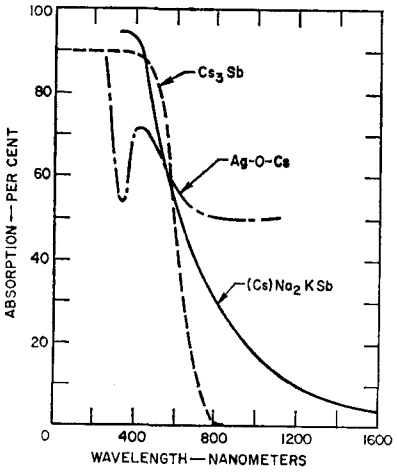

Fig. 5 — Radiation absorption for three commonly used semitransparent photocathode materials. Note loss of absorption in red region.

Photocathodes of Practical Importance

The photocathodes most commonly used in photomultipliers are silver-oxygen-cesium (Ag-0-Cs), cesium-antimony (Cs_3Sb), multialkali or trialkali [(Cs) Na_2KSb]*, and bialkali (K_2CsSb). Typical spectral-response curves for these materials are shown in Fig. 4 and Fig. 6. Additional information about these and other photocathodes of practical importance is shown in Table I.

The long-wavelength response of the multialkali photocathode has been extended recently by processing changes including the use of an increased photocathode-film thickness at the expense of the short-wavelength response. A typical spectral-response curve for one of these Extended Red Multi-Alkali (ERMA) photocathodes is shown in Fig. 7 in comparison with a conventionally processed multialkali photocathode.

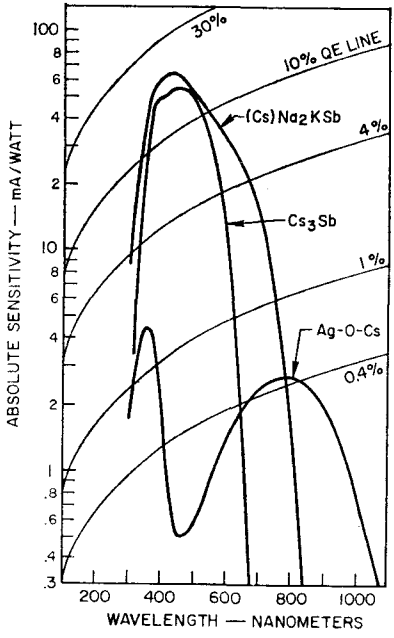

Fig. 6 — Typical spectral-response curves, with 008 lime-glass window, for (a) silver-oxygen-cesium (Ag-O-Cs), (b) cesium-antimony (Cs_3Sb), (c) multialkali or trialkali [(Cs)Na_2KSb].

* The parenthetical expression (Cs) indicates trace quantities of the element.

Table I — *Nominal Composition and Characteristics of Various Photocathodes.*

Nominal Composition	Response Designation	Type of Photocathode	Envelope Material[a]	Conversion Factor[b] (lumen/watt at λmax)	Luminous Sensitivity (μA/lumen)	Wavelength of Maximum Response, λmax (nm)	Sensitivity at λmax (mA/watt)	Quantum Efficiency at λmax (percent)	Dark Emission at 25°C A x 10^{-15}/cm²
Ag-O-Cs	S-1	O	0080	92.7	25	800	2.3	0.36	900
Ag-O-Rb	S-3	O	0080	285	6.5	420	1.8	0.55	—
Cs_3Sb	S-19	O	SiO_2	1603	40	330	64	24	0.3
Cs_3Sb	S-4	O	0080	1044	40	400	42	13	0.2
Ca_3Sb	S-5	O	9741	1262	40	340	50	18	0.3
Cs_3Bi	S-8	O	0080	757	3	365	2.3	0.77	0.13
Ag-Bi-O-Cs	S-10	S	0080	509	40	450	20	5.6	70
Cs_3Sb	S-13	S	SiO_2	799	60	440	48	14	4
Cs_3Sb	S-9	S	0080	683	30	480	20	5.3	—
Cs_3Sb	S-11	S	0080	808	60	440	48	14	3
Cs_3Sb	S-21	S	9741	783	30	440	23	6.7	—
Cs_3Sb	S-17	O[g]	0080	667	125	490	83	21	1.2
Na_2KSb	S-24	S	7056	1505	32	380	64	23	0.0003
K-Cs-Sb	—	S	7740	1117	80	400	89	28	0.02
$(Ca)Na_2KSb$	—	S	SiO_2	429	150	420	64	18.9	0.4
$(Cs)Na_2KSb$	S-20	S	0080	428	150	420	64	19	0.3
$(Cs)Na_2KSb$	S-25	S	0080	276	160	420	44	13	—
$(Cs)Na_2KSb$	ERMA[c]	S	7056	169	265	575	45	10	1
Ga-As	—	O[h]	9741	148	250	450	37	10	0.1
Ga-As-P	—	O[i]	Sapphire	310	200	450	61	17	0.01
InGaAs-CsO[d]	—	O[h]	0080	266	260	400	71	22	1[d]
Cs_2Te	—	S	LiF	[e]	[e]	120	12.6	13	[f]
CsI	—	S	LiF	[e]	[e]	120	24	20	[f]
CuI	—	S	LiF	[e]	[e]	150	13	10.7	[f]

[a] Numbers refer to the following glasses:
0080—Corning Lime Glass
9741—Corning Ultraviolet Transmitting Glass
7056—Corning Borosilicate Glass
7740—Corning Pyrex Glass
SiO_2—Fused Silica (Suprasil—Trademark of Englehard Industries, Inc., Hillside, New Jersey)

[b] These conversion factors are the ratio of the radiant sensitivity at the peak of the spectral response characteristic in amperes per watt to the luminous sensitivity in amperes per lumen for a tungsten test lamp operated at a color temperature of 2854°K.

[c] An RCA designation for "Extended-Red Multialkali."

[d] An experimental photocathode, private communication from B. F. Williams, RCA Laboratories, Princeton, New Jersey. The dark emission indicated is a calculated value based on a bandgap of 1.1 eV for the particular composition studied. See also B. F. Williams, "InGaAs-CsO, A Low Work Function (Less Than 1.0 eV) Photoemitter," Appl. Phys. Letters 14, No. 9, p. 273 (1969).

[e] Not relevant.

[f] Data unavailable; expected to be very low.

[g] Reflecting substrate.

[h] Single crystal.

[i] Polycrystalline.

O = Opaque

S = Semitransparent

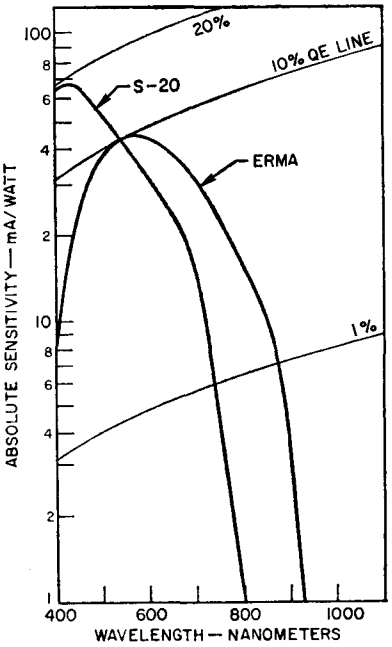

Fig. 7 — Typical spectral-response curve for one of the Extended Red Multi-Alkali (ERMA) photocathodes in comparison with a conventionally processed multialkali photocathode.

New Photocathode Materials

The negative-electron-affinity materials described earlier are used in opaque photocathodes. Typical spectral-response curves for GaAs(Cs) and $GaAs_xP_{1-x}(Cs)$ opaque photocathodes are shown in Fig. 8. Development of negative-electron-affinity materials is proceeding rapidly. Therefore, improved sensitivities and extended spectral ranges may be anticipated.

SECONDARY EMISSION

When electrons strike the surface of a material with sufficient kinetic energy, secondary electrons are emitted. The secondary-emission ratio or yield, δ, is defined as follows:

$$\delta = \frac{N_s}{N_e} \qquad (3)$$

where N_s is the average number of secondary electrons emitted for N_e primary electrons incident upon the surface.

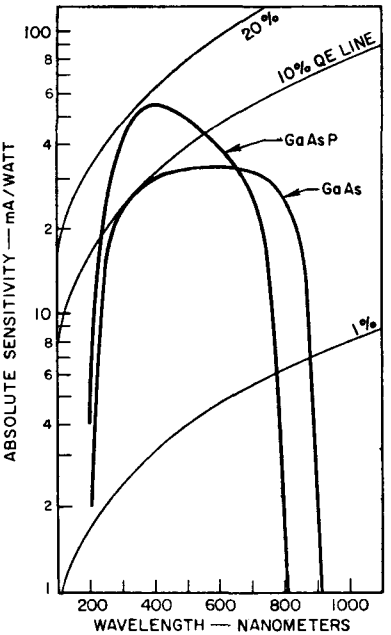

Fig. 8 — Typical spectral-response curves for GaAs(Cs) and $GaAs_xP_{1-x}(Cs)$ opaque photocathodes.

Fundamentals of Secondary Emission

The physical processes involved in secondary emission are in many respects similar to those already described under **Fundamentals of Photoemission.** The main difference is that the impact of primary electrons rather than incident photons causes the emission of electrons. The steps involved in secondary emission can be stated briefly as follows:

1. The incident electrons interact with electrons in the material and excite them to higher energy states.
2. Some of these excited electrons move toward the vacuum-solid interface.
3. Those electrons which arrive at the surface with energy greater than that represented by the surface barrier are emitted into the vacuum.

When a primary beam of electrons impacts a secondary-emitting material, the primary-beam energy is dissipated within the material and a number of excited electrons are produced within the material. Based on experimental data, approximations have been made [2] based on the assumption that the range of primary electrons varies as the 1.35 power of the primary energy and that the number of electrons excited is uniform throughout the primary range. The numbers of excited electrons produced are indicated in Fig. 9 for primary energies varying from 400 to 2200 electron-volts. The total number of excited electrons produced by a primary is indicated by the area of the individual rectangles in the figure.

As an excited electron in the bulk of the material moves toward the vacuum-solid interface, it loses energy as a result of collisions with other electrons and optical phonons. The energy of the electron is very rapidly dissipated as a result of these collisions, and it is estimated that the energy of such an electron will decay to within a few times the mean thermal energy above the bottom of the conduction band within 10^{-12} second. If the electron arrives at the vacuum-solid interface with energy below that required to traverse the potential barrier, it cannot escape as a secondary electron. Therefore, only those electrons excited near the surface of the material are likely to escape as secondary electrons. The probability of

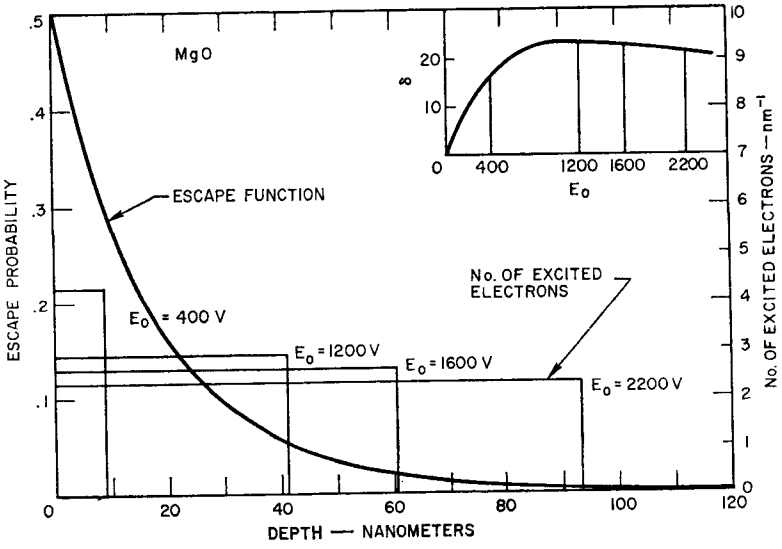

Fig. 9 — An illustration showing the processes of secondary emission. See text for explanation.

escape for an excited electron is assumed to vary exponentially with the excitation depth, as indicated in Fig. 9. If the product of the escape function and the number of excited electrons (which is a function of primary energy and depth) is integrated, a secondary-emission-yield function may be obtained, as indicated in the insert at the top of Fig. 9. The model which has been assumed thus explains the general characteristics of secondary emission as a function of primary energy. Secondary-emission yield increases with primary energy, provided the excited electrons are produced near the surface where the escape probability is high. As the primary-electron energy increases, the number of excited electrons also increases, but the excitation occurs at greater depths in the material where escape is much less probable. Consequently, the secondary-emission yield eventually reaches a maximum and then decreases with primary energy.

Experimental secondary-emission-yield values are shown as a function of primary-electron energy in Fig. 10 for MgO, a traditional secondary-emission material, and for GaP(Cs), a recently developed negative-electron-affinity material. Although both of these materials display the general characteristics of secondary emission as a function of primary energy, as expected from the model illustrated in Fig. 8, the secondary-emission yield for GaP(Cs) increases with voltage to much higher values. Even though electrons are excited rather deep in the negative-electron-affinity material and lose most of their excess energy as a result of collisions, many still escape into the vacuum because of the nature of the surface barrier.

When secondary electrons are emitted into the vacuum, the spread of emission energies may be quite large, as illustrated in the curve of Fig. 11 for a positive-affinity emitter. The peak at the right of the

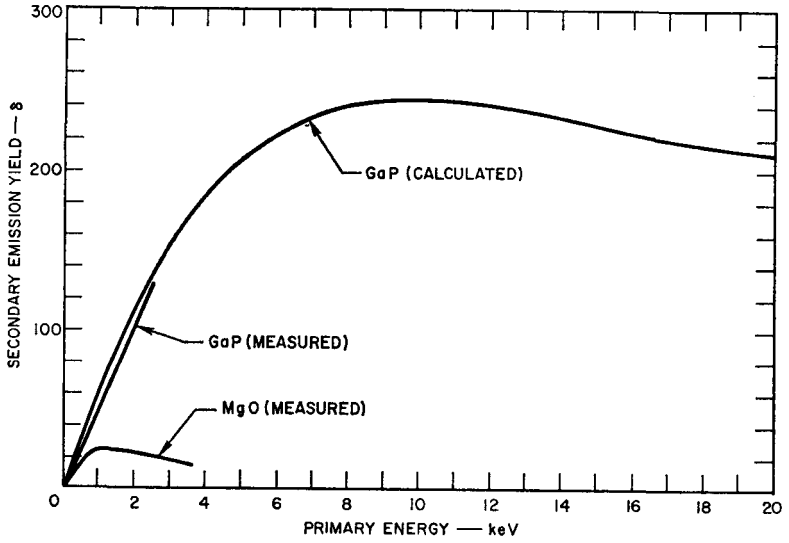

Fig. 10 — Typical curve of secondary-emission yield as a function of primary-electron energy in GaP(Cs) and MgO.

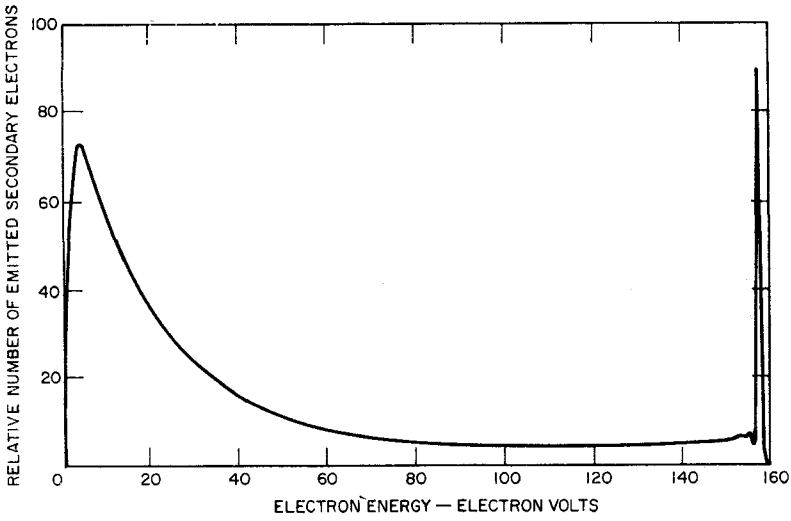

Fig. 11 — Typical secondary-electron energy distribution; peak at right is caused by reflected primary electrons.

curve does not represent a true secondary, but rather a reflected primary. Data are not available for the emission energies from a negative-electron-affinity material, but they are expected to be considerably less than for positive-affinity materials.

Negative electron affinity has not only expanded the field of photoemission, but has proved very important in the development of greatly improved secondary-emitting materials for use as dynodes in photomultipliers. With negative-electron-affinity materials, such as GaP, the secondary-emission ratio increases almost linearly up to very high primary energies; factors up to 130 have been measured. This factor compares with typical values of less than 10 for previously used dynode materials.

Effects of Secondary-Emission Statistics

The statistical distribution of secondary-emission yields tends to degrade the signal-to-noise ratio in a photomultiplier; the greatest contribution to the noise occurs at the first dynode. If the secondary-emission ratio of the first dynode is improved through the use of a negative-electron-affinity material, such as GaP, the emission statistics of the first dynode are markedly improved and the performance of the multiplier more closely resembles that of a perfect amplifier. Photomultiplier statistics are explained in greater detail in the section on **Statistical Fluctuation and Noise.**

The incorporation of high-gain secondary-emission materials throughout the dynode chain makes it possible to design photomultipliers with fewer stages for given amplifications. The use of fewer stages also reduces the variation of gain with voltage changes.

Time Lag in Photoemission and Secondary Emission

Because both photoemission and secondary emission can be described

in terms of the excitation of electrons within the volume of the solid and the subsequent diffusion of these electrons to the surface, a finite time interval occurs between the instant that a primary (photon or electron) strikes a surface and the emergence of electrons from the surface. Furthermore, in the case of secondary emission, the secondaries can be expected to reach the surface over a period of time. Within the limitations of a mechanistic approach to a quantum phenomenon, time intervals for metals or insulators of the order of 10^{-13} to 10^{-14} second may be estimated from the known energy of the primaries, their approximately known range, and the approximately known diffusion velocities of the internal electrons. In negative-electron-affinity semiconductors, it is known that the lifetime of internal "free" electrons having quasi-thermal energies (i.e. electrons near the bottom of the conduction band) can be of the order of 10^{-10} second.

Thus far experiments have provided only upper limits for the time lag of emission. In the case of secondary emission, a variety of experiments have established limits. Several investigators [3, 4, 6] have deduced limits from the measured performance of electron tubes using secondary emitters. Others, making direct measurements of these limits, determined the time dispersion of secondary emission by letting short electron bunches strike a target and comparing the duration of the resulting secondary bunches with the measured duration of the primary bunch. By this means an upper limit of 6×10^{-12} second was determined for platinum [7] and an upper limit of 7×10^{-11} second for an MgO layer [5] formed on the surface of an AgMg alloy.

The upper limit for the time lag in photoemission, however, is not well established. One investigation [8] determined a limit of 3×10^{-9} second. From careful measurements [9] of the time performance of fast photomultipliers it can be inferred that the limit must be at least an order of magnitude smaller.

While these limits are a useful guide to the type of time performance to be expected in present photomultipliers, they will probably have less significance as new photomultipliers using semiconducting photoemitters and secondary emitters are developed. Semiconductors having minority-carrier lifetimes of the order of microseconds are now available. Probably, by combination of this characteristic with negative electron affinity, higher gains and quantum efficiencies can be achieved, but at a sacrifice of time response or band width. However, the first generation of negative-electron-affinity emitters (e.g., GaP) has actually resulted in photomultipliers having better time performance because a smaller number of stages operating at higher voltage can be used. At this time it can only be concluded that in the future photomultipliers will probably be designed to match in more detail the requirements of a particular use.

REFERENCES

1. A. H. Sommer, *Photoemissive Materials,* John Wiley, New York (1968)
2. R. E. Simon and B. F. Williams, "Secondary Electron Emission," *IEEE Trans. Nucl. Sci., Vol. NS–15,* No. 3, p. 167 (1968)
3. G. Diemer and J. L. H. Jonker, "On the Time Delay of Secondary Emission," *Philips Research Repts., Vol. 5,* p. 161 (1950)

4. M. H. Greenblatt and P. A. Miller, Jr., "A Microwave Secondary-Electron Multiplier," *Phys. Rev., Vol. 72,* p. 160 (1947)
5. M. H. Greenblatt, "On the Measurement of the Average Time Delay in Secondary Emission," *RCA Rev., Vol. 16,* p. 52 (1955)
6. C. G. Wang, "Reflex Oscillators Using Secondary-Emission Current," *Phys. Rev., Vol. 68,* p. 284 (1945)
7. E. W. Ernst and H. Von Foerster, "Time Dispersion of Secondary Electron Emission," *J. Appl. Phys., Vol. 26,* p. 781 (1955)
8. E. O. Lawrence and J. W. Beams, "Instantansity of the Photoelectric Effect," *Phys. Rev., Vol. 29,* p. 903 (1927)
9. M. Birk, Q. A. Kerns, and R. F. Tusting, "Evaluation of the C-70045A High-Speed Photomultiplier," *IEEE Trans. Nucl. Sci. Vol. NS-11,* p. 129 (1964)

Principles of Photomultiplier Design

THIS section describes the physical and electrical parameters of interest in the design of photomultipliers. The effects of dynode and anode structures on such parameters as time response, sensitivity, and dark current are discussed. A section covering ruggedized photomultipliers describes their structure and method of testing.

PHOTOCATHODE-TO-FIRST DYNODE REGION

As mentioned in the preceding section, two classes of photocathodes are used in photomultipliers: opaque and semitransparent. Because opaque photocathodes are an integral part of the electron-multiplier structure, they are discussed later in connection with the electron multiplier. Semitransparent photocathodes are formed on planar or spherical-section windows which are part of the photocathode-to-first dynode region. Semitransparent photocathodes have large, readily accessible light-collection areas which may be directly coupled to scintillation crystals.

A planar-photocathode design, such as that shown in Fig. 12(a), provides excellent coupling to a scintillation crystal, but its time response is not as good as that of a spherical-section photocathode. The spherical-section photocathode shown in Fig. 12(b) when coupled to a high-speed electron multiplier provides a photomultiplier having a very fast time response. Some tube types utilize a spherical-section photocathode on a plano-concave faceplate to facilitate scintillator coupling. This design is usually limited to faceplate diameters of two inches or less because of the excessive thickness of the glass at the edge. The plano-concave faceplate may also contribute to some loss in uniformity of sensitivity because of internal reflection effects near the thick edge of the photocathode.

Design Analysis

Photocathode-to-first-dynode structures are usually axially symmetric, with the symmetry axis passing through the center of the photocathode. This symmetry simplifies the electron-optical analysis of the photocathode-to-first-dynode region because the problem is reduced from three dimensions to two. The first step in the analysis is the solution of the Laplace equation, $\nabla^2 V = 0$. Because a solution of this equation in closed form is impossible for most geometries, numerical solutions are obtained;[1] one solution[2] results in the photocathode-to-first-dynode region shown in Fig. 12(b). Performance is determined by use of a computer to trace equipotential lines and electron trajectories which can

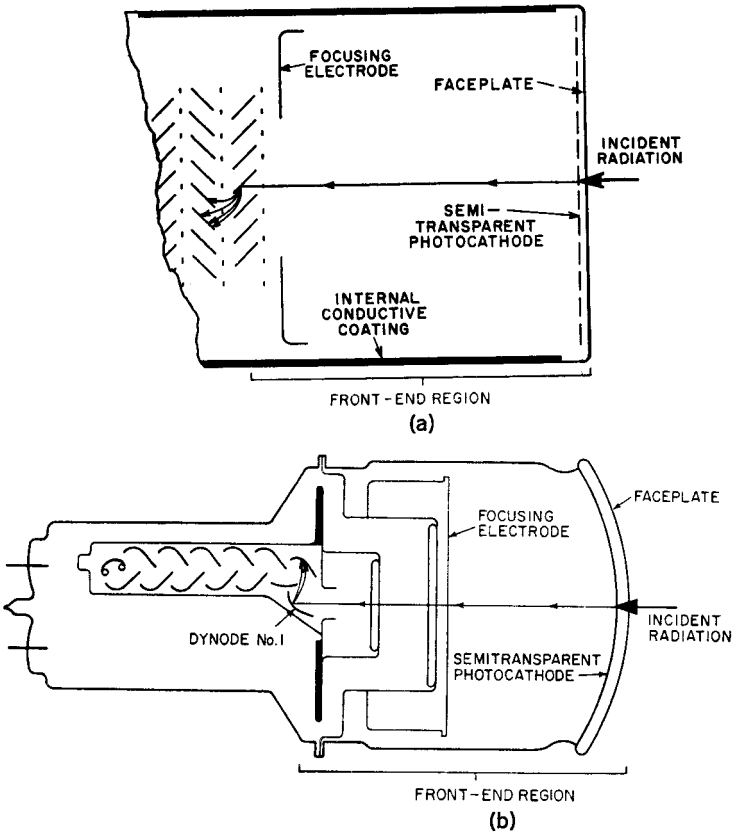

Fig. 12 — Front-end region of a photomultiplier with (a) a planar photocathode, and (b) a spherical-section photocathode.

then be superimposed on a schematic diagram of the tube structure as shown in Fig. 13.

Collection efficiency and time response may be predicted from an analysis of the electron trajectory. The collection efficiency is defined as the ratio of the number of photoelectrons which land upon a useful area of the first dynode to the number of photoelectrons emitted by the photocathode. If all the photoelectrons began their trajectories at the surface of the photocathode with zero velocity, a collection efficiency of 100 per cent would be possible; however, because of the finite initial velocities,[3] some photoelectrons begin their trajectories with unfavorable angles of launch and are not collected on the useful area of the first dynode. Although collection efficiency is difficult to measure, it can be calculated by computer by the use of Monte Carlo simulations.[4]

In modern photomultiplier structures, first-dynode collection efficiencies vary from 85 to 98 per cent. Ideally, the emitted photoelectrons should converge to a very small area on the first dynode; in practice this electron-spot diameter is approximately 1/8 to 1/20 of the cathode diameter, depending upon tube type.

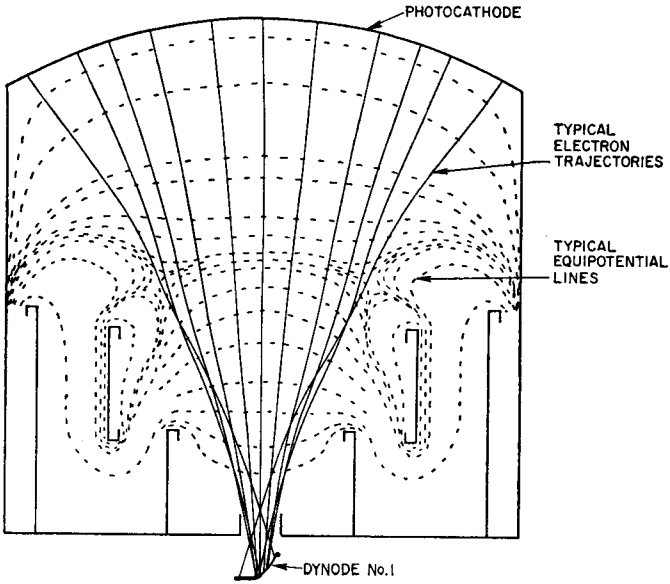

Fig. 13 — Cross section of a photomultiplier showing equipotential lines and electron trajectories that were plotted by computer.

ELECTRON MULTIPLIERS

In a photomultiplier having an opaque photocathode, the photocathode is part of the electron-multiplier or dynode-chain structure. The circular cage structure, shown in Fig. 14(a) for a "side-on" type of photomultiplier, employs an opaque photocathode and is one of the earliest multiplier configurations. Its relatively fast time response is a result of its small size and high interdynode field strengths. This same structure is also used in "head-on" type photomultipliers, as shown in Fig. 14(b). Because of the type of symmetry in the design, the number of dynodes in these structures can be reduced by units of two.

The "venetian-blind" dynode structure shown in Fig. 15 has a compact, rugged geometry and is generally used with planar photocathodes because the relatively large area of the first dynode allows simple photoelectron collector systems to be used. This structure is used only when time response is not of prime consideration. The relatively slow time response is a result of the weak electric field at the surfaces of the dynode vanes. This structure is the most flexible as to the number of stages.

The box-and-grid dynode structure, shown in Fig. 16, also has a large first-dynode collection area. The time response of this structure is similar to that of a venetian-blind multiplier (slow) because of the weak electric field within the box.

A linear-multiplier structure, such as that shown in Fig. 17, offers good time response. Because the dynode stages (with the exception of the first three and the last two) are iterative, the number of stages in this structure may be varied without electron-optic redesign.

The continuous-channel multiplier structure [5] shown in Fig. 18 is very

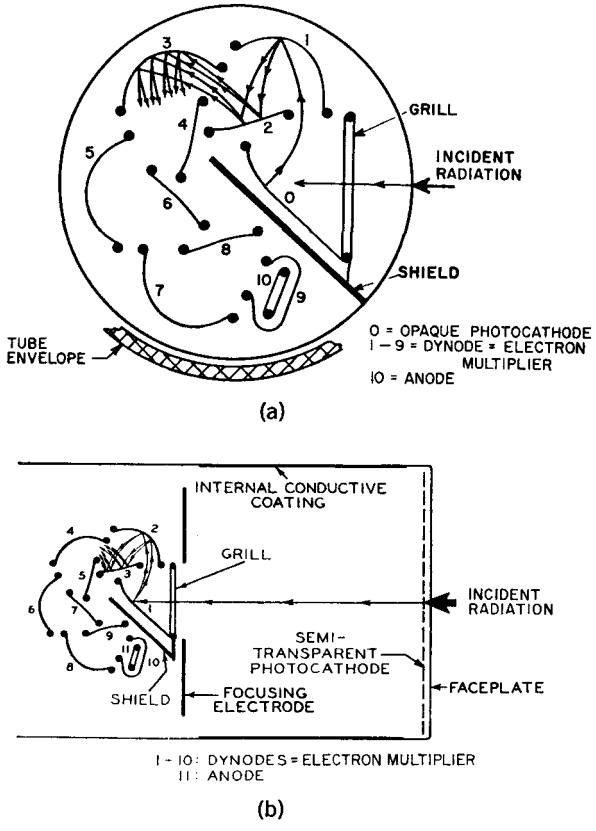

Fig. 14 — The circular-cage multiplier structure (a) in a "side-on" photomultiplier, (b) in a "head-on" photomultiplier.

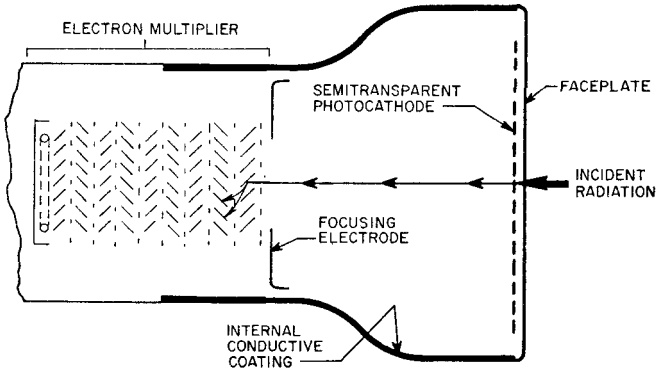

Fig. 15 — The venetian-blind multiplier structure.

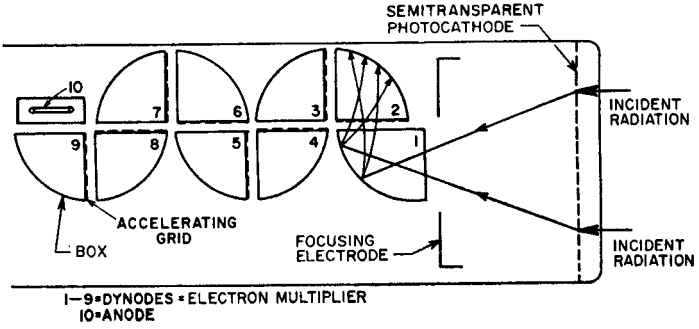

Fig. 16 — The box-and-grid multiplier structure.

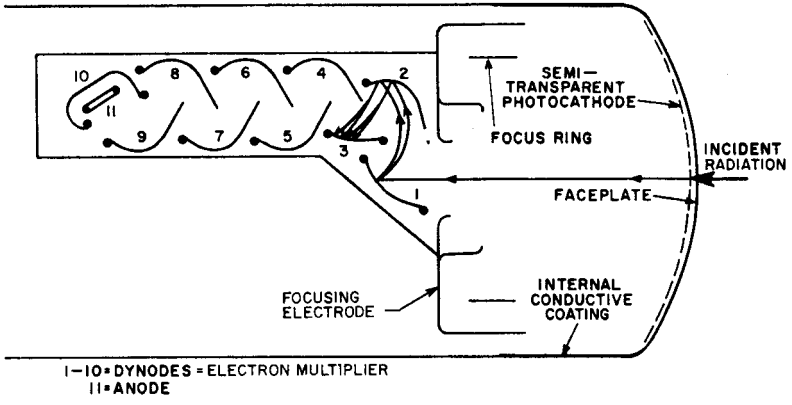

Fig. 17 — The linear-multiplier structure.

compact and utilizes a resistive emitter on the inside surface of a cylinder rather than a discrete number of dynodes. The lack of discrete dynodes causes the electron-multiplication statistics to be poor because of the variable path lengths and the variable associated voltages. The gain of a continuous-channel multiplier is determined by the ratio of length, l, to inside diameter, d; a typical value of this ratio is 50 but it may range from 30 to 100.

An interesting multiplier structure which has potentially good time response is a series of close-spaced parallel-plane structures that use transmission dynodes. The dynodes consist of thin membranes on which primary electrons impinge to cause secondary emission from the opposite side. There are, however, difficulties in this construction: (1) in obtaining rugged self-supporting dynodes of reasonable size, and (2) in preventing transmission of primary electrons which tend to degrade the statistics of electron transit time.

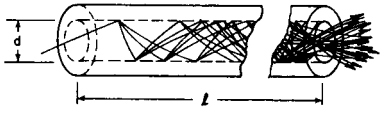

Fig 18 — The continuous-channel multiplier structure.

Multiplier Analysis

The analysis of the multiplier structure requires solution of the Laplace equation. This solution can be obtained with an analog model, such as the rubber membrane,[6] or in digital form by use of a computer.[1] Initial analysis requires that electrons from a large area of one dynode be converged onto a smaller area on the next dynode. Convergence must take place in two dimensions to keep the electron cascade from spilling off the ends of the dynodes. The over-all rounded shape of the dynode shown in Fig. 19 converges the electrons in one dimension, while the field-forming ridges at or near the dynode ends converge the electrons in the second dimension.

In an analysis of multiplier structures, space-charge effects may be ignored in the early stages because of the low current densities. However, space-charge effects must be taken into account in the output

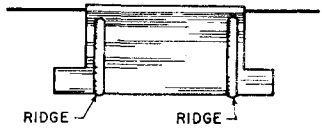

Fig. 19 — A dynode whose over-all rounded shape and field-forming ridges converge the electron cascade.

stages of tube designs requiring large anode pulse currents. Such tubes usually require higher interstage potential differences near the anode to overcome space-charge saturation effects.

ANODES

The primary function of the anode is to collect secondary electrons from the last dynode. The anode should exhibit a constant-current characteristic of the type shown in Fig. 20. The simplest anode structure, shown in Fig. 21, is a grid-like collector used in some venetian-blind structures. The secondary electrons from the next-to-last dynode pass

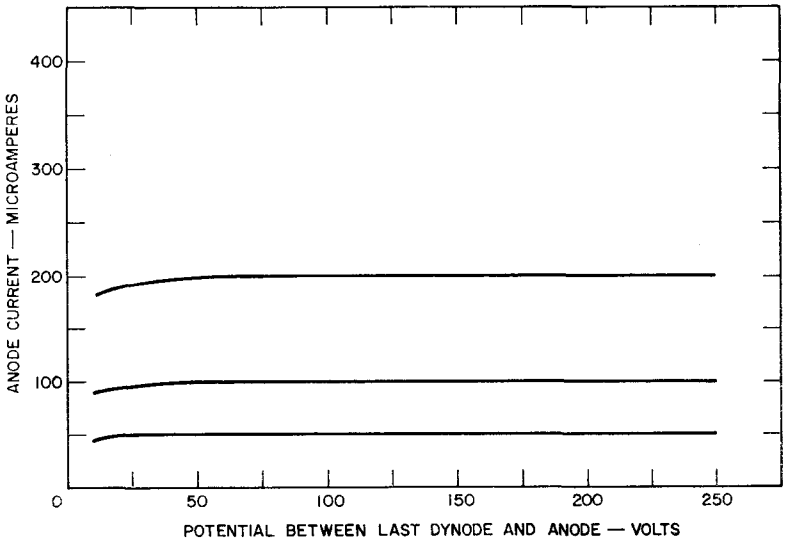

Fig. 20 — Constant-current characteristic required of an anode.

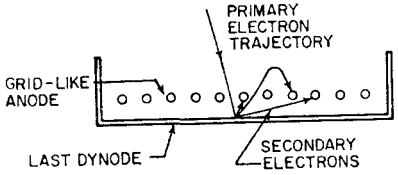

Fig. 21 — The simplest anode structure, a grid-like collector.

through the grid to the last dynode. Secondary electrons leaving the last dynode are then collected on the grid-like anode. Photomultipliers designed to have fast time responses require anodes with matched-impedance transmission lines. Most high-speed circuits are designed to utilize a 50-ohm impedance, which requires a 50-ohm transmission line within the tube and a suitable connector or lead geometry outside the tube to permit proper interface. A more detailed description of these requirements is given in the section on **Voltage-Divider Considerations.**

Anode configurations and internal transmission lines may be analyzed by use of the standard methods of cavity and transmission-line analysis. These methods yield approximate design parameters,[7] which are optimized experimentally by means of time-domain reflectometry, TDR [8, 9]. TDR provides information about the discontinuities in the characteristic impedance of a system as a function of electrical length and is an extremely useful approach in the design of voltage-divider circuits and mating sockets which do not readily lend themselves to mathematical analysis.

Certain anode structures in fast-rise-time photomultipliers exhibit a small-amplitude pulse (prepulse) that can be observed a nanosecond or two before the true signal pulse. In grid-like anode structures this prepulse is induced when electrons from the next-to-last dynode pass through the anode grid. In more sophisticated photomultiplier designs this phenomenon may be suppressed by auxiliary grids that shield the anode from the effects of the impinging electron cloud.

TRANSIT-TIME CONSIDERATIONS

Photocathode Transit-Time Difference

A time parameter of interest is the photocathode transit-time difference, the time difference between the peak current outputs for simultaneous small-spot illumination of different parts of the photocathode. (In practice, of course, one small area at a time is illuminated and the spread in illumination-peak output intervals is measured.) In a planar-cathode design, the transit time is longer for edge illumination than for center illumination because of the longer edge trajectories and the weaker electric field near the edge of the photocathode. The center-to-edge transit-time difference may be as much as 10 nanoseconds. The spherical-section photocathode affords more uniform time response than the planar photocathode because all the electron paths are nearly equal in length; however, the transit time is slightly longer for edge trajectories than for axial trajectories because of the weaker electric field at the edge.

The photocathode transit-time difference is ultimately limited by the initial-velocity distribution of the photoelectrons; this distribution causes time-broadening of the electron packet during its flight from the photocathode to the first dynode. The broadening effect can be minimized by increasing the strength of

the electric field at the surface of the photocathode.

Electron-Multiplier Time Response

Because the energy spread of secondary electrons is even larger than that of photoelectrons, initial-velocity effects are the major limitation on the time response of the electron multiplier. Multiplier time response is usually improved by the use of high electric-field strengths at the dynode surfaces and compensated design geometries. In a compensated design, such as that shown in Fig. 22, longer electron paths and weaker fields alternate with shorter electron paths and stronger fields from dynode to dynode to produce nearly equal total transit time.

Excellent time response is achieved with crossed-field multipliers which use both magnetic and electrostatic focusing fields. Crossed-field multipliers yield nearly isochronous electron trajectories because of their compensation characteristics; the higher-velocity electrons have longer path lengths between stages, and thus arrive at the same time as electrons which began with lower initial velocities. Because this type of multiplier must be operated at a unique voltage for a given magnetic field strength, gain is not adjustable unless electromagnets are used.

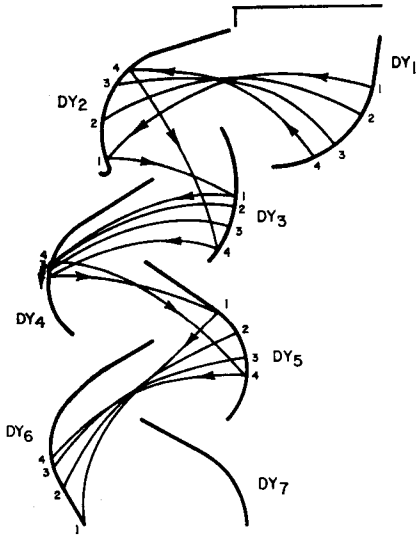

Fig. 22 — A compensated-design multiplier.

Certain materials have advantages over other materials in providing good multiplier time performance. For example, a standard dynode material, copper beryllium (CuBe), has a maximum gain per stage of 8 at a 600-volt interstage potential difference. In contrast, gallium phosphide (GaP) exhibits a gain of 50 or more at a 1000-volt interstage potential difference.[10] The advantage in time performance of the GaP dynode over one of the CuBe type is that the number of stages, and thus the total transit time, may be reduced, and that the energy spread of the secondary electrons is less.

RUGGEDIZED PHOTOMULTIPLIERS

New and increased demands on the capabilities of photomultipliers to survive severe vibrational environments have resulted in the development of a series of ruggedized photomultiplier types. The ruggedization of these photomultipliers has been achieved without degradation of electrical characteristics.

Ruggedization of glass-envelope photomultipliers has been accomplished by moving the dynode cage extremely close to the stem (thereby drastically shortening the lead lengths and raising their mechanical resonant frequency), and by using heavier leads, extra spacers to hold the dy-

node cage in place, and a special heavy-duty welding process on the metal-to-metal joints. A new type of tube, the stacked-ceramic photomultiplier, has been developed for use in the most severe mechanical environments. In this type, each dynode is mounted on the inside of a flat metal ring which is separated from the next dynode ring by a ceramic-ring spacer. The metal rings and ceramic spacers are then brazed together to form the vacuum envelope.

Ruggedized tubes are tested for their ability to withstand sinusoidal and random vibrations and for their resistance to shock. Test-parameter values for RCA ruggedized photomultipliers are given in the **Data Section.**

The "sinusoidal vibration test" is performed on apparatus that applies a variable sinusoidal vibration to the tube. The sinusoidal frequency is varied logarithmically with time from a minimum to a maximum to a minimum value. Each tube is vibrated in each of the three orthogonal axes shown in Fig. 23. The total time for the vibration of all three axes for ruggedized photomultipliers is given in the **Data Section.**

The peak acceleration is expressed in units of the acceleration of gravity at the earth's axis (32.17 ft/s^2) and is denoted by the symbol g. The distance over which the tube is vibrated is referred to as the "double amplitude." Double amplitude is the distance between the limits of travel of the tube in both directions of the sinusoidal vibration.

The shock test is performed on apparatus that applies a half-wave sinusoidal shock pulse to the photomultiplier tube. The tube is subjected to the shock in each of three orthogonal axes shown in Fig. 23.

The shock pulse is expressed in terms of the peak acceleration of the pulse and the time duration of the pulse. The tubes may receive more than one shock pulse in each of the orthogonal axes.

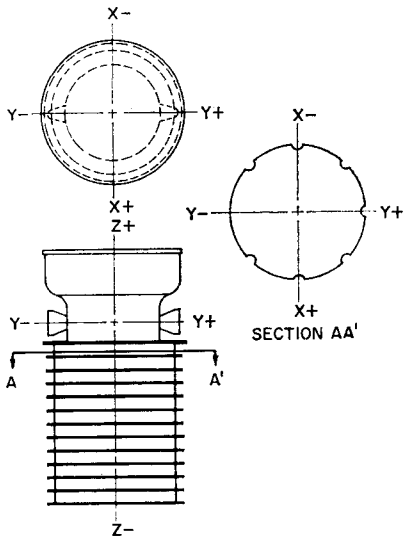

Fig. 23 — Test axes used in random-vibration and shock testing of stacked-ceramic photomultipliers.

BASING CONSIDERATIONS

Photomultiplier tubes may have either a temporary or a permanently attached base. Dimensional outline diagrams such as those shown in Fig. 24 are provided in the Technical Data Section of this manual and in individual tube bulletins. Indicated on the diagrams are the type of base employed, maximum mechanical dimensions, radii of curvature where applicable, pin/lead details, location and dimensions of magnetic parts used (in tubes utilizing minimum number of magnetic materials), and notes regarding restricted mounting areas, again where applicable.

Photomultiplier tubes intended to be soldered directly to circuit boards or housings are supplied with semi-flexible or "flying" leads and a tem-

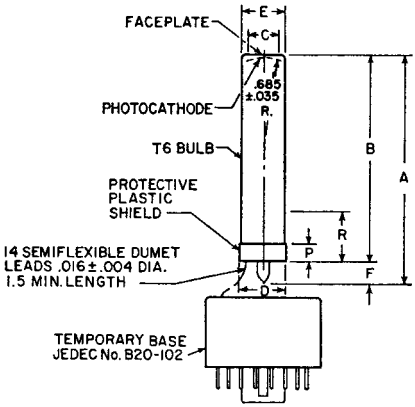

Dimensions	Inches	mm
A	3.94 max.	100.0 max.
B	3.50 $^{+.06}_{-.12}$	88.9 $^{+1.5}_{-3}$
C	.5 min. dia.	12.7 min. dia.
D	.78 max. dia.	19.8 max. dia.
E	.755 max. dia.	19.18 max. dia.
F	.38 max.	9.7 max.
H	.75 min.	19.0 min.
P	.30 max.	7.6 max.
R	1.0 max.	25 max.

The dimensions in millimeters are derived from the basic inch dimensions (1 inch = 25.4 mm)

Fig. 24 — Typical dimensional-outline drawings showing the type of base supplied with each tube and pertinent notes.

porary base, intended for testing purposes only, that should be removed prior to permanent installation.

A lead-terminal diagram that shows photomultiplier-tube lead orientation with the temporary base removed, shown in Fig. 25, provides a lead indexing reference. A lead-connection diagram, such as the one shown in Fig. 26, relates terminal to

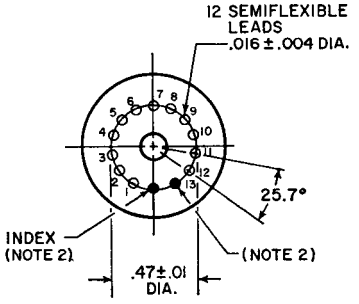

Fig. 25 — Lead-orientation diagram.

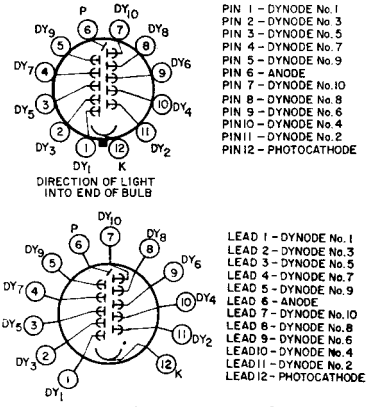

Fig. 26 — Lead-connection diagram: (a with base connected, (b) with tempora base removed.

electrode. Care must be exercised in interpreting basing and lead-terminal diagrams to insure against possible damage to the photomultiplier resulting from incorrect connections.

REFERENCES

1. H. E. Kulsrud, "A Programming System for Electron Optical Simulation," *RCA Rev., Vol. 28,* No. 2, p. 351 (1967)
2. R. W. Engstrom and R. M. Matheson, "Multiplier-Phototube Development Program at RCA-Lancaster," *IRE Trans. Nucl. Sci., Vol. NS–7,* No. 2–3, p. 52 (1960)
3. E. A. Taft and H. R. Philipp, "Structure in the Energy Distribution of Photoelectrons from K_3Sb and Cs_3Sb," *Phys. Rev., Vol. 115,* No. 6, p. 1583 (1959)
4. D. E. Persyk, "Computer Simulation of Photomultiplier-Tube Operation," RCA Reprint PE–473 (1970)
5. K. C. Schmidt and C. F. Hendee, "Continuous-Channel Electron Multiplier Operated in the Pulse-Saturated Mode," *IEEE Trans. Nucl. Sci., Vol. NS–13,* No. 3, p. 100 (1966)
6. A. D. White and D. L. Perry, "Notes on the Use of a Rubber Membrane Model for Plotting Electron Trajectories," *Rev. Sci. Instr., Vol. 32,* No. 6, p. 730 (1961)
7. I. A. D. Lewis and F. H. Wells, *Milli-Microsecond Pulse Techniques,* Pergamon Press (1959)
8. "Time-Domain Reflectometry," Hewlett Packard Application Note 62
9. "Time-Domain Reflectometry," Tektronix Publication 062–0703–00
10. G. A. Morton, H. M. Smith, Jr., and H. R. Krall, "The Performance of High-Gain First-Dynode Photomultipliers," *IEEE Trans. Nucl. Sci., Vol. NS–16,* No. 1, p. 92 (1969)

Basic Performance Characteristics

THIS section discusses the operational characteristics of photomultipliers that are listed in the **Technical Data** section of this Manual and in the technical data bulletins that describe each type of photomultiplier. The index at the back of the Manual gives the location of particular characteristics of interest within the pages of this section.

CLASSES OF DATA

Ratings

Photomultiplier ratings are established to help equipment designers utilize the performance and service capability of each device to best advantage. These ratings are based on careful study and extensive testing and indicate limits within which the operating conditions must be maintained to insure satisfactory performance. The maximum ratings given are based on the **Absolute Maximum System,** a system initiated by the Joint Electron Device Engineering Council (JEDEC) and subscribed to by the National Electrical Manufacturers Association (NEMA) and Electronic Industries Association (EIA).

Equipment Design Parameters

Characteristic Range Values for Equipment Design are included in this Manual and in individual data bulletins in addition to the maximum ratings described above. Minimum, maximum, and typical values of selected parameters for a given tube of a particular type are listed under this heading to assist an equipment designer in selecting the proper device for his application. Knowledge of parameter values allows the designer to specify the proper latitude of voltage and gain controls, additional amplification, etc., which will permit optimum utilization of the device he has chosen. Of the parameters listed, some are measured and some calculated from the measured quantities. Not all parameters are described for every device because many parameters are important only in specific infrequent applications.

RATINGS AND DESIGN PARAMETERS

Voltage

The maximum voltage ratings for photomultipliers are usually given as

the maximum voltage to be applied between the anode and cathode, between the anode and the last dynode, between consecutive dynodes, and between the cathode and the first dynode. A maximum anode-to-cathode voltage is specified so that the tube does not become regenerative. At excessive values of voltage the output current will become very noisy and may become so large as to exceed the current rating and cause damage to the secondary-emitting surfaces of the dynodes which could result in eventual tube failure. Maximum-voltage ratings are also specified between the last dynode and the anode. This rating is usually made somewhat lower in value than the ratings between consecutive dynodes to reduce the possibility of breakdown between the last dynode and the anode as a result of the close proximity of the two. Maximum voltages between consecutive dynodes are specified to prevent the possibility of breakdown between these elements and also to prevent excessive ohmic leakage in the region of the stem leads. The inter-dynode maximum voltage rating maintains operation below the point of maximum secondary emission above which the gain actually decreases. The specification of a maximum cathode-to-first-dynode-voltage rating also reduces the possibility of leakage, breakdown, and reduction in secondary emission.

The sum of the individual maximum voltage ratings may exceed the maximum anode-to-cathode voltage rating. This statement does not mean that the over-all voltage rating can be exceeded, but that, depending upon the application, special voltage distributions may be made. A detailed discussion of voltage distribution is given in the section on **Voltage-Divider Considerations.** One possible application in which special or "tapered" voltage distribution may be desirable is in equipment in which large anode pulse currents may be encountered. To reduce the possibility of space-charge limiting, it is often desirable to increase the voltage between the last few successive dynodes and between the last dynode and the anode. It may also be desirable to increase the normal cathode-to-first-dynode potential when optimum pulse-height resolution is desired.

Cathode Current

The magnitude of the maximum permissible cathode current depends upon the type of photocathode and the type of substrate or conductive layer upon which the photocathode is placed. In a tube having a semitransparent bialkali photocathode up to approximately one inch in diameter, a peak cathode current of 1×10^{-8} ampere at a tube temperature of 22°C or 1×10^{-10} ampere at −100°C should not be exceeded. Tubes having larger photocathodes should not be subjected to cathode currents exceeding 1×10^{-9} ampere at a tube temperature of 22°C or 1×10^{-11} ampere at −100°C. Because of the resistivity of the photocathode, the voltage drop caused by higher peak cathode currents could produce radial electric fields across the photocathode, and result in poor photoelectron collection at the first dynode. Photosurface resistivity also increases with decreasing temperature and thus reduces the maximum permissible current still further.

Opaque cesium-antimony photocathodes can be operated at peak cathode currents as high as 100 microamperes per square centimeter. Semitransparent cesium-anti-

mony photocathodes (CsSb) should be operated at currents less than 1 microampere per square centimeter at room temperature, and proportionally less as the ambient temperature is reduced. Semitransparent multialkali and Ag-O-Cs (S-1) photocathodes have lower resistivities than the CsSb types and can be operated at currents as high as 100 microamperes per square centimeter at room temperature; again, derating is required as temperature is reduced.

Anode Current

All photomultipliers have a maximum anode current rating. The primary reason for such a rating is to limit the anode power dissipation to approximately one-half watt or less. Consequently, the magnitude of the maximum anode current is restricted to a few milliamperes when the tube is operated at 100 to 200 volts between the last dynode and the anode. Space-charge effects must also be considered in computation of the magnitude of the maximum recommended anode current. As the anode current increases, operation becomes nonlinear because of the space-charge buildup between the last few dynodes and the last dynode and the anode. Even though a photomultiplier acts essentially as a constant-current device, the signal voltage developed across the load is in series with the last-dynode-to-anode voltage and consequently opposes it. Nonlinear operation may occur as the load resistance and load current become large.

Another possible adverse effect of operating a given photomultiplier at an excessively high anode current is the increased fatigue that occurs as the average anode current increases.

Temperature

A maximum ambient temperature, and in some instances a minimum temperature, is specified for all photomultipliers. The specification of maximum ambient temperatures reduces the possibility of heat damage to the tube. Because dark current (noise) increases with temperature, it is possible that a point of instability may be reached at high temperatures at which the tube will break down and the resulting large currents permanently damage the secondary-emitting surfaces of the dynodes. Even if the dark current does not increase to a level that causes regeneration, the tube might be damaged as a result of changes in the composition of the photocathode and dynode materials. Cesium, for example, is very volatile and may be driven from the photocathode and dynode surfaces to condense on the cooler portions of the tube and thereby reduce gain and cathode sensitivity or both.

It is recommended that photomultipliers be operated at or below room temperature so that the effects of dark current are minimized. The variation of dark current, or noise, is most important because of its effect on ultimate low-light-level sensitivity. Various cryostats and solid-state thermionic coolers have been designed that reduce dark current at low temperatures in low-light-level applications. An important consideration in the use of these devices is to prevent condensation of moisture on the photomultiplier window. A controlled low-humidity atmosphere or special equipment configuration may be necessary to prevent such condensation.

When the temperature is varied, small changes in the spectral response characteristics of the photo-

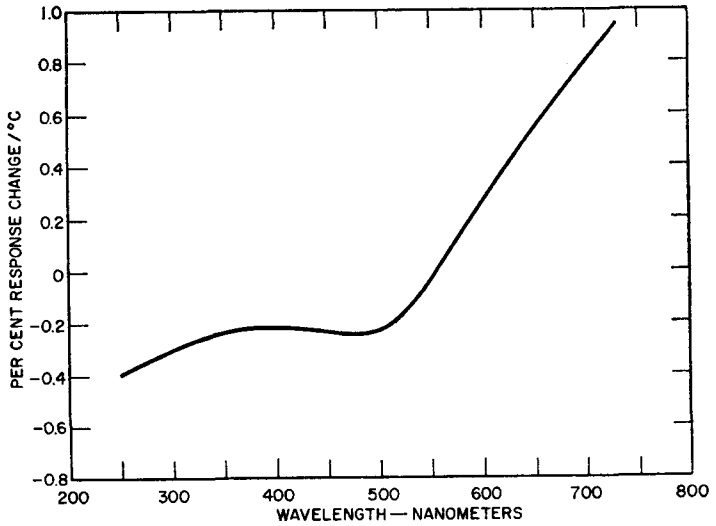

Fig. 27 — Temperature coefficient of cesium-antimony cathodes as a function of wavelength at 20°C. Note the large positive effect near the threshold.

cathode may be observed. Fig. 27 shows a temperature coefficient of sensitivity of a CsSb photocathode as a function of wavelength.[1] The increase of red sensitivity with temperature is typical for photoemission.

Alhough it is recommended that photomultipliers be operated at or below room temperature, many devices have minimum operating temperatures. The materials used in producing photocathodes are semiconductors. Their conductivity decreases with decreasing temperature until the photocathode becomes so resistive that a sizable voltage drop may occur across the cathode surface when cathode current flows. Such a voltage drop may result in loss of linearity of the output current as a function of light level. Fig. 28 shows the resistance per square of common semitransparent photocathode materials; measurements were made in special tubes having conections to parallel conducting lines on the photocathode. Semitransparent photocathodes of the bialkali and cesium antimony types have particularly high resistivity. Consequently, the operating temperatures of these photocathodes

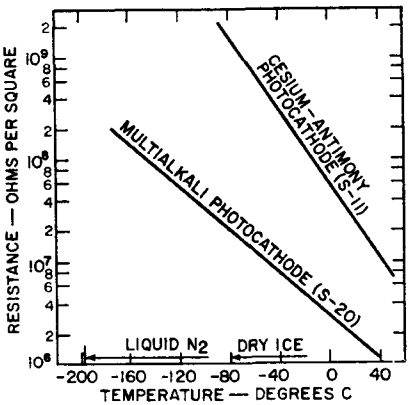

Fig. 28 — Resistance per square as a function of temperature for the cesium-antimony and the multialkali semitransparent photocathodes. These data were obtained with special tubes having connections to parallel conducting lines on the photocathode.

should be kept above −100°C, depending somewhat upon the photocathode diameter, the light-spot diameter, and the cathode current. The larger the photocathode diameter and the smaller the light-spot diameter, the more severe the effect. Opaque photocathodes and photocathodes having conductive substrates can be operated at cryogenic temperatures.

Another reason for avoiding the operation of photomultipliers at extremely low temperatures is the possible phase change that this type of operation may cause in some of the metal parts. These changes are particularly probable when Kovar is used in metal-to-glass seals. Tubes utilizing Kovar in their construction should not be operated at temperatures below that of liquid nitrogen (−196°C).

In some tubes, particularly those with multialkali photocathodes, it is sometimes observed that the noise actually increases as the temperature of the photocathode is reduced below about −40°C. The reason for this noise increase is not understood. However, most of the dark-current reduction has already been achieved at temperatures above −40°C.

In general, it is recommended that all wires and connections to the tube be encapsulated for refrigerated operation. Encapsulation minimizes breakdown of insulation, especially that caused by moisture condensation.

Exterior Magnetic and Electrostatic Fields

All photomultipliers are to some extent sensitive to the presence of magnetic and electrostatic fields. These fields may deflect electrons from their normal path between stages and cause a loss of gain. Tubes designed for scintillation counting are generally very sensitive to magnetic fields because of the relatively long path from the cathode to the first dynode; consequently, such tubes ordinarily require electrostatic and magnetic shielding. Magnetic fields may easily reduce the anode current by as much as 50 per cent or more of the "no-field" value.

The three curves in Fig. 29 show the effect on anode current of magnetic fields parallel and perpendicular to the main tube axis and parallel to the dynodes. The curves are usually provided for one or more values of over-all applied voltage and indicate the relative anode current in per cent as a function of magnetic field intensity in oersteds. Fig. 30 shows the variation of output current of several photomultiplier tubes as a function of magnetic-field intensity directly parallel to the major axis of the tube. The magnitude of the effect depends to a great extent upon the structure of the tube, the orientation of the field, and the operating voltage. In general, the higher the operating voltage, the less the effect of these fields.

High-mu material in the form of foils or preformed shields is available commercially for most photomultipliers. When such a shield is used, it must be at cathode potential. The use of an external shield may present a safety hazard because in many applications the photomultiplier is operated with the anode at ground potential and the cathode at a high negative potential. Adequate safeguards are therefore required to prevent personnel from coming in contact with the high potential of the shield. The application of high voltage, with respect to the cathode, to insulating or other materials supporting or shielding the photomultiplier at the photocathode end of the

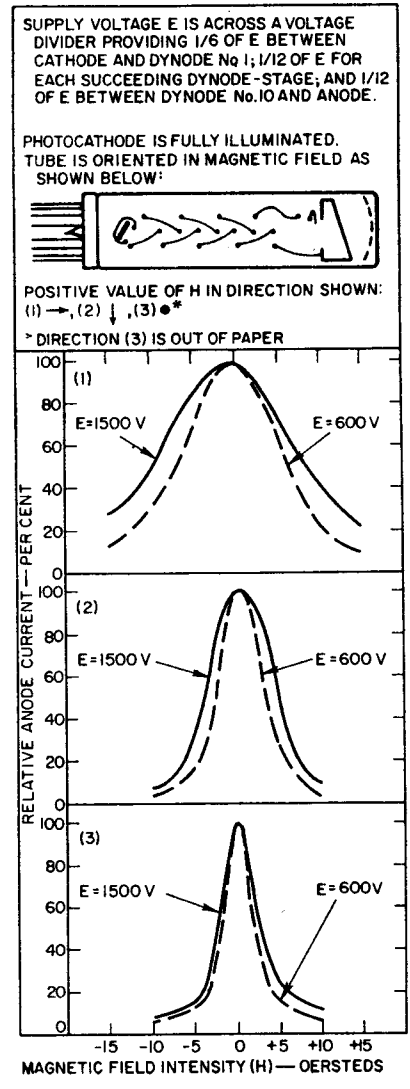

Fig. 29 — Curves showing the effect on anode current of magnetic fields parallel and perpendicular to the main tube axis and parallel to the dynodes.

tube should not be permitted unless the materials are of the type that will limit the leakage current to the tube envelope to 1×10^{-12} ampere or less. In addition to increasing dark current and noise output because of voltage gradients developed across the envelope wall, the application of high voltage may produce leakage current to the cathode through the tube envelope and insulating materials; this current can permanently damage the tube.

It is possible to modulate the output current of a photomultiplier with a magnetic field. The application of a magnetic field generally causes no permanent damage to a photomultiplier although it may magnetize those internal parts of a tube that contain ferromagnetic materials (tubes are available which contain practically no ferromagnetic materials). If tube parts do become magnetized, the performance of the tube may be degraded somewhat; however, the condition is easily corrected by degaussing, a process in which a tube is placed in and then gradually withdrawn from the center of a coil operated at an alternating current of 60 Hz with a maximum fiield strength of 100 oersteds.

Environments of Excessive Vibration or Shock

Most photomultipliers will survive only a reasonable amount of shock or vibration (less than 10-g shock, depending on shock duration and direction). Although special photomultipliers have been designed to survive in extreme environments (shock values from 30 to 1500 g), the user should make every effort to avoid excessive shock or vibration, possibly by the use of special vibration-isolation fixtures. The photomultiplier tube should be handled as the delicate instrument that it is. Excessive shock or vibration can actually cause physical damage to the tube to the point of shorting out some of the elements or even resulting in break-

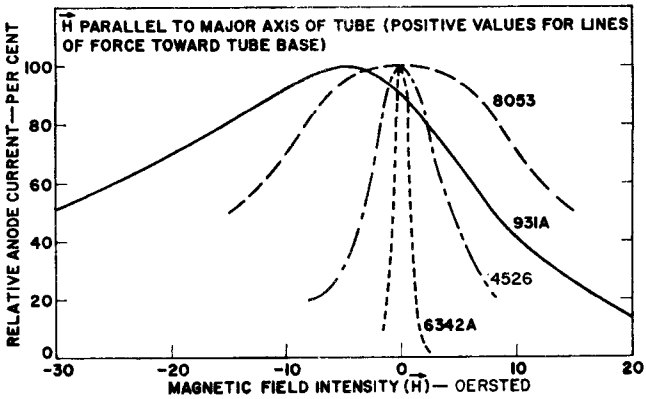

Fig. 30 — Variation of output current of several photomultiplier tubes as a function of magnetic-field intensity directly parallel to the major axis of the tube.

age of the envelope and loss of vacuum. A lesser degree of shock may result in deformation of the elements of the tube which can result in loss of gain or deterioration of other performance parameters. If measurements are being made while a tube is vibrated, it is likely that the output will be modulated by the vibration not only because the light spot may be deflected to different positions on the photocathode but because some of the dynodes may actually vibrate and cause modulation of the secondary-emission gain.

Many photomultipliers have been designed for use under severe environmental conditions of shock and vibration and, in many cases, specifically for use in missile and rocket applications. Such tubes, however, find uses in many other applications including oil-well logging or other industrial control appulications where the tube may be subjected to rough usage. These tubes are available with most of the electrical and spectral characteristics typical of the more-general-purpose types. These types differ primarily in mechanical construction in that additional supporting members may be employed and an improved cathode connection may be used to insure positive contact when the tube is subjected to these environments.

Tubes recommended for use under severe environmental conditions are usually designed to withstand environmental tests equivalent to those specified in the applicable portions of MIL-E-5272C or MIL-STD-810B in which the specified accelerations are applied directly to the tubes. Certain other types of photomultipliers, particularly those utilizing stacked ceramic-to-metal brazed construction, have an environmental capability in excess of those specified in the above military specifications. These types find use in applications in which the tube must not only survive but operate reliably during periods of extreme shock and vibration such as those encountered during an actual rocket launch.

Unusual Atmospheric Environments

Photomultipliers may be operated in environments in which the pressure varies from that of a nearly perfect vacuum such as would be

encountered in space to several atmospheres as perhaps would be present in an underwater application. Although photomultipliers themselves may operate at very low pressures, precautions must be taken to reduce the possibility of breakdown between external tube and circuit elements in partial-pressure environments as predicted by Paschen's Law. The gas contributing to the partial pressure could be the result of outgassing of encapsulating and other materials used external to the photomultiplier.

High-pressure operation of photomultipliers depends primarily upon the physical size and strength of the materials employed in their construction. Although a two-inch-diameter tube employing stacked ceramic-to-metal brazed construction can easily withstand 4 or 5 atmospheres, other all-glass two-inch-diameter tubes with very thin entrance windows are limited to only slight additional loading above atmospheric pressure.

Helium Penetration. Because helium permeates through glass, the operation or storage of photomultipliers in environments where helium is present must be avoided. Tubes subjected to such an environment will exhibit a noise increase and possibly an increase in afterpulsing. Depending upon the degree of permeation, a point will soon be reached at which complete ionization takes place and makes the tube unusable. Continued operation will result in the deterioration of the photocathode response and lead to an inoperative tube.

PHOTOMULTIPLIER DATA

Sensitivity

Sensitivity provides an indication of the magnitude of the signal that may be expected for a given light input. Photocathode and anode sensitivities are stated in terms of luminous or radiant sensitivity.

Current amplification is stated in terms of the ratio of anode output current to photocathode current and is measured at specified values of electrode voltage. Typical photomultiplier current-amplification values range from 10^4 to 10^9 when the tubes are operated at the voltages recommended for the number of stages and dynode materials used.

Fig. 31 describes the anode sensitivity in amperes per lumen and the typical amplification characteristics of a photomultiplier as a function of the applied voltage. These curves

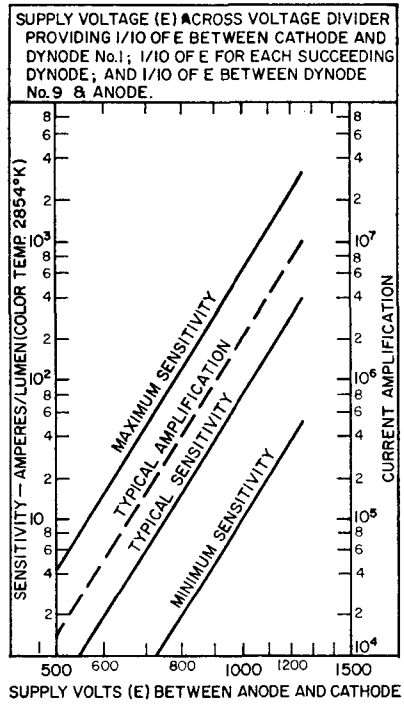

Fig. 31 — Typical anode sensitivity and amplification characteristics of a photomultiplier tube as a function of applied voltage.

illustrate the wide range of amplification of which a photomultiplier is capable, provided a well regulated voltage power supply is available. It is customary to present these sensitivity, amplification, and voltage data on logarithmic scales that cover the normal range of operation; the resultant curves are then closely approximated by straight lines. Curves of minimum and maximum sensitivity are shown, as well as those of the typical sensitivity and amplification.

Luminous sensitivity is defined as the output anode current divided by the luminous flux incident on the photocathode, measured at a specified electrode voltage; it is expressed in amperes per lumen, A/lm. Luminous sensitivity is most frequently stated in terms of a tungsten-filament light source in a lime-glass envelope operated at a color temperature of 2854°K. A typical luminous flux for test purposes is in the range of 10^{-8} to 10^{-5} lumen.

Cathode luminous sensitivity is the photocurrent emitted per lumen of incident light flux on the photocathode at constant electrode voltage, and is also expressed in terms of amperes per lumen, A/lm. In the measurement of cathode luminous sensitivity in a photomultiplier, a dc voltage of 100 to 250 volts is applied between the cathode and all other electrodes connected together as an anode. Light flux in the order of 10^{-2} to 10^{-4} lumen is then applied, and the measured photocurrent is divided by the specified light level to yield the required amperes per lumen.

It is customary in sensitivity measurements to subtract any dark current which may be present so that only the effect of the radiation is recorded.

Radiant sensitivity is the output anode current divided by the incident radiant power at a given wavelength, measured at a constant electrode voltage. **Cathode radiant sensitivity** is the amount of current leaving the photocathode divided by the incident radiant power at a given wavelength, usually the wavelength of peak response. Values at other wavelengths can be computed from the relative-spectral-response curve. Alhough radiant sensitivity may be measured directly with suitable *monochromatic* sources and radiation-measuring equipment, it is usually computed from the measured anode and cathode luminous-sensitivity values and expressed in terms of amperes per watt, A/W. This computation uses conversion factors and is dependent upon established typical spectral-response characteristics.

Some users prefer to use **integral radiant sensitivity** instead of luminous sensitivity because the latter expression, although very commonly used, does have an element of inappropriateness especially when used to express the sensitivity of devices which have sensitivity beyond the visible range of radiation.

Integral radiant sensitivity is the ratio of the anode or photocathode current to the total radiation in watts impinging on the photocathode from a tungsten test lamp operating at a color temperature of 2854°K. Because it is very difficult to calibrate a test lamp in total radiant watts, it is customary to use a luminous calibration and a conversion factor for the lamp of 20 lumens per watt.

Another sensitivity parameter often specified for tubes, especially those intended for scintillation detectors, is **blue sensitivity.** Because most scintillators produce radiation in the blue region of the spectrum,

tubes intended for these applications are processed for maximum sensitivity in this region. It has been found, during processing of such photomultipliers, that the maximum sensitivity for blue and for white light often does not occur at the same time. The anode blue sensitivity is measured with rated voltages applied to the electrodes and a source of blue light incident upon the cathode. The blue-light source has a spectral output as indicated in Fig. 32 and consists of the flux of tungsten radiation at a color temperature

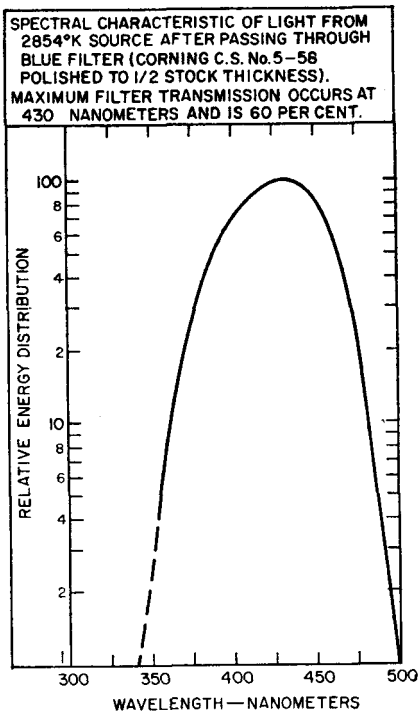

Fig. 32 — Spectral output of a blue light source used in measuring anode blue sensitivity.

of 2854°K which is transmitted through a blue filter. Sensitivities are termed "blue" but are expressed in terms of the light flux which is incident upon the filter. Incident light fluxes range between 10^{-5} and 10^{-7} lumen, depending upon the tube sensitivity, when the anode blue sensitivity is measured, and between 10^{-2} and 10^{-4} lumen when the cathode blue sensitivity is measured. Blue sensitivity is expressed in amperes per "blue" lumen.

A **spectral response** curve provides the most complete specification of the sensitivity of a photocathode. Fig. 33 shows a set of typical spectral-response characteristics. Spectral-response characteristics may be given in terms of absolute radiant sensitivity, relative sensitivity, or quantum efficiency as a function of wavelength. These quantities are discussed in detail in the following paragraphs.

The uppermost curve of Fig. 33, the relative-sensitivity curve, shows the per-cent relative sensitivity of the

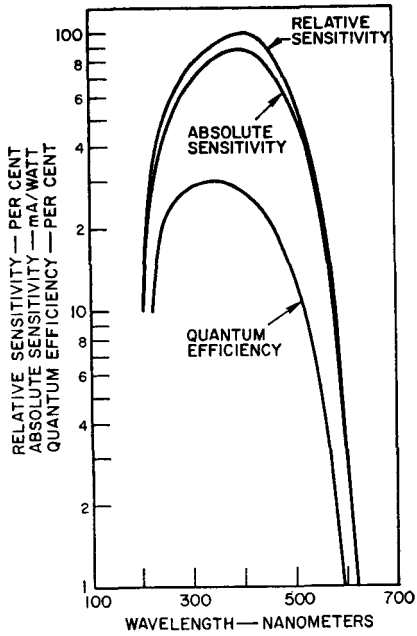

Fig. 33 — A set of typical spectral-response characteristics.

peak sensitivity at each wavelength over the useful spectral range of the device. The center curve provides the absolute radiant sensitivity in units of milliamperes per watt. The third curve shows the per-cent quantum efficiency at each wavelength.

The wavelength of peak response and the long-wavelength cutoff are primarily functions of the photocathode material. The short-wavelength cutoff is primarily a function of the window material. Each window material has its characteristic cutoff region that varies from about 300 nanometers for commonly used lime glass to 105 nanometers for lithium fluoride.

Cathode quantum efficiency may be defined as the average number of photoelectrons emitted per incident photon. The cathode quantum efficiency, QE, in per cent at any given wavelength can be calculated from the following formula:

$$QE = S \frac{1239.5}{\lambda} (100)$$

where S is the cathode radiant sensitivity at the wavelength λ in amperes per watt, and λ is the wavelength in nanometers. From this relation and the absolute (radiant) spectral-response characteristic it is possible to calculate the typical quantum efficiency at any wavelength within the spectral range of the photomultiplier under consideration.

The relative spectral response can also be used to calculate cathode quantum efficiency if the radiant sensitivity at the wavelength of peak response is known. This calculation is made by multiplying the peak radiant sensitivity by the percentage of the peak response (obtained from the relative-response curves) for the wavelength in question. The resultant product is the absolute (radiant) spectral sensitivity for the desired wavelength.

Dark Current

Current flows in the anode circuit of a photomultiplier even when the tube is operated in complete darkness. The dc component of this current is called the anode dark current, or simply the dark current. This current and its resulting noise component usually limit the lower level of photomultiplier light detection; as a result, the anode dark-current value is nearly always given as part of the data for any tube.

It is important to understand the variation of dark current in the photomultiplier as a function of various parameters so that the ultimate in low-light-level detection can be achieved. Although not all the mechanisms by which dark current is generated within a photomultiplier are understood, they can be categorized by origin into three types: ohmic leakage, emission of electrons from the cathode and other elements of the tube, and regenerative effects.

Interior **ohmic leakage,** the predominant source of dark current at low operating voltage that can be identified by its proportionality with applied voltage, results from the imperfect insulating properties of the glass stem, the supporting members, or the base, and is always present but usually negligible. Contamination consisting of dirt, water vapor, or grease on the outside of the tube may also contribute to ohmic leakage. A source of leakage inside the tube may be residual alkali metals used in the photomultiplier processing.

As the operating voltage of the photomultiplier increases to mid-range values, the dark current begins to follow the gain characteristic of

the tube. The source of this gain-proportional dark current is the dark or **thermionic emission** of electrons from the photocathode or the dynodes. Because each thermionically generated electron emitted from the photocathode is multiplied by the secondary-emission gain of the tube, the output is a pulse having a magnitude equal to the charge of one electron multiplied by the gain of the tube. This process, involving statistical variations, is discussed in detail in the section on **Statistical Fluctuation and Noise.** Because the emission of thermionic electrons is random in time, the output dark current consists of random unidirectional pulses. The time average of these pulses may be measured on a dc meter and is usually the main component of the dc dark current at normal operating voltages. The variable nature of the thermionic dark current limits the sensitivity of a tube at very low light levels. It is not possible to balance out the effect of this current in the same manner as the effect of a steady dc current resulting from ohmic leakage. It is usually advantageous to operate a photomultiplier in the range where the thermionic component is dominant because in this range the signal-to-noise ratio of the tube is maximum.

Regenerative effects occur in all photomultipliers at higher dynode voltages and cause the dark current to increase and become very erratic. At times the dark current may increase to the practical limitations of the tube and circuit. Permanent damage may be caused to the sensitized surfaces.

Regenerative effects may be triggered by the electrostatic potential of the walls surrounding the photocathode and dynode-structure region. As shown in Fig. 34, a positive

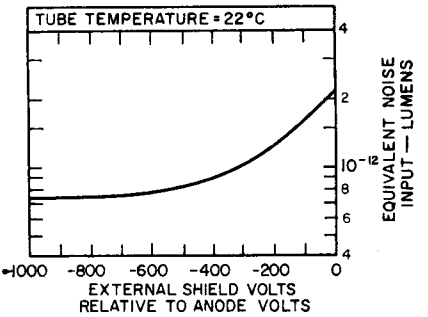

Fig. 34 — Effect of external-shield potential on the noise of a 1P21 photomultiplier. Note the desirability of maintaining a negative bulb potential.

potential with respect to the cathode on the envelope wall can cause noisy operation by contributing to the generation of minute ionic currents which flow through the glass and produce light at the cathode as a result of fluorescence within the glass. This noise need not arise from direct connection of the envelope wall to a positive potential; close proximity of the tube to such a potential will yield the same effect. In addition to the increased dark current and noise, the life of the photocathode is usually shortened when regenerative effects are present. To prevent this deterioration, the envelope wall should be maintained near photocathode potential by wrapping or painting it with a conductive material and connecting this material to cathode potential. The connection is usually made through a high impedance to reduce the shock hazard. Insulating materials must be selected to limit the leakage currents in the vicinity of the photocathode to less than 1×10^{-12} ampere.

Excess noise or dark current can also result from a number of other sources: fluorescent effects produced on the inner surfaces of the bulb during high-current operation, light generated within the tube at the

various dynodes and at the anode as a result of electrons striking these elements, field emission occurring at sharp points within the tube, ionic bombardment of the photocathode as the result of minute quantities of residual gases, and scintillations in the glass envelope of the tube caused by radioactive elements within glass (most glasses contain some radioactive K^{40}).

Photomultipliers with bialkali photocathodes, and to a lesser extent those with cesium antimony photocathodes, exhibit a temporary increase in dark current and noise by as much as three orders of magnitude when the tube is exposed momentarily to blue light or ultraviolet radiation from sources such as fluorescent room lighting, as shown in Fig. 35. This increase in dark current occurs even though voltage is not applied to the tube, and may persist for a period of from 6 to 24 hours after such irradiation.

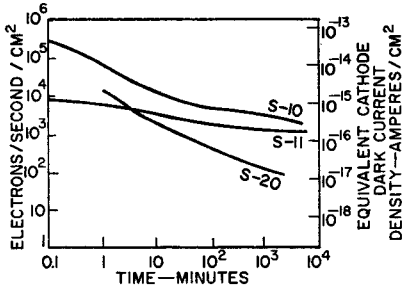

Fig. 35 — Variation of dark current following exposure of photocathode to cool white fluorescent-lamp radiation. The various photocathodes are identified by their spectral-response symbols.

Dark-Current Specification. Dark-current values are often specified at a particular value of anode sensitivity rather than at a fixed operating voltage. Specifications of dark current in this manner are more closely related to the actual application of the photomultiplier.

The best operating range for a given photomultiplier can usually be predicted from the quotient of the anode dark current and the luminous sensitivity at which the dark current is measured. This quotient is identified as the **Equivalent Anode Dark Current Input** (EADCI) in the **Technical Data** section of this Manual and in individual tube bulletins, and is the value of radiant flux incident on the photocathode required to produce an anode current equal to the dark current observed. The units used in specifying EADCI are either lumens or watts.

The curves in Fig. 36 show both typical anode dark current and equivalent anode dark current input (EADCI) as functions of luminous

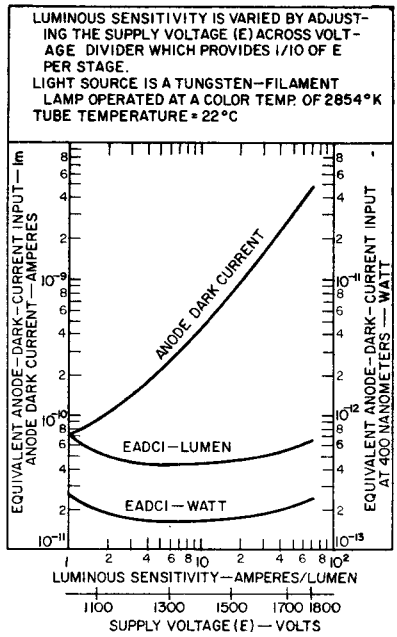

Fig. 36 — Typical and equivalent anode-dark-current input (EADCI) as a function of luminous sensitivity.

sensitivity. These curves can be used to predict the best operating range for a tube by considering the ratio of the dark current to the output sensitivity. The optimum operating range occurs in the region of the minimum on the EADCI curve, the region in which the signal-to-noise ratio is also near its maximum. The increase in the EADCI curve at higher values of sensitivity indicates the onset of a region of unstable and erratic operation. Many curves of this type also include a scale of anode-to-cathode supply voltage corresponding to the sensitivity scale.

Dark-Current Reduction. Dark current may be reduced by cooling the photomultiplier in a refrigerant, such as dry ice. This procedure is recommended in those applications in which maximum current amplification with minimum dark current is required. It should be noted, however, that at reduced temperature the resistance of the cathode increases and may reduce the maximum peak anode current.

If care is taken to avoid damage to the photomultiplier by operation with excessive current, the dark current can often be reduced by a process of operating the photomultiplier in the dark at or near the maximum operating voltage. This process, called **dark aging,** may require several hours to several days. After such a process of aging, it is recommended that a photomultiplier be operated for several minutes at the reduced voltage before measurements are attempted.

Equivalent Noise Input. Dark current is the average or dc value of discrete pulses occurring at random intervals. The fluctuations or noise associated with these pulses limit the measurement precision. Noise is evaluated in terms of a signal-to-noise-ratio measurement under specified operating conditions. If the type of modulation and bandwidth used in the measurement is known, an equivalent noise input, ENI, can be calculated from the signal-to-noise ratio. Equivalent noise input is defined as the value of incident luminous or radiant flux which, when modulated in a stated manner, produces an rms output current equal to the rms noise current within a specified bandwidth, usually 1 Hz.

To determine the ENI for any other bandwidth, it is necessary only to multiply the published ENI value by the square root of that bandwidth. The conditions under which a value of ENI is obtained are similar to those used to measure luminous sensitivity, except that the light incident upon the photocathode is modulated by a light chopper so that a square-wave signal with equal on and off periods is produced at the photomultiplier output.

It is of interest to consider what ENI may be expected for a photomultiplier if it is assumed that the only source of noise is the photocathode dark emission, i_t. If the photocathode sensitivity is given by S in amperes per lumen and the unmodulated light flux by F in lumens, the unmodulated output signal is equal to $SF\mu$, where μ is the gain of the multiplier. When the light is chopped in an equal on and off square wave with its peak amplitude the same as that of the unmodulated light flux, the rms signal output at the fundamental frequency (with a narrow-bandpass measuring device) is $SF\mu(2)^{1/2}/\pi$. The rms noise current from the dark emission in a band pass of Δf is given by the expression $\mu(2ei_t\Delta f)^{1/2}$, where e is the charge of an electron. This expression neglects the noise increase from dynode amplification statistics which

may increase this noise current by a few per cent. (See the section on **Statistical Fluctuation and Noise.**) In an evaluation of the expression for ENI, the signal must be equated to the dark noise, as follows:

$$\frac{SF\mu(2)^{1/2}}{\pi} = \mu(2ei_t\Delta f)^{1/2}$$

The value of ENI is then approximately the value of F for the condition of this equation:

$$ENI = F = \frac{\pi(ei_t\Delta f)^{1/2}}{S}$$

For $\Delta f = 1$, $i_t = 10^{-15}$ ampere (a reasonably low value of photocathode dark-emission current), and S = 100 microamperes per lumen, the ENI is equal to 4×10^{-13} lumen. This value is equivalent to a photocathode peak signal current of 4×10^{-17} ampere. Because this signal current is almost two orders of magnitude less than the photocathode dark-emission current, the noise in the signal current is negligible.

Because the dark emission is reduced as the temperature of the photocathode is reduced, ENI may be reduced by cooling the photomultiplier. Fig. 37 shows the variation of ENI for a 1P21 (opaque CsSb photocathode) over a wide range of temperature.

The **differential dark-noise spectrum** shown in Fig. 38 displays the number of pulses counted per unit of time as a function of their height. Such a spectrum indicates the numbers of single and multiple electron events originating at the photocathode. Submultiple electron emission results from electron emission at one of the dynode surfaces.

A differential dark-noise spectrum is obtained with a multichannel pulse-height analyzer. The calibration of the single-photoelectron pulse height is determined by illuminating the photocathode with a light level so low that there is a

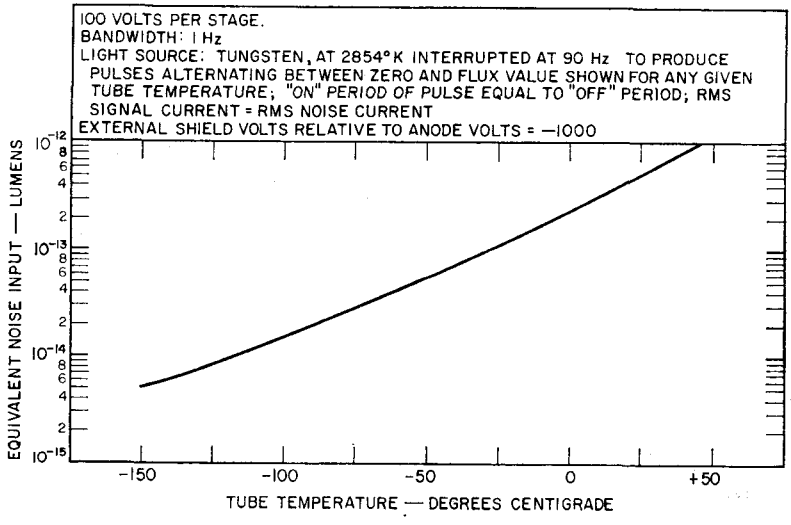

Fig. 37 — Equivalent noise input in lumens for a 1P21 photomultiplier as a function of temperature.

very low probability of coincident photoelectron emission. The dark-pulse distribution is then subtracted from the subsequent combination of dark pulses and single-photoelectron pulses, so that the remainder represents only that distribution resulting from single-photoelectron events. By adjusting the gain of the pulse-height analyzer, the single-electron photopeak can be placed in the desired channel to provide a normalized distribution.

The dark-pulse spectrum of Fig. 38 is characteristic of photomultipliers intended for use in scintillation counting and other low-light-level pulse applications. The dashed portion at the left of the curve is an extrapolation to show the location of the single photoelectron peak; the solid portion shows the actual differential dark-noise spectrum. The rapid change in slope of this curve in the pulse-height region of less than one-half photoelectron is assumed to be the result of electron emission from the first- and second-dynode surfaces.

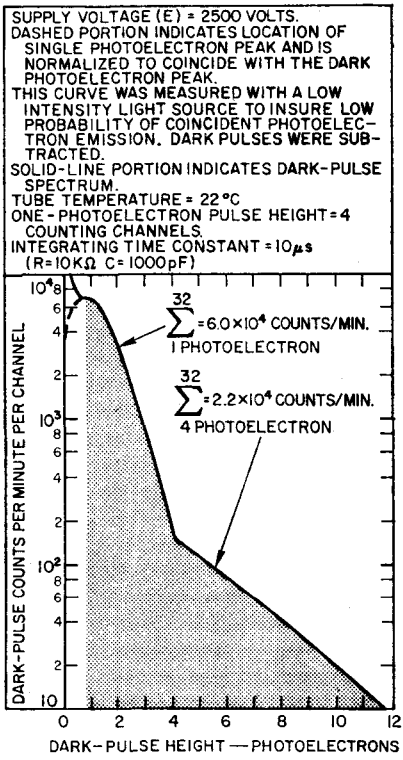

Fig. 38 — Typical dark-noise pulse spectrum.

The slope of the curve for the pulse-height region between 1 and 4 photoelectrons is as expected for single-electron emission, when the statistical nature of secondary-emission multiplication is considered. The number of pulses in this region may be reduced by cooling the photomultiplier.

The slope of the curve for the pulse-height region greater than 4 photoelectrons is presumed to be caused by multiple-electron-emission events. These multiple pulses are caused by processes such as ionic bombardment of the photocathode. Other mechanisms contributing to the noise spectrum include cosmic rays, field emission, and radioactive contaminants that produce scintillations within the glass envelope. Cooling has little effect upon reduction of the number of these multiple-electron pulses, but extended operation of the tube may improve performance. Operation of the tube may result in erosion of sharp points and reduce the possible contribution of field effects. In addition, improvement occurs because residual gases are absorbed within the tube, ion bombardment of the photocathode is reduced, and the resulting multiple secondary-electron emission is lessened.

For many applications it is useful to have a summation of the total number of dark pulses. In Fig. 38, for example, the sum of dark-pulse counts from one electron equivalent

height to 32 electron equivalent heights is 3×10^4 counts per minute. The value of 32 is chosen to be essentially equivalent to infinity. Another useful figure is the summation of pulses in the range from 4 to 32 equivalent electron heights. This sum for this particular distribution is 2.2×10^3 counts per minute and corresponds to the rate of multiple-electron events.

Pulse Counting

Pulse-Height Resolution. An important application of photomultipliers is in scintillation counting. (For a more detailed account of scintillation counting, see the section on **Photomultiplier Applications.**) In many scintillation-counting applications, a photomultiplier is coupled to a thallium-activated sodium iodide NaI(T1) crystal in which scintillations are produced by gamma rays resulting from nuclear disintegrations. Because the output of a photomultiplier is linear with light input and because the light energy of scintillations is directly proportional to the gamma-ray energy over a certain range, an electrical pulse is obtained which is a direct measure of the gamma-ray energy. Consequently, an important requirement of photomultipliers used in nuclear spectrometry is the ability to discriminate between pulses of various heights. The parameter indicating the ability of a tube to perform this discrimination is called pulse-height resolution.

A typical pulse-height distribution curve obtained with a Cs^{137} source and an NaI(T1) crystal is shown in Fig. 39. The main peak of the curves at the right is associated with monoenergetic gamma rays which lose their entire energy by photoelectric conversion in the crystal. Pulse-height resolution is defined as the

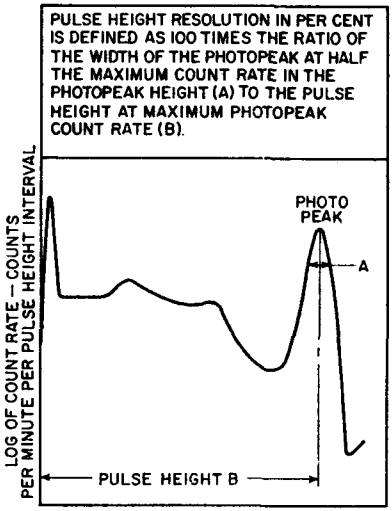

Fig. 39 — Typical pulse-height distribution curve.

width of the photopeak at half the maximum count rate divided by the pulse height at maximum count rate. Consequently, the lower the pulse-height resolution, the greater the ability of the photomultiplier to discriminate between pulses of nearly equal height.

The pulse-height resolution parameter is often measured by using the 662-keV photon from an isotope of cesium, Cs^{137}, and a cylindrical thallium-activated sodium-iodide scintillator. The Cs^{137} source is placed in direct contact with the metal end of the scintillator package and the faceplate end of the crystal is coupled to the tube by means of an optical coupling fluid. The load across which the pulse height is measured may consist of a 100,000-ohm resistor and a capacitance of 100 picofarads in parallel. This combination provides a 10-microsecond time constant.

Peak-to-Valley Ratio. In many low-energy scintillation-counting applications, noise as well as resolution

becomes important. A parameter which provides an indication of photomultiplier usefulness in resolving low-energy X-rays is the pulse-height spectrum obtained for an Fe^{55} radioactive isotope and shown in Fig. 40. This parameter is measured by using an NaI(Tl) scintillator with a thin beryllium window and an Fe^{55} source. The decay of this isotope of iron results in a 5.9-keV X-ray. From the resulting spectrum a peak-to-valley ratio and a pulse-height resolution can be calculated.

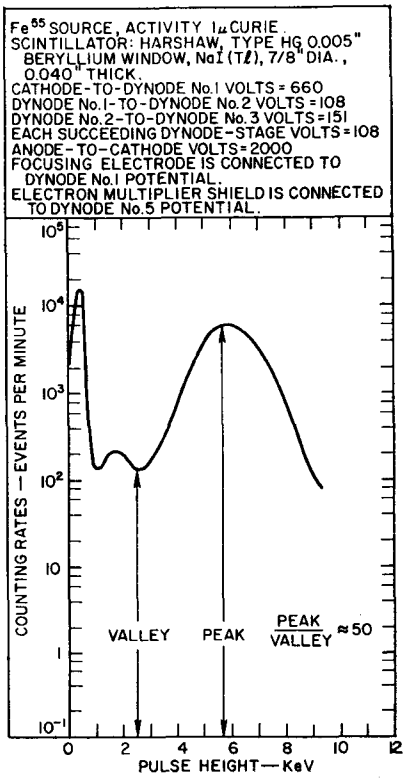

Fig. 40 — Typical pulse-height spectrum obtained for an Fe^{55} radioactive isotope.

The peak-to-valley ratio of the measured spectrum is a measure of the extent to which tube noise obscures the observation of low-energy gamma rays. However, at the larger values of peak-to-valley ratio (30 to 50), the properties of the crystal become dominant.

Afterpulsing. Afterpulses, which may be observed when photomultipliers are used to detect very short light flashes as in scintillation counting or in detecting short laser pulses, are identified as minor secondary pulses that follow a main anode-current pulse. There are two general types of afterpulses; both are characterized by their time of occurrence in relation to the main pulse. The first type results from light feedback from the area of the anode, or possibly certain dynodes, to the photocathode; the intensity of the light is proportional to the tube currents. When this light feedback reaches the cathode, the afterpulse is produced. Afterpulses of this type, characterized by a delay in the order of 40 to 50 nanoseconds, may be a problem in many older photomultipliers having open dynode structures. The time delay experienced with this type of afterpulse is equal to the total transit time of the signal through the photomultiplier plus the transit time of the light that is fed back.

The second type of afterpulse has been shown to be the result of ionization of gas in the region between the cathode and first dynode. The time of occurrence of the afterpulse depends upon the type of residual gas involved and the mass of the gas ion, but usually ranges from 200 nanoseconds to well over 1 microsecond after the main pulse. When the ion strikes the photocathode, several secondary electrons may be emitted; thus, the resulting afterpulse has an amplitude equal to sev-

eral electron pulse-height equivalents. These pulses appear to be identical to the larger dark-current pulses, and it is suspected that many of the dark-current pulses are the result of photocathode bombardment by gas ions.

Several gases, including N_2+ and H_2+, are known to produce afterpulses. Each gas produces its own characteristic delay following the main pulse. The most troublesome, perhaps, is the afterpulse caused by the H_2+ ion; this afterpulse occurs approximately 300 nanoseconds after the main pulse. One source of hydrogen in the tube is water vapor absorbed by the multiplier section before it is sealed to the exhaust system. Other gases which may cause afterpulsing may be present as a result of outgassing of the photomultiplier parts during processing or operation. Present photomultiplier processing techniques are designed to eliminate or at least to minimize the problem of afterpulsing.

Time Response

The commonly used methods of specifying time response involve frequency-domain and time-domain parameters. Frequency response is usually characterized in terms of the frequency at which the ac component of the output current decreases to 3 dB below the low-frequency output level, and may be measured with an electro-optic modulator and a variable-frequency driving oscillator. Time-response measurements are made with small-spark sources,[2] light-emitting diodes, or mode-locked lasers[3] that approximate delta-function light sources. In most measurements the entire photocathode is illuminated.

The frequency response of a photomultiplier is related to the anode-pulse rise time, a parameter usually provided for each photomultiplier type. The anode-pulse rise time of a tube, illustrated in Fig. 41, is affected primarily by the mechani-

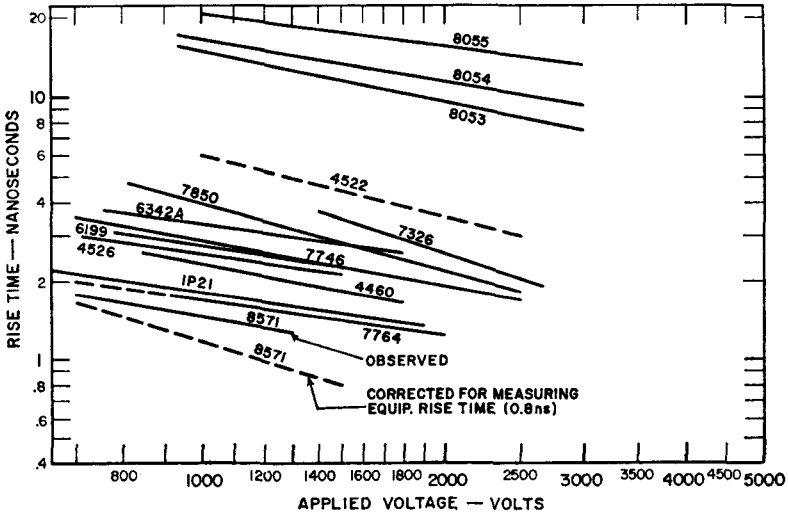

Fig. 41 — Anode-pulse rise times as a function of anode-to-cathode applied voltage for a number of photomultipliers.

cal configuration and the operating values of a device and is specified as the time for the current to increase from 10 to 90 per cent of maximum anode-pulse height when the tube is illuminated with a delta-function light source.

Frequency response is also limited by the **transit-time spread.** This spread is the time interval between the half-amplitude points of the output pulse at the anode terminal, as shown in Fig. 42. Transit-time spread is seldom measured directly because it is difficult to determine whether the fall time of the pulse results from the fall time of the light source or the tube. Figs. 41 and 42 indicate that transit and rise times are reduced as over-all applied voltage is increased. Tubes utilizing focus structures of either the linear or the circular-cage type exhibit better time-resolution characteristics than tubes of the venetian-blind type; in many high-speed applications this difference is of major importance.

STABILITY

The operating stability of a photomultiplier depends on the magnitude of the average anode current; when stability is of prime importance, the use of average anode currents of 1 microampere or less is recommended. Additional considerations affecting stability are discussed in the subsequent paragraphs.

Fatigue

Tube fatigue or loss of anode sensitivity is a function of output-current level, dynode materials, and previous operating history. The amount of average current that a given photomultiplier can withstand varies widely, even among tubes of the same type; consequently, only typical patterns of fatigue may be cited.

The sensitivity changes that are a direct function of large currents imposed for great lengths of time are thought to be the result of erosion of the cesium from the dynode surfaces

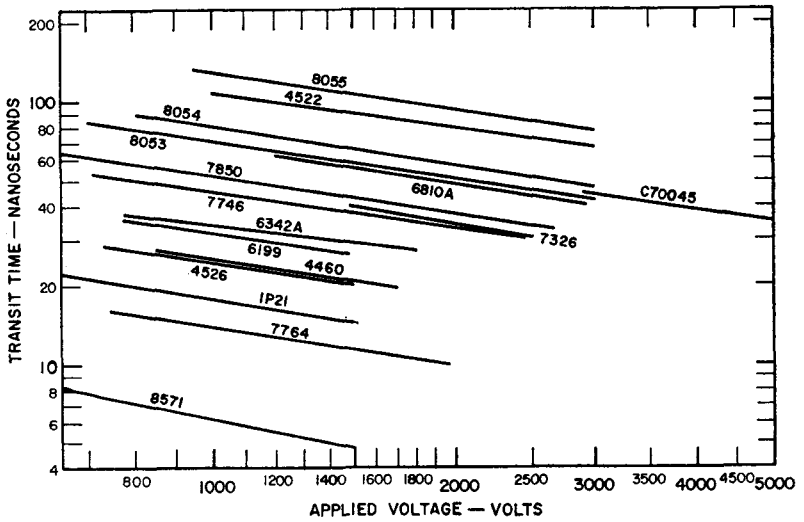

Fig. 42 — Transit-time spreads as a function of supply voltage for a number of photomultipliers.

during periods of heavy electron bombardment, and the subsequent deposition of the cesium on other areas within the photomultiplier. Sensitivity losses of this type, illustrated in Fig. 43 for a 1P21 operated at an output current of 100 microamperes, may be reversed during periods of non-operation when the cesium may again return to the dynode surfaces. This process of return

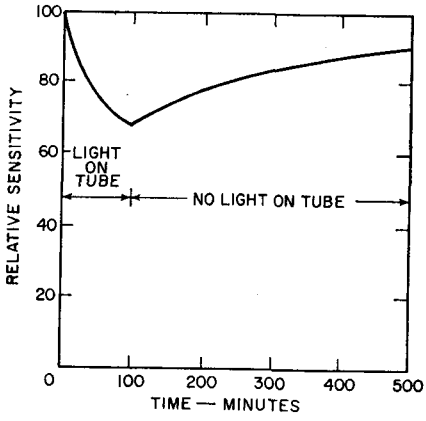

Fig. 43 — Short-time fatigue and recovery characteristics of a typical 1P21 operating at 11 volts per stage and with a light source adjusted to give 100 microamperes initial anode current. At the end of 100 minutes the light is turned off and the tube allowed to recover sensitivity. Tubes recover approximately as shown, whether the voltage is on or off.

may be accelerated by heating the photomultiplier during periods of non-operation to a temperature within the maximum temperature rating of the tube; heating above the maximum rating may cause a permanent loss of sensitivity.

Sensitivity losses for a given operating current normally occur rather rapidly during initial operation and at a much slower rate after the tube has been in use for some time. Fig. 44 shows this type of behavior for a

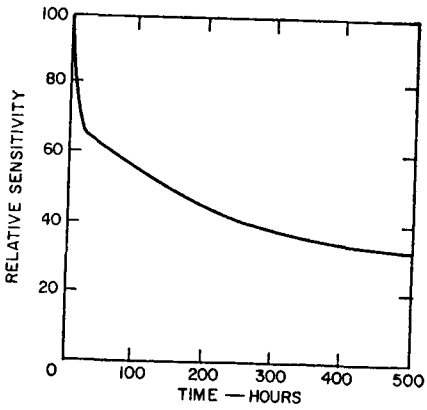

Fig. 44 — Typical sensitivity loss for a 1P21 operating at 100 volts per stage for a period of 500 hours. Initial anode current is 100 microamperes and is readjusted to this operating value at 48, 168, and 360 hours.

1P21 having CsSb dynodes, operating at an output current of 100 microamperes. Tubes operated at lower current levels, of the order of 10 microamperes or less, experience less fatigue than those operated at higher currents, and, in fact, may actually recover from high-current operation during periods of low-current operation.

Fatigue rates are also affected by the type of dynode materials used in a tube. Copper beryllium or silver magnesium dynodes are generally more stable at high operating currents than the cesium antimony types. The sensitivity for tubes utilizing these dynodes very often increases during initial hours of operation, after which a very gradual decrease takes place, as illustrated in Fig. 45.

Photocathode Fatigue

A photomultiplier with a multialkali photocathode (S-20 spectral response) tends to decrease in sensi-

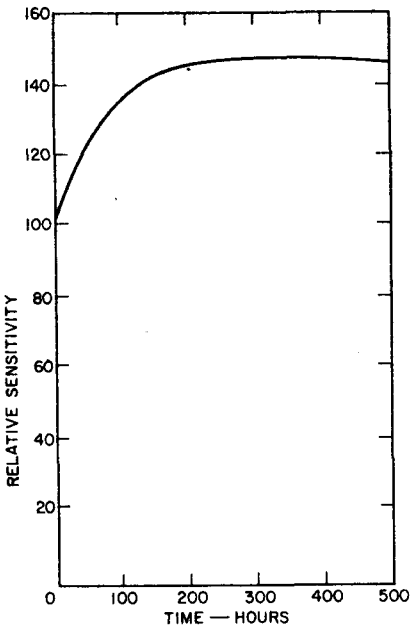

Fig. 45 — Typical sensitivity variation on life for a photomultiplier having silver-magnesium dynodes. Initial anode current was 2 milliamperes and was re-adjusted to this operating value at 48, 168, and 360 hours.

tivity upon extended exposure to high ambient room lighting. The mechanism by which this sensitivity loss occurs is not clearly understood. The decreased cathode sensitivity occurs primarily in the red portion of the spectrum and is usually permanent. It is interesting to note that photocathodes of the extended red multi-alkali (ERMA) type apparently do not exhibit this loss.

The Ag-0-Cs photocathode (S–1 spectral response) also suffers a decrease in sensitivity, particularly during operation, when exposed to high radiant-energy levels normally not harmful to other types of photocathode materials. The decreased sensitivity occurs primarily in the infrared portion of the spectrum. Sensitivity may decrease quite rapidly upon application of light and voltage during the first few minutes of operation. With a few hours of continued operation, the sensitivity usually increases until it has regained its initial value. If the source of the high radiant energy is removed from the tube, the sensitivity also tends to return to its initial value.

"Hysteresis"

Many photomultipliers exhibit a temporary instability in anode current and change in anode sensitivity for several seconds after voltage and light are applied. This instability, sometimes called hysteresis because of cyclic behavior, may be caused by electrons striking and charging the dynode support spacers and thus slightly changing the electron optics within the tube. Sensitivity may overshoot or undershoot a few per cent before reaching a stable value. The time to reach a stable value is related to the resistance of the insulator, its surface capacitance, and the local photomultiplier current. This instability may be a problem in applications such as photometry where a photomultiplier is used in a constant-anode-current mode by varying the photomultiplier voltage as the light input changes.

Hysteresis has been eliminated in many tubes by coating the dynode spacers with a conductive material and maintaining them at cathode potential. Tubes treated by this method assume final sensitivity values almost immediately upon application of light and voltage.

Counting Stability

In scintillation counting it is particularly important that the photomultiplier have very good stability.

There are two types of gain stability tests which have been used to evaluate photomultipliers for this application: (1) a test of long-term drift in pulse-height amplitude measured at a constant counting rate; and (2) a measure of short-term pulse-height amplitude shift with change in counting rate.

In the **time stability test,** a pulse-height analyzer, a Cs^{137} source, and a NaI(T1) crystal are employed to measure the pulse height. The Cs^{137} source is located along the major axis of the tube and crystal so that a count-rate of 1000 counts per second is obtained. The entire system is allowed to warm up under operating conditions for a period of one-half to one hour before readings are recorded. Following this period of stabilization, the pulse height is recorded at one-hour intervals for a period of 16 hours. The drift rate in per cent is then calculated as the mean gain deviation (MGD) of the series of pulse-height measurements, as follows:

$$MGD = \frac{\sum_{i=1}^{i=n} |p - p_i|}{n} \cdot \frac{100}{p}$$

where p is the mean pulse height, p_i is the pulse height at the i^{th} reading, and n is the total number of readings. Typical maximum mean-gain-deviation values for photomultipliers with high-stability CuBe dynodes are usually less than 1 per cent when measured under the conditions specified above. Gain stability becomes particularly important when photopeaks produced by nuclear disintegrations of nearly equal energy are being differentiated.

In the **count-rate stability test,** the photomultiplier is first operated at 10,000 counts per second. The photopeak counting rate is then decreased to 1000 counts per second by increasing the source-to-crystal distance. The photopeak position is measured and compared with the last measurement made at a counting rate of 10,000 per second. The count-rate stability is expressed as the percentage gain shift for the count-rate change. It should be noted that count-rate stability is related to the hysteresis effect discussed above. Photomultipliers designed for counting stability may be expected to have a value of no greater than 1 per cent gain shift as measured by this count-rate stability test.

Life Expectancy

The life expectancy of a photomultiplier, although related to fatigue, is very difficult to predict. Most photomultipliers will function satisfactorily through several thousand hours of conservative operation and proportionally less as the severity of operation increases. Although photomultipliers do not have elements which "burn out" as in the case of a filament in a vacuum tube, photomultiplier dynodes do lose sensitivity with operation; however, as pointed out earlier, this loss occurs at an extremely low rate and even tends to recover during conservative operation.

Factors which are known to affect life adversely are high-current operation, excessive-voltage operation, high photocathode illumination, and high temperature.

Operation of photomultipliers in regions of intense nuclear radiation or X-rays may result in an increase in noise and dark current as a result of fluorescence and scintillation within the glass portions of the tubes.

Continued exposure may cause darkening of the glass and a resultant reduction in transmission capability. Photomultipliers having glass envelopes should not be operated in helium environments because helium can permeate the tube envelope and lead to eventual tube destruction.

Extremely high illumination focused onto a spot on the photocathode actually destroys a portion of the photocathode. It is usually better to defocus such a light source and utilize a larger area of the photocathode.

Loss of photocathode sensitivity may sometimes result from the proximity of a high-potential gradient in the region of the photocathode. Such a gradient may result from applications in which the photomultiplier is operated with the anode near ground potential. Metal fixtures, clamps, or shields at ground potential may provide such a gradient through the glass near the photocathode either by proximity or direct contact. The result may be increased noise output and a deterioration of the photocathode through an electrolysis process through the glass. The destructive process may take a few hours or several hundred hours depending upon the material in contact with the envelope and the amount of potential difference. The deterioration process is greatly accelerated as the temperature is increased above normal ambients.

LINEARITY

The anode currents produced by photomultipliers are proportional to the level of incident radiation over a wide range of values. A linearity plot over a wide range of light level is shown in Fig. 46 for a type 931A. The limit of linearity occurs when space charge begins to form. Space-charge-limiting effects usually occur in the space between the last two dynodes. The voltage gradient between anode and last dynode is usually much higher than between dynodes and, therefore, results in a limitation at the previous stage, even though the current is less. The maximum output current, at the onset of space charge, is proportional to the 3/2 power of the voltage gradient in the critical dynode region. By use of an unbalanced dynode-voltage distribution increasing the interstage voltages near the output end of the multiplier, it is possible to increase the linear range of output current.

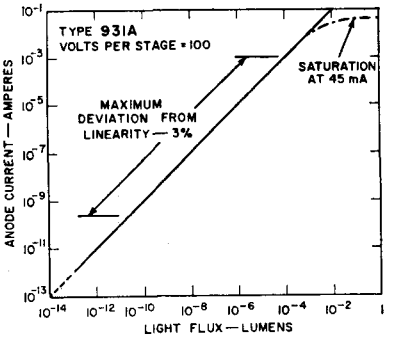

Fig. 46 — Range of anode-current linearity as a function of light flux for a 931A photomultiplier.

Some photomultipliers used in applications requiring high output pulse current use an accelerating grid between the last dynode and the anode to reduce the effects of space-charge limiting. The potential of such a grid is usually between that of the last and the next-to-last dynode and is adjusted by observing and maximizing the value of the anode output current.

Another factor that may limit anode-output-current linearity is cathode resistivity; cathode resistivity is a problem only in tubes with semitransparent photocathodes, particularly of the CsSb or bialkali type.

Individual tube bulletins and data listed in the **Technical Data** section of this manual give values of the peak linear and the peak saturated pulse currents. The limits of linear operation are determined, of course, by the particular geometry of the output stages and by the applied voltage.

Peak linear and saturation currents are measured by both dc and pulsed methods. One common method makes use of a cathode-ray tube with a P15 or P16 phosphor. The grid is double-pulsed with pulses of unequal amplitudes but fixed amplitude ratio. As the amplitude of the two pulses is increased, a point is observed at which the amplitude of the larger of the anode pulses does not increase in the same proportion as the smaller pulse. At this point the tube is assumed to become nonlinear. The current value at this point is then measured by means of an oscilloscope and load resistor. The maximum saturation current is found when a further increase in radiation level yields no further increase in output.

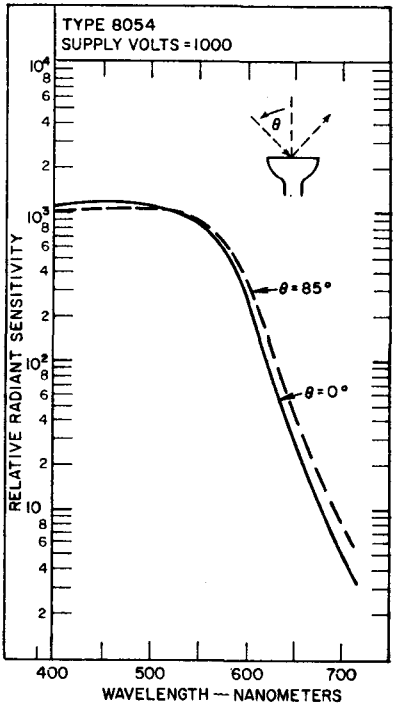

Fig. 47 — Spectral-response characteristics for a CsSb transmission-type photocathode for two different incident angles of radiation. The increased red response for the large angle of incidence may be explained in part by the increase in absorption caused by the longer path.

USE OF REFLECTED LIGHT AT THE PHOTOCATHODE

Because, in general, photocathodes absorb less red light than blue, the spectral response of the photocathode is somewhat sensitive to the angle of incidence of light on the photocathode. There is an increase in red sensitivity at larger angles of incidence, as shown in Fig. 47. It is possible to take advantage of this characteristic of photocathodes to enhance the photoemission significantly.

If a prism is optically coupled to the faceplate of a transparent photocathode, the angle of the incident radiation may become such that total internal reflection occurs at both the photocathode-to-vacuum interface and the glass-to-air interface. Several passes of the light through the photocathode become possible and thus increase the probability of producing photoemission. For total internal reflection to occur, the minimum angle at which light may impinge upon the faceplate is given by arcsine (1/n), where n is the refractive index of the photomultiplier window material.

The greatest enhancement produced by the total internal-reflection method occurs in the red region of

the photomultiplier spectral response; gains greater than 5 have been achieved at 700 nanometers in tubes having an S–20 spectral response.

OUTPUT-CURRENT CONTROL AND SPATIAL UNIFORMITY

Many photomultipliers are equipped with a focusing electrode, or grid, between the photocathode and the first dynode to provide optimum collection of the photoelectrons emitted from the photocathode. The focusing-grid voltage is usually set at the point at which maximum anode output current is obtained. In some applications, spatial uniformity, i.e., the variation of anode current with position of photocathode illumination, may be more important than maximizing output current. In such cases, however, the final adjustment of the focusing-grid potential should not differ significantly from the adjustment that provides optimized collection efficiency. Fig. 48 shows a typical focusing-electrode characteristic.

Spatial uniformity is determined by photocathode uniformity and by the uniformity of collection efficiency, i.e., the proportion of the emitted photoelectrons which strike a useful area on the first dynode.

Photomultipliers with venetian-blind structures usually exhibit the best spatial uniformity because they have a large aperture area, and thus a relatively large first-dynode area. Modern high-speed tubes with focused structures designed specifically for scintillation-counting applications also provide excellent spatial uniformity; the collection efficiency in these tubes approaches unity.

Cathode uniformity is determined by the uniformity of the deposition of the photocathode material. In general, large tubes having relatively large distances between the activating elements and the photocathode exhibit the best cathode uniformity. In these tubes, the activating elements, of which there may be several, approach point sources.

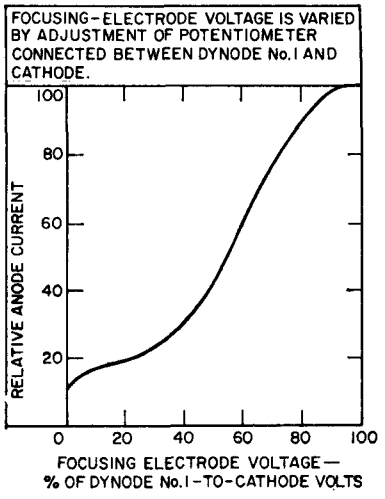

Fig. 48 — A typical focusing-electrode characteristic.

REFERENCES

1. M. Lontie-Bailliez and A. Messen, "L'Influence de la Temperature sur les Photomultiplicateurs," *Annales de la Societe Scientifique de Bruxelles, Vol. 73,* Series 1, p. 390 (1959)
2. A. Kerns, A. Kirsten, and C. Cox, "Generator of Nanosecond Light Pulses for Phototube Testing," *Rev. Sci. Instr., Vol. 30,* No. 1, p. 31 (1959)
3. A. J. DeMaria, W. H. Glenn, Jr., M. J. Brienza, and M. E. Mack, "Picosecond Laser Pulses," *Proc. IEEE, Vol. 57,* No. 1, p. 2 (1969)

Statistical Fluctuation and Noise

IN this section, some of the sources of noise and output fluctuations in photomultipliers are examined. These sources may be roughly divided into two classes: (1) those resulting from the processes by which the photomultiplier operates, and (2) those resulting from the way in which a tube is designed and manufactured and the conditions under which it is operated. The first class is more fundamental because it comprises the statistical processes of photoelectric emission and electron multiplication through secondary emission. Most of the discussion of class 1 sources deals with these processes and their effect on photomultiplier output. Class 2 sources include thermionic emission from the photocathode, spurious gas ionization within the tube, light feedback from the output stages to the photocathode, and random emission caused by the natural radioactivity of the various materials within the tube.

A photomultiplier is so sensitive a radiation detector that it can operate at the lower limit of detectability where output pulses are initiated by single photoelectrons from the photocathode. A count of the number of output pulses in a given time interval provides a measure of the rate at which photons strike the photocathode. This mode of operation is called the photon-counting mode; it is at this lower limit of photomultiplier operation that noise sources become most important. Therefore, most of the discussion in this section centers upon the effect of the noise sources on tube output in this mode.

PHOTON NOISE

If the photon flux impinging upon the photocathode originates from a thermal broad-band source, the photons can be assumed to be emitted at random time intervals. Under such conditions, the probability that n photons will strike the photocathode in a time interval τ is given by a Poisson distribution, as follows:

$$P(n, \tau) = \frac{(I_p\tau)^n}{n!} \exp(-I_p\tau) \quad (4)$$

where I_p is the average photon-arrival rate. The average value for n and the variance in n, σ_p^2, can be obtained directly from $P(n, \tau)$:

$$n = I_p\tau \quad (5)$$

$$\sigma_p^2 = I_p\tau = \bar{n} \quad (6)$$

The signal-to-noise ratio $\bar{n}/\sigma_p$ is given by

$$SNR = (I_p\tau)^{\frac{1}{2}} \quad (7)$$

Thus the signal-to-noise ratio of the photon flux increases as $\sqrt{I_p\tau}$.

There are a few cases in which the fluctuation in the photon flux has an additional term.[1] In broadband thermal sources, however, Eq. (6) yields the proper expression for the noise in the input photon flux.

NOISE CONTRIBUTIONS FROM THE PHOTOCATHODE

The physics of photoemission and photocathodes is discussed in the section on **Photoemission and Secondary Emission.** In the following discussion it is assumed that the time between the absorption of a photon and the subsequent emission of an electron, when emission occurs, is short (about 10^{-12} second). In addition, it is assumed that all the statistical processes of absorption, electron transport within the photocathode, and photoemission can be described and characterized by one number, the quantum efficiency η. For a given photocathode, η is a function of the photon wavelength, as explained in the section on **Photoemission and Secondary Emission.**

A simple model of photoemission will aid in understanding the noise contributions of the photocathode. For each photon that strikes the photocathode, an electron is emitted with probability η. Optical-reflection effects at the various cathode interfaces are accounted for in the value of η. The chance that no electron is emitted is $1-\eta$.

The statistics for this process can be found through the use of the generating function $Q_{P.C.}(s)$ derived in Appendix A at the end of this section. In the simplified model of the photocathode this function is given by

$$Q_{P.C.}(s) = (1-\eta) + s\eta \qquad (8)$$

From the expressions developed in Appendix A for the average and variance, the average output $\bar{n}$ and the variance σ^2 are given by

$$\bar{n} = \eta \qquad (9)$$

$$\sigma^2 = \eta\,(1-\eta) \qquad (10)$$

The discussion of these expressions is best understood by imagining a steady stream of photons impinging upon the photocathode. The photons are equally spaced in time and arrive at a rate of I_p photons per second. In an interval τ (where τ is much larger than $1/I_p$), the number of photons N striking the photocathode is equal to $I_p\tau$. Because by hypothesis I_p is constant, the number N does not fluctuate. In a time τ, the average number of photoelectrons n emitted from the photocathode is equal to ηN. The fluctuations in photoelectron number can be computed by use of Eq. (84) in Appendix A for the total variance for two statistical processes in series. Because the photon flux does not fluctuate, the total variance in the photoelectron number is given by

$$\sigma^2_{p.e.} = N\,(1-\eta)\,\eta \qquad (11)$$

Eq. (11) can be derived from Eq. (84) in Appendix A with the following substitutions:
$\bar{n}_A = N$, $\bar{n}_B = \eta$, $\sigma_A{}^2 = 0$, and $\sigma_B{}^2 = \eta(1-\eta)$. The signal-to-noise ratio of the photon flux is infinite because it does not fluctuate; however, the photoelection number has a signal-to-noise ratio given by

$$SNR_{p.e.} = \left[\frac{\eta N}{(1-\eta)}\right]^{\frac{1}{2}} \qquad (12)$$

Thus, for quantum efficiencies less than unity, the statistics of the photocathode result in a finite signal-to-

noise ratio for the photoelectron number. As shown below, this statement is valid even when the input photon beam fluctuates.

Fig. 49 shows a curve of the signal-to-noise ratio of the photoelectron number produced by the hypothetical noiseless photon flux. When $\eta = 1$, the photocathode is a perfect converter and no noise is impressed on the photoelectron number. When η is less than 1, the signal-to-noise ratio decreases with decreasing η until, for values much smaller than 1, the signal-to-noise ratio becomes proportional to the square root of η.

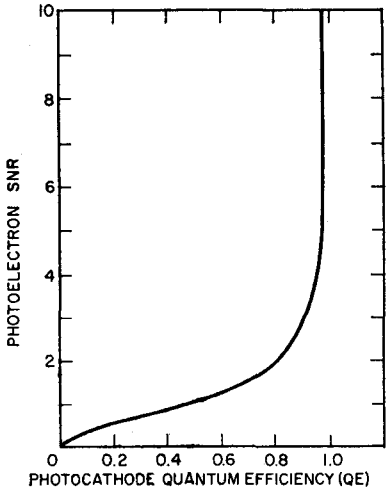

Fig. 49 — The photoelectron signal-to-noise ratio resulting from a noiseless photon flux impinging upon the photocathode.

In practice, the signal-to-noise ratio of the input photon flux is never infinite; the flux always contains some noise. In most sources, the signal-to-noise ratio of the photon flux is given by Eq. (7) and the variance of the photon beam is given by

$$\sigma^p = \bar{n}_p \tag{13}$$

and

$$\mathrm{SNR}_p = [\bar{n}_p]^{\frac{1}{2}} \tag{14}$$

where $\bar{n}_p$ is the average number of photons arriving in a time interval τ. The average photoelectron number and its variance are calculated from Eqs. (81) and (84), respectively, in Appendix A. The average number of photoelectrons and the variance in the photoelectron number are stated, respectively, as

$$\bar{n}_{p.e.} = \eta\, \bar{n}_p \tag{15}$$

and $$\sigma^2_{p.e.} = \bar{n}_p\, \eta\, (1-\eta) + \eta^2\, \bar{n}_p$$

or

$$\sigma^2_{p.e.} = \eta\, \bar{n}_p \tag{16}$$

It should be noted that the statistical conversion process within the photocathode has not altered the functional form of the variance; it is still proportional to the average number of particles. The photoelectrons appear to emanate from a random source of electrons with average value $\eta\bar{n}_p$. It is as though the average photon number were reduced by a factor η in the conversion process, a result that depends on the variance of the photon flux being equal to $\bar{n}_p$.

The photoelectron signal-to-noise ratio is

$$\mathrm{SNR}_{p.e.} = [\eta\, \bar{n}_p]^{\frac{1}{2}} \tag{17}$$

A quantum efficiency of 40 per cent reduces the signal-to-noise ratio of the photoelectron flux to about 63 per cent of that of the photon flux.

It is important to realize that the degradation in signal-to-noise ratio as a result of η being less than unity is irreversible in that no amount of noise-free amplification can improve the photoelectron signal-to-noise ratio.

In some applications, multiphoton pulses form the input signal. In these applications, integral numbers of photoelectrons are emitted from the photocathode within a time that is short with respect to the resolution capabilities of the photomultiplier as a result of a multiphoton input pulse. Examples of this type of input can be found in radioactive tracer scintillations, such as those observed in tritium and carbon spectroscopy.

If, with η equal to 1, the input signal consists of a steady train of photon pulses widely spaced in time, each pulse consisting of m photons, a steady train of photoelectron pulses would result, each consisting of m electrons. For values of η less than 1, the number of electrons in each pulse, r, can vary from 0 to m ($0 \leq r \leq m$). The probability that r electrons are emitted is obtained through the use of the multiple-input-particle generation function described by Eq. (86) in Appendix A. For m-photon input pulses, the generating function $Q_m(s)$ is given by $[Q(s)]^m$, where Q(s) is the single-particle generating function. Thus, the function $Q_m(s)$ is given by

$$Q_m(s) = [(1-\eta) + \eta s]^m \qquad (18)$$

The probability that r photoelectrons will be emitted is given by

$$P_r(\eta) = \frac{1}{(r)!} \frac{\partial^r Q_m(s)}{\partial s^r}\bigg|_{s=0} \qquad (19)$$

or

$$P_r(\eta) = \eta^r (1-\eta)^{m-r} \left[\frac{m!}{r!\,(m-r)!}\right] \qquad (20)$$

Eq. (20) is just the coefficient of s^r in the expression for $Q_m(s)$. $P_r(\eta)$ is composed of the chance of r successful photoemissions (η^r), the chance of (m−r) failures to photoemit $[(1-\eta)^{m-r}]$, and the binomial coefficient $\left[\frac{m!}{r!\,(m-r)!}\right]$ which describes the number of ways such an output can occur among the m-photon inputs.

Figs. 50 and 51 show the probability distribution for photoemission from the photocathode for a train of 4-photon input pulses and for two different values of η. The spectrum in Fig. 50 is computed with

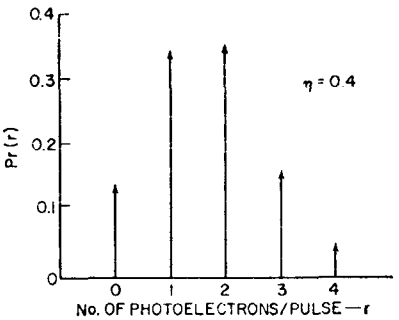

Fig. 50 — Photoelectron output pulse spectra resulting from a flux of 4-photon input pulses computed with $\eta = 0.4$.

$\eta = 0.4$ and that of Fig. 51 with $\eta = 0.01$. The difference is striking. With $\eta = 0.4$, there is no photoemission only 13 per cent of the time; most of the photoemission is divided between 1- and (2-, 3-, or 4-) photoelectron pulses in the ratio of 13 to 20. In sharp contrast, when $\eta = 0.01$, photoemission does not occur 96 per cent of the time. Of the times when photoelectrons are emitted, single-electron pulses occur 70 times more often than any others; 3- and 4-photoelectron pulses almost never occur. It should be clear that in multiphoton-pulse spectroscopy it is important that η be as high as possible.

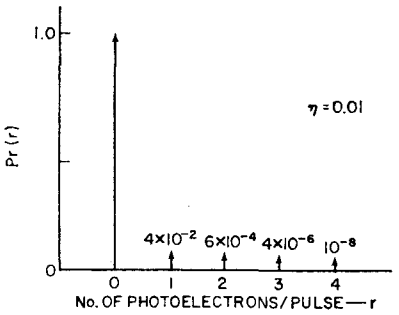

Fig. 51 — Photoelectron output pulse resulting from a flux of 4-photon input pulses computed with $\eta = 0.01$.

As in the case of a single-photon pulse train, the average photoelectron number and the variance in that number can be found from $Q_m(s)$ by use of Eqs. (87) and (88) of Appendix A. If α is the average rate of randomly emitted m-photon pulses, then the average number of photoelectrons emitted in a time τ (where τ is much greater than $1/\alpha$) is given by

$$\overline{n}_{p.e.} = \eta\, m(\alpha\tau) \qquad (21)$$

and the variance is given by

$$\sigma^2_{p.e.} = \eta m(\alpha\tau) \qquad (22)$$

The signal-to-noise ratio is given by

$$SNR_{p.e.} = [\eta\, m(\alpha\tau)]^{\frac{1}{2}} \qquad (23)$$

The input signal-to-noise ratio $(m\alpha\tau)^{1/2}$ is degraded by a factor of 0.63 for $\eta = 0.4$ and by a factor of 0.1 for $\eta = 0.01$.

The effect of the imperfect conversion of photons from a purely random source into photoelectrons within the cathode is a reduction in the input signal-to-noise ratio by a factor equal to the square root of η. Deviations from this result indicate that the photon source may not be purely random. Such effects have been observed but are small in ordinary thermal sources.[1]

Another source of photocathode noise is the thermionic emission of single electrons. The strength of the emission varies with photocathode type. In the bialkali cathode, for example, thermionic emission is virtually absent; electron emission exists in the absence of a photo signal, but it is not temperature-dependent as is thermionic dark emission, and it probably arises from a different source. S-1 photocathodes, on the other hand, exhibit relatively large dark currents as a result of thermionic emission; these currents can be eliminated to some extent, however, by cooling the tube.

Randomly emitted thermionic electrons add a term to the fluctuation in the photoelectron current proportional to their number. Because of their independence with respect to any usual signal current, the term adds to that of the signal noise in quadrature. That is,

$$\sigma^2_{p.e.} = \eta\, \overline{n}_p + \overline{n}_{th} \qquad (24)$$

where n_{th} is the average number of thermionic electrons emitted in a time τ, and $\eta\overline{n}_p$ is the average number of photoelectrons emitted in the same time.

NOISE CONTRIBUTIONS FROM THE MULTIPLIER CHAIN

Although the amplification (multiplication) of the photoelectron current in the dynode chain of a photomultiplier is often referred to as noise-free, careful examination of the statistics of the gain mechanisms involved shows that this statement is not entirely correct. Approximately noise-free operation can be attained, however, with the use of proper elec-

tron optics and newly developed dynode materials. In the following discussion the statistical gain processes in the individual dynodes are examined and then combined to yield the statistical properties of the entire multiplier chain. Much of the work presented was accomplished at a very early stage in photomultiplier history.[2]

Secondary Emission

Photomultiplier dynodes provide gain through the process of secondary emission, which was discussed in detail in the section on **Photoemission and Secondary Emission.** Most practical dynodes consist of semiconductors or of conducting substrates surfaced with a thin insulating film. An energetic primary electron penetrates the surface and, ideally, excites electrons from the valence band to the conduction band within the dynode material. These excited electrons drift and diffuse toward the dynode-vacuum interface where they escape with a certain probability into the vacuum as secondary electrons. For a given primary energy, it is possible to obtain any number of secondaries n_s from zero to a maximum $n_{s(max)}$. The maximum number is given by the quotient of the primary energy E_p and the energy required to produce a hole-electron pair within the dynode ϵ_p, as follows:

$$n_{s(max)} = E_p/\epsilon_p \qquad (25)$$

Over many repeated measurements using primary electrons of the same energy, a truncated distribution is obtained for n_s. A model that describes the observed distributions from most practical dynodes is developed in Appendix B at the end of this section.

Statistics for a Series of Dynodes

Using the formulas for the gain and fluctuation for a single dynode developed in Appendix A, the expressions of Appendix B may be used to find the combined gain and variances for the string of dynodes that make up a multiplier. It is assumed that one primary electron impinging on the first dynode releases, on the average, δ_1 secondaries with variance σ_1^2. The output of the first dynode striking the second dynode produces an average gain at the second stage of $\overline{m}_2$ and a variance of σ^2_{m2}. From Eq. (84) in Appendix A, $\overline{m}_2$ and σ^2_{2m} can be related to the individual dynode statistics as follows:

$$\overline{m}_2 = \delta_1 \cdot \delta_2 \qquad (26)$$

and

$$\sigma_{m_2}^2 = \delta_2^2\,\sigma_1^2 + \delta_1\,\sigma_2^2 \qquad (27)$$

where δ_2 and σ_2^2 are the average secondary emission and variance for the second dynode for a single input electron. Continuing in this manner, the gain and fluctuation from the third stage are given by

$$\overline{m}_3 = \delta_1 \cdot \delta_2 \cdot \delta_3 \qquad (28)$$

and

$$\sigma^2_{m3} = \delta_3^2[\delta_2^2\,\sigma_1^2 + \delta_1\,\sigma_2^2] + \delta_1\,\delta_2\,\sigma_3^2 \qquad (29)$$

Eq. (29) can be rearranged to read

$$\sigma^2_{m3} = [\delta_1\,\delta_2\,\delta_3]^2 \left\{\frac{\sigma_1^2}{\delta_1^2} + \frac{\sigma_2^2}{\delta_1\,\delta_2^2} + \frac{\sigma_3^2}{\delta_1\,\delta_2\,\delta_3^2}\right\} \qquad (30)$$

The extension of Eqs. (29) and (30) to k stages is accomplished by adding terms to Eqs. (26) and (27) as follows:

$$\overline{m}_k = \delta_1 \cdot \delta_2 \cdot \cdots \cdot \delta_k \qquad (31)$$

$$\sigma^2_{mk} = (\overline{m}_k)^2 \left\{ \frac{\sigma_1^2}{\delta_1^2} + \frac{\sigma_2^2}{\delta_1 \cdot \delta_2^2} + \cdots \cdot \frac{\sigma_k^2}{(\delta_1 \cdot \delta_2 \cdots \delta_{k-1})\,\delta_k^2} \right\} \qquad (32)$$

Eq. (31) states the expected results: that the total average gain for a series of k dynodes is the product of the secondary-emission yields of the individual dynodes in the series. Eq. (32) shows that the relative contribution of any stage to the total fluctuation decreases with the proximity of the dynodes to the output end of the chain. The first stage contributes most to the total variance. The higher the first-stage gain, the less each subsequent stage contributes to the total variance. This property is an important feature of the new high-gain GaP first-dynode photomultipliers.

The signal-to-noise ratio for the multiplier chain is given by

$$\frac{\overline{m}_k}{\sigma_{mk}} = \left[\frac{\sigma_1^2}{\delta_1^2} + \frac{\sigma_2^2}{\delta_1\,\delta_2^2} + \cdots \cdot \frac{\sigma_k^2}{(\delta_1 \cdot \delta_2 \cdots \delta_{k-1})\,\delta_k^2} \right]^{-\frac{1}{2}} \qquad (33)$$

For large first-stage gains, the multiplier signal-to-noise ratio is high. Most of the noise contribution is from the first stage. If, in addition to a large gain, the first stage exhibits Poisson statistics, as explained in Appendix B, the signal-to-noise ratio becomes

$$SNR_k \equiv \frac{\overline{m}_k}{\sigma_{mk}} \approx \sqrt{\delta_1} \qquad (34)$$

The noise added to the input signal is very small. It is in this sense that the multiplication chain is said to provide noise-free gain.

Multiple-Particle Inputs

The output-pulse distribution for multiple-particle inputs is obtained from the generating function for the multiplier chain. A multiplier chain consisting of k dynodes has a generating function $Q_k(s)$ given by

$$Q_k(s) = Q_1\,\{Q_2\,[\cdots\cdots Q_k(s)]\} \qquad (35)$$

The probability $P_k(n)$ of observing n electrons (for a one-electron input) at the output of a k-stage chain is derived from Eq. (74) in Appendix A, as follows:

$$P_k(n) = \frac{1}{n!} \left. \frac{\partial^n Q_k(s)}{\partial s^n} \right|_{s=0} \qquad (36)$$

The generating function for a k-stage multiplier chain for multiple-particle inputs is given by Eq. (86) of Appendix A, as follows:

$$Q_k(s,m) = [Q_k(s)]^m \qquad (37)$$

The probability of observing n output electrons from m input particles is given by

$$P_k(n,m) = \frac{1}{n!} \left. \frac{\partial_n [Q_k(s)]^m}{\partial s^n} \right|_{s=0} \qquad (38)$$

When identical dynodes are used, the output distribution for single-electron input pulses evolves toward a steady-state distribution after four or five stages, and exhibits little change thereafter. Fig. 52 shows some single-electron distributions[3] computed by use of the Polya statistics for each stage in the chain as explained in Appendix B. As b ap-

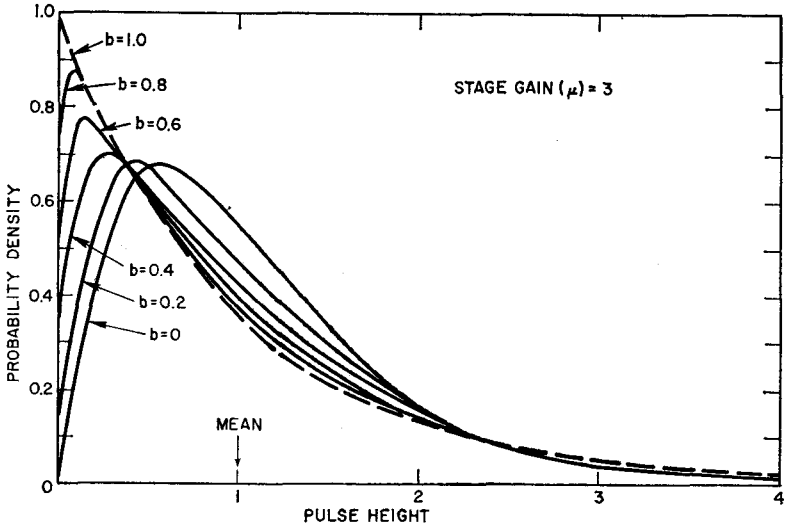

Fig. 52 — Computed single-electron distribution for a range of values of parameter b. Parameter b is defined in Appendix B.

proaches 1, the distribution becomes more sharply peaked.

Computer values of multiple-particle outputs for a two-stage structure are shown in Fig. 53.[4] The two curves relate to two different structures that have the same dynode as a first stage. The solid-line curve

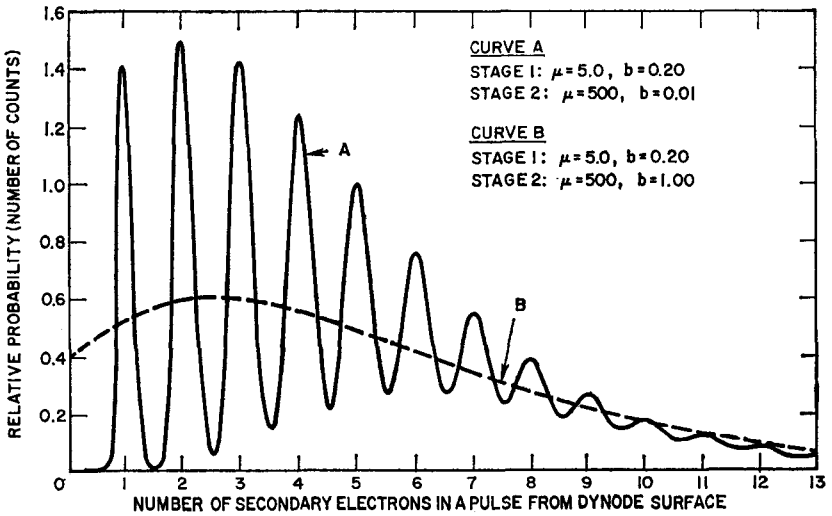

Fig. 53 — Theoretical pulse-height distribution.

shows the output when the first stage is followed by a high-gain ($\mu = 500$) second stage having nearly pure Poisson statistics (b = 0.01). The output peaks are sharply defined, and pulses up to a ten-electron input pulse are clearly resolvable. The dashed line describes the final output distribution when the first stage is followed by a high-gain ($\mu = 500$) dynode having an exponential output distribution. Individual peaks are no longer discernible; the large variance associated with the exponential statistics of the second stage eliminates all the structure in the output of the first stage.

RCA has recently developed a high-gain gallium phosphide (GaP) dynode which, when used as the first stage in a conventional copper beryllium (CuBe) multiplier chain, greatly increases the pulse-height resolution of the photomultiplier. The high-gain first stage in a photomultiplier having multiple photoelectron events originating from the photocathode is similar to the case illustrated in Fig. 53 for a multiplier where the high-gain second dynode amplifies the multiple pulses originating from the first dynode which in turn are initiated by single electrons. Typical gains for the new RCA gallium phosphide dynodes are 30 to 45, and their statistics are nearly Poisson. Fig. 54 shows the multiple-particle pulse-height distribution for the tube, and Fig. 55 shows the pulse-height curves for a tritium scintillation input for a conventional tube using the standard copper-beryllium first dynode along with that for a tube with a gallium phosphide first dynode. The increased resolution of the gallium phosphide dynode is clearly shown.

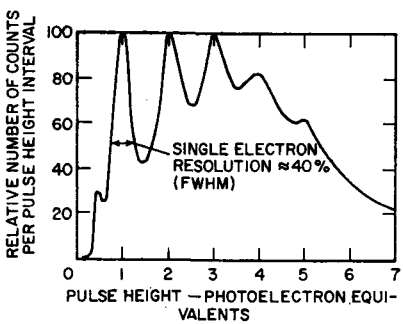

Fig. 54 — Typical photoelectron pulse-height spectrum for a photomultiplier having a GaP first dynode.

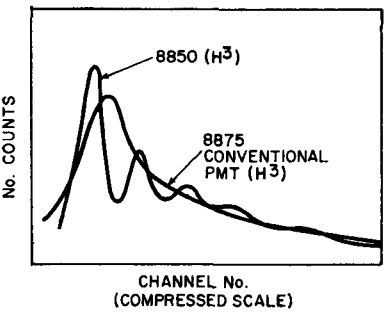

Fig. 55 — A comparison of the tritium scintillation pulse-height spectra obtained using a conventional photomultiplier having all CuBe dynodes and a photomultiplier having a GaP first stage.

Note: The first photoelectron peak of the 8850 spectra includes dark noise from the photomultiplier, chemiluminescence and phosphorescence from the vial and cocktail, and well as H^3 disintegration.

FLUCTUATIONS IN THE TUBE AS A WHOLE

In the previous sections the noise contributions from the photocathode and the multiplier chain were considered; these results can be combined to obtain the signal-to-noise ratio for the photomultiplier as a whole.

The average number of photoelectrons from the photocathode in a time τ is given by

$$\bar{n}_{p.e.} = \eta \cdot \bar{n}_p \tag{39}$$

The variance is given by

$$\sigma^2_{p.e.} = \eta \cdot \bar{n}_p \tag{40}$$

It is assumed that $\sigma_p{}^2 = n_p$ or that the input flux of photons displays Poisson statistics. If the form for $\sigma_p{}^2$ is not the result of a Poisson process, Eq. (84) in Appendix A must be used to obtain $\sigma_{pe}{}^2$.

Using these expressions to describe the input to the photomultiplier chain, the average number of electrons collected at the anode can be stated as follows:

$$\bar{n}_a = \eta \cdot \bar{n}_p \cdot \bar{m}_k \tag{41}$$

where $\bar{m}_k$ is given in Eq. (31) and is the average gain of a k-stage multiplier. The variance for the output electron stream is given by

$$\sigma^2_a = \bar{m}^2_k \cdot \eta \cdot \bar{n}_p + \eta \cdot \bar{n}_p \cdot \sigma^2_{mk} \tag{42}$$

where $\sigma_{mk}{}^2$ is given by Eq. (32) and is the variance in the average gain of a k-stage multiplier chain.

Eq. (42) can be rearranged as follows:

$$\sigma^2_a = \eta\, \bar{n}_p\, (\bar{m}^2_k + \sigma^2_{mk}) \tag{43}$$

For equal-gain stages described by Poisson statistics in the multiplier chain, Eq. (42) becomes

$$\sigma^2_{mk} = \frac{\bar{m}^2_k}{(\delta - 1)} \left[1 - \frac{1}{\delta^k} \right] \tag{44}$$

Neglecting the $1/\delta^k$ term and substituting the result and δ^k for $\bar{m}_k$ in Eq. (43),

$$\sigma^2_a = \eta\, \bar{n}_p \left[\delta^{2k} \left(1 + \frac{1}{\delta - 1} \right) \right] \tag{45}$$

In this case

$$\mathrm{SNR}_a = \sqrt{\eta \bar{n}_p \Big/ \left(\frac{\delta}{\delta - 1} \right)}. \tag{46}$$

High dynode gains imply that $1/(\delta - 1)$ is much less than 1 and hence that

$$\sigma^2_a = \eta \bar{n}_p (\delta^{2k}) \tag{47}$$

The signal-to-noise ratio at the anode is given by

$$\mathrm{SNR}_a = \frac{\bar{n}_a}{\sigma_a} = (\eta \bar{n}_p)^{\frac{1}{2}} \tag{48}$$

For high-gain dynodes exhibiting Poisson statistics, therefore, SNR_a is essentially that of the photoelectrons, $\mathrm{SNR}_{p.e.}$, as given in Eq. (17).

In a photomultiplier in which the dynode gain is not high but still exhibits Poisson statistics, SNR_a is given by

$$\mathrm{SNR}_a = \frac{(\eta\, \bar{n}_p)^{\frac{1}{2}}}{\left(\frac{\delta}{\delta - 1} \right)^{\frac{1}{2}}} \tag{49}$$

As an example, with $\delta = 4$ the SNR_a is decreased by a factor of 0.87 from its value for very large δ. Doubling δ to a value of 8 changes the degradation factor to 0.94. Further increases in δ do not improve the SNR_a very much.

In the case of fully exponential dynode statistics, the variance for each dynode in a chain of identical dynodes is given by Eq. (94) in Appendix B; i.e.,

$$\sigma^2_a = \delta^2 + \delta \tag{50}$$

where δ is the average gain per stage. The total anode fluctuation then becomes

$$\sigma^2_a = (\eta\, \bar{n}_p) \left[\delta^{2k} \left(1 + \frac{(\delta + 1)}{(\delta - 1)} \right) \right] \tag{51}$$

For large dynode gains,

$$\sigma^2_a \approx 2(\eta\, \bar{n}_p)\, \delta^{2k} \tag{52}$$

Even for large dynode gains, exponential statistics increase σ_a^2 by a factor of 2, with the result that SNR_a decreases by $1/\sqrt{2}$. This drop in SNR_a is accompanied by a severe loss in single- and multiple-electron pulse-height resolution, as shown in Fig. 53. To resolve single-photoelectron pulses, the multiplier chain must exhibit both high gain and good (i.e., Poisson) statistics.

A significant improvement in SNR_a results when the photocathode quantum efficiency η is increased. At present the peak value of η for the S-20 cathode is 0.35; doubling η to 0.7 would improve SNR_a by a factor of 1.4. The ideal photomultiplier, for which $\eta = 1$, would have an SNR_a equal to the square root of n_p. The present value of $\eta = 0.35$ degrades the ideal SNR_a by a factor of 0.59. Considerable improvement can be expected with the development of photocathode materials of increased sensitivity.

The application of these equations to present photomultipliers indicates that the available photocathode quantum efficiency is the principal degrading influence on SNR_a. Values of η less than 1 also decrease the multiple-photon input-pulse resolution of a photomultiplier. High dynode gains (δ greater than 6) do not significantly degrade the input signal-to-noise ratio of photoelectrons provided the dynode statistics are nearly Poisson.

OTHER SOURCES OF NOISE IN PHOTOMULTIPLIER TUBES

Within a photomultiplier there are sources of noise that are not associated directly with the processes of photoelectric conversion and electron multiplication. These sources can, in general, be separated into two groups: (1) those that are not correlated with and (2) those that are correlated with the signal pulse.

GROUP 1 NOISE SOURCES

Radioactivity within the Photomultiplier

The materials used to fabricate the internal structure and the glass envelope of a photomultiplier may contain amounts of certain radioactive elements that decay and give off gamma rays or other high-energy particles. If one of these emitted particles strikes the photocathode or one of the first few dynodes, it will produce an anode dark pulse. The size of the anode pulse may be equivalent to one or more photoelectrons emitted at the photocathode. These pulses are randomly emitted. In tube manufacture this type of emission is minimized through the careful selection of materials.

Dark Pulses of Unknown Origin

Dark pulses of unknown origin in a photomultiplier result primarily from single-electron pulses; a small fraction consists of 2- and 3-electron pulses. The rate of occurrence of these dark pulses varies among multipliers; the lowest rate is about 150 counts per minute for the new RCA-8855 series. These dark pulses are randomly emitted, but may be accompanied by one or more of the noise effects correlated with the signal pulse. The problem of the origin of unknown pulses is at present a very active field of research.

GROUP 2 CORRELATED NOISE SOURCES

Gas Ionization

A gas atom or molecule within the photomultiplier may be ionized by a

photoelectron pulse. This ionization may occur at the first-dynode surface or in the vacuum between the photocathode and the first dynode. The positive ion thus created travels backward to the cathode where it may release one or more electrons from the photocathode. Because there is a time delay in the ion-emitted electron pulse equal to the time of flight of the ion to the photocathode, the resulting pulse, usually referred to as an afterpulse, occurs after the true signal pulse at the anode. Afterpulses are caused mainly by hydrogen ions and their occurrence can be minimized in tube processing.

Light Feedback

Primary electrons produce photons as well as secondary electrons within the dynodes of the multiplier chain. Despite the low efficiency of this process, some of the emitted photons may eventually reach the photocathode and release additional electrons. A time delay is observed corresponding to the transit time for the regenerated electron pulse to reach the point of origin of the light. Depending upon the type of dynode multiplier cage, this time may be of the order of 20 nanoseconds. Most of the photons comprising the light feedback originate in the region of the last few dynodes or of the anode.

If the voltage across the tube is increased, the dark-pulse rate also increases and usually produces some observable light near the anode region, a fraction of which is fed back to the photocathode. The result of this positive feedback is that, at a certain voltage, the photomultiplier becomes unstable and allows the output dark-pulse rate to increase to an intolerably high level. The voltage at which this increase occurs is generally above the recommended maximum operating voltage.

Not every signal pulse initiates an afterpulse. Therefore, coincidence techniques, using more than one photomultiplier, can be employed in some instances to eliminate this source of noise as well as the uncorrelated sources discussed above.

Analytically, the fluctuations resulting from Group 1 non-correlated random sources add in quadrature to those of the signal. Because they are random, the dark-pulse variances σ_{dp}^2 are proportional to the average dark-pulse rate $\bar{n}_{dp}$, as follows:

$$\sigma_{dp}^2 = \bar{n}_{dp} \tag{53}$$

The total anode variances are given by:

$$\sigma_a^2 = (\eta \bar{n}_p + \bar{n}_{dp}) \left[\bar{m}_k^2 \left(1 + \frac{1}{\delta - 1}\right)\right] \tag{54}$$

where $\eta\bar{n}_p$ and $\bar{n}_{dp}$ are the average single-photoelectron and the average single-dark-emitted electron numbers observed in a time τ. The factor $\bar{n}_{dp}$ sets a real limit on the anode signal-to-noise ratio. Again, in those instances where the incoming radiation signal comprises more than one photon, coincidence techniques can be employed to reduce the effect of randomly emitted electrons originating at the cathode.

Electrons may originate at dynodes well along in the multiplier chain. At the anode, these electrons appear as fractional-photoelectron pulses. Such pulses also result from interstage skipping, generally near the beginning of the chain. With good statistics in the chain, the fractional pulses may be discriminated against because the single-electron peak in the pulse-height spectrum stands out sharply.

NOISE AND THE BANDWIDTH OF THE OBSERVATION

At high counting rates, noise calculations are performed with the average and variance of the photoelectron current rather than with individual photoelectron pulses. The expressions which have been developed for signal-to-noise ratio by consideration of the average number of events in a time τ and the variance from average may be converted to expressions of signal-to-noise ratio involving currents and bandwith, Δf, by considering the reciprocal nature of the observation time and the bandwidth.

Noise equivalent bandwidth Δf may be defined [5] as follows:

$$\Delta f = \frac{1}{A_m^2} \int_0^\infty |H(j\omega)|^2 \, df \quad (55)$$

where $H(j\omega)$ is the complex frequency transfer response of the circuit, and A_m is the maximum absolute value of $H(j\omega)$. The "circuit" in this case counts pulses in a time τ. The network transfer function is the Laplace transform of the impulse response. The impulse response is a rectangular pulse of width τ, like a camera shutter. For this case,

$$H(j\omega) = \frac{1}{j\omega}(1 - e^{-j\tau\omega}) \quad (56)$$

and A_m is found to be equal to τ. The noise equivalent bandwidth is then readily found to be

$$\Delta f = 1/2\tau. \quad (57)$$

It is of interest to compare this relation with the equivalent noise bandwidth for exponential impulse response as in an RC circuit; in this case

$$\Delta f = 1/4RC \quad (58)$$

From Eq. (7), the SNR for a random photon flux is given by

$$SNR_p = \sqrt{I_p \tau} \quad (59)$$

where I_p is the average photon arrival rate and τ is the time interval of the count. When $\tau = 1/(2\Delta f)$ is substituted,

$$SNR_p = \sqrt{I_p/2\Delta f} \quad (60)$$

In the case of the photocathode electron current,

$$SNR_{p.e.} = \sqrt{\frac{\eta I_p}{2\Delta f}} = \sqrt{\frac{i}{2e\Delta f}} \quad (61)$$

where i is the photocathode emission current in amperes and e is the charge of the electron. If the signal current is considered as i, the noise in the bandwidth Δf for the photocurrent is the familiar shot noise formula $(2ei\Delta f)^{1/2}$.

The equation for the photon noise squared is given by

$$I_{pN}^2 = 2 I_p \Delta f \quad (62)$$

The photocurrent noise squared is given by

$$I_{peN}^2 = 2 \eta e^2 I_p \Delta f \quad (63)$$

Both these equations involve the photon "current" I_p.

If the photons are not randomly emitted, Eq. (62) must be modified. In the case in which the variance in the photon current is given by σ_p^2, the equation becomes

$$I_{peN}^2 = 2e^2 \Delta f \left[\eta I_p (1-\eta) + \frac{\sigma_p^2 \eta^2}{\tau} \right] \quad (64)$$

For a randomly emitted photon, the noise current squared at the anode is given by

$$\Delta I_{aN}^2 = 2 e^2 \eta \delta^{2k} I_p \Delta f \quad (65)$$

where the multiplier chain is assumed to be composed of k high-gain dynodes exhibiting Poisson statistics, each with an average gain δ.

At the anode, the input resistance and capacitance of a preamplifier generate a noise current squared given by

$$i_n^2 = 4kTg\,\Delta f \left[1 + R_n g + \frac{4\pi^2}{3} \cdot \frac{R_n}{g} \Delta f^2 C^2\right] \quad (66)$$

where $g = 1/R$ is the shunt conductance in the anode lead, C is the shunt capacitance, Δf is the bandwidth, k is Boltzmann's constant, T is the absolute temperature, and R_n is the equivalent noise resistance of the preamplifier input. The total noise current squared through R is $\Delta I^2_{aN} + i_n^2$, and SNR_a is given by

$$SNR_a = \eta \delta^k I_p e \Big/ \left[2 e^2 \eta \delta^{2k} I_p \Delta f + 4k\,Tg\,\Delta f \left(1 + R_n g + \frac{4\pi^2}{3} \frac{R_n}{g} \Delta f^2 C^2\right)\right]^{1/2} \quad (67)$$

To maintain the input SNR, ΔI^2_{aN} must be greater than i_n^2. For example, with $\Delta I^2_{aN} = 10\ i^2_n$, and $R = 100$ ohms, $C = 100$ picofarads, $R_n = 100$ ohms, $T = 300°K$, and $\Delta f = 10^6$ Hz, at room temperature,

$$i_n^2 = 3.2\ 10^{-16} \text{ amperes}^2 \quad (68)$$

With $\eta = 0.3$ and $\delta^k = 10^6$,

$$I_p = 10\ i_n^2/(2e^2\ \eta\ \delta^{2k}\ \Delta f) \quad (69)$$

or

$$I_p \simeq 2 \times 10^5 \text{ photons per second}$$

The value of I_p shown in Eq. (69) is the lower limit for the average photon current and makes the squared anode-current fluctuation greater than the squared noise current in the photomultiplier preamplifier input by a factor of ten. The resulting value of the average photon current corresponds to a photoelectric current of about 10^{-14} ampere, or about 6×10^4 photoelectrons per second. In cases in which the dark current is effectively higher than 6×10^4 photoelectrons per second, the photomultiplier sensitivity limit is set by the dark current and not by the preamplifier noise. It is the noise-free gain of the multiplier chain which increases the rms photocurrent shot noise by a factor of δ^k and permits the low-input-level operation.

SUMMARY

The more important expressions relating to signal and noise discussed in this section are summarized below. Beginning at the input to the photomultiplier, the signal is followed through the tube, and the variance and the SNR associated with the signal are noted.

First, a randomly emitted photon flux exhibiting Poisson statistics has an average value $\bar{n}$ given by

$$\bar{n} = I_p \tau$$

for the number of photons present in a time interval τ when the average rate of emission is I_p photons

per second. The variance σ^2 is given by

$$\sigma_p^2 = I_p\tau = \bar{n}$$

and the signal-to-noise ratio is given by

$$SNR = \bar{n}_p/\sigma_p = \sqrt{I_p\tau} = \sqrt{\bar{n}_p}$$

The number of photoelectrons emitted from a photocathode of quantum efficiency η is given by

$$\bar{n}_{p.e.} = \eta I_p\tau$$

and the variance is given by

$$\sigma_{p.e.}^2 = \eta I_p\tau$$

The signal-to-noise ratio of the photoelectron flux is given by

$$SNR_{p.e.} = \sqrt{\eta I_p\tau}$$

If the photocathode contributes randomly emitted thermionic electrons to the signal of photoelectrons, then the variance of the electron flux is increased, as follows:

$$\sigma_{p.e.}^2 = \eta I_p\tau + \bar{n}_{th},$$

where $\bar{n}_{th}$ is the average number of thermionic electrons emitted in a time τ. The SNR is decreased and becomes

$$SNR_{p.e.} = (\eta I_p\tau)/(\eta I_p\tau + \bar{n}_{th})^{\frac{1}{2}}$$

The signal-to-noise ratio of the multiplier chain with k dynodes alone is given by

$$SNR_k = \frac{\bar{m}_k}{\sigma_{mk}} = \left[\frac{\sigma_1^2}{\delta_1^2} + \frac{\sigma_2^2}{\delta_1\delta_2^2} + \cdots \frac{\sigma_k^2}{(\delta_1\cdot\delta_2\cdots\delta_{k-1})\,\delta_k^2}\right]^{-\frac{1}{2}}$$

where δ_j and σ_j^2 are the gain and variance of the j_{th} stage, respectively, and $\bar{m}_k$ and σ_{mk} are the total gain and the total deviation, respectively, for the entire multiplier chain.

For the photomultiplier tube as a whole, the anode SNR is given by

$$SNR_a = \sqrt{\eta\,\bar{n}_p}/[1+\sigma_1^2/\delta_1^2+\sigma_2^2/(\delta_1\cdot\delta_2^2) + \cdots + \sigma_k^2/((\delta_1\cdot\delta_2\cdots\delta_{k-1})\delta_k^2)]^{\frac{1}{2}}$$

If each stage is identical and has Poisson statistics,

$$SNR_a \simeq (\eta\,\bar{n}_p\,(\delta-1)/\delta)^{\frac{1}{2}}$$

and for large gain (i.e., $\delta >> 1$),

$$SNR_a \simeq \sqrt{\eta\,\bar{n}_p}$$

In this case the multiplier chain has not reduced the photoelectron SNR.

If each stage in the multiplier chain is identical and has exponential statistics, then

$$SNR_a = [\eta\,\bar{n}_p(\delta-1)/2\delta]^{\frac{1}{2}}$$

and for large gain,

$$SNR_a \simeq \sqrt{\eta\,\bar{n}_p/2}$$

The SNR for exponential statistics is decreased by $1/\sqrt{2}$ below that of a high-gain multiplier chain with Poisson statistics.

When the photomultiplier is operated at high photon counting rates:

$$SNR_a = \eta\delta^k I_p e \Big/ \left[2\,e^2\,\eta\delta^{2k} I_p\,\Delta f + 4k\,Tg\,\Delta f\left(1 + R_n g + \frac{4\pi^2}{3}\frac{R_n}{g}\,\Delta f^2 C^2\right)\right]^{1/2}$$

where I_p is the average photon current in photons per second, e is the electronic charge, Δf is the frequency bandwidth, T is the absolute temperature (°K), k is the Boltzman constant, R_n is the equivalent noise resistance of the input of the preamplifier that processes the anode signal, g is the shunt conductance in the anode lead, and C is the shunt capacitance in the anode lead.

APPENDIX A— STATISTICAL PROCESSES AND THE GENERATING FUNCTION

Statistical processes are characterized by randomly distributed outputs for a given input. The relative frequency of occurrence of any particular output is given by the probability that this output occurs. As an example, for a single-particle input, the output of a particle-multiplication device such as a photomultiplier may consist of from zero to N particles. A particular output n occurs with probability P_n. The distribution of P_n sums to unity as follows:

$$\sum_{n=0}^{N} P_n = 1 \qquad (70)$$

The average number of output particles is given by

$$\bar{n} = \sum_{n=0}^{N} n\, P_n \qquad (71)$$

On any given single measurement, an output consisting of n particles is not expected. In fact, n may not be integral, even though all possible outputs must be. There will be fluctuations in the output which are given by the variance σ^2, or by the rms or standard deviation σ, such that

$$\sigma = \left[\sum_{n=0}^{N} (n-\bar{n})^2 \cdot P_n \right]^{\frac{1}{2}} \qquad (72)$$

The expression $\bar{n}/\sigma$ is the signal-to-noise ratio for the device in question ($\sigma/\bar{n}$ is the relative deviation). Obviously, the smaller the value of σ, the more precisely determined is the output.

An alternative and more powerful method of obtaining the results above, as well as others of a more complex nature, involves the use of the generating function of the distribution $[P_n]$.[6] The generating function Q(s) in terms of the auxiliary variable s is defined as follows:

$$Q(s) = \sum_{n=0}^{N} s^n\, P_n \qquad (73)$$

and has the following properties:

$$P_n = \frac{1}{n!} \cdot \frac{\partial^n Q(s)}{\partial s^n}\bigg|_{s=0} \qquad (74)$$

$$Q(s)\,|_{s=1} = 1 \qquad (75)$$

$$\frac{\partial Q(s)}{\partial s}\bigg|_{s=1} = \bar{n} \qquad (76)$$

and

$$\frac{\partial^2 Q(s)}{\partial s^2}\bigg|_{s=1} + \frac{\partial Q(s)}{\partial s}\bigg|_{s=1} - \left[\frac{\partial Q(s)}{\partial s}\bigg|_{s=1}\right]^2 = \sigma^2 \qquad (77)$$

The statistical properties of a number of individual devices in series (the multiplier chain of a photomultiplier is an example) and the average output and fluctuation for a single device when the input consists of more than one particle can now be obtained through the use of the generating function Q(s) of the single-particle-input probability distribution $[P_n]$.

Fig. 56 shows the series combination of two statistical devices. The first has an output distribution $[P_n]_A$ which yields an average gain $\bar{n}_A$ and variance σ_A^2. The generating function for $[P_n]_A$ is $Q_A(s)$. Similarly, for the second device the output distribution is $[P_n]_B$, the average gain is $\bar{n}_B$, the variance is σ_B^2, and the generating function is $Q_B(s)$. The relationships between these individual device functions and the total average output n_{AB} and the variance σ_{AB}^2 for the entire serial combination are required. The first step is to state the generating function $Q_{AB}(s)$ for the serial combination shown in Fig. 56.

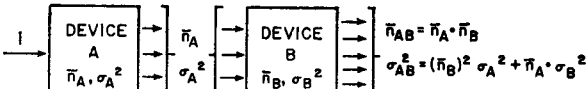

Fig. 56 — A schematic representation of the serial combination of two statistical devices A and B. For a single-particle input the gain and variance of the signal at each stage in the device are shown. The total gain and total variance for the entire combination in terms of each of the individual device characteristics for a single-particle input is given by Eqs. (81) and (84) in the text.

The generating function for the serial combination is given by the following relation:

$$Q_{AB}(s) = Q_A[Q_B(s)] \qquad (78)$$

This relation can be understood more clearly if the two devices are considered to have only two possible outputs, either one particle or two particles. Then the generating functions are $Q_A(s) = sP_1 + s^2P_2$ and $Q_B(s) = sP_1' + s^2P_2'$. When these functions are inserted, Eq. (78) becomes

$$Q_{AB}(s) = sP_1P_1' + s^2P_1P_2' + s^2P_2P_1'P_1' + 2s^3P_2P_1'P_2' + s^4P_2P_2'P_2'$$

or

$$Q_{AB}(s) = sP_1P_1' + s^2(P_1P_2' + P_2P_1'P_1') + s^3(2\,P_2P_1'P_2') + s^4P_2P_2'P_2' \qquad (79)$$

The coefficients of s^j ($j = 1, 2, 3, 4$) give the probability of a j-particle output for the entire series combination. Each coefficient comprises the sum of all possible ways to obtain that particular number of particles at the output.

From Eq. (78), the output probability distribution $[P_n]_{AB}$, the total average output $\bar{n}_{AB}$, and the total variance σ_{AB}^2 for the series combination can be obtained through the use of Eqs. (74), (76), and (77). Of most interest are the total average output and the total variance. From Eq. (76),

$$\bar{n}_{AB} = \left.\frac{\partial Q_{AB}}{\partial s}\right|_{s=1} \qquad (80)$$

or

$$\bar{n}_{AB} = \left.\frac{\partial Q_A}{\partial Q_B} \cdot \frac{\partial Q_B}{\partial s}\right|_{s=1} = \left[\frac{\partial Q_A}{\partial s} \cdot \frac{\partial Q_B}{\partial s}\right]_{s=1} = \bar{n}_A \cdot \bar{n}_B \qquad (81)$$

As expected, the average output for the series combination is the product of the average outputs of the indi-

vidual devices. The variance σ_{AB}^2 is given by

$$\sigma_{AB}^2 = \frac{\partial^2 Q_{AB}}{\partial s^2} + \frac{\partial Q_{AB}}{\partial s} - \left[\frac{\partial Q_{AB}}{\partial s}\right]^2 \quad (82)$$

After the differentiation is performed,

$$\sigma_{AB}^2 = Q_A'' [Q_B']^2 + Q_A' Q_B'' + Q_A' Q_B' - [Q_A']^2 [Q_B']^2 \quad (83)$$

where the prime indicates differentiation with respect to s and evaluation of the derivative at s = 1. By addition and subtraction of a term $[Q_A'][Q_B']^2$, Eq. (83) can be rearranged as follows:

$$\sigma_{AB}^2 = [Q_B]^2 [Q_A'' + Q_A' - [Q_A']^2] + Q_A' [Q_B'' + Q_B - [Q_B']^2]$$

or, in terms of the individual-device average outputs and variances, as follows:

$$\sigma_{AB}^2 = [\bar{n}_B]^2 \cdot \sigma_A^2 + \bar{n}_A \cdot \sigma_B^2 \quad (84)$$

The physical interpretation of Eq. (84) is straightforward. If device B had no fluctuations ($\sigma_B^2 \doteq 0$), σ_{AB}^2 would comprise only the variance σ_A^2 from device A multiplied by the square of the average output of device B. Each particle from device A is multiplied by $\bar{n}_B$, a constant, and therefore the coefficient of σ_A^2 in Eq. (84) is $[\bar{n}_B]^2$. On the other hand, if device A had no output fluctuations, each of the $\bar{n}_A$ particles would undergo independent fluctuations in device B. As independent fluctuations, they add in quadrature, and thus $\sigma_{AB}^2 = \bar{n}_A \sigma_B^2$.

More devices could be strung in series. In general, for a series of devices A, B, C, etc., the generating function is given by

$$Q_{ABC\cdots Z} = Q_A \{Q_B [\cdots\cdots Q_Z(s)]\} \quad (85)$$

Eqs. (81) and (84) provide a recursion relation between any two devices in the series so that the total gain and variance from any number of devices can be obtained. These recursion relations are used in discussions of photocathode and multiplier-chain statistics.

When the input to a particular device consists of multiple, simultaneous, independent events, the generating function for the combination is obtained by taking the product of the separate generating functions. Thus, for two such parallel inputs to a statistical device, the corresponding generating functions are:

$$Q_A = \sum_{m=0}^{N} s^m P_{Am} \text{ and } Q_B = \sum_{m=0}^{M} s^m P_{Bm}$$

When the product is formed, the individual coefficients of s_j represent the sum of the event probabilities which yield j particles in the output, as follows:

$$Q_{AB} = Q_A \cdot Q_B = P_{A0} P_{B0} + (P_{A0} P_{B1} + P_{A1} P_{B0}) s + (P_{A0} P_{B2} + P_{A1} P_{B1} + P_{A2} P_{B0}) s^2 + \cdots$$

It is obvious that this treatment may be extended to multiple simultaneous events. In particular, for an m-particle input, where the generating function is Q(s) for each particle, the output generating function $Q_m(s)$ is given by

$$Q_m(s) = [Q(s)]^m \cdots\cdots \quad (86)$$

This situation is shown schematically in Fig. 57.

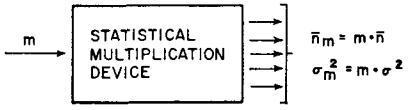

Fig. 57 — A schematic representation of a statistical, multiplicative device with an m-particle input. The total gain and variance for the output in terms of the single-particle input characteristic are given by Eqs. (87) and (88) in the text.

By use of Eqs. (76) and (77)

$$\bar{n}_m = m \cdot \bar{n} \qquad (87)$$

and

$$\sigma_m^2 = m \cdot \sigma^2 \qquad (88)$$

The output probability distribution $[P_n]_m$ is obtained by using the m-particle generating function [Eq. (86)] in Eq. (74).

Eqs. (87) and (88) can be obtained from Eqs. (81) and (84) by assuming in that case (see Fig. 56) that the first serial device is a perfect multiplier with no variance ($\sigma_A^2 = 0$). Under this restriction, the input to device B is a constant m, and the gain and variance found from Eqs. (81) and (84) are identical to those given in (87) and (88).

APPENDIX B— MODEL FOR DYNODE STATISTICS

The observed number distributions for secondary electrons vary among the different types of dynodes used commercially. Nearly all the distributions fall within the class limited by a Poisson distribution [7] at one extreme and an exponential distribution at the other.[4] To describe this wide variety of distributions the Polya, or compound Poisson, distribution is employed.[3] Through the adjustment of one parameter, the distribution runs from purely Poisson to exponential. Therefore, this one distribution can be used to describe and to interpret the bulk of the observed secondary-emission statistics.

The distribution has the following form:

$$P(n,b) = \frac{\mu^n}{n!}(1+b\mu)^{-n-1/b}\prod_{j=1}^{n-1}(1+jb) \qquad (89)$$

where P(n, b) is the probability of observing n secondaries, μ is the mean value of the distribution, and b is the parameter controlling the shape of the distribution. With b = 0, the distribution is Poisson, as follows:

$$P(n,o) = \frac{\mu^n}{n!}e^{-\mu} \qquad (90)$$

With b = 1, an exponential distribution results, as given by:

$$P(n,1) = \mu^n(1+\mu)^{-(n+1)} \qquad (91)$$

Fig. 58 shows a family of distributions for various values of b.

The generating function for P(n, b) is given by

$$Q(s) = [1+b\mu(1-s)]^{-1/b} \qquad (92)$$

From Eqs. (76) and (77) of Appendix A,

$$\bar{n} = \mu \qquad (93)$$

and

$$\sigma^2 = b\mu^2 + \mu \qquad (94)$$

The fluctuations increase as μ^2 for an exponential distribution (b = 1), but increase only as μ for the Poisson distribution. The signal-to-noise ratio is given by

$$\frac{\bar{n}}{\sigma} = \mu/(b\mu^2+\mu)^{\frac{1}{2}} \qquad (95)$$

Fig. 59 shows a log-log plot of the signal-to-noise ratio as a function of μ with b as a parameter. The signal-to-noise ratio improves with increasing μ for the Poisson distribution, but approaches unity with large μ in

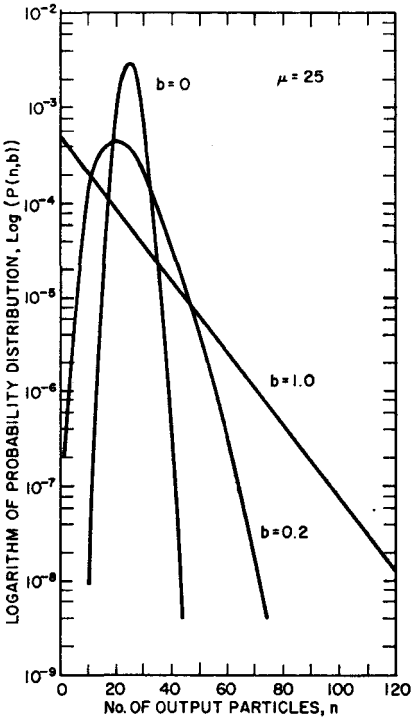

Fig. 58 — Single-particle output distribution for a dynode displaying Polya statistics. A value of b = 1 gives a probably exponential distribution; b = 0 gives a Poisson distribution; b = 0.2 is intermediate between the two extreme values.

the exponential distribution. In fact, for any non-zero value of b, the signal-to-noise ratio approaches $b^{-1/2}$ for large μ. As shown in Fig. 59, even small departures from Poisson statistics significantly reduce the signal-to-noise ratio at moderately high gains of 10 to 20. It can be anticipated that departures from Poisson statistics degrade the single-electron pulse-height resolution.

The Polya distribution has an interesting interpretation with respect to secondary-emission statistics.[3] For non-zero values of b, the distributions described by Eq. (89) can be shown to be composed of a number of different Poisson processes, each with a different mean value. The mean values are, in turn, distributed according to the Laplace distribution.

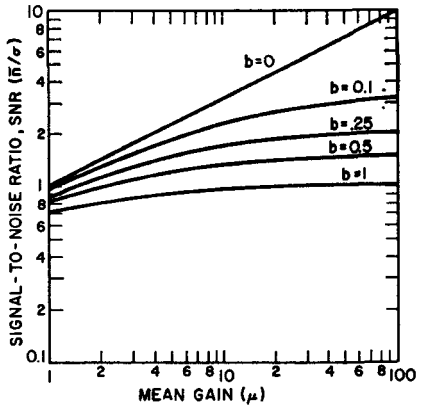

Fig. 59 — A comparison of the SNR as a function of the mean value μ for a number of Polya distributions. For Poisson statistics (b = 0), the SNR increases as the square root of μ. With 0 < b ≤ 1, the SNR approaches the square root of b^{-1} for large mean gains.

When b equals 0, the distribution of the mean values collapses to a delta function at the value μ, leading to a purely Poisson distribution. For b equals 1, the distribution of the mean values is exponential. The physical interpretation for a dynode displaying non-Poisson statistics is that physical non-uniformities on the dynode surface cause each element of the surface to have a different mean value for emission. Although each small element exhibits Poisson statistics with respect to emission, the total emission from the entire dynode is non-Poisson because it comprises a distribution of Poisson distributions. It is possible that the basic emission process from a given dy-

node is not a Poisson process. However, high-gain GaP dynodes exhibit nearly Poisson statistics [7] and at present it is believed that departures from this norm are caused, to a large extent, by dynode non-uniformities.

The departure from Poisson statistics affects the single-particle pulse-height resolution. Fig. 60 shows the output-pulse distribution from a single dynode for a number of multiple-particle inputs. The resolution is clearly degraded in passing from a Poisson distribution to an exponential one. With the exponential distribution shown in Fig. 60, it would be difficult to distinguish among one-, three-, and five-particle input pulses, whereas the problem virtually disappears for a Poisson distribution.

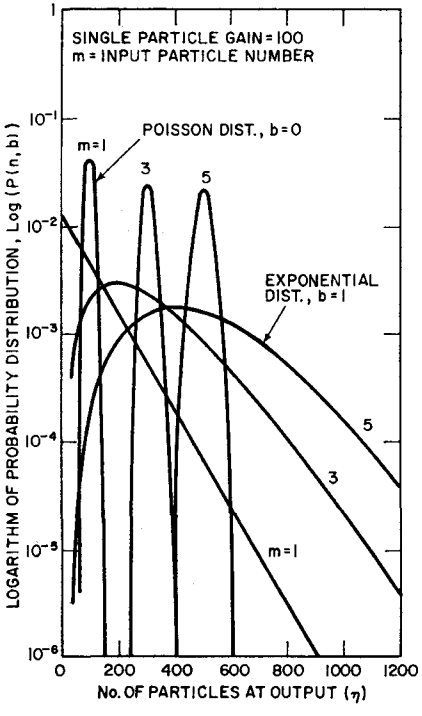

Fig. 60 — A comparison of multiple-particle distributions from a single dynode having Poisson and exponential distribution. Clearly, the particle resolution characteristics of the exponential distribution are much poorer.

REFERENCES

1. R. H. Brown and R. Q. Twiss, "Interferometry of the Intensity Fluctuations in Light", *Proc. Royal Soc. London, Vol. 242A*, p. 300 (1957), *Vol. 243A*, p. 291 (1958).
2. W. Shockley and J. R. Pierce, "A Theory of Noise for Electron Multipliers", *Proc. IRE, Vol. 26*, p. 321 (1938); V. K. Zworykin, G. A. Morton, L. Malter, "The Secondary Emission Multiplier—A New Electronic Device", *Proc. IRE, Vol. 24*, p. 351 (1936).
3. J. R. Prescott, *Nuc. Instr. Methods*, A Statistical Model for photomultiplier Single-Electron Statistics", *Vol. 39*, p. 173 (1966).
4. L. A. Dietz, L. R. Hanrahan and A. B. Hance, "Single-Electron Response of a Porous KCl Transmission Dynode and Application of Polya Statistics to Particle Counting in an Electron Multiplier", *Rev. Sci. Inst., Vol. 38*, p. 176 (1967).
5. M. Schwartz, *Information Transmission, Modulation, and Noise*, McGraw-Hill, p. 207 (1959).
6. T. Jorgensen, "On Probability Generating Functions", *Am. J. Phys., Vol. 16*, p. 285 (1948); E. Breitenberger, "Scintillation Spectrometer Statistics", *Prog. Nuc. Phys., Vol. 4*, (Ed. O. R. Frisch, Pergamon Press, London, p. 56 (1955).
7. G. A. Morton, H. M. Smith, and H. R. Krall, "Pulse Height Resolution of High Gain First Dynode Photomultipliers", *Appl. Phys. Lett., Vol. 13*, p. 356 (1968).

Application of Photomultipliers

THIS section discusses the major applications of photomultipliers and describes some of the special considerations for each application. The applications covered include scintillation counting, Cerenkov radiation detection, time spectroscopy, laser range finding, flying-spot scanning, detection of low light levels, photometry, and spectrometry. This listing is not complete even for presently known applications, and new ones are being continually devised. The applications discussed, however, are some of the major ones and the information given can be readily adapted to other applications or to new ones.

SCINTILLATION COUNTING AND CERENKOV RADIATION DETECTION

A scintillation counter is a device used to detect and register individual light flashes caused by ionizing radiation, usually in the form of an alpha particle, beta particle, gamma ray, or neutron, whose energy may be in the range from just a few thousand electron-volts to many million electron-volts. The most common use of scintillation counters is in gamma-ray detection and spectroscopy.

The gas, liquid, or solid in which a scintillation or light flash occurs is called the scintillator. A photomultiplier mounted in contact with the scintillator provides the means for detecting and measuring the scintillation. Fig. 61 is a diagram of a basic scintillation counter. The three most probable ways in which incident gamma radiation can cause a scintillation are by the photoelectric effect, Compton scattering, or pair

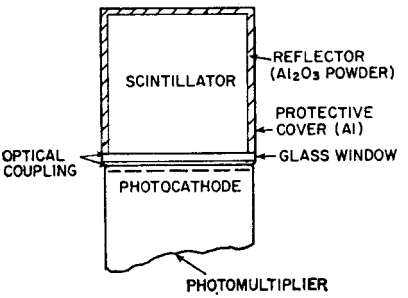

Fig. 61 — Diagram of a scintillation counter.

production. The reaction probabilities associated with each of these types of interaction are a function of the energy of the incident radiation as well as the physical size and atomic number of the scintillator material. In general, for a given scintillator, the photoelectric effect predominates at small quantum energies, the Compton effect at medium energies, and pair production at energies above 1.02 MeV.

Scintillation Processes

In the photoelectric effect, a gamma-ray photon collides with a bound electron in the scintillator and imparts virtually all its energy to the electron. In the Compton effect, a gamma-ray photon with energy $E = h\nu$ interacts with a free electron in the scintillator and transmits only part of its energy to the electron, as shown in Fig. 62. A scattered photon of lower energy also results. To satisfy the conditions of conservation

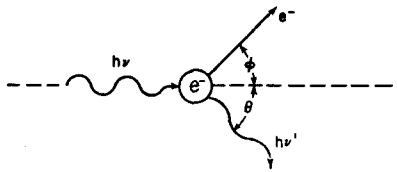

Fig. 62— Compton-effect mechanism.

of energy and momentum, there is a maximum energy that can be transferred to the electron. This maximum energy, known as the Compton edge, occurs when Θ in Fig. 62 is 180 degrees and ϕ is 0 degrees; it is given by

$$T_{CM} = \frac{E}{1 + (1/2\alpha)} \qquad (96)$$

where E is the photon energy, $\alpha = E/m_0c^2$, m_0 is the rest mass of an electron, and c is the speed of light. The resultant energy imparted to the electron can then range from zero to a maximum of T_{CM}.

In pair production, as shown in Fig. 63, the energy of a gamma ray is converted to an electron-positron pair in the field of a nucleus. The gamma ray must have energy at least equal to two times the rest-mass-energy equivalent of an electron, 2 (m_0c^2), or 1.02 MeV; any additional

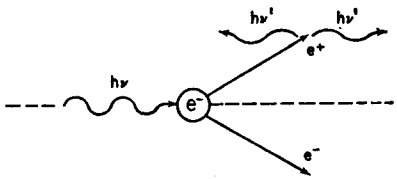

Fig. 63 — Pair-production mechanism.

energy is transferred as kinetic energy. When the positron is annihilated, two photons are produced 180 degrees apart, each with an energy of 0.51 MeV. The photons are then subject to the normal probabilities of interaction with the scintillator.

In neutron detection, unlike alpha- or beta-particle or gamma-ray detection, the primary interaction is with the nuclei of the scintillator rather than its atomic electrons. The interaction may consist of scattering or absorption; in either case, some or all of the energy of the neutron is transferred to the recoil nucleus which then behaves similarly to an alpha particle.

In each interaction between a form of ionizing radiation and a scintillator, an electron having some kinetic energy is produced. A secondary process follows which is independent of both the kind of ionizing radiation incident on the scintillator and the type of interaction which occurred. In this secondary process, the kinetic energy of the excited electron is dissipated by exciting other electrons from the valence band in the scintillator material into the conduction band. When these excited electrons return to the valence band, some of them generate light or scintillation photons. The number of photons produced is essentially proportional to the energy of the incident radiation. In the photoelectric interaction described above, all of the incident

photon energy is transferred to the excited electrons; therefore, the number of photons produced in this secondary process, and hence the brightness of the scintillation, is proportional to the energy of the incident photon.

Scintillation Mechanism

The exact mechanism of the scintillation or light-producing process is not completely understood in all types of materials; however, in an inorganic scintillator, the phenomenon is known to be caused by the absorption of energy by a valence electron in the crystal lattice and its subsequent return to the valence band. Fig. 64 shows a simplified energy-band diagram of a scintillation crystal. The presence of energy levels or centers between the valence and conduction bands is the result of imperfections or impurities in the crystal lattice. Three types are important: fluorescence centers in which an electron, after excitaton, quickly returns to the valence band with the emission of a photon; quenching centers in which the excited electron returns to the valence band with the dissipation of heat without emission of light; and phosphorescence centers in which the excited electron can be trapped in a metastable state until it can absorb some additional energy and return to the valence band with the emission of a photon. An important process in the transfer of energy to the fluorescence, or activator, centers is the generation of excitons or bound hole-electron pairs. These pairs behave much like hydrogen atoms and, being electrically neutral, can wander freely through the crystal until captured by fluorescence centers. The emission of a photon from a phosphorescence center is a relatively slow or delayed process. Of the three types of centers through which an excited electron can return to the valence band, the first, fluorescence, is that sought for in the preparation of scintillators. The second type, quenching, tends to lessen the efficiency of the scintillator because it does not cause the emission of photons, and the third, phosphorescence, produces an undesirable background glow.

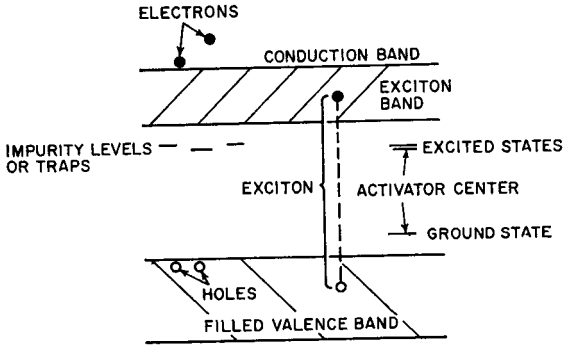

Fig. 64 — A simplified energy-band diagram of a scintillation crystal: (a) electrons in phosphorescence center; (b) electrons in fluorescence center; (c) electrons in quenching center.

Scintillator Materials

The most popular scintillator materials for gamma-ray energy spectrometry is thallium-activated sodium iodide, NaI(Tl). This material is particularly good because its response spectrum contains a well-defined photoelectric peak; i.e., the material has a high efficiency or probability of photoelectric interaction. In addition, the light emitted by the material covers a spectral range from approximately 350 to 500 nanometers with a maximum at about 410 nanometers, a range particularly well matched to the spectral response of conventional photomultipliers, NaI(Tl) does not, however, have a fast decay time in comparison to other scintillators, and, therefore, is generally not used for fast-time resolution. As a comparison, the decay time constant for NaI(Tl) is approximately 250 nanoseconds, while for a fast plastic scintillator the dominant decay time constant is approximately 10 nanoseconds.

The decay time of a scintillator involves the time required for all the light-emitting luminescence centers to return excited electrons to the valence band. In some of the better scintillators the decay is essentially exponential, with one dominant decay time constant. Unfortunately, most scintillators have a number of components each with different decay time.

Collection Considerations

Because scintillations can occur anywhere in the bulk of the scintillator material and emit photons in all directions, there exists the problem of collecting as many of these photons as possible on the faceplate of the photomultiplier. The relative standard deviation in the number of photons arriving at the faceplate of a photomultiplier as a result of a single ionizing event E is given by

$$\text{relative standard deviation} \approx (N_p)^{1/2}/N_p \qquad (97)$$

were N_p is the average number of photons arriving at the faceplate of the photomultiplier per incident ionizing event. N_p is equal to c E ξ, where c is the average number of photons per unit energy for the scintillation, E is the energy of the incident radiation, and ξ is the fraction of the total number of photons produced which arrive at the faceplate of the photomultiplier.

Eq. (97) implies that it is highly desirable that all emitted photons be collected at the photomultiplier faceplate. This collection problem can be simplified by careful selection of the shape and dimensions of the scintillator to match the photomultiplier photocathode dimensions. The coating of all sides of the scintillator except that which is to be exposed to the photomultiplier faceplate with a material which is highly reflective for the wavelengths of the photons emitted by the scintillator also proves helpful. Because NaI (Tl) is damaged by exposure to air, it is usually packaged in an aluminum case lined with highly reflective Al_2O_3 powder; the NaI(Tl) scintillator is provided with an exit window of glass or quartz. To avoid total internal reflection, it is important that the indices of refraction of the scintillator material, its window, any light guide, and the photomultiplier faceplate match as closely as possible.

If it is not convenient for the photomultiplier to be directly coupled to the scintillator, as when the photomultiplier entrance window is

not flat, light guides can be used. Again, care should be taken in designing the light guide to assure maximum light transmission. The outer side or surface of the light guide should be polished and coated with a highly reflective material. In some cases, a flexible fiber-optics bundle can be used. An optically transparent silicone-oil coupling fluid should be applied at the scintillator (-light guide, if used)-photomultilier interface regardless of the light-conduction method used.

The next important consideration in scintillation counting is the conversion of the photons to photoelectrons in the photocathode. The photocathode should have the greatest quantum efficiency possible over the spectral range defined by the spectral emissivity curve of the scintillator. The method of determining the quantum efficiency of a photocathode as a function of wavelength is explained in the section on **Basic Performance Characteristics.** The bialkali photocathode K_2CsSb provides the highest quantum efficiency (approximately 30 per cent at 385 nanometers) of all photocathodes presently available for matching to most scintillators.

The uniformity of the photocathode, i.e., the variation in quantum efficiency at a given wavelength as a function of position on the photocathode, is also important. Because the number of photoelectrons emitted for a constant number of photons incident on the photocathode is proportional to the quantum efficiency, any variation in quantum efficiency as a function of position results in an undesirable variation in the number of photoelectrons emitted as a function of position.

When the scintillation is fairly bright, i.e., when a large number of photons are produced per scintillation, and when the scintillator is thick in comparison to its diameter, as shown in Fig. 65(a), the photocathode is approximately uniformly illuminated during each scintillation. However, if the scintillator is thin in comparison to its diameter, as shown in Fig. 65(b), or if the scintillation is very weak, the illumination of the photocathode as a function of position is closely related to the position of origin of the scintillation; therefore, photocathode uniformity is much more important when a thin scintillator is used. Photocathode uniformity also becomes more important as the energy of the incident radiation becomes less and the number of photons per disintegration is reduced.

In some photomultipliers, the collection efficiency for photoelectrons decreases near the outer edges of the photocathode; therefore, best results are obtained when the scintillator is slightly smaller in diameter than the photocathode.

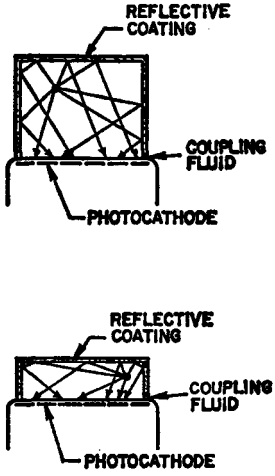

Fig. 65 — Scintillator geometries: (a) thick in comparison to diameter; (b) thin in comparison to diameter.

Multiplier Considerations

The two multiplier configurations most commonly used in photomultipliers in scintillation-counter applications are the venetian-blind and focused (either in-line or circular-cage) structures. The advantage of the venetian-blind structure is that the useful portion of the first dynode area is quite large in comparison to the photocathode area. On the other hand, the focused structure has a small first-dynode area and, therefore, requires a more complex front-end design to provide good collection efficiency. However, a well designed focused structure, although more complex, can provide a better collection efficiency than the venetian-blind structure. In addition, the focused structure is several times faster than the venetian-blind type, as discussed in the section on **Principles of Photomultiplier Design.**

Significant Photomultiplier Characteristics

Photomultiplier dark noise is of particular importance in scintillation-counting applications when the energy of the ionizing radiation is small, or when very little energy is transferred to the scintillation medium; in short, when the flash per event represents only a few photons. If a photomultiplier is coupled to a scintillator and voltage is applied, the composite of all noise pulses coming from the photomultiplier is referred to as the background of the system. The plot of a frequency distribution of these pulses as a function of energy is shown in Fig. 66. The well-defined peaks seen in the figure are caused by external radiations and can be reduced by placing the photomultiplier and scintillator in a lead or steel vault to reduce background radiation.

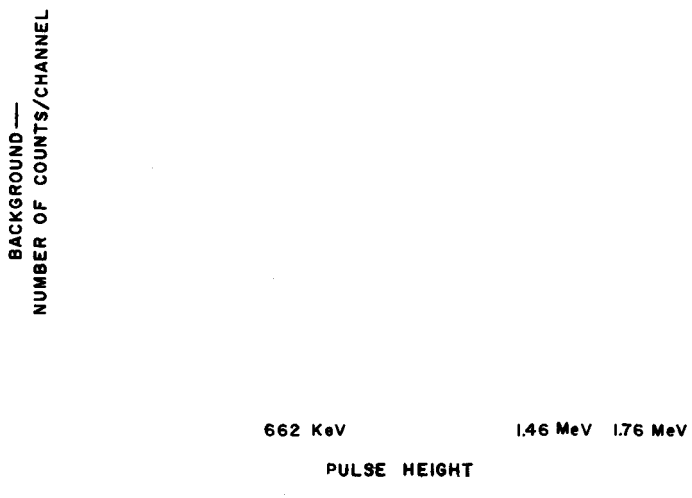

Fig. 66 — Distribution of radiation background pulses as a function of energy. A calibration spectrum showing the Cs^{137} photopeak is included for reference.

It is desirable that the background of the scintillation counter be as low as possible. Photomultipliers have been developed in which the background is kept low by the use of radioactively clean metal cans in-

liquid scintillation counting has developed rapidly. The beta-ray energies from these radioisotopes may vary over a fairly broad range; for example, H^3 emits betas with energies varying from zero to a maximum

scintillator. The three most commonly used radioisotopes in liquid scintillation counting are tritium, H^3; carbon, C^{14}; and phosphorus, P^{32}. Because these elements are the most suitable radioactive tracers used in biological experiments, the field of

by the following equation:

$$C = \frac{2N_1N_2\tau}{60} \qquad (98)$$

where C is the chance coincidence rate per minute, N_1 is the dark-noise count rate in counts per minute from tube No. 1, N_2 is the dark-noise count

* Registered Trade Name for General Electric Co. material.

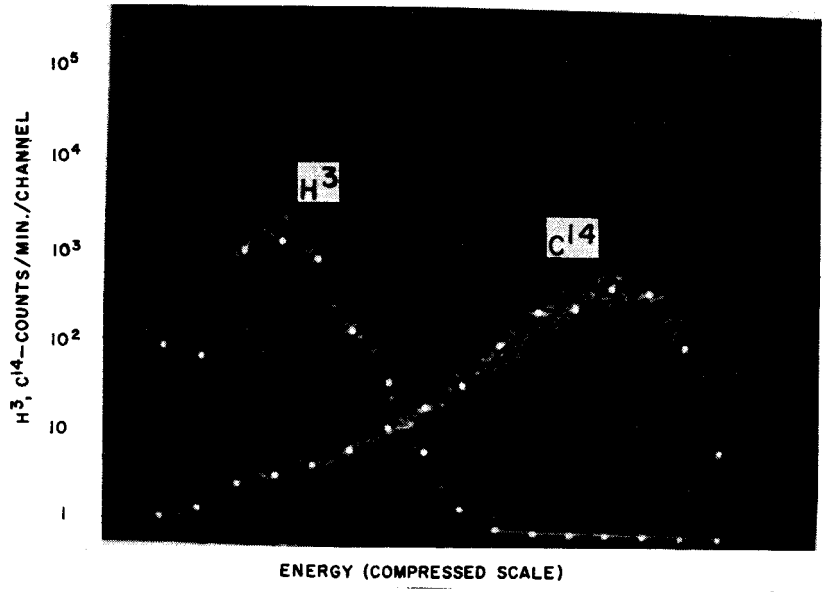

Fig. 67 — Scintillation count showing distribution of beta-ray energies.

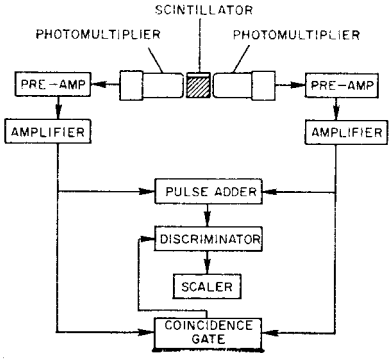

Fig. 68 — Block diagram of a liquid-scintillation spectrometer.

rate in counts per minute from tube No. 2, and τ is the resolving time of the coincidence circuit in seconds.

In a liquid-scintillation spectrometer employing two tubes with dark-noise ratings of 30,000 counts per minute each and a coincidence circuit having a resolving time of 10 nanoseconds, the number of accidental coincidences is approximately 0.3 count per minute. Scintillations resulting in at least one photoelectron being emitted from the photocathode of each tube should produce a signal pulse from the coincidence circuit. Because a scintillation of at least two photons is required to initiate a pulse from both photomultipliers, the over-all detection efficiency for both tubes together is slightly lower than for a single tube having a very low background count rate.

When a vial filled only with a scintillator is placed between the photomultipliers, and the output from the coincidence circuit is examined by use of a multichannel analyzer, a pulse-height distribution such as that shown in Fig. 69 is obtained. Clearly, not many of the background pulses shown are caused by the accidental coincidences of dark-noise pulses from the photomultipliers, but are caused by cosmic rays or scintillations in the material of the vial and photomultiplier envelope resulting from the presence of radioisotopes in the materials of which they are constructed. Light originated internally in either photomultiplier and trans-

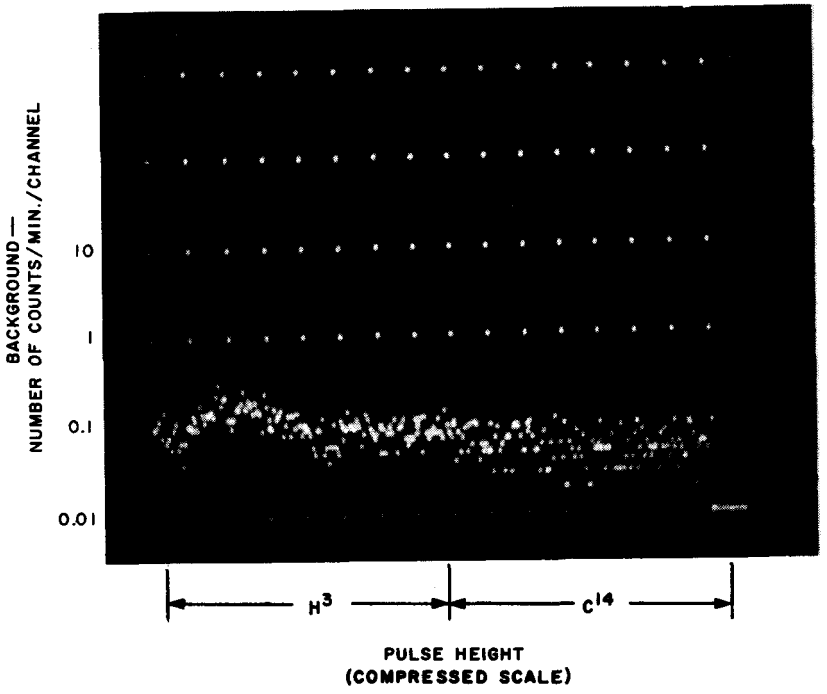

Fig. 69 — Background distribution obtained from a liquid scintillator using a coincidence system.

mitted to the other also causes background pulses; this phenomenon is sometimes referred to as crosstalk.

The counting efficiency E for a liquid scintillation counter is defined in per cent as follows:

$$E = \frac{\text{(counting rate from coincidence circuit)-(background)}}{\text{disintegration rate of sample}} \times 100 \quad (99)$$

The best counting efficiency for a given radioisotope is obtained when a highly efficient scintillator and a photomultiplier with a high quantum efficiency in the spectral emissivity range of the scintillator are used. The optical system containing the two photomultipliers and the counting vial is also of major importance; it should be designed so that, as far as possible, the photons produced in a scintillation are equally divided between the photomultipliers. This division assures that a coincidence pulse results from as many scintillations as possible. In some cases, two or more different isotopes may be counted simultaneously; therefore, it is desirable that the photomultipliers have matched gains and good energy (pulse-height) resolution capability to provide best isotope separation.

A figure of merit E^2/b has been developed to aid in the evaluation of systems used in liquid scintillation counting; E is the counting efficiency of the system for a given isotope, and b is the background of the system in an energy range including the energy range of pulses from the radioisotope. The figure of merit is, however, not necessarily the best way of evaluating all systems. It is valid at very low counting rates where the background is the dominant factor, but is not of great help at high counting rates where the background of the system becomes less important than the efficiency in determining the merit of the system.

In selecting a photomultiplier tube for a liquid-scintillation application, the following items are of major importance: high photocathode quantum efficiency, low dark-noise count rate, minimum internal-light generation, low radioactive-background envelope, low scintillation-efficiency envelope, fast time response, and good energy resolution. The RCA-4501V3 photomultiplier has been specifically designed to meet these requirements.

Cerenkov Radiation Detection

Cerenkov radiation is generated when a charged particle passes through a dielectric with a velocity greater than the velocity of light in the dielectric (i.e., v greater than c/n, where n is the index of refraction of the dielectric). Polarization of the dielectric by the particle results in the development of an electromagnetic wave as the dielectric relaxes. If the velocity of the particle is greater than the velocity of light, constructive interference occurs and a conical wavefront develops, as illustrated in Fig. 70. Cerenkov radiation is the electromagnetic counterpart of the shock wave produced in a gas by an object traveling faster than sound. It is highly directional, and occurs mostly in the near-ultraviolet part of the electromagnetic spectrum. Because the radiation is propagated in the forward direction of motion of the charged particle, as shown in Fig. 70, Cerenkov detectors can be made to detect only those particles that enter the system from a restricted solid angle.

Cerenkov radiation produced in an aqueous solution by beta emitters can be useful in radioassay techniques because it is unaffected by

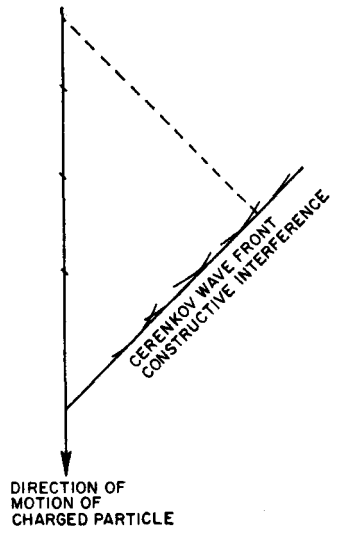

Fig. 70 — Diagram of the Cerenkov radiation mechanism.

chemical quenching and because it offers the advantages, over liquid-scintillation counting techniques, of simplified sample preparation and the ability to accommodate large-volume samples. Because a fast particle is required to produce Cerenkov radiation, rather high-energy beta rays are required; e.g., the threshold for Cerenkov radiation is 261 keV for electrons in water. Because the photon yield for Cerenkov light is usually very low, the same considerations concerning photomultiplier selection apply for the Cerenkov detection as for liquid-scintillation counting. The tube selected should also be equipped with a faceplate capable of good ultraviolet transmission.

Time Spectroscopy

In addition to the energy spectroscopy described above, there are occasions when it is of advantage to measure time differences such as between a pair of gamma rays or a combination of gamma rays and particles in cascade de-exciting some level in a nucleus. In time spectroscopy, some special considerations must be made in selecting the scintillator, photomultipliers, and technique of analyzing the signals from the photomultipliers.

In a photomultiplier, time resolution is proportional to $(\bar{n})^{-1/2}$, where $\bar{n}$ is the average number of photoelectrons per event. It is therefore important to choose a scintillator material that provides a high light yield for a given energy of detected radiation. It is also important that the variation of the time of interaction of the radiation with the scintillator be as small as possible. This minimum variation is assured by attention to scintillator thickness and source-to-detector geometry. The decay time constant of the light-emitting states in the scintillator should be as short as possible, and the geometry and reflective coatings of the scintillator should be selected so that variations in path lengths of photons from the scintillator to the photocathode of the photomultiplier are minimized. The photocathode of the photomultiplier selected should have a high quantum efficiency. In addition, the transit-time dispersion or jitter (variations in the time required for electrons leaving the photocathode to arrive at the anode of the tube) should be small over the entire photocathode area.

The major contribution to transit-time spread occurs in the photocathode-to-first-dynode region and may be a result of the initial kinetic energies of the emitted photoelectrons and their angle of emission. Focusing aberrations, and the single-electron response or rise time, i.e., the output-pulse shape at the anode

for a single photoelectron impinging on the first dynode, may also be of some importance. Although the single-electron response theoretically does not have much effect on time resolution, it does change the triggering threshold at which the best time resolution can be obtained.

The most commonly used time-spectroscopy techniques include leading-edge timing, zero-crossover timing, and constant-fraction-of-pulse-height-trigger timing; the technique used depends on the time resolution and counting efficiency required and the range of the pulse heights encountered. A block diagram of a basic time spectrometer is shown in Fig. 71.

Leading-edge timing makes use of a fixed threshold on the anode-current pulse and provides good time resolution over a narrow range of pulse heights. The fractional pulse height F at which the triggering threshold is set is defined as follows:

$$F = \frac{V_t}{V_a} \qquad (100)$$

where V_t is the discriminator threshold, and V_a is the peak amplitude of the anode-current pulse. The fractional pulse height has a considerable effect on the time resolution obtained; best results are usually obtained with F equal to 0.2.

In fast zero-crossover timing, the anode pulse is differentiated twice. This double-differentiation produces a bipolar output pulse that triggers the timing discriminator at the zero crossover, the time required to collect approximately 50 per cent of the total change in the photomultiplier pulse. Zero-crossover timing is second to leading-edge timing for time-resolution work with narrow pulse-height ranges, but is better than the leading-edge method for large pulse-height ranges.

In constant-fraction triggering, the point on the leading edge of the anode-current pulse at which leading-edge timing data indicate that the best time resolution can be obtained is used regardless of the pulse height. For this reason, constant-fraction-of-pulse-height timing is the best method

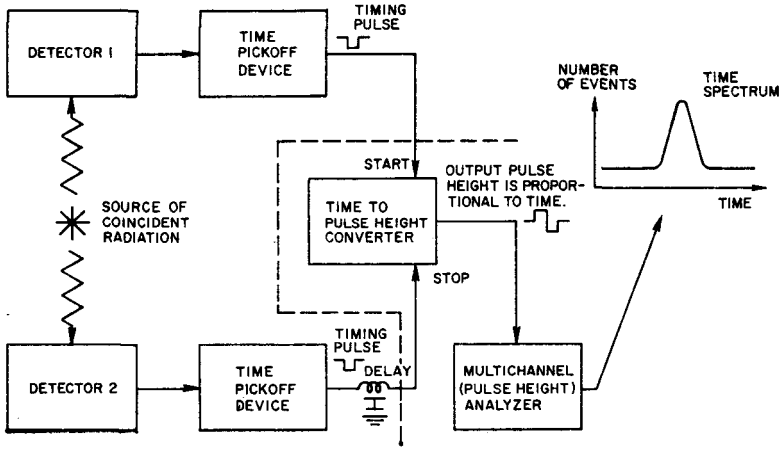

Fig. 71 — Generalized block diagram of a time spectrometer.

for obtaining optimum time resolution no matter what the pulse-height range.

Interpretation of Counting Data

A number of techniques can be used to interpret the data obtained from a scintillation counter; one of the most popular employs a multichannel analyzer. The analyzer sorts the pulses according to their amplitude and records the number of pulses in a "channel" whose position is proportional to the amplitude of the pulse. Many pulses are analyzed in this manner and a frequency distribution of pulse heights is obtained. Fig. 72 shows a pulse-height distribution for a scintillation counter counting pulses from a sample of Cs^{137}.

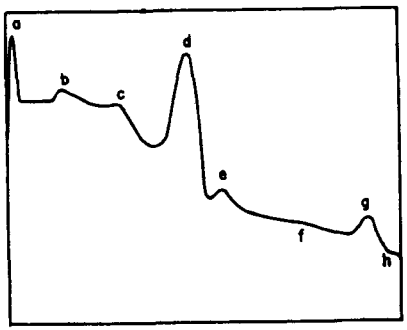

a. 32 keV Barium x-ray line.
b. Backscatter peak.
c. Compton edge.
d. Photopeak, cesium 137, 0.662 MeV.
e. 749 keV photopeak of cesium 134 impurity.
f. Continuum due to accidental self-coincidences producing partial sum pulses.
g. Accident sum coincidence peak.
h. Detail due to background radiation.

Fig. 72 — Pulse-height distribution for a scintillation counter counting pulses from a sample of Cs^{137}.

LASER RANGE FINDING

A simplified block diagram of a laser range finder is shown in Fig. 73. The interference filter is used to pass the wavelength of radiant energy of the laser with a minimum of background radiation. Photomultipliers used in laser range finding may have a relatively small photocathode, but they must exhibit high quantum efficiency, low dark noise, and fast rise time or an equivalent large bandwidth. Most photomultipliers can provide bandwidths exceeding 100 MHz and at the same time maintain relatively large output signals. The bandwidth of a photomultiplier can be limited by the RC time constant of the anode circuit.

The range of a laser-range-finding system depends on system parameters and operational environment. The maximum range of a given system may be signal-photon limited or background limited. The photon-limited case exists when the background and detector noise can be considered negligible. The maximum range in this case is determined by the signal-to-noise ratio in the photoelectron pulse corresponding to the scattered laser return beam. As noted in the section on **Statistical Fluctuation and Noise,** the signal-to-noise ratio of such a pulse is proportional to the square root of the product of the number of incident photons on the photomultiplier and the quantum efficiency of the photoelectric conversion. If the atmospheric attenuation is neglected and it is assumed that the laser spot falls entirely within the target, the maximum range in this case would be increased as the square root of the quantum efficiency of the photocathode. This increase follows because the number of photons collected by the aperture of the receiving

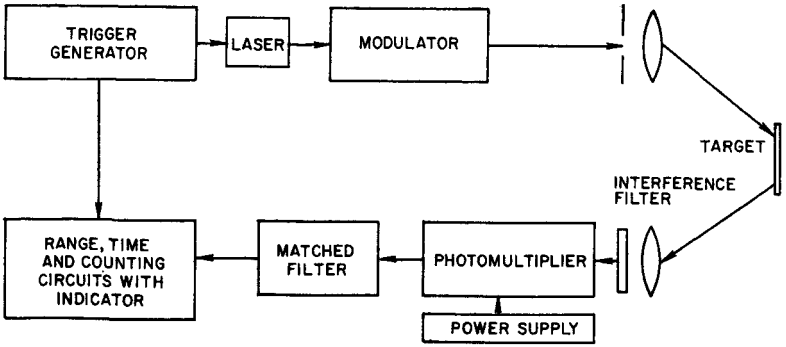

Fig. 73 — Simplified block diagram of a laser range finder.

system varies inversely as the square of the distance from the target. Recent improvements in the multialkali photocathode, resulting in the ERMA cathode, described in the section on **Photoemission and Secondary Emission,** have increased the quantum efficiency at 860 nanometers from 0.01 per cent to 1.5 per cent. In terms of laser range in the photon-limited case, this quantum-efficiency improvement implies more than a 10-to-1 range increase. The use of a GaAs photocathode is even more promising at this wavelength.

In cases where the laser pulse must be detected against the background of a daylight scene, it is said to be background limited. If atmospheric attenuation again is neglected, the signal is proportional to the number of incident photons times the quantum efficiency of the photocathode. The number of incident photons from the return beam is inversely proportional to the square of the range, again assuming that the target is larger than the laser spot. The noise, however, is independent of the range and is determined by the square root of the product of the incident background radiation and the quantum efficiency. Thus, to a first approximation the range is increased in the background-limited case only by the fourth root of the quantum efficiency. Because the photomultiplier current caused by the background radiation is proportional to the solid angle of the scene from which the photomultiplier collects radiation, the background current in the photomultiplier may be minimized by the use of a photocathode having a small area or by the use of a limiting aperture on the faceplate of the photomultiplier. No loss in collected laser light need result because the return beam may generally be considered as originating from a point source. The system aperture, of course, must be large enough to avoid optical alignment problems.

FLYING-SPOT SCANNING

An important application for which photomultipliers are particularly well suited is flying-spot scanning, a system for generating video signals for television display from a photographic transparency. The elements of a flying-spot scanning system are shown in Fig. 74. A cathode-ray tube, in conjunction with its power supplies and deflection cir-

cuits, provides a small rapidly moving light source which forms a raster on its face. This raster is focused by the objective lens in the optical system onto the object being scanned, a slide transparency or a motion-picture film. The amount of light passing through the film varies with the film density. This modulated light signal is focused upon the photomultiplier by means of the condensing-lens system; the photomultiplier converts the radiant-energy signal into an electrical video signal. The amplifier and its associated equalization circuits increase the amplitude of the video signal as required.

The flying-spot scanning system is capable of providing high-resolution monochromatic performance. With the addition of (a) appropriate dichroic mirrors which selectively reflect and transmit the red, blue, and green wavelengths, (b) two additional photomultipliers with video amplifiers, and (c) appropriate filters, color operation is possible. In color operation, the primary wavelengths are filtered after separation by the light-absorbing filters before being focused upon each of three photomultipliers, one for each color channel. The output of each photomultiplier is then fed to a separate video amplifier.

Flying-spot video-signal generators are used in the television industry primarily for viewing slides, test patterns, motion-picture film, and other fixed images. Systems have been developed for the home-entertainment industry that allow slides and motion-picture film to be shown on the picture tube of any type of commercial television receiver.

Cathode-Ray Tube

Several important considerations must be taken into account if the cathode-ray tube in the system is to produce a light spot capable of providing good resolution. The cathode-ray tube should be operated with as small a light spot as possible. The cathode-ray-tube faceplate should be as blemish-free as possible and the tube should employ a fine-grain phos-

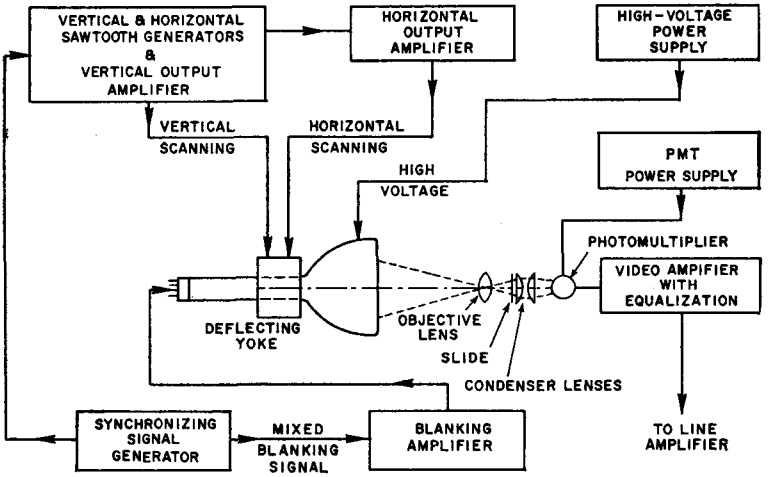

Fig. 74 — Elements of a flying-spot scanning system.

phor; blemishes adversely affect signal-to-noise performance and contribute to a loss of resolution.

The spectral output of the cathode-ray-tube phosphor should match the spectral characteristic of the photomultiplier. This match can be rather loose in a monochromatic flying-spot generator; however, the spectral output of the phosphor of the cathode-ray tube used in a three-color version must include most of the visible spectrum. Phosphors used in monochromatic systems may provide outputs in the ultraviolet region of the spectrum and still perform satisfactorily. Phosphors such as P16 and P15, when used with an appropriate ultraviolet filter, display the necessary short persistence required in a monochromatic system.

The visible portion of the P15 or P24 phosphor is used in color systems. The P15 and P14 phosphors are, however, much slower than the P16 phosphor and cause a lag in buildup and decay of output from the screen.

The phosphor lag results in trailing, a condition in which the persistence of energy output from the cathode-ray tube results in a continued and spurious input to the photomultiplier as the flying spot moves across the picture being scanned. The result is that a light area may trail into the dark area in the reproduced picture.

Similarly, the lag in buildup of screen output causes a dark area to trail over into the light area. The result of these effects on the reproduced picture is an appearance similar to that produced by a video signal deficient in high frequencies; consequently, high-frequency equalization is necessary in the video amplifier.

Objective Lens

The objective lens used in a flying-spot generator should be of a high-quality enlarger type designed for low magnification and, depending upon the cathode-ray-tube light output, should be corrected for ultraviolet radiation. The diameter of the objective lens should be adequate to cover the slide to be scanned. An enlarging f/4.5 lens with a focal length of 100 millimeters is suitable for use with 35-millimeter slides.

Photomultiplier Tube

The spectral characteristics of the photomultiplier (or photomultipliers in the case of the three-color system) and the cathode-ray-tube phosphor should match. Usually an S-4 or S-11 spectral response is suitable for use in a monochromatic system or as the detector for the blue and green channels; an S-20 response is very often utilized for the red channel. The bialkali cathode (K-Cs-Sb) is also well suited for the blue channel. The speed of the detector must be sufficient to provide the desired video bandwidth. Most requirements do not exceed 6 to 8 MHz, a figure well within photomultiplier capabilities.

The anode dark current of the photomultiplier should be small compared to the useful signal current. The signal-to-noise ratio will be maximized by operation of the photomultiplier at the highest light levels possible. If necessary, the over-all photomultiplier gain should be reduced to prevent excessive anode current and fatigue.

The amplitude of the light input is usually a compromise between an optimum signal-to-noise ratio and maximum cathode-ray-tube life, which may be reduced as a result

of loss of phosphor efficiency at high beam-current levels. The signal-to-noise ratio can also be improved by the selection of photomultipliers having the highest photocathode sensitivities possible. However, because the spread of photocathode sensitivities is seldom greater than two or three to one, the improvement afforded by such selection is limited to two or three dB, an improvement difficult to detect while observing a television display but desirable and necessary in some critical applications.

Video Amplifier

Photomultiplier gain need only be sufficient to provide a signal of the required level to the succeeding video-amplifier stages. These stages, in addition to providing the necessary amplification and bandwidth to assure good picture quality, incorporate equalization circuits composed of networks with different time constants. The relatively long decay time of these circuits generally results in appreciable reduction of the useful signal-to-noise ratio. Therefore, the use of short-persistence phosphors is recommended to reduce the required amount of equalization.

In addition to the video amplifier, a gamma-correction amplifier is required in each channel. The gamma-correction amplifier assures maximum color fidelity by making the linearity or gamma of the system unity.

LOW-LIGHT-LEVEL DETECTION

Systems for the detection of low light levels make use of two basic techniques: charge integration, in which the output photocurrent is considered as an integration of the anode pulses which originate from the individual photoelectrons, and the digital technique in which individual pulses are counted.

Charge-Integration Method

In the charge-integration method, either the transit-time spread of the photomultiplier or the time characteristics of the anode circuit cause the anode pulses to overlap and produce a continuous, though perhaps noisy, anode current. The current is modulated by turning the light off and on by means of some mechanical device such as a shutter or light "chopper". The signal becomes the difference between the current in the light-on and light-off conditions.

Detection is limited by noise in the anode current. At low light levels the noise is caused primarily by the fluctuations in dark current of the photomultiplier (as discussed in the sections on **Basic Performance Characteristics** and **Statistical Fluctuation and Noise**). The noise may be minimized by reducing the bandwidth of the measuring system. For example, a dc system may be used with a bandwidth of only a few hertz if an appropriate low-level current meter is selected. Bandwidth can also be reduced by some technique of averaging the current fluctuations over a period of time.

Another technique of charge integration is to chop the light signal with a motor-driven chopper disk having uniformly spaced holes or slots. The output current is then fed through an amplifier having a narrow bandwidth tuned to the frequency of chop. Bandwidths of the order of 1 Hz are typical.

The earlier discussions on **Equivalent Noise Input** and on **Noise Formulas Relative to Photomultipliers** contain the information neces-

sary to evaluate the performance of photomultipliers in the charge-integration method.

Digital Method

In the digital method for the detection of low light levels a series of output pulses, each corresponding to a photoelectron leaving the photocathode of a photomultiplier, appears at the anode. All of the output pulses from the tube are shaped by a preamplifier before they enter a pulse-amplitude discrimination circuit. Only those pulses having amplitudes greater than some predetermined value and having the proper rise-time characteristics pass through to the signal-processing circuits. The digital technique is superior to charge integration at very low light levels because it eliminates the dc leakage component of the dark current as well as dark-current components originating at places other than the photocathode. Fig. 75 shows a digital system in block form.

In the special case in which the digital technique is used to count single photons incident upon the photocathode of a photomultiplier, signal pulses appear at the anode with an average pulse amplitude PH equal to $e\bar{m}$, where e is the electron charge and $\bar{m}$ is the photomultiplier gain. The number of signal pulses N_a arriving at the anode is given by

$$N_a = N_p \eta\lambda \qquad (101)$$

where N_p is the number of photons incident on the photocathode window, and $\eta\lambda$ is the quantum efficiency of the photocathode at the photon wavelength including a factor for the loss of light by reflection and absorption, and a factor for the loss resulting from imperfect electron-collection efficiency of the front end of the photomultiplier.

The dark-noise pulses present in addition to the signal pulses originate mainly from single electrons and have a pulse-height distribution as shown in the simplified dark-noise pulse-height-distribution spectrum of Fig. 76. Region A of Fig. 76 includes circuit-originated noise, some

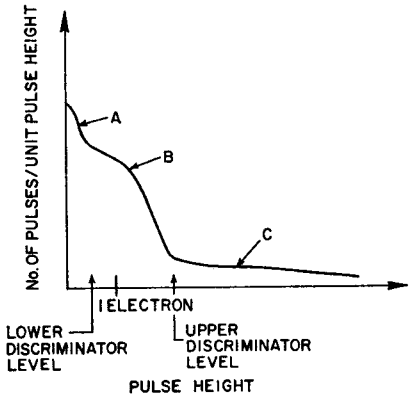

Fig. 76 — Dark-noise pulse-height-distribution spectrum.

single-electron pulses, and pulses caused by electrons originating at the dynodes in the multiplier section.

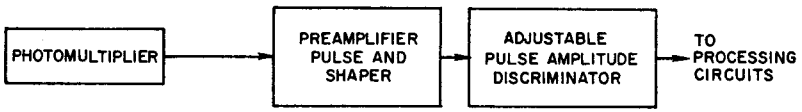

Fig. 75 — Block diagram illustrating a digital system for detection of low light levels.

Pulses originating at the dynodes exhibit less gain than the single-electron pulses from the cathode. Region B represents the single-electron pulse-height distribution and is the region in which the single-photon signal pulses appear. Region C is caused by cosmic-ray muons, afterpulsing, and radioactive contaminants in the tube materials and in the vicinity of the tube. To maximize the ratio of signal pulses to noise pulses in single-photon counting, lower- and upper-level discriminators should be located as shown in the figure.

If the rate of photon arrival is I_p, the net quantum efficiency is η, and the counting interval is τ, the number of signal pulses is $I_p\eta\tau$. The rate of single-electron dark pulses is referred to as I_d. At the limit of detection the number of dark pulses will greatly exceed the pulses which are photon originated. Two counts must be made, one with the light on and one with it off. The difference in the number of counts is the signal, $I_p\eta\tau$, in numbers of electrons for the count interval. The variance for this measurement is given by

$$\sigma^2 = I_p \eta \tau + I_d \tau + I_d \tau \quad (102)$$

The reason for the double entry of the variance for the dark counts $I_d\tau$ is that the determination involves the subtraction of the light-on and light-off counts. If it is assumed that the number of dark pulses greatly exceeds the light-originated pulses, the signal-to-noise ratio is given by the following expression:

$$\mathrm{SNR} = \frac{I_p \eta \tau^{\frac{1}{2}}}{[2I_d]^{\frac{1}{2}}} \quad (103)$$

(The section on **Statistical Fluctuation and Noise** contains a further discussion of the statistics of photon counting.)

The signal-to-noise ratio may be improved by the square root of the time of count. Increasing the time of count is analogous to decreasing the bandwidth in the charge-integration method. The signal-to-noise ratio can also be improved by a square-root factor by decreasing the number of dark-noise pulses. Because these pulses originate at the photocathode surface, the number can be reduced by reducing the area of the photocathode or by reducing the effective photocathode area by using electron optics to image only a small part of the photocathode on the first dynode. It may also be desirable to cool the photomultiplier and thereby reduce the thermionic emission from the photocathode (as discussed in the section on **Basic Performance Characteristics**).

Very-Low-Light-Level Photon-Counting Technique

Before beginning very-low-light-level photon counting, the following special precautions must be taken:

1. The power supply and interconnecting circuits must have low-noise characteristics.

2. The optical system must be carefully designed to minimize photon loss and to prevent movement of the image of the object on the photocathode, a possible cause of error if the cathode is non-uniform. It is generally good practice to defocus the image on the photocathode, especially in the case of a point source, to minimize problems which may result from a non-uniform photocathode.

3. The photomultiplier must be allowed to stabilize before photon

counting is begun. The tube should not be exposed to ultraviolet radiation before use and should, if possible, be operated for 24 hours at the desired voltage before the data are taken.

4. The photomultiplier should be operated with the cathode at ground potential if possible. If the tube is operated with the photocathode at negative high voltage, care must be taken to prevent the glass envelope of the tube from coming into contact with conductors at ground potential or noisy insulators such as bakelite or felt. Without this precaution, a very high dark noise may result as well as permanent damage to the photocathode.

5. Large thermal gradients must not be permitted across the tube as it is cooling. In addition, care must be taken to avoid excessive condensation across the leads of the tube or on the faceplate.

Photomultiplier Selection for Photon Counting

In the selection of a photomultiplier for use in photon counting, several important parameters must be considered. First, and most important, the quantum efficiency of the photocathode should be as high as possible at the desired wavelength. To minimize the thermionic dark-noise emission, the photocathode area should be no larger than necessary for signal collection; the multiplier structure should utilize as large a fraction as possible of the electrons from the photocathode. The over-all tube should have as low a dark noise as possible. In some applications, the rise time and time-resolution capabilities of the tube may also be important.

A number of more recent developments in photomultiplier design are of considerable significance in photon counting. These developments fall into two major categories, secondary-emission materials and photocathodes. Because of the superior statistics of gallium phosphide (one of the more recently developed secondary-emission materials discussed in the section on **Photoemission and Secondary Emission**), a tight single-electron distribution curve can be obtained, as shown in Fig. 77. The tight distribution permits easy location of the pulse-height discriminator, as is particularly evident when some

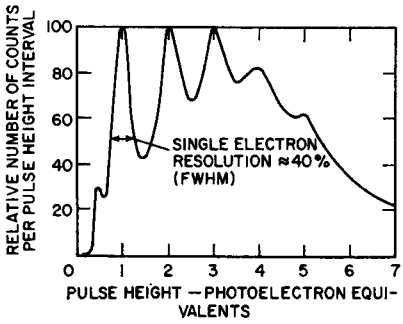

Fig. 77 — Single-electron distribution curve taken with a photomultiplier having a gallium phosphide first dynode.

of the signal pulses are originated by two or more photoelectrons leaving the cathode simultaneously. If the average number of photoelectrons leaving the photocathode per pulse were three, a pulse-height distribution similar to that shown in Fig. 78 would be obtained. Gallium phosphide provides a higher signal-to-noise ratio than would conventional secondary-emitting materials such as BeO or Cs_3Sb when used in the same tube.

Photocathode developments include ERMA (Extended Red Multi-Alkali), a semitransparent photocathode having a response to 900

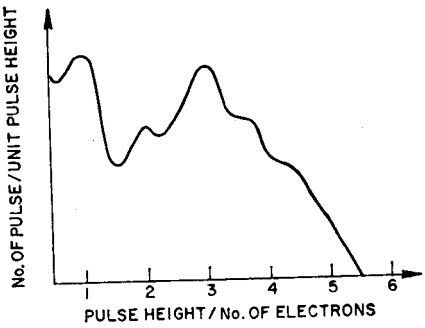

Fig. 78 — Pulse-height distribution obtained with a photomultiplier having a gallium phosphide first dynode. Light level is such that three photoelectrons per pulse time is the most probable number.

nanometers, and several negative-electron-affinity materials. Perhaps the most significant of these materials is indium gallium arsenide, whose threshold wavelength increases with increasing indium content. Spectral-response curves for some of the more recent photocathodes are shown in the section on **Basic Performance Characteristics.**

PHOTOMETRIC APPLICATIONS

Photometry is concerned with the measurement of luminous intensity and other parameters related to the radiant energy which produces visual sensation. Photometric units and conversion from radiant power are discussed in a later section of this Manual. Photometric measurements may be made either by visual comparison or by more accurate photoelectric methods. This section discusses some of the applications of photomultipliers in photometry.

Spectrophotometry

Spectrophotometers measure the optical density of materials as a function of wavelength and require photomultipliers having a broad spectral range. The results of measurements of the absorption characteristics of substances are frequently expressed in terms of optical density. This logarithmic method correlates with the way the human eye discriminates differences in brightness.

The transmission density D is defined by

$$D = \log_{10} \frac{P_o}{P_t} = \log_{10} \frac{1}{T} \qquad (104)$$

where P_o is the radiant flux incident upon a sample, P_t is the radiant flux transmitted by a sample, and T is the transmission figure or P_t/P_o. Density measurements are useful in various applications to films and other transparencies in addition to chemical analysis where concentration of a solution is studied as a function of wavelength.

Color-Balancing Photometry

A color-balancing photometer is used to determine color balance and exposure times necessary to produce photographic color prints from color negatives. Such a device is shown in block diagram form in Fig. 79; it allows the matching of the relative proportions of red, blue, and green light transmitted by a production negative to those of a master color negative. As the first step in the matching process, the master negative is used to make an acceptable print. This first print is produced through trial and error by measurement of the relative proportions of red, blue, and green light transmitted through a key area of the master negative; the key area usually consists of a flesh tone or a gray area. The amount of light transmitted is

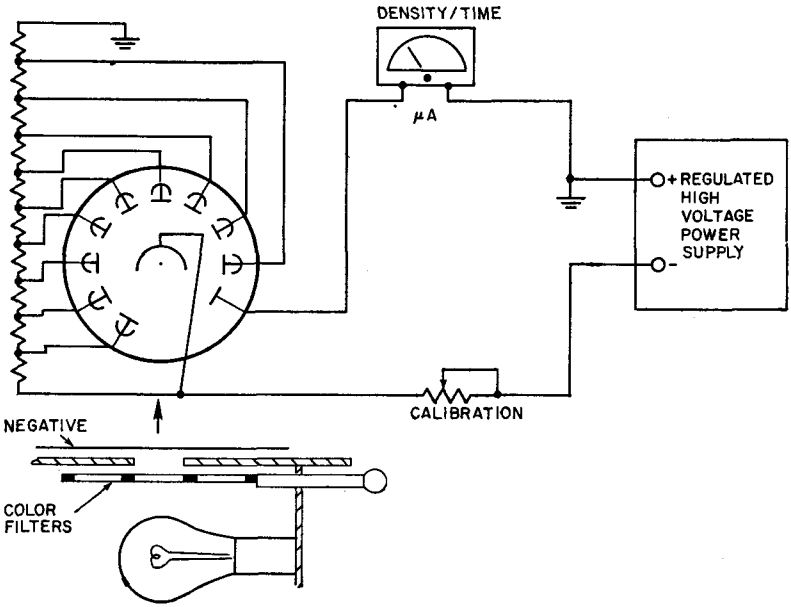

Fig. 79 — Block diagram of a color-balancing photometer.

a measure of the density. The exposure time using white light and the lens opening used to obtain the satisfactory print are noted.

Next, an area of the production negative similar to that on the master negative is chosen and the relative proportions of the red, blue, and green light transmitted are measured again. By use of magenta and yellow correcting filters, the color transmitted by the production negative can be balanced with that of the master negative. When the production negative is used, the lens opening is adjusted so that the exposure time with white light is the same as it was for exposure of the master negative. When the values of color-correcting filters and exposure times thus determined are used, prints from the production negative can be obtained which are very nearly as good as those obtained with the master color negative.

Most color-balancing photometers employ steady light sources and handle small-amplitude signals. Consequently, the photomultiplier used must have low values of dark current and good stability. The life expectancy of tubes used in this application is long because the small signal levels reduce the effects of fatigue which might otherwise adversely affect measurement accuracy and repeatability. Low-current operation also provides for linear operation where the anode current is proportional to the input flux over the range of transmission values measured. The intensity range of a color-balancing photometer, given in terms of the ratio of the radiant flux incident upon a sample to the radiant flux transmitted by a sample, is usually of the

order of 1000 to 1 or more. It must be remembered that as in most photomultiplier applications, the power supplies used must be capable of providing voltages sufficiently regulated and free from ripple to assure minimum variation in sensitivity with possible line-voltage variation.

Densitometry

A second example of the use of the equivalent photoelectric method in photometry measurements is in densitometry, or the measurement of diffuse transmission density.

Although techniques such as those employed in the color-balancing photometer may be used successfully to measure density over an intensity range of 10 or 100 to 1 (density 1 to density 2), their use becomes increasingly difficult as the range is increased to 1000 to 10,000 to 1 (density 3 to density 4) or more. The large dynamic ranges encountered in color-film processing place severe requirements upon the photomultiplier because it must be operated in a constant-voltage mode. Problems develop in this mode at high-density values at which the dark current may become a significant proportion of the signal current. The random nature of this dark current, which precludes its being "zeroed out", may lead to output-signal instability. As a result of the type of operation needed to produce the dynamic range required in density measurements, the photomultiplier anode current is high at low density values. These high currents may result in excessive fatigue, and, depending upon the operating point, perhaps non-linear operation. As with the color-balancing photometer, a well regulated low-ripple power supply is needed to assure accurate measurements.

Logarithmic Photometry

In the measurement of absorption characteristics, the changes in brightness levels vary over such a large range that it is advantageous to use a photometer whose response is approximately logarithmic. This response enables the photometer to be equipped with a meter or read-out scale that is linear and provides precise readings even at high optical densities.

A simplified circuit of a logarithmic photometer capable of measuring film density with high sensitivity and stability and of providing an appropriate logarithmic electrical response and linear meter indication of density over three or four density ranges is shown in Fig. 80.

The circuit of Fig. 80, in which the photomultiplier operates at a constant current, minimizes photomultiplier fatigue and eliminates the need for a regulated high-voltage supply. The feedback circuit illustrated develops a signal across R1 proportional to the anode current. This signal controls the bias applied to the control tube and automatically adjusts the current in the voltage-divider network. By this means, the dynode voltage is maintained at a level such that the anode current is held constant at a value selected to minimize the effects of fatigue. At optical densities of 3, the dynode supply voltage may be 1000 volts; at optical densities of less than 1, the dynode voltage may be as low as 300 volts. Dynode voltage is translated into density by means of the scale on voltmeter V1.

Because there is an approximately exponential variation of sensitivity of a photomultiplier with applied voltage (as discussed in the section on **Basic Performance Characteristics**) in a constant-current

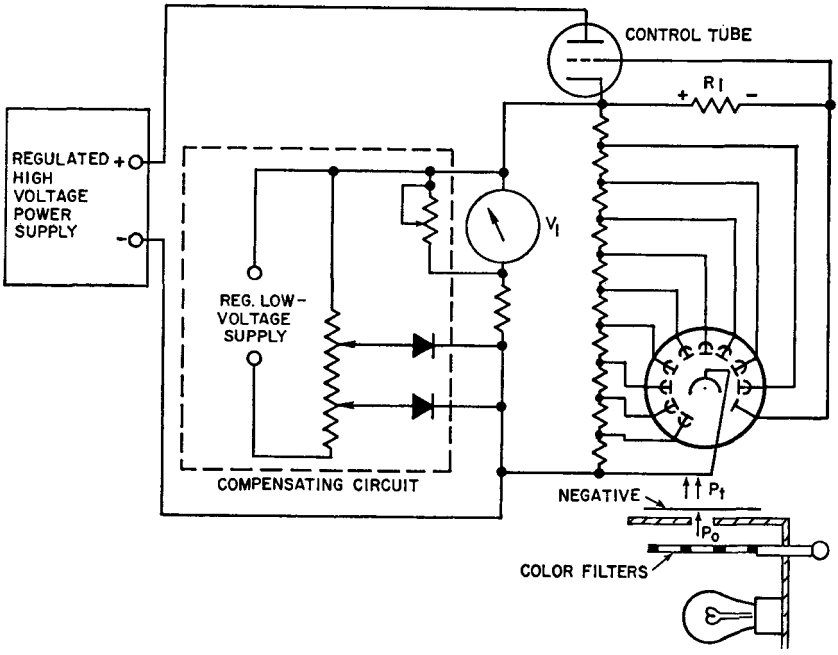

Fig. 80 — Block diagram of a logarithmic photometer.

mode, the voltage becomes a logarithmic function of the input light flux and thus a linear measure of density.

In photometric equipment, the relationship between dynode voltage and the logarithm of the incident radiant flux P_o is not quite linear and, consequently, some compensation is required. This compensation is provided in the circuit of Fig. 80 by the incorporation of a variable and automatic shunt across the voltmeter V1. As the density values increase, the effective value of the shunt resistance is reduced. This circuit not only compensates for photomultiplier non-linearity, but also for the non-linearity of the optical system employed so that the measurements obtained through its use will conform to American Standards Association standards for the determination of diffuse density.

SPECTROMETRIC APPLICATIONS

Spectrometry, the science of spectrum analysis, applies the methods of physics and physical chemistry to chemical analysis. Spectrometric applications include absorption, emission, Raman, solar, and vacuum spectrometry, and fluorometry. The uses made of photomultipliers in these applications are described in the following paragraphs.

Absorption Spectrometry

Absorption spectrometry, used to detect radiant energy in the visible,

ultraviolet, and infrared ranges, is one of the most important of the instrumental methods of chemical analysis. It has gained this importance largely as a result of the development of equipment employing photomultipliers as detectors. The principle underlying absorption spectrometry is the spectrally selective absorption of radiant energy by a substance. The measurement of the amount of absorption aids the scientist in determining the amount of various substances contained in a sample.

The essential components of an absorption spectrometer are a source of radiant energy, a monochromator for isolating the desired spectral band, a sample chamber, a detector for converting the radiant energy to electrical energy, and a meter to measure the electrical energy. The spectral ranges of the source and detector must be appropriate to the range in which measurements are to be made; in some cases this range may include one wavelength; in others, it may scan all wavelengths between the near-ultraviolet and the near-infrared.

The side-on photomultiplier has, in general, been the most widely used in spectrometric applications. The side-on tube is relatively small and has a rectangularly shaped photocathode that is compatible with the shape of the light beam from an exit slit. Spectrometric applications require tubes with good stability, high anode sensitivity, low dark current, and broad spectral sensitivity.

Before the development of the new negative-electron-affinity type photoemitters, such as gallium arsenide, it was necessary to use more than one detector in the measurement of radiant energy from the near-ultraviolet to the near-infrared part of the spectrum. A photomultiplier having a gallium arsenide photoemitter can now be used to detect radiant energy from 940 nanometers to the cut-off point of the photomultiplier window in the near-ultraviolet.

Raman Spectroscopy

There are two types of molecular scattering of light, Rayleigh and Raman. Rayleigh scattering is the elastic collision of photons with the molecules of a homogeneous medium. Because the scattered photons do not gain energy from or lose energy to the molecule, they have the same energy $h\nu_0$ as the incident photons. A classic example of Rayleigh scattering of light from gas molecules is the scattering of the sun's light rays as they pass through the earth's atmosphere; the scattering accounts for the brightness and the blueness of the sky.

Raman scattering is the inelastic collision of photons with molecules that produces scattered photons of higher or lower energy than the initial photons. During the collision there is a quantized exchange of energy which, depending on the state of the molecules, determines whether the initial photon gains or loses energy. The differences in energy levels are characteristic of the molecule. If the excitation frequency is ν_1 and the photon emitted after the interaction has a frequency of ν_2, the interaction results in a change in the energy of an initial photon by $h\nu_0$, where $h\nu_0 = |h\nu_2 - h\nu_1|$. When $h\nu_2$ is greater than $h\nu_1$, the initial photon has gained energy from the molecule that was in the excited state; in the reverse case, the initial photon has given up energy to the molecule in the unexcited state.

Early Raman instruments had a number of disadvantages and were difficult to use; it was difficult to

find a stable high-intensity light source and to discriminate against Rayleigh scattering of the exciting line. With the recent development of high-quality monochromators and the advent of the laser light source, a renewed interest in the Raman effect as an analytical method of chemical analysis has taken place. Raman spectrophotometers are generally used to investigate the structure of molecules and to supplement other methods of chemical analysis, particularly infrared-absorption spectrometry.

The scattered photons from a Raman interaction are so few in number that only the highest-quality photomultipliers can be used as detectors. The tube should have high collection efficiency, high gain, good multiplication statistics, low noise, and high quantum efficiency over the spectral range of interest. Fig. 81 shows a Raman spectrum. To reduce the effects of Rayleigh scattering, a source of noise in Raman spectroscopy, the photomultiplier is placed at right angles to the light beam, whose wavelength has been chosen as long as possible within the range of interest.

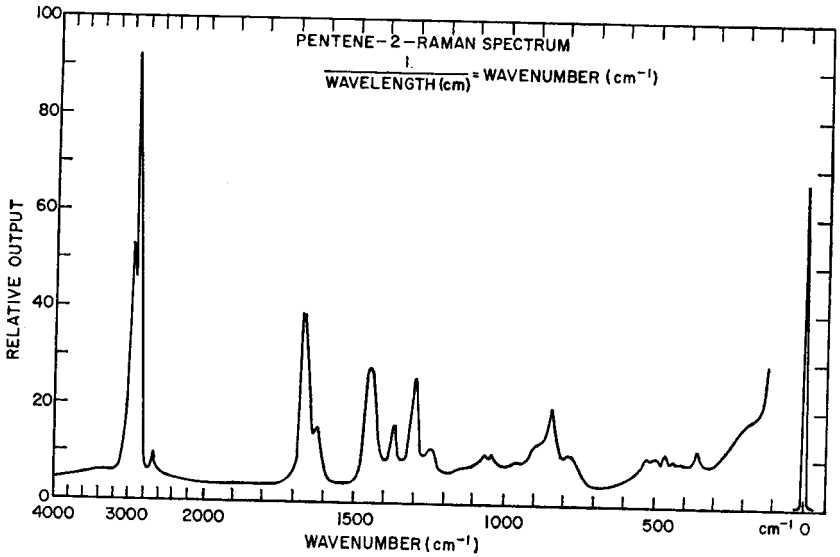

Fig. 81 — Typical Raman spectrum.

Voltage-Divider Considerations

THE interstage voltage gradients for the photomultiplier elements may be supplied by individual voltage sources; however, the usual source is a resistive voltage divider placed across a high-voltage source, as shown in Fig. 82.

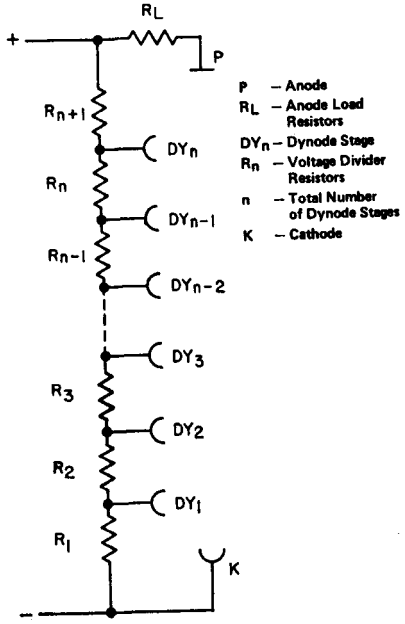

Fig. 82 — Schematic diagram of a resistive voltage divider.

RESISTANCE VOLTAGE DIVIDER

The response of a 931A photomultiplier using a conventional voltage divider, as shown in Fig. 82, with equal voltage per stage is shown in Fig. 83 as a function of the light flux input.[1] (The value of R_L was essentially zero for this measurement.) The anode current is shown relative to the divider current at zero

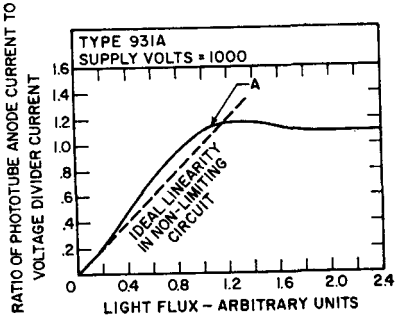

Fig. 83 — The relative response of a 931A photomultiplier as a function of the light flux using the circuit of Fig. 82 with equal stage voltage (at zero light level). Curve is taken from Fig. 2 of Ref. 1.

light level. The superlinearity region is explained by the fact that the increase in dynode voltage resulting from the redistribution of the voltage loss across the anode-to-last-dynode

divider resistor tends to reduce anode collection efficiency. The decrease in sensitivity which occurs beyond region A of Fig. 83 results from the extension of voltage losses to the last two or three dynode resistors causing defocusing and skipping in the associated dynode stages. In order to prevent this loss and assure a high degree of linearity, the current through the voltage-divider network should be at least ten times the maximum average anode current required to prevent the dynode voltages from varying. In calculating the voltage-divider current, the average anode current must first be estimated; this estimate requires knowledge of the value of the input (light) signal and the required output (electrical) signal.

VOLTAGE RATIO

A resistance voltage divider must be designed to divide the applied voltage equally or unequally among the various stages as required by the electrostatic system of the tube. The most common voltage between stages is usually referred to as the stage voltage and the voltage between other stages as relative to the most common stage voltage.

The voltage distribution is normally specified in the following way:

Between	Relative Voltage
$K - Dy_1$	$r_{(1)}$
$Dy_1 - Dy_2$	$r_{(2)}$
$Dy_{n-1} - Dy_n$	$r_{(n)}$
Dy_n – Anode	$r_{(n+1)}$

where n represents the number of the dynode stage and $r_{(j)}$ (j = 1 to n+1) represents the relative interstage voltage. There is always one more interstage voltage than there are dynode stages.

The following formula may be used to calculate the voltage between stages:

$$V_j = \frac{(E_{supply})\ r_j}{r_t}$$

where $r_t = \sum_{i=1}^{n+1} r_i$, and V_j is the voltage between the elements K – Dy_1, $Dy_1 - Dy_2$, and Dy_n – Anode.

VOLTAGE-DIVIDER RESISTORS

The voltage-divider resistor values required for each stage can be determined from the value of the total resistance required of the voltage divider and the voltage-divider ratios of the particular tube type. The interstage resistance values are in proportion to the voltage-divider ratios as follows:

$$R_j = R_t \frac{r_j}{r_t}$$

where R_j is the resistance between elements Dy_j and Dy_{j-1}. The recommended resistance values for a photomultiplier voltage divider range from 20,000 ohms per stage to 5 megohms per stage; the exact values are usually the result of a compromise. If low values of resistance per stage are utilized, the power drawn from the regulated power supply may be excessively large. The resistor power rating should be at least twice the calculated rating to provide a safety margin and to prevent a shift in resistance values as a result of overheating.

Photomutliplier noise or a shift in gain may result from heat emanating from the voltage-divider resistors; therefore, the divider network and

other heat-producing components should be located so that they will not increase the tube temperature. Resistance values in excess of five megohms should be avoided because current leakage between the photomultiplier terminals could cause a variation of the interstage voltage.

The type of resistor used in a divider depends on the dynode structure with which the divider will be used. Close tolerance resistors, such as the wire-wound types, are normally required with the focused or in-line structures. On the other hand, interdynode voltages in the venetian-blind structures can vary widely with but little effect on the photomultiplier. For this reason, the resistors used with a venetian-blind structure need only be of a less stable variety, such as carbon.

CATHODE-TO-FIRST-DYNODE REGION

The over-all performance of a tube can be improved by maintaining a high electric field in the cathode-to-first-dynode region to reduce the transit-time spread of photoelectrons arriving at the first dynode and minimize the effect of magnetic fields. A high first-dynode gain, which implies a high cathode-to-first-dynode voltage, is particularly important in the detection of extremely low light levels where the statistics of photoemission become important.

A high cathode-to-first-dynode voltage of approximately 600 to 800 volts is recommended in photomultipliers having a gallium phosphide first dynode. Otherwise, the higher secondary-emission capability of this material and its improved statistics are not utilized.

It is frequently useful to control the gain of the photomutiplier by varying the over-all voltage. This arrangement, however, may have the disadvantage of reducing the gain in the critical first stage. This disadvantage can be avoided by using a zener diode to hold this critical voltage constant.

INTERMEDIATE STAGES

In applications in which it is desirable to control the anode sensitivity without changing the over-all voltage, the voltage of a single dynode may be varied. Fig. 84 shows the variation of anode current for a 931A photomultiplier when one of the dynode voltages is varied while the total supply voltage is held constant. The dynode should be selected from the middle of the dynode string because a variation of dynode potentials near the cathode or anode would have a detrimental effect on photomultiplier operation.

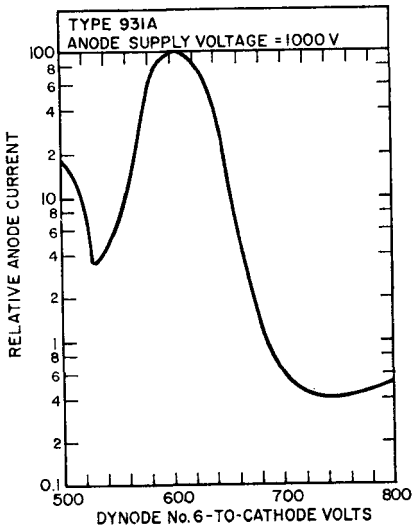

Fig. 84 — The output-current variation of a 931A when the voltage on one dynode (No. 6) is varied while the total anode voltage remains fixed.

VOLTAGE DIVIDERS FOR PULSED OPERATION

In applications in which the input signal is in the form of pulses, the average anode current can be determined from the average pulse amplitude and the duty factor. The total resistance of the voltage-divider network is calculated for the average anode current for dc operation.

In cases in which the average anode current is orders of magnitude less than a peak pulse current, dynode potentials can be maintained at a nearly constant value during pulse durations of 100 nanoseconds or less by use of charge-storage capacitors at the tube socket. The voltage-divider current need only be sufficient to provide the average anode current for the photomultiplier; the high peak currents required during the large-amplitude light pulses may be supplied by the capacitors.

The capacitor values depend upon the value of the output charge associated with the pulse or train of pulses. The value of the final-dynode-to-anode capacitor C is given by

$$C = 100 \frac{q}{V}$$

where C is in farads, q is the total anode charge per pulse in coulombs, and V is the voltage across the capacitor. The factor 100 is used to limit the voltage change across the capacitor to a 1-per-cent maximum during a pulse. Capacitor values for preceding stages should take into account the smaller values of dynode currents in these stages. Conservatively, a factor of approximately 2 per stage is used. Capacitors are not required across those dynode stages at which the peak dynode current is less than 1/10 of the average current through the voltage-divider network.

MEDIUM-SPEED PULSE APPLICATIONS

In applications in which the output current consists of pulses of short duration, the capacitance C_L of the anode circuit to ground becomes very important. The capacitance C_L is the sum of all capacitances from the anode to ground: photomultiplier-anode capacitance, cable capacitance, and the input capacitance of the measuring device. For pulses with a duration much shorter than the anode time constant R_LC_L, the output voltage is equal to the product of the charge and $1/C_L$ because the anode current is simply charging a capacitor. The capacitor charge then decays exponentially through the anode load resistor with a time constant of R_LC_L. To prevent pulses from piling up on each other, the maximum value of R_LC_L should be much less than the reciprocal of the repetition rate.

An important example of this type of operation is scintillation counting, for example with NaI(Tl). The time constant of the scintillations is 0.25 microsecond and, because the integral of the output current pulse is a measure of the energy of the incident radiation, the current pulse is integrated on the anode-circuit capacitance for a period of about 1 microsecond. To prevent pulse pile-up, the anode-circuit time constant is selected to be about 10 microseconds. Because the scintillations occur at random, the maximum average counting rate is limited to about 10 kHz.

FAST-PULSE APPLICATIONS

In fast-pulse light applications, it is recommended that the photomultiplier be operated at negative high voltage with the anode at ground potential. A typical voltage-divider circuit with series-connected capacitors used with a positive ground is shown in Fig. 85. The parallel configuration of capacitors may also be used, as shown in Fig. 86. This circuit permits lower-inductance connections to the ground plane. The parallel arrangement requires capacitors of higher voltage ratings. Regardless of the configuration, the capacitors must be located at the socket. The capacitor arrangements just described may also be applied to negative-ground applications.

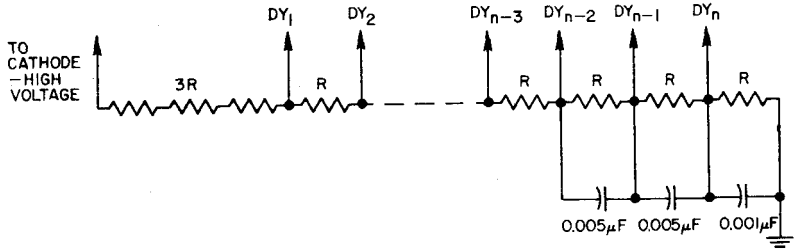

Fig. 85 — Series-connected capacitors in voltage-divider circuit using positive ground for pulse-light applications.

The wiring of the anode is very critical in pulse applications if linearity and pulse shape are to be preserved. Most pulse circuitry is based on a 50-ohm source and a 50-ohm load impedance; careful wiring technique is required to assure the best impedance match. A good impedance match to the transmission line and anode of the tube is provided by capacitively coupling the last, and sometimes the next to last, dynode to the ground braid of the 50-ohm coaxial signal cable.

Fig. 87 illustrates the use of bypass capacitors (C_{BP}) on the anode signal line. Because of the bypass capacitors, the transmission-line elements in the figure are viewed by a fast pulse as a single line between two ground planes.

WIRING TECHNIQUES

Good high-frequency wiring techniques must be employed in wiring photomultiplier sockets and associated voltage dividers if loss of time

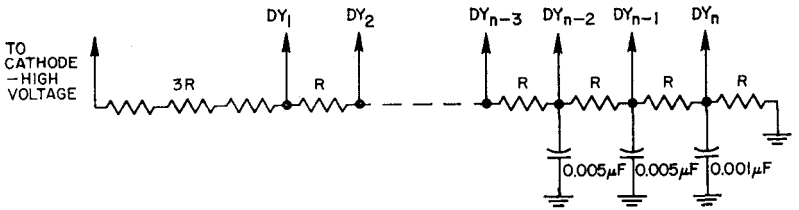

Fig. 86 — Parallel-connected capacitors in voltage-divider circuit for pulsed-light application.

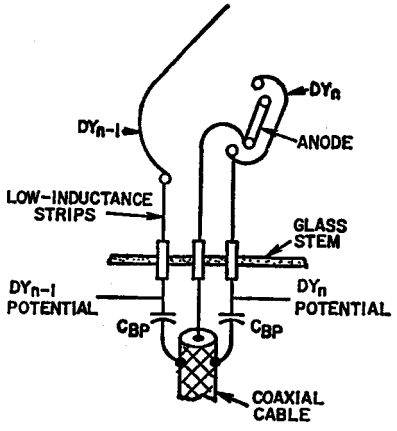

Fig. 87 — Bypass capacitors used to make the last two dynodes appear as a ground plane to a fast-pulsed signal.

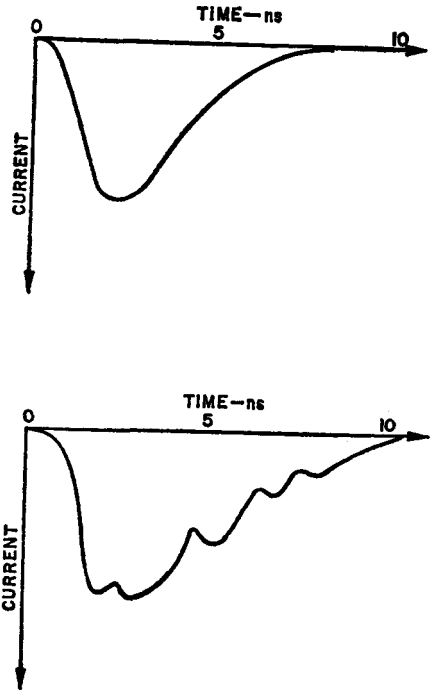

Fig. 88 — (a) Pulse shape obtained from photomultiplier excited by a 0.5-nanosecond-rise-time light pulse, and (b) distortion encountered with improper charge-storage capacitors and ringing in an improperly wired socket.

resolution in pulse operation is to be minimized. Fig. 88(a) illustrates the pulse shape obtained from an 8575 photomultiplier excited by a 0.5-nanosecond rise-time light pulse. The pulse shape is most easily seen with the aid of a repetitive light pulser and a sampling oscilloscope. Fig. 88(b) indicates the general type of distortion encountered with the use of improper charge-storage capacitors, capacitors either too small in value or too inductive. The output pulse appears clipped in comparison to that of Fig. 88(a) and illustrates the ringing that may occur in an improperly wired socket, a condition that worsens as pulse amplitude increases.

Fig. 89 shows a socket wired for a negative high-voltage application. The disk-type bypass capacitors are mounted in series with minimum lead length because the self-inductance of a few millimeters of wire becomes critical in nanosecond-pulse work; care should also be taken in dressing the bypass capacitors and coaxial cable. The resistors for the voltage divider are shown mounted on the socket. In applications requiring minimum dark current, the resistors should be remote from the photomultiplier to minimize heating effects. In negative-high-voltage applications, the socket should be mounted in a copper or brass coaxial cylinder to provide a suitable ground plane to which the capacitors can be connected; this construction is shown in Fig. 90.

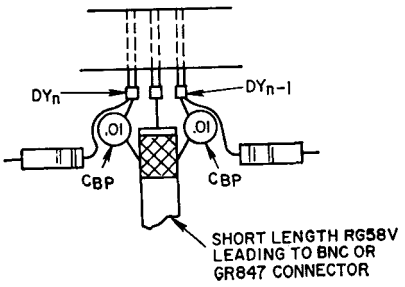

Fig. 89 — Anode detail of socket wired for a negative high-voltage application.

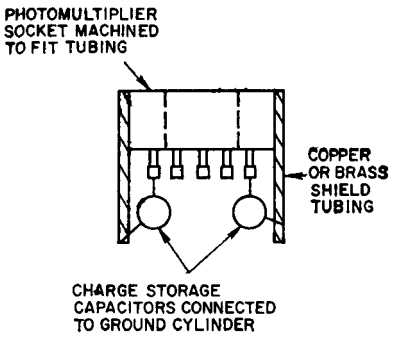

Fig. 90 — Tube socket mounted in copper or brass coaxial cylinder for negative-high-voltage applications.

CHECKING SOCKET AND TUBE PERFORMANCE

Some photomultipliers typically display a reflected-pulse rise time of the order of 1.5 nanoseconds for an initiating pulse of the order of 50 picoseconds when the tube and socket are tested with a time-domain reflectometer, the instrument used to test the anode-pin region of the socket. The socket should simulate an open circuit. If the output pulse can be viewed with a sampling oscilloscope, the pulse shape can be inspected for signs of clipping or ringing, effects more prominent at high pulse amplitudes. Output-pulse amplitude may be increased by increasing the tube voltage and may be measured with a multichannel analyzer or an oscilloscope.

The effectiveness of the charge-storage capacitors can be verified with a simple linearity test. The output of a photomultiplier varies as $V\alpha$, where V is the applied voltage and alpha (α) is a constant; thus a plot of pulse amplitude as a function of the logarithm of the voltage value should yield a straight line.

A two-pulse technique may be employed to test linearity at constant operating voltage. This technique requires a means for attenuating the light signals by a factor of 0.5 to 0.1; a filter in the light beam suffices. In applying the technique, the ratio of the amplitude of the two pulses is established at low pulse amplitudes where linear operation is assured. Next, the pulse amplitude is increased, either by increasing the tube voltage or by increasing the light intensity; a constant pulse-amplitude ratio indicates linear operation.

TAPERED DIVIDERS

Some applications require that photomultipliers sustain high signal currents for short time intervals, tens of nanoseconds or less. In general, photomultipliers are capable of supplying 0.2 ampere or more into a 50-ohm load for short durations. However, the voltage divider must be tailored to the application to allow a photomultiplier to deliver these high currents.

The principal limitation on current output (into a 50-ohm system) is space charge at the last few stages. This space charge can be overcome if the potential difference across the last few stages is increased by use

of a tapered divider rather than an equal-volts-per-stage divider. The tapered divider places 3 to 4 times the normal interstage potential difference across the last stage. The progression leading to the 4-times potential difference should be gradual to maintain proper electrostatic focus between stages; a progression of 1, 1 . . . 1, 1, 1.5, 2.0, 2.5, 3 is recommended.

Anode signals 400 to 500 volts in amplitude can be obtained from photomultipliers. These large voltage excursions are often useful, for example, in driving electro-optical modulators. Because the photomultiplier is nearly an ideal constant-current source, its output voltage into a high-impedance load is limited only by the potential difference between the last dynode and the anode. If the potential difference is 100 volts, the anode cannot swing through more than a 100-volt excursion. By impressing a much higher potential difference between the anode and last dynode by means of a tapered divider, greater voltage swings can be obtained.

DYNAMIC COMPRESSION OF OUTPUT SIGNAL

Most photomultipliers operate linearly over a dynamic range of six or seven orders of magnitude, a range few monitor devices can accommodate without requiring range changes. When compression of the dynamic range is desired, a logarithmic amplifier is sometimes used. The photomultiplier may be operated in a compressed-output mode, however, without the need for additional compression circuitry.

The voltage excursion of the anode is limited by the potential difference between the last dynode and the anode (with no signal current flowing). If the potential difference is reduced from, for example, 100 volts to 10 volts, several orders of magnitude can be compressed into a single decade. The exact relationship between input-light intensity and the compressed output voltage developed across a load resistor varies among tube types and voltage dividers, and must be determined empirically.

CURRENT PROTECTION OF PHOTOMULTIPLIER

If a photomultiplier is accidentally exposed to an excessive amount of light, it may be permanently damaged by the resultant high currents. To reduce this possibility, the resistive voltage-divider network may be designed to limit the anode current. The average anode current of a photomultiplier cannot much exceed the voltage-divider current; therefore, the voltage-divider network serves as an overload protection for the tube. If overexposure is expected frequently, interdynode currents which can be quite excessive, may cause loss of gain. In some applications it may be worth while to protect against dynode damage by using resistors in series with each dynode lead.[1]

HIGH-VOLTAGE SUPPLY

The recommended polarity of the photomultiplier power-supply voltage with respect to ground depends largely on the application intended. Of course, the cathode is always negative with respect to the anode; however, in some pulsed applications, such as scintillation counting, the cathode should be grounded and the anode operated at a high positive potential with a capacitance-coupled output. The scintillator and any magnetic or electrostatic shields should

also be connected to ground potential to eliminate leakage currents from ground to the photocathode and to prevent the shock hazard caused by the scintillator being at high voltage.

In applications in which the signal cannot be passed through a coupling capacitor, the positive side of the power supply should be grounded. The cathode is then at a high negative potential with respect to ground. When this arrangement is used, extra precautions must be taken in the mounting and shielding of the photomultiplier. If a potential gradient exists across the tube wall, scintillations occurring in the glass will increase dark noise. If this condition exists for a sufficiently long period of time, the photocathode will be permanently damaged by the ionic conduction through the glass. To prevent this situation when a shield is used, the shield is connected to photocathode potential. Light-shielding or supporting materials used in photomultipliers must limit leakage currents to 10^{-12} ampere or less. Fig. 91 shows a curve of the effect of external-shield potential on photomultiplier noise.

To reduce the shock hazard to personnel, a very high resistance should be connected between the shield and the negative high voltage.

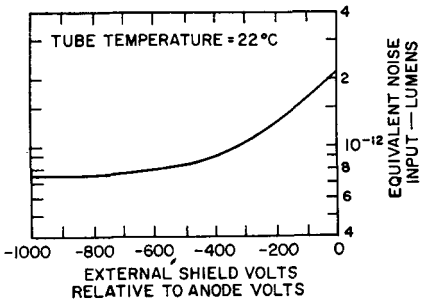

Fig. 91 — Curve of effect of external-shield potential on noise in a photomultiplier.

POWER-SUPPLY STABILITY

The output signal of a photomultiplier is extremely sensitive to variations in the supply voltage. Therefore, the power supply should be very stable and exhibit minimum ripple. As an approximate "rule of thumb", power-supply stability (in per-cent variation) should be at least ten times less than the maximum output-current variation (in per cent) that can be tolerated.

REFERENCES

1. R. W. Engstrom and E. Fischer, "Effects of Voltage-Divider Characteristics on Multiplier Phototube Response", *Rev. Sci. Instr., Vol. 28,* p. 525 (1957).

Photometric Units and Photometric-to-Radiant Conversion

PHOTOMETRY is concerned with the measurement of light; the origins of the photoelectric industry were associated with the visible spectrum. It was appropriate, therefore, that the units for evaluating photosensitive devices be photometric. Today, however, although many of the applications of photosensitive devices are for radiation outside the visible spectrum, for many purposes the photometric units are still retained. Because these units are based on the characteristics of the eye, it is appropriate that the introduction to this discussion begin with a consideration of some of the characteristics of the eye.

CHARACTERISTICS OF THE EYE

The sensors in the retina of the human eye are of two kinds: "cones" which predominate the central (or foveal) vision and "rods" which provide peripheral vision. The cones are responsible for our color vision; rods provide no color information but in the dark-adapted state are more sensitive than the cones and thus provide the basis of dark-adapted vision. Because there are no rods in the foveal region, faint objects can more readily be observed at night when the eye is not exactly directed toward the faint object. The response of the light-adapted eye (cone vision) is referred to as the **Photopic eye response;** the response of the dark-adapted eye (rod vision) is referred to as **Scotopic eye response.**

Although characteristics of the human eye vary from person to person, standard luminosity coefficients for the eye were defined by the Commission Internationale d'Eclairage (International Commission on Illumination) in 1931. These standard C.I.E. luminosity coefficients, listed in Table II, refer to the Photopic eye response. They represent the relative luminous equivalents of an equal-energy spectrum for each wavelength in the visible range, assuming foveal vision. An absolute "sensitivity" figure established for the standard eye relates photometric units and radiant power units. At 555 nanometers, the wavelength of maximum sensitivity of the eye, one watt of radiant power corresponds to 680 lumens.

For the dark-adapted eye, the peak sensitivity increases and is shifted toward the violet end of the spectrum. A tabulation of the relative scotopic vision is given in Table III. The peak luminosity for scotopic vision occurs at 511 nanometers and is the equivalent of 1746 lumens/watt. Fig. 92 shows the comparison of the absolute

Table II — *Standard Luminosity Coefficient Values.*

Wavelength (nanometers)	C.I.E. Value	Wavelength (nanometers)	C.I.E. Value	Wavelength (nanometers)	C.I.E. Value
380	0.00004	510	0.503	640	0.175
390	0.00012	520	0.710	650	0.107
400	0.0004	530	0.862	660	0.061
410	0.0012	540	0.954	670	0.032
420	0.0040	550	0.995	680	0.017
430	0.0116	560	0.995	690	0.0082
440	0.023	570	0.952	700	0.0041
450	0.038	580	0.870	710	0.0021
460	0.060	590	0.757	720	0.00105
470	0.091	600	0.631	730	0.00052
480	0.139	610	0.503	740	0.00025
490	0.208	620	0.381	750	0.00012
500	0.323	630	0.265	760	0.00006

luminosity curves for scotopic and photopic vision as a function of wavelength.

The sensitivity of the eye outside the wavelength limits shown in Tables II and III is very low, but not actually zero. Studies with intense infrared sources have shown that the eye is sensitive to radiation of wavelength at least as long as 1050 nanometers. Fig. 93 shows a composite curve given by Griffin, Hubbard, and Wald [1] for the sensitivity of the eye for both foveal and peripheral vision from 360 to 1050 nanometers. According to Goodeve [2] the ultraviolet sensitivity of the eye extends to between 302.3 and 312.5 nanometers. Below this level the absorption of radiation by the proteins of the eye lens apparently limits further extension of vision into the ultraviolet. Light having a wavelength of 302 nanometers is detected by its fluorescent effect in the front part of the eye.

PHOTOMETRIC UNITS

Luminous intensity (or candlepower) describes luminous flux per unit solid angle in a particular direction from a light source. The measure of luminous intensity is the fundamental standard from which all other

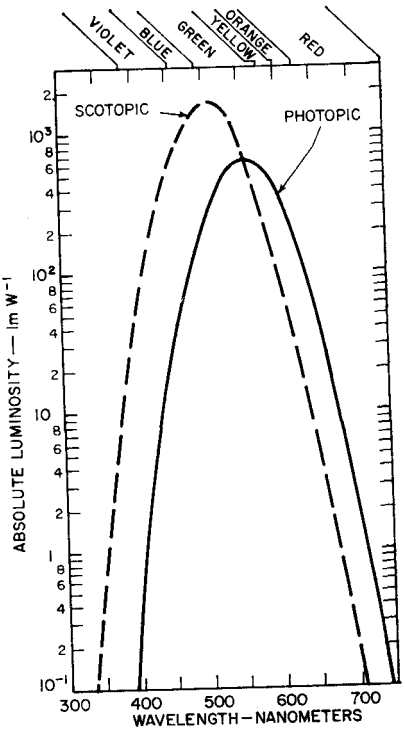

Fig. 92 — Absolute luminosity curves for scotopic and photopic eye response.

Table III — *Relative Luminosity Values for Photopic and Scotopic Vision.*

WAVELENGTH (nm)	PHOTOPIC $V\lambda$ ($B > 3$ cd m^{-2})	SCOTOPIC $V\lambda$ ($B < 3 \times 10^{-5}$ cd m^{-2})
350	—	0.0003
360	—	0.0008
370	—	0.0022
380	0.00004	0.0055
390	0.00012	0.0127
400	0.0004	0.0270
410	0.0012	0.0530
420	0.0040	0.0950
430	0.0116	0.157
440	0.023	0.239
450	0.038	0.339
460	0.060	0.456
470	0.091	0.576
480	0.139	0.713
490	0.208	0.842
500	0.323	0.948
510	0.503	0.999
520	0.710	0.953
530	0.862	0.849
540	0.954	0.697
550	0.995	0.531
560	0.995	0.365
570	0.952	0.243
580	0.870	0.155
590	0.757	0.0942
600	0.631	0.0561
610	0.503	0.0324
620	0.381	0.0188
630	0.265	0.0105
640	0.175	0.0058
650	0.107	0.0032
660	0.061	0.0017
670	0.032	0.0009
680	0.017	0.0005
690	0.0082	0.0002
700	0.0041	0.0001
710	0.0021	—
720	0.00105	—
730	0.00052	—
740	0.00025	—
750	0.00012	—
760	0.00006	—
770	0.00003	—

photometric units are derived. The standard of luminous intensity is the **candela;** the older term candle is sometimes still used, but refers to the new candle or candela.

The candela is defined by the radiation from a black body at the temperature of solidification of platinum. A candela is one-sixtieth of the luminous intensity of one square centimeter of such a radiator.

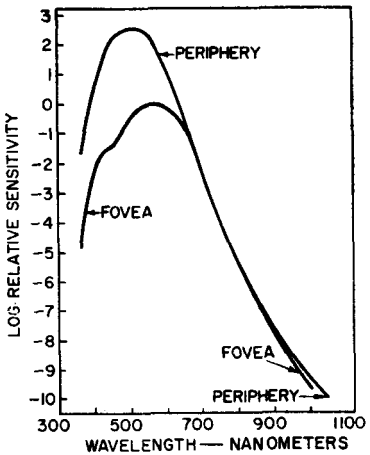

Fig. 93 — Relative spectral sensitivity of the dark-adapted foveal and peripheral retina.

A suitable substandard for practical photoelectric measurements is the developmental-type calibrated lamp, RCA Dev. No. C70048, which operates at a current of about 4.5 amperes and a voltage of 7 to 10 volts. A typical lamp calibrated at a color temperature of 2854°K provides a luminous intensity of 55 candelas. The luminous intensity of a tungsten lamp measured in candelas is usually numerically somewhat greater than the power delivered to the lamp in watts. (The photoelectric industry is in the process of changing the color-temperature standard for the tungsten test lamp. A color temperature of 2870°K has served as the basic test standard for photoelectric measurements in this country for about 30 years. In order to provide a more universal standard, most industries and government laboratories are changing to 2854°K color temperature. This latter temperature is in common use in Europe. Illuminant A as designated by the C.I.E. is a tungsten lamp operated at 2854°K color temperature. The text of this Manual utilizes the 2854°K figure, although tube data are still based on 2870°K. The difference, however, is generally negligible.[3] Test lamps may be obtained with either temperature calibration.)

Luminous flux is the rate of flow of light energy, that characteristic of radiant energy which produces visual sensation. The unit of luminous flux is the **lumen,** which is the flux emitted per unit solid angle by a uniform point source of one candela. Such a source produces a total luminous flux of 4π lumens.

A radiant source may be evaluated in terms of luminous flux if the radiant-energy distribution of the source is known. If $W(\lambda)$ is the total radiant power in watts per unit wavelength, total radiant power over all wavelengths is $\int_0^\infty W(\lambda)\, d\lambda$, and the total luminous flux L in lumens can be expressed as follows:

$$L = 680 \int_0^\infty W(\lambda)\ y(\lambda)\ d\lambda$$

where $y(\lambda)$ represents the luminosity coefficient as a function of wavelength. At a wavelength of 555 nanometers, one watt of radiant power corresponds to 680 lumens. The lumen is the most widely used unit in the rating of photoemissive devices; for photomultipliers the typical test levels of luminous flux range from 10^{-7} to 10^{-5} lumen (0.1 to 10 microlumens).

Table IV — *Luminance Values for Some Common Sources.*

Source	Luminance (Footlamberts)
Sun, as observed from Earth's surface at meridian	4.7×10^8
Moon, bright spot, as observed from Earth's surface	730
Clear blue sky	2300
Lightning flash	2×10^{10}
Atomic fission bomb, 0.1 millisecond after firing, 90-feet diameter ball	6×10^{11}
Tungsten filament lamp, gas-filled, 16 lumen/watt	2.6×10^6
Plain carbon arc, positive crater	4.7×10^6
Fluorescent lamp, T-12 bulb, cool white, 430 mA, medium loading	2000

Illuminance (or **illumination**) is the density of luminous flux incident on a surface. A common unit of illumination is the **footcandle,** the illumination produced by one lumen uniformly distributed over an area of one square foot. It follows that a source of one candela produces an illumination of one footcandle at a distance of one foot.

Table IV lists some common values of illumination encountered in photoelectric applications. Further information concerning natural radiation is shown in Fig. 94, which indicates the change in natural illumination at ground level during, before, and after sunset for a condition of clear sky and no moon.[4]

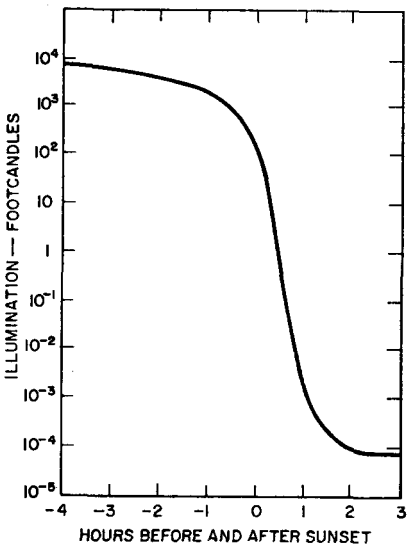

Fig. 94 — Natural illuminance on the earth for the hours immediately before and after sunset with a clear sky and no moon.

Photometric luminance (or **brightness**) is a measure of the luminous flux per unit solid angle leaving a surface at a given point in a given direction, per unit of projected area. The term photometric luminance is used to distinguish a physically measured luminance from a subjective luminance. The latter varies with illuminance because of the shift in spectral response of the eye toward the blue region at lower levels of illuminance. The term luminance describes the light emission from a surface, whether the surface is self-luminous or receives its light from some external luminous body.

For a surface which is uniformly diffusing, luminance is the same regardless of the angle from which the

surface is viewed. This condition results from the fact that a uniformly diffusing surface obeys Lambert's law (the cosine law) of emission. Thus, both the emission per unit solid angle and the projected area are proportional to the cosine of the angle between the direction of observation and the surface normal.

A logical unit of luminance based on the definition given above is a candela per unit area. When the unit of area is the square meter, this unit is called a **nit;** when the unit of area is a square centimeter, the unit is a **stilb.** It is also possible to refer to a candela per square foot. However, none of these units is as commonly used in photoelectric measurement as the **footlambert,** a unit of photometric luminance equal to $1/\pi$ candela per square foot. The advantage of using the footlambert for a uniform diffuser is that it is equivalent to a total emission of one lumen per square foot from one side of the surface. This relationship can be demonstrated by the following conditions, as shown in Fig. 95. An elementary portion of a diffusing surface having an area of A square feet has a luminance of one footlambert, or $1/\pi$ candela per square foot. The light flux of interest is that emitted into an elementary solid angle, $2\pi \sin\theta \, d\theta$. At an angle of θ, the projection of the elementary area is equal to A cos θ. Because the luminous flux in a particular direction is equal to the product of the source strength in candelas and the solid angle, the total luminous flux L in lumens from the area A may be obtained by integration over the hemisphere as follows:

$$L = \int_0^{\pi/2} \frac{1}{\pi} (A \cos\theta)(2\pi \sin\theta)\, d\theta = A \quad (1.6)$$

In other words, the total flux from a uniform diffuser having a luminance of one footlambert is one lumen per square foot.

An advantage of the above relationship is that the illumination at a surface in front of and parallel to an extended and uniformly diffusing surface having a luminance of one footlambert is equal to one lumen per square foot or one footcandle. As a result, an instrument reading illuminance in footcandles indicates photometric luminance or brightness in footlamberts if the instrument is illuminated essentially from the entire hemisphere. (This statement neglects the possible perturbation caused by the measurement instrument.)

In a typical application, a uniformly diffusing radiating surface may be of such small size that it can be considered practically a point source. However, if the radiator is assumed to be a flat surface radiating according to Lambert's law, the distribution of flux about the point is not the same as for an ordinary point source. In this case, if the surface luminance is one footlambert and the area is A square foot, the flux per steradian in a direction normal to the surface would be

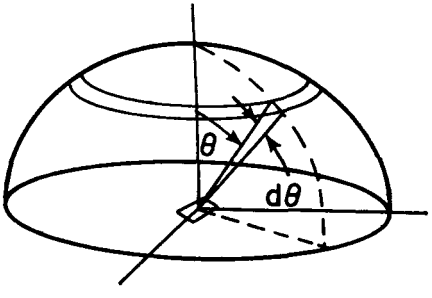

Fig. 95 — Diagram illustrating Lambert's law and the calculation of total luminous flux from a diffuse radiator.

$A(1/\pi)$ lumens, or at an angle θ with respect to the normal line the flux would be $A(1/\pi)$ (cos θ) lumens per steradian.

All photometric data in this Manual are presented in units of candelas, lumens, footcandles, and footlamberts; Table V is a conversion table for various photometric units.

Table V — *Conversion Table for Various Photometric Units.*

Luminous Intensity

1 candela (cd) = 1 lumen/steradian (1m sn^{-1})

Luminous Flux

4π lumens = total flux from uniform point source of 1 candela.

Illuminance

1 footcandle (fc) = 1 lumen/ft^2

= 10.764 lux (meter candle) (lumen/$meter^2$)

= 0.001076 phot (lumen/cm^2)

Luminance

1 footlambert (fL) = $1/\pi$ candela/ft^2

= 0.0010764 lambert ($1/\pi$ candela/cm^2)

= 1.0764 millilamberts

= 3.426 nits (candela/$meter^2$)

= 0.0003426 stilbs (candela/cm^2)

= 0.3183 candela/ft^2

= 10.764 apostilbs ($1/\pi$ candela/$meter^2$)

REFERENCES

1. D. R. Griffin, R. Hubbard, and G. Wald, "The Sensitivity of the Human Eye to Infrared Radiation," *JOSA, Vol. 37,* No. 7 (1947).
2. C. F. Goodeve, "Vision in the Ultraviolet," *Nature* (1934).
3. R. W. Engstrom and A. L. Morehead, "Standard Test Lamp Temperature for Photosensitive Devices—Relationship of Absolute and Luminous Sensitivities," *RCA Review, Vol. 28* (1967).
4. *I.E.S. Lighting Handbook,* Illuminating Engineering Society, New York, New York (1959).
5. R. Kingslake, *Applied Optics and Optical Engineering, Vol. 1,* Chapter 1, Table II, Academic Press, New York and London (1965).
6. J. W. Walsh, *Photometry,* Constable and Co., Ltd., London (1953).

Radiant Energy and Sources

RADIANT energy is energy traveling in the form of electromagnetic waves; it is measured in joules, ergs, or calories. The rate of flow of radiant energy is called radiant flux; is it expressed in calories per second, in ergs per second, or, preferably, in watts (joules per second).

BLACK-BODY RADIATION

As a body is raised in temperature, it first emits radiation primarily in the invisible infrared region. Then, as the temperature is increased, the radiation shifts toward the shorter wavelengths. A certain type of radiation called black-body radiation is used as a standard for the infrared region; other sources may be described in terms of the black body.

A black body is one which absorbs all incident radiation; none is transmitted and none is reflected. Because, in thermal equilibrium, thermal radiation balances absorption, it follows that a black body is the most efficient thermal radiator possible. A black body radiates more total power and more power at a particular wavelength than any other thermally radiating source at the same temperature. Although no material is ideally black, the equivalent of a theoretical black body can be achieved in the laboratory by providing a hollow radiator with a small exit hole. The radiation from the hole approaches that from a theoretical black radiator if the cross-sectional area of the cavity is large compared with the area of the exit hole. The characteristic of 100-per-cent absorption is achieved because any radiation entering the hole is reflected many times inside the cavity.

The radiation distribution for a source which is not black may be calculated from the black-body radiation laws provided the emissivity as a function of wavelength is known. Spectral emissivity is defined as the ratio of the output of a radiator at a specific wavelength to that of a black body at the same temperature. Tungsten sources, for which tables of emissivity data are available,[1] are widely used as practical standards, particularly for the visible range. Tungsten radiation standards for the visible range are frequently given in terms of color temperature, instead of true temperature. The color temperature of a selective radiator is determined by comparison with a black body: when the outputs of the selective radiator and a black body are the closest possible approximation to a perfect color match in the range of visual sensitivity, the color temperature of the selective radiator is numerically the same as the black-body true temperature. For a tungsten source, the relative distribution

of radiant energy in the visible spectral range is very close to that of a black body although the absolute temperatures differ. However, the match of energy distribution becomes progressively worse in the ultraviolet and infrared spectral regions.

SOURCE TYPES

Tungsten lamps are probably the most important type of radiation source because of their availability, reliability, and constancy of operating characteristics. Commercial photomultiplier design has been considerably influenced by the characteristics of the tungsten lamp. A relative spectral-emission characteristic for a tungsten lamp at 2854°K color temperature is shown in Fig. 96.

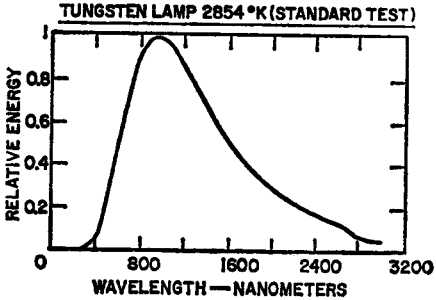

Fig. 96 — Relative spectral-emission characteristic for a tungsten lamp at a color temperature of 2854°K.

The common **fluorescent lamp,** a very efficient light source, consists of an argon-mercury glow discharge in a bulb internally coated with a phosphor that converts ultraviolet radiation from the discharge into useful light output. There are numerous types of fluorescent lamps, each with a different output spectral distribution depending upon the phosphor and gas filling. The spectral response shown in Fig. 97 is a typical curve for a fluorescent lamp of the daylight type.

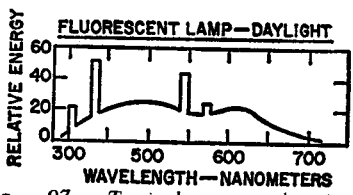

Fig. 97 — Typical spectral-emission curve for a daylight-type fluorescent lamp.

A very useful point source [2] is the **zirconium concentrated-arc lamp.** Concentrated-arc lamps are available with ratings from 2 to 300 watts, and in point diameters from 0.003 to 0.116 inch. Operation of these lamps requires one special circuit to provide a high starting voltage and another well filtered and ballasted circuit for operation.

Although many types of electrical discharge have been used as radiation sources, probably the most important are the **mercury arc** and the **carbon arc.** The character of the light emitted from the mercury arc varies with pressure and operating conditions. At increasing pressures, the spectral-energy distribution from the arc changes from the typical mercury-line spectral characteristic to an almost continuous spectrum of high intensity in the near-infrared, visible, and ultraviolet regions. Fig. 98 shows the spectral-energy distribution from a water-cooled mercury

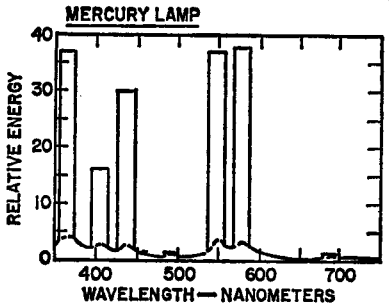

Fig. 98 — Typical spectral-emission curve for a water-cooled mercury-arc lamp at a pressure of 130 atmospheres.

arc at a pressure of 130 atmospheres. The carbon arc is a source of great intensity and high color temperature. A typical energy-distribution spectrum of a dc high-intensity arc is shown in Fig. 99. Figs. 100 and 101 show relative spectral-emission characteristic curves for xenon and argon arcs; Table VI specifies typical parameters for all sources described.

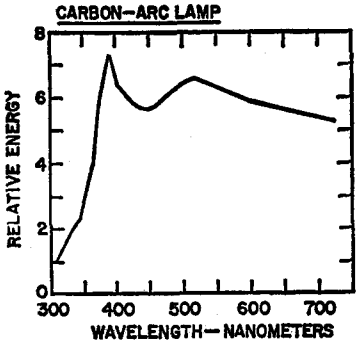

Fig. 99 — Typical spectral-emission curve for a dc high-intensity carbon-arc lamp.

In recent years the development of various types of **lasers** and **p-n light-emitting diodes** with very high modulation frequencies and short rise times has increased the types of sources that photomultipliers are called upon

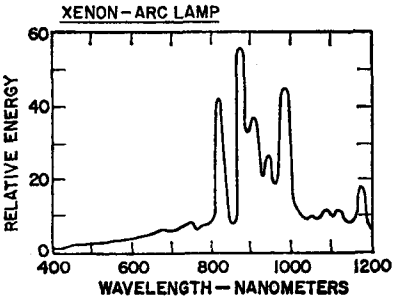

Fig. 100 — Typical spectral-emission curve for a xenon-arc lamp.

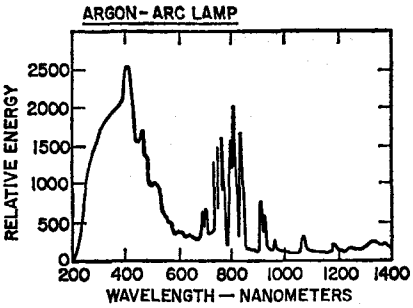

Fig. 101— Typical spectral-emission curve for an argon-arc lamp.

to detect. Although many of these interesting devices have their principal wavelengths of emission in the infrared beyond the sensitivity range of photomultiplier tubes, some do not. Because of the growing importance of laser applications and the use of photomultipliers for detecting their radiation, Tables VII through XI are provided as reference data on crystalline, gas, and liquid lasers, and on p-n junction light-emitting diodes.

LIGHT SOURCES FOR TESTING

Monochromatic sources of many wavelengths may be produced by narrow-band filters or monochromators. Narrow-band filters are more practical for production testing, but, at best, such tests are time-consuming and subject to error. Monochromatic sources are not used in general-purpose testing because most applications involve broader-band light sources; a monochromatic test might grossly misrepresent the situation because of spectral-response variations.

A broad-band source is probably more useful as a single test because it tends to integrate out irregularities in the spectral-response characteristic and more nearly represents the

Table VI — *Typical Parameters for the Most Commonly Used Radiant Energy Sources.*

LAMP TYPE	DC INPUT POWER (WATTS)	ARC DIMENSIONS (mm)	LUMINOUS FLUX (lm)	LUMINOUS EFFICIENCY (lm W^{-1})	AVERAGE LUMINANCE (cd mm^{-2})
Mercury Short Arc (high pressure)	200	2.5 × 1.8	9500	47.5	250
Xenon Short Arc	150	1.3 × 1.0	3200	21	300
Xenon Short Arc	20,000	12.5 × 6	1,150,000	57	3000 (in 3 mm × 6 mm)
Zirconium Arc	100	1.5 (diam)	250	2.5	100
Vortex-Stabilized Argon Arc	24,800	3 × 10	422,000	17	1400
Tungsten Light Bulbs	10	—	79	7.9	10 to 25
	100	—	1630	16.3	
	1,000	—	21,500	21.5	
Fluorescent Lamp Standard Warm White	40	—	2,560	64	—
Carbon Arc Non-Rotating	2,000	≈5 × 5	36,800	18.4	175 to 800
Rotating	15,800	≈8 × 8	350,000	22.2	
Sun	—	—	—	—	1600

Table VII — *Typical Characteristics of a Number of Useful Crystal Laser Systems.*

HOST	DOPANT	WAVELENGTH OF LASER (μm)	MODE AND HIGHEST TEMPERATURE OF OPERATION (°K)
Al_2O_3	0.05% Cr^{3+}	0.6934	CW, P 350
		0.6929	P 300
Al_2O_3	0.5% Cr^{3+}	0.7009	P 77
		0.7041	P 77
		0.7670	P 300
MgF_2	1% Ni^{2+}	1.6220	P 77
MgF_2	1% Co^{2+}	1.7500	P 77
		1.8030	P 77
ZnF_2	1% Co^{2+}	2.6113	P 77
$CaWO_4$	1% Nd^{3+}	1.0580	CW 300
		0.9145	P 77
		1.3392	P 300
CaF_2	1% Nd^{3+}	1.0460	P 77
$CaMoO_4$	1.8% Nd^{3+}	1.0610	CW 300
$Y_3Al_5O_{12}$	Nd^{3+}	1.0648	CW 360
			P 440
LaF_3	1% Nd^{3+}	1.0633	P 300

Table VII — *Typical Characteristics of a Number of Useful Crystal Laser Systems. (cont'd.)*

HOST	DOPANT	WAVELENGTH OF LASER (μm)	MODE AND HIGHEST TEMPERATURE OF OPERATION (°K)
LaF_3	1% Pr^{3+}	0.5985	P 77
$CaWO_4$	0.5% Pr^{3+}	1.0468	P 77
Y_2O_3	5% Eu^{3+}	0.6113	P 220
CaF_2	Ho^{3+}	0.5512	P 77
$CaWO_4$	0.5% Ho^{3+}	2.0460	P 77
$Y_3Al_5O_{12}$	Ho^{3+}	2.0975	CW 77 P 300
$CaWO_4$	1% Er^{3+}	1.6120	P 77
$Ca(NbO_3)_2$	Er^{3+}	1.6100	P 77
$Y_3Al_5O_{12}$	Er^{3+}	1.6602	P 77
$CaWO_4$	Tm^{3+}	1.9110	P 77
$Y_3Al_5O_{12}$	Tm^{3+}	2.0132	CW 77 P 300
Er_2O_3	Tm^{3+}	1.9340	CW 77
$Y_3Al_5O_{12}$	Yb^{3+}	1.0296	P 77
CaF_2	0.05% U^{3+}	2.6130	P 300 CW 77
SrF_2	U^{3+}	2.4070	P 90
CaF_2	.01% Sm^{2+}	0.7083	P 20
SrF_2	.01% Sm^{2+}	0.6969	P 4.2
CaF_2	.01% Dy^{2+}	2.3588	CW 77 P 145
CaF_2	0.01% Tm^{2+}	1.1160	P 27 CW4.2

Table VIII — *Comparison of Characteristics of Continuous Crystalline Lasers.*

MATERIAL ACTIVE SYSTEM	SENSITIZER	OPTICAL PUMP	WAVE-LENGTH (μm)	EFF. (%)	POWER (WATTS)	OPERATING TEMP. (°K)
$Dy^{2+}CaF_2$	—	W	2.36	0.06	1.2	77
$Cr^{3+}Al_2O_3$	—	Hg	0.69	0.1	1.0	300
$Nd^{3+}Y_3Al_5O_{12}$	—	W	1.06	0.2	2	300
			1.06	0.6	15	300
$Nd^{3+}Y_3Al_5O_{12}$	—	Plasma Arc	1.06	0.2	200	300
$Nd^{3+}Y_3Al_5O_{12}$	—	Na Doped Hg	1.06	0.2	0.5	300
$Nd^{3+}Y_3Al_5O_{12}$	Cr^{3+}	Hg	1.06	0.4	10	300
$Ho^{3+}Y_3Al_5O_{12}$	[Er^{3+}, Yb^{3+}, Tm^{3+}]	W	2.12	5.0	15	77

typical application. The tungsten lamp has been used for many years because it is relatively simple, stable, and inexpensive, and maintains its calibration. The tungsten lamp emits a broad band of energy with relatively smooth transitions from one end of the spectrum to the other. Its principal disadvantage as a general source is its lack of ultraviolet output and relatively low blue output.

Sources such as arcs and glow discharges are difficult to calibrate and show serious time variations.

Filters are frequently used to narrow the spectral range for specific purposes; however, they sometimes contribute to errors because of significant transmission outside the band of interest. Filters are also subject to change in transmission with time and are very difficult to reproduce with identical characteristics.

Table IX — *Typical Characteristics of p-n Junction Light-emitting Diodes.*

CRYSTAL	WAVELENGTH (μm)	LASER ACTION
PbSe	8.5	Yes
PbTe	6.5	Yes
InSb	5.2	Yes
PbS	4.3	Yes
InAs	3.15	Yes
$(In_x Ga_{1-x}) As$	0.85-3.15	Yes
$In (P_x As_{1-x})$	0.91-3.15	Yes
GaSb	1.6	No
InP	0.91	Yes
GaAs	0.90	Yes
$Ga (As_{1-x} P_x)$	0.55-0.90	Yes
CdTe	0.855	No
$(Zn_x Cd_{1-x}) Te$	0.59-0.83	No
CdTe-ZnTe	0.56-0.66	No
BP	0.64	No
Cu_2Se-ZnSe	0.40-0.63	No
$Zn (Se_x Te_{1-x})$	0.627	No
ZnTe	0.62	No
GaP	0.565	No
GaP	0.68	No
SiC	0.456	?

Table X — *Typical Characteristics of a Number of Useful Gas Lasers.*

GAS	PRINCIPAL WAVELENGTHS (μm)	OUTPUT POWER		PULSED OR CONTINUOUS
		TYPICAL	MAXIMUM	
Ne (ionized)	0.3324	—	10 mW	Pulsed
			10 mW	CW
Ne (unionized)	0.5401	—	1 kW	Pulsed
He-Ne (unionized)	0.5944–0.6143	10 μW —		Pulsed
	0.6328	1 mW —	150 mW	CW
	1.1523	1-5 mW —	25 mW	CW
	3.3913	<1 mW —	10 mW	CW
Xe (ionized)	0.4603–0.6271	5 mW —	—	Pulsed
	0.5419–0.6271	10 mW —	1 W	CW
	0.4965–0.5971	1 mW —	1 W	Pulsed
Xe (unionized)	2.026	1 mW —	10 mW	CW
	3.507	—	1 mW	CW
	5 575	0.5 mW —	5 mW	CW
	9 007	0.5 mW	5 mW	CW
A (ionized)	0 4880	0.5 W —	5 W	CW
	0 5145	0.5 W —	5 W	CW
	0 4545 to 0 5287	1.5 W —	40 W	CW
N_2 (ionized)	0 33	—	200 kW	Pulsed
		—	100 mW	CW
Kr (ionized)	0.3507	—	300 mW	CW
	0.5208–0.6871	—	3 W	CW
	0.5682	—	100 mW	CW
CO_2 (molecular excitation)	10.552 10.572 10.592	50 W	3.2 kW	CW
CF_3I	1.315	—	10 kW	Pulsed
H_2O (molecular excitation)	27.9	—	1.2 W	Pulsed
	118	—	1 mW	Pulsed
	118	—	10 μW	CW
CN (molecular excitation)	337	—	50 mW	Pulsed

Table XI — *Typical Characteristics for Two Liquid Lasers.*

LIQUID	PRINCIPAL WAVELENGTH (μm)	PULSE ENERGY (PULSEWIDTH)
Eu(o-Cl BTFA)$_4$DMA*	0.61175	0.1J
Nd^{+3}:$SeOCl_2$**	1.056	10J (150 μs)

* dimethylammonium salt of tetrakis europium - ortho - chloro - benzoyltrifluoracetonate

** trivalent neodymium in selenium oxychloride

As a result of the work of industrial committees, virtually the entire photosensitive-device industry in the United States uses the tungsten lamp at 2870°K color temperature* as a general test source. The lamp is calibrated in lumens and is utilized in the infrared spectrum as well as the visible. Typical as well as maximum and minimum photosensitivities are quoted in microamperes per lumen.

The principal disadvantages of using the tungsten lamp as an industry standard test are that it does not provide a direct measure of radiant sensitivity as a function of wavelength and that it is a somewhat misleading term when the response of the photomultiplier lies outside the visible range. To assist the scientist in using photomultipliers, technical specifications for RCA photomultiplier types include photocathode spectral-response curves which give the sensitivity in absolute terms such as amperes per watt and quantum efficiency as a function of wavelength. Methods of computing the response of a given photodetector to a particular radiation source are outlined in the following section on **Spectral Response and Source-Detector Matching.**

FUNCTIONAL TESTING

In many applications it is appropriate to test photomultipliers in the same manner in which they are to be utilized in the final application. For example, photomultipliers to be used in scintillation counting may be tested by means of an NaI(Tl) crystal and a Cs^{137} source or a simulated NaI light source utilizing a tungsten lamp whose light passes through a one-half stock-thickness Corning 5113 glass-type CS-5-58 filter. Interference-type filters are becoming increasingly important in isolating specific wavelengths for testing photomultiplier tubes for laser applications.

TESTING FOR SCIENTIFIC AND MULTIPURPOSE APPLICATIONS

When a photomultiplier is manufactured for a variety of purposes, including scientific applications, it would be highly desirable if sensitivity were specified by a complete spectral response in terms of quantum efficiency or radiant sensitivity. This information could then be utilized in conjunction with the known spectral emission of any source to compute the response of the photomultiplier to that source. Complete spectral sensitivity data, however, are rarely provided because it is unnecessary for most practical situations and would considerably increase device costs.

REFERENCES

1. J. C. DeVos, *Physica, Vol. 20* (1954).
2. W. D. Buckingham and C. R. Deihert, "Characteristics and Applications of Concentrated Arc Lamps," *Journal of the Society of Motion Picture Engineers, Vol. 47* (1946).

* Now being changed to 2854°K color temperature to agree with international standards.

Spectral Response and Source-Detector Matching

THIS section covers the significance of the spectral response of photomultiplier tubes, describes some of the methods used for measuring this response; and discusses in some detail the calculations and other considerations useful for matching the radiation source and the photomultiplier tube type for a specific application.

SPECTRAL-RESPONSE CHARACTERISTICS

A spectral-response characteristic is a display of the response of a photosensitive device as a function of the wavelength of the exciting radiation. Such curves may be on an absolute or a relative basis. In the latter case the curves are usually normalized to unity at the peak of the spectral-response curve. For a photocathode the absolute radiant sensitivity is expressed in amperes per watt. Curves of absolute spectral response may also be expressed in terms of the quantum efficiency at the particular wavelength. If the curve is presented in terms of amperes per watt, lines of equal quantum efficiency may be indicated for convenient reference. Typical curves are usually included in tube data bulletins. Because there are variations in spectral response from tube to tube, the typical spectral-response characteristic usually includes an indication of the range over which the peak of the curve may be expected to vary, as well as an indication of the range over which the cut-off at either end of the spectral response may vary. These cut-off points are usually expressed at 10 per cent of the maximum value.

The spectral-response characteristic, and particularly the long-wavelength cut-off, are dependent upon the chemical composition and the processing of the particular photocathode. On the other hand, the ultraviolet cut-off characteristic is determined primarily by the characteristic cut-off transmission of the window of the tube.

MEASUREMENT TECHNIQUES

In order to determine a spectral-response characteristic, a source of essentially monochromatic radiation, a current-sensitive instrument to measure the output of the photocathode, and a method of calibrating the monochromatic radiation for its magnitude in units of power are required.

The source of monochromatic radiation is often a prism or a grating type of monochromator. Interference filters may also be used to isolate narrow spectral bands. Although interference filters do not provide the flexibility of a mono-

chromator, they may be indicated in situations in which repeated measurements are required in a particular region of the spectrum.

The width of the spectral transmission band in these measurements must be narrow enough to delineate the spectral-response characteristic in the required detail. However, for the most part, spectral-response characteristics do not require fine detail and generally have broad peaks with exponential cut-off characteristics at the long-wavelength limit and rather sharp cut-offs at the short-wavelength end. For spectral measurements, therefore, a reasonably wide band is used. Such a band has the following important advantages: (1) because the level of radiation is higher, measurements are easier and more precise; and (2) spectral leakage in other parts of the spectrum is relatively less important. Spectral leakage is a problem in any monochromator because of scattered radiation, and in any filter because there is some transmission outside the desired pass band. A double monochromator may be used and will greatly reduce the spectral leakage outside the pass band. The double monochromator is at a disadvantage in cost and complexity. If a pass band of 10 nanometers is used, spectral leakage can be insignificant for most of the spectral measurements. At the same time, this pass band is narrow enough to avoid distortion in the measured spectral-response characteristic. It is often advisable to vary the pass band depending upon what part of the curve is being measured. For example, at the long-wavelength cut-off where the response of the photocathode may be very small, the leakage spectrum may play a rather important part; thus it is advisable to increase the spectral bandpass of the measurement. Wide pass-band color filters which exclude the wavelength of the measurement and include the suspected spectral leakage region, or vice versa, are used in checking the magnitude of the possible leakage spectrum.

ENERGY SOURCES

Various radiant-energy sources are used to advantage in spectral-response measurements. A tungsten lamp is useful from about 450 nanometers to beyond 1200 nanometers because of its uniform and stable spectral-emission characteristic. The linear type of filament also provides good optical coupling to the slits used in monochromators. A mercury-vapor discharge lamp provides a high concentration in specific radiation lines and thus minimizes the background scattered-radiation problem. The mercury lamp is particularly useful in the ultraviolet end of the spectrum where the tungsten lamp fails.

MEASUREMENT OF RADIANT POWER OUTPUT

A radiation thermocouple or thermopile with a black absorbing surface is commonly used to measure the radiation power output at a specific wavelength. Although these devices are relatively low in sensitivity, they do provide a reasonably reliable means of measuring radiation independent of the wavelength. The limitation to their accuracy is the flatness of the spectral absorption characteristic of the black coating on the detector. Throughout the visible and near-infrared regions there is usually no problem. There is some question, however, as to the flatness of the response in the ultraviolet part of the spectrum.

The output of the thermocouple or thermopile is a voltage proportional to the input radiation power. This voltage is converted by means of a suitable sensitive voltmeter to a calibrated measure of power in watts. The calibration may be accomplished by means of standard radiation lamps obtained from the National Bureau of Standards. It is theoretically possible to calculate the monochromatic power from a knowledge of the emission characteristic of the source, the dispersion characteristic of the monochromator or the transmission characteristic of the filter, and from the transmission characteristic of the various lenses. This procedure is difficult, subject to error, and is not recommended except perhaps in the case of a tungsten lamp source combined with a narrow-band filter system.

MEASUREMENT OF PHOTOCATHODE OUTPUT

For measuring the spectral characteristic of a photocathode, a very sensitive ammeter is required. When the output of the photocathode of a photomultiplier is measured, the tube is usually operated as a photodiode by connecting all elements other than the photocathode together to serve as the anode. When the photomultiplier is operated as a conventional photomultiplier, the output is very easy to measure. It is necessary, however, to be careful to avoid fatigue effects which could distort the spectral-response measurement. It should be noted that the spectral response of a photomultiplier may be somewhat different than that of the photocathode alone because of the effect of initial velocities and their effect on collection efficiency at the first dynode and because of the possibility of a photoeffect on the first dynode by light transmitted through the photocathode, especially if the first dynode is a photosensitive material such as cesium-antimony.

A diagram of a typical arrangement for measurement of spectral response is shown in Fig. 102. In this arrangement a mirror is used in two angular orientations to reflect the radiation alternately to the thermocouple and to the photocathode. Other methods are also used to split the monochromatic beam so that both thermocouple and photocathode can be sampled alternately or simultaneously.

SOURCE AND DETECTOR MATCHING

One of the most important parameters to be considered in the selection of a photomultiplier type for a specific application is the photocathode spectral response. The spectral response of RCA photomultiplier

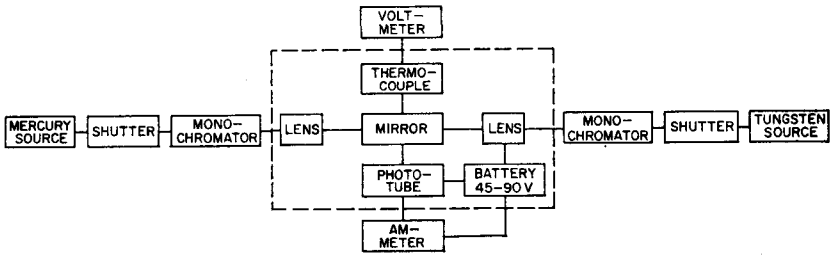

Fig. 102 — Diagram of typical arrangement for spectral-response measurements.

tubes covers the spectrum from the ultraviolet to the near-infrared region. In this range there are a large variety of spectral responses to choose from. Some cover narrow ranges of the spectrum while others cover a very broad range. The data sheet for each photomultiplier type shows the relative and absolute spectral-response curves for a typical tube of that particular type. The relative typical spectral-response curves published may be used for matching the detector to a light source for all but the most exacting applications. The matching of detector to source consists of choosing the photomultiplier tube type that has a spectral response providing maximum overlap of the spectral distributions of detector and light source.

MATCHING CALCULATIONS

The average power radiating from a light source may be expressed as follows:

$$\bar{P} = P_o \int_0^\infty W(\lambda)\, d\lambda \quad (105)$$

where P_o is the incident power in watts per unit wavelength at the peak of the relative spectral radiation characteristic, $W(\lambda)$, which is normalized to unity.

If the absolute spectral distribution for the light source and the absolute spectral response of the photomultiplier tube are known, the resulting photocathode current I_k when the light is incident on the detector can be expressed as follows:

$$I_k = \sigma P_o \int_0^\infty W(\lambda)\, R(\lambda)\, d\lambda \quad (106)$$

where σ is the radiant sensitivity of the photocathode in amperes per watt at the peak of the relative curve, and $R(\lambda)$ represents the relative photocathode spectral response as a function of wavelength normalized to unity at the peak. When Eq. (106) is solved for the peak power per unit wavelength, P_o, and this solution is substituted into Eq. (107), the cathode current is expressed as follows:

$$I_k = \sigma P \frac{\int_0^\infty W(\lambda)\, R(\lambda)\, d\lambda}{\int_0^\infty W(\lambda)\, d\lambda} \quad (107)$$

The ratio of the dimensionless integrals can be defined as the matching factor, M. The matching factor is the ratio of the area under the curve defined by the product of the relative source and detector spectral curves to the area under the relative spectral source curve.

$$M = \frac{\int_0^\infty W(\lambda)\, R(\lambda)\, d\lambda}{\int_0^\infty W(\lambda)\, d\lambda} \quad (108)$$

Fig. 103 shows an example of the data involved in the evaluation of the matching factor, M, as given in Eq. (108).

If the input light distribution incident on the detector is modified with a filter or any other optical device, the matching-factor formulas must be changed accordingly. If the transmission of the filter or optical device is $f(\lambda)$, the matching factor will be

$$M = \frac{\int_0^\infty W(\lambda)\, R(\lambda)\, f\lambda\, d\lambda}{\int_0^\infty W(\lambda)\, f(\lambda)\, d\lambda}$$

Table XII shows a number of matching factors for various light sources

Table XII — *Spectral Matching Factors.***

	Notes	PHOTOCATHODES S1 k	S4 k	S10 k	S11 k	S17 k	S20 k	S25 k	OTHER DETECTORS Photopic eye l	Scotopic eye m
Phosphors										
P1	a	0.278	0.498	0.807	0.687	0.892	0.700	0.853	0.768	0.743
P4	a,b	0.310	0.549	0.767	0.661	0.734	0.724	0.861	0.402	0.452
P7	a	0.312	0.611	0.805	0.709	0.773	0.771	0.882	0.411	0.388
P11	a	0.217	0.816	0.949	0.914	0.954	0.877	0.953	0.201	0.601
P15	a	0.385	0.701	0.855	0.787	0.871	0.802	0.904	0.376	0.495
P16	a	0.830	0.970	0.853	0.880	0.855	0.902	0.922	0.003	0.042
P20	a	0.395	0.284	0.612	0.427	0.563	0.583	0.782	0.707	0.354
P22B	c	0.217	0.893	0.974	0.960	0.948	0.927	0.979	0.808	0.477
P22G	c	0.278	0.495	0.807	0.686	0.896	0.699	0.855	0.784	0.747
P22R	c	0.632	0.036	0.264	0.055	0.077	0.368	0.623	0.225	0.008
P24	a	0.279	0.545	0.806	0.696	0.827	0.725	0.869	0.540	0.621
P31	a,d	0.276	0.533	0.811	0.698	0.853	0.722	0.868	0.626	0.651
NaI	e	0.534	0.923	0.885	0.889	0.889	0.900	0.933	0.046	0.224
Lamps										
2870/2854 std	f	0.516*	0.046*	0.095*	0.060*	0.072*	0.112*	0.227*	0.071*†	0.040*
Fluorescent	g	0.395	0.390	0.650	0.496	0.575	0.635	0.805	0.502	0.314
Sun										
In space	h	0.535*	0.308*	0.388*	0.328*	0.380*	0.406*	0.547*	0.179*	0.172*
+2 air masses	h,i	0.536*	0.236*	0.348*	0.277*	0.315*	0.360*	0.513*	0.197*	0.175*
Day sky	j	0.537*	0.520*	0.556*	0.508*	0.589*	0.581*	0.700*	0.170*	0.218*
Blackbodies										
6000°K	—	0.533*	0.308*	0.376*	0.320*	0.375*	0.397*	0.521*	0.167*	0.159*
3000°K	—	0.512*	0.053*	0.102*	0.067*	0.080*	0.120*	0.232*	0.075*	0.044*
2870°K	—	0.504*	0.044*	0.090*	0.057*	0.069*	0.106*	0.216*	0.067*	0.038*
2854°K	—	0.500*	0.042*	0.088*	0.055*	0.068*	0.103*	0.211*	0.065*	0.037*
2810°K	—	0.493*	0.039*	0.081*	0.051*	0.062*	0.097*	0.150*	0.061*	0.034*
2042°K	—	0.401*	0.008*	0.023*	0.011*	0.014*	0.033*	0.090*	0.018*	0.007*

* Entry valid only for 300-1200-nm wavelength interval.

† For the total wavelength spectrum this entry would be 0.0294.

Notes: **a** Registered spectral distribution. Data extrapolated as required.
b Sulfide type.
c RCA data.
d Low brightness type.
e Harshaw Chemical Co. data.
f Standard test lamp distribution.
g General Electric Co. data.
h From **Handbook of Geophysics.**
i Approximately noon sealevel flux at 60° latitude.
j From Gates between 300 nm and 530 nm. A 12,000°K blackbody spectral distribution was assumed between 530 nm and 1200 nm.
k Registered spectral distribution. Data extrapolated as required.
l Standard tabulated photopic visibility distribution.
m Standard tabulated scotopic visibility distribution.

** Data from E. H. Eberhardt, "Source-Detector Spectral Matching Factors", Applied Optics, 7, 2037, (1968)

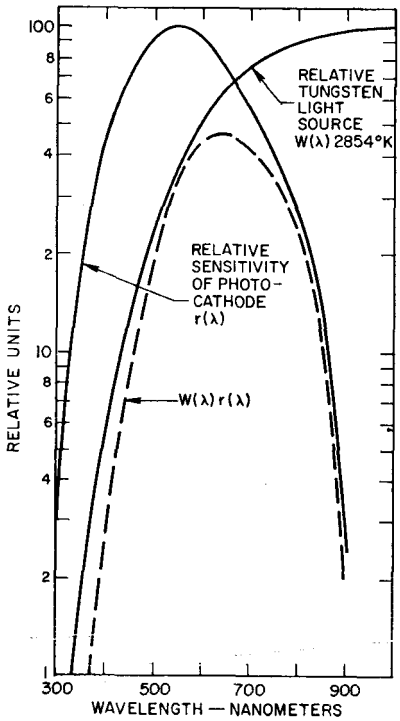

Fig. 103 — Graphic example of factors used in evaluation of matching factor M.

and spectral response characteristics. When the spectral range of a source exceeded 1200 nanometers, the integration was terminated at this wavelength. Because none of the photoresponses exceed 1200 nanometers, conclusions as to the relative merit of various combinations are still valid.

When M is substituted for the integral ratio in Eq. (107), the photocathode current becomes

$$I_k = \sigma \overline{P} M \qquad (109)$$

Matching Factor

In any photomultiplier application it is desirable to choose a detector having a photocathode spectral response that will maximize the photocathode current, I_k, for a given light source. Maximizing the cathode current is important to maximize the signal-to-noise ratio. From Eq. (109) it can be seen that the product of the matching factor M and the peak absolute photocathode sensitivity σ must be maximized to maximize the cathode current. It is advantageous then to define the product of the peak absolute cathode sensitivity σ and the matching factor M as N, a value to be selected as a maximum for a given light source:

$$N = \sigma M \qquad (110)$$

Therefore,

$$I_k = \overline{P} N \qquad (111)$$

The importance of taking into account the absolute photocathode sensitivity, as well as the matching factor, is illustrated by a comparison of the S-1 and S-20 photocathodes with a tungsten light source operating at a color temperature of 2854°K. The S-1 and the S-20 matching factors are 0.516 and 0.112, respectively. From the matching factors alone it appears that the S-1 is the best choice of photocathode spectral response. The S-1 has a peak absolute sensitivity of 2.5 milliamperes per watt and the S-20 has a peak absolute sensitivity of 64 milliamperes per watt. Calculation of the variable N for the two photocathodes yields the following results:

$$N\,(S\text{-}1) = 0.0025 \times 0.516 = 0.00129$$
$$N\,(S\text{-}20) = 0.064 \times 0.112 = 0.00716$$

These calculations show that the S-20 photocathode will provide a substantially larger response to the tungsten lamp than the S-1.

REFERENCES

1. E. H. Eberhardt, "Source-Detector Spectral Matching Factors," *Applied Optics, Vol. 7*, p. 2037 (1968).

Technical Data

THE tabulated data on the following pages are believed to be accurate and reliable for the listed types at the date of printing. However the data, especially for developmental types, are subject to change. It is recommended that RCA distributors or RCA field sales representatives be contacted for current information on the individual types.

The data shown have been measured using a tungsten-filament lamp operated at a color temperature of 2870°K. It is intended that future

PRELIMINARY SELECTION GUIDES
For Photomultiplier Tubes by Spectral Response

Spectral Response[a]	Nominal Tube Diameter Inches	Number of Stages	Viewing Configuration[b]	Cage Structure[c]	RCA Type No.●	Outline, Basing Diagram	MAXIMUM RATINGS	
							Supply Voltage (E) V	Average Anode Current mA
101 (S-1)	3/4	10	H	I	C70102B	4	1500	0.01
	1-1/8	9	S	C	C31004A	11	1500	0.01
	1-1/2	10	H	C	7102	18	1500	0.01
	1-1/2	10	H	C	C70114D	19	1500	0.01
	2	12	H	I	C70007A	25	2000	0.01
102 (S-4)	1/2	9	S	C	8571	1	1250	0.02
	1-1/8	9	S	C	1P21	11	1250	0.1
	1-1/8	9	S	C	931A	11	1250	1.0
	1-1/8	9	S	C	4471	11	1250	1.0
	1-1/8	9	S	C	4472	11	1250	1.0
	1-1/8	9	S	C	4473	11	1250	0.1
	1-1/8	9	S	C	6328	12	1250	0.1
	1-1/8	9	S	C	6472	13	1250	0.1
	1-1/8	9	S	C	7117	12	1250	0.1
	1-1/8	9	S	C	C7075J	11	1250	0.1
103	1-1/8	9	S	C	1P28/V1	11	1250	0.5
	1-1/8	9	S	C	1P28A/V1	11	1250	0.5

data for RCA photomultipliers be measured using the international color temperature of 2854°K.

Variants of the listed photomultipliers are also available having electrostatic and magnetic shielding and/or integral voltage-divider networks.

Photomultiplier variants of each of the listed types are also available with permanently attached bases, with temporary bases attached to semiflexible leads, or with flexible leads only.

TYPICAL CHARACTERISTICS AT THE SPECIFIED SUPPLY VOLTAGE AND 22° C

Supply Voltage V	Sensitivity				Current Amplification (Approx.)	Anode Dark Current nA@ Anode Luminous Sensitivity A/lm	Spectral Response*
	Radiant		Luminous				
	Cathode mA/W	Anode A/W	Cathode uA/lm	Anode A/lm			
1250	2.8	310	30	3.3	1.1×10^5	800 @ 4	
1250	1.9	235	20	2.5	1.25×10^5	300 @ 2	
1250	2.8	660	30	7	2.3×10^5	1900 @ 4	101 (S-1)
1250	2.8	420	30	4.5	1.5×10^5	1700 @ 4	
1250	2.8	940	30	10	3.3×10^5	400 @ 4	
1000	34	73,000	35	75	2.1×10^6	2 @ 20	
1000	40	120,000	40	120	3×10^6	1 @ 20	
1000	40	83,000	40	80	2×10^6	5 @ 20	
1000	40	100,000	40	100	2.5×10^6	5 @ 20	
1000	40	100,000	40	100	2.5×10^6	5 @ 20	
1000	40	160,000	40	160	4×10^6	1 @ 20	102 (S-4)
1000	—	35,000	—	35	—	—	
1000	—	32,500	—	35	—	—	
1000	—	35,000	—	35	—	—	
1000	40	83,000	40	80	2×10^6	5 @ 20	
1000	48	160,000	60	200	3.3×10^6	2 @ 40	103
1000	48	160,000	60	200	3.3×10^6	2 @ 40	

PRELIMINARY SELECTION GUIDES
For Photomultiplier Tubes by Spectral Response (cont'd)

Spectral Response[a]	Nominal Tube Diameter Inches	Number of Stages	Viewing Configuration[b]	Cage Structure[c]	RCA Type No.[d]	Outline, Basing Diagram	MAXIMUM RATINGS: Supply Voltage (E) V	MAXIMUM RATINGS: Average Anode Current mA
	1/2	9	S	C	C70129H	2	1250	0.02
104 (S-5)	1-1/8	9	S	C	1P28	11	1250	0.5
	1-1/8	9	S	C	1P28A	11	1250	0.5
105 (S-8)	1-1/8	9	S	C	1P22	11	1250	1.0
106 (S-10)	2	10	H	C	6217	26	1250	0.75
	3/4	6	H	I	7764	5	1500	0.5
	3/4	10	H	I	4460	4	1500	0.5
	3/4	10	H	I	7767	4	1500	0.5
	3/4	10	H	I	C70102E	4	1500	0.5
	3/4	12	H	I	C31005B	6	2000	0.5
	1-1/2	10	H	C	2060	18	1250	0.75
	1-1/2	10	H	C	2067	20	1250	0.75
	1-1/2	10	H	C	4438	21	1250	0.75
	1-1/2	10	H	C	4439	21	1250	0.75
	1-1/2	10	H	C	4440	21	1250	0.75
	1-1/2	10	H	C	4441	19	1250	0.75
	1-1/2	10	H	C	4441A	19	1250	0.75
	1-1/2	10	H	C	4461	19	1500	1.0
107 (S-11)	1-1/2	10	H	C	6199	18	1250	0.75
	1-1/2	10	H	C	C7151N	22	1600	0.5
	1-1/2	10	H	C	C70132B	20	1600	0.5
	2	10	H	C	2020	27	1500	2.0
	2	10	H	C	2061	28	1500	2.0
	2	10	H	C	2062	28	1250	0.75
	2	10	H	V	2063	29	2000	2.0
	2	10	H	C	5819	26	1250	0.75
	2	10	H	C	6342A	30	1500	2.0
	2	10	H	C	6655A	30	1250	0.75
	2	10	H	I	7746	31	2500	2.0
	2	10	H	V	8053	29	2000	2.0
	2	12	H	I	7850	25	2600	2.0
	2	14	H	I	7264	32	2400	2.0
	2	14	H	I	6810A	32	2400	2.0

TYPICAL CHARACTERISTICS AT THE SPECIFIED SUPPLY VOLTAGE AND 22° C

Supply Voltage V	Sensitivity				Current Amplification (Approx.)	Anode Dark Current nA@ Anode Luminous Sensitivity A/lm	Spectral Response*
	Radiant		Luminous				
	Cathode mA/W	Anode A/W	Cathode uA/lm	Anode A/lm			
1000	44	44,000	35	35	1×10^6	20 @ 20	
1000	50	120,000	40	100	2.5×10^6	5 @ 20	104 (S-5)
1000	50	250,000	40	200	5×10^6	5 @ 20	
1000	2.3	7500	3	10	3.3×10^6	6 @ 0.8	105 (S-8)
1000	20	50,000	40	100	2.5×10^6	200 @ 20	106 (S-10)
1200	48	480	60	0.6	1×10^4	2 @ 0.3	
1250	48	6000	60	7.5	1.25×10^5	6 @ 7.5	
1250	48	12,800	60	16	2.7×10^5	4 @ 7.5	
1250	56	8800	70	11	1.6×10^5	1.4 @ 7.5	
1500	56	120,000	70	155	2.2×10^6	100 @ 100	
1000	36	36,000	45	45	1×10^6	4.5 @ 20	
1000	60	16,000	74	20	2.7×10^5	2.6 @ 20	
1000	36	22,000	45	27	6×10^5	16 @ 20	
1000	36	22,000	45	27	6×10^5	16 @ 20	
1000	36	22,000	45	27	6×10^5	16 @ 20	
1000	36	22,000	45	27	6×10^5	16 @ 20	
1000	36	22,000	45	27	6×10^5	16 @ 20	
1250	48	8000	60	10	1.7×10^5	5 @ 10	
1000	36	36,000	45	45	1×10^6	4.5 @ 20	107 (S-11)
1500	70	56,000	85	70	8.1×10^5	0.8 @ 20	
1500	70	56,000	85	70	8.1×10^5	0.8 @ 20	
1250	40	4800	50	6	1.2×10^5	4 @ 20	
1250	64	—	80	—	—	—	
1000	61	96,000	76	120	1.6×10^6	6 @ 20	
1500	56	—	70	—	—	—	
1000	40	80,000	50	100	2×10^6	6 @ 20	
1250	64	25,000	80	31	3.9×10^5	4 @ 20	
1000	61	96,000	76	120	1.6×10^6	6 @ 20	
1500	56	100,000	70	130	1.8×10^6	16 @ 20	
1500	56	34,000	70	42	6×10^5	4 @ 9	
1800	56	510,000	70	640	9.1×10^6	64 @ 160	
2000	56	3,400,000	70	4200	6.1×10^7	1000 @ 2000	
2000	56	3,000,000	70	3800	5.4×10^7	1000 @ 2000	

PRELIMINARY SELECTION GUIDES
For Photomultiplier Tubes by Spectral Response (cont'd)

Spectral Response[a]	Nominal Tube Diameter Inches	Number of Stages	Viewing Configuration[b]	Cage Structure[c]	RCA Type No.●	Outline, Basing Diagram	MAXIMUM RATINGS	
							Supply Voltage (E) V	Average Anode Current mA
	3	10	H	V	2064B	38	2000	2.0
107 (S-11)	3	10	H	V	8054	38	2000	2.0
(Cont'd)	5	10	H	V	2065	41	2000	2.0
	5	10	H	V	8055	41	2000	2.0
108 (S-13)	2	10	H	C	6903	30	1250	0.75
109 (S-19)	1-1/8	9	S	C	7200	14	1250	0.5
	3/4	10	H	I	8644	4	2100	0.5
	3/4	10	H	I	8645	8	1800	0.1
	1-1/2	10	H	C	C70114C	19	1800	1.0
	2	10	H	V	4463	29	2500	1.0
110 (S-20)	2	10	H	I	7326	33	2400	1.0
	2	12	H	I	4459	25	2800	1.0
	2	14	H	I	7265	32	3000	1.0
	3	10	H	V	4464	38	2500	1.0
	5	10	H	V	4465	41	2500	1.0
111	1-1/2	10	DW	C	4526	23	2000	0.1
112	1-1/2	10	H	C	C70114E	19	1800	1.0
	3	14	S	I	C70045C	39	6000	1.0
113	2	12	H	I	C31000A	34	3000	1.0
	2	12	H	I	C31000B	34	3000	1.0
	3/4	10	H	I	C70042D	4	2100	0.5
114	2	10	H	V	C70109E	29	2500	1.0
	2	14	H	I	C7268	32	3000	1.0
	3/4	10	H	I	4516	4	1800	0.5
	3/4	10	H	I	C70102M	4	1800	0.5
	1	10	H	C	C31016A	9	1500	0.02
	1	10	H	C	C31016B	9	1500	0.02
	1-1/2	10	H	C	4517	18	1800	0.5
115	1-1/2	10	H	C	C7151Q	22	1800	0.5
	1-1/2	10	H	C	C70114F	19	1800	0.5
	1-1/2	10	H	C	C70132A	20	1800	0.5
	2	10	H	C	4518	30	2000	0.5
	2	10	H	V	4523	29	2500	0.5

TYPICAL CHARACTERISTICS AT THE SPECIFIED SUPPLY VOLTAGE AND 22° C

Supply Voltage V	Sensitivity				Current Amplification (Approx.)	Anode Dark Current nA@ Anode Luminous Sensitivity A/lm	Spectral Response*
	Radiant		Luminous				
	Cathode mA/W	Anode A/W	Cathode uA/lm	Anode A/lm			
1500	64	—	80	—	—	—	
1500	64	35,000	80	43	5.4×10^5	4 @ 9	107 (S-11)
1500	88	—	110	—	—	—	(Cont'd)
1500	88	35,000	110	44	4×10^5	4 @ 9	
1000	48	72,000	60	90	1.5×10^5	10 @ 20	108 (S-13)
1000	65	65,000	40	40	1×10^6	4 @ 20	109 (S-19)
1500	64	5100	150	12	8×10^4	1.2 @ 30	
1500	64	5100	150	12	8×10^4	1.2 @ 30	
1500	77	11,000	180	25	1.4×10^5	4 @ 10	
2000	68	11,000	160	25	1.6×10^5	4.8 @ 12	
1800	64	38,000	150	88	5.9×10^5	3 @ 20	110 (S-20)
2300	64	430,000	150	1000	6.6×10^6	30 @ 300	
2400	64	3,000,000	150	7200	4.8×10^7	50 @ 1000	
2000	68	11,000	160	25	1.6×10^5	4.8 @ 12	
2000	68	11,000	160	25	1.6×10^5	4.8 @ 12	
1250	89	4400	300	15	5×10^4	2 @ 20	111
1500	77	11,000	180	25	1.4×10^5	4 @ 10	112
5000	60	—	140	—	5×10^6	500 @ 1000	
2000	77	270,000	200	700	3.5×10^6	5 @ 200	113
2000	77	270,000	200	700	3.5×10^6	5 @ 200	
1500	60	4300	140	10	7.1×10^4	6 @ 30	
1500	68	3400	160	8	5×10^4	0.2 @ 6	114
2400	64	2,200,000	150	5200	3.4×10^7	50 @ 1000	
1500	71	56,000	60	47	8×10^5	0.2 @ 7	
1500	79	32,000	67	27	4×10^5	0.2 @ 7	
1250	71	12,000	60	10	6×10^5	0.5 @ 7	
1250	79	15,000	67	13	1.9×10^5	0.5 @ 7	
1500	79	56,000	67	47	7×10^5	0.2 @ 7	115
1500	79	39,000	67	33	5×10^5	0.3 @ 7	
1500	79	39,000	67	33	5×10^5	0.3 @ 7	
1500	79	65,000	67	55	8.2×10^5	0.4 @ 6.7	
1500	79	39,000	67	33	5×10^5	0.24 @ 7	
1500	71	32,000	60	27	4.5×10^5	0.5 @ 13	

PRELIMINARY SELECTION GUIDES
For Photomultiplier Tubes by Spectral Response (cont'd)

Spectral Response[a]	Nominal Tube Diameter Inches	Number of Stages	Viewing Configuration[b]	Cage Structure[c]	RCA Type No.●	Outline, Basing Diagram	MAXIMUM RATINGS: Supply Voltage (E) V	MAXIMUM RATINGS: Average Anode Current mA
115 (Cont'd)	3	10	H	V	4524	38	2500	0.5
	5	10	H	V	4525	41	2500	0.5
	5	10	H	V	C31027	42	2000	0.5
	5	12	H	V	C31029	43	2500	0.5
116	2	12	H	I	8575	34	3000	0.2
	2	12	H	I	8850	34	3000	0.2
	2	12	H	I	8851	34	3000	0.2
117	1-1/2	10	H	C	C70114J	19	1800	0.5
	3	14	S	I	C70045D	39	6000	1.0
118	5	14	H	I	4522	44	3000	0.5
	5	14	H	I	C70133B	44	3000	0.5
119	2	12	H	I	C31000E	34	2500	1.0
	2	12	H	I	C31000F	34	2500	1.0
120	2	10	H	V	8664	35	2000	2.0
	2	10	H	V	8664/V1	35	2000	2.0
121	3/4	12	H	I	C31005	6	2500	0.5
122	3	10	H	V	4521	40	2000	0.5
123	1/2	9	S	C	C70129E	3	1250	0.02
	1-1/8	9	S	C	C31022	15	1250	0.1
124	3/4	10	H	I	C70102N	4	1500	0.5
125	3/4	12	H	I	C70128	7	1800	0.5
126	2	5	H	I	C31024	36	6000	0.5
127	1-1/2	10	H	C	C7151U	24	1250	0.75
128	1-1/8	9	S	C	C31025C	16	1500	0.1
129	1-1/8	9	S	C	C31025B	16	1800	0.1
	1-1/8	9	S	C	C31025G	16	1800	0.1
130	2	10	H	C	C7164R	30	1500	0.5
131	3/4	10	H	I	C70042K	4	2100	0.5

TYPICAL CHARACTERISTICS AT THE SPECIFIED SUPPLY VOLTAGE AND 22° C

Supply Voltage V	Sensitivity: Radiant Cathode mA/W	Sensitivity: Radiant Anode A/W	Sensitivity: Luminous Cathode uA/lm	Sensitivity: Luminous Anode A/lm	Current Amplification (Approx.)	Anode Dark Current nA@ Anode Luminous Sensitivity A/lm	Spectral Response[a]
1500	71	32,000	60	27	4.5×10^5	1 @ 13	115 (Cont'd)
1500	80	32,000	67	27	4×10^5	1.5 @ 13	
1500	88	13,000	77	11.5	1.5×10^5	2 @ 0.9 A/incident lm[d]	
1750	88	130,000	77	115	1.5×10^6	20 @ 9 A/incident lm[d]	
2000	97	970,000	85	850	1×10^7	1 @ 200	116
2000	97	710,000	85	620	7.3×10^6	0.6 @ 200	
2000	97	710,000	85	620	7.3×10^6	0.6 @ 200	
2500	79	39,000	67	33	5×10^5	0.3 @ 7	117
5000	72	—	—	—	1×10^7	1000 @ 1000	
2000	88	2,600,000	77	2300	3×10^7	60 @ 2000	118
2000	88	2,600,000	77	2300	3×10^7	60 @ 2000	
1500	45	18,000	250	100	4×10^5	10 @ 30	119
1500	45	18,000	250	100	4×10^5	10 @ 30	
1500	69	18,000	67	17	2.6×10^5	1 @ 7.5	120
1500	69	18,000	67	17	2.6×10^5	1 @ 7.5	
2100	9.2 min. @ 253.7 nm	9200 min. @ 253.7 nm	—	—	1×10^6	0.1 @ 3000 A/W	121
1500	87	19,000	83	18	2.2×10^5	2 @ 7.5	122
1000	31	21,000	30	20	6.7×10^5	8 @ 15	123
1000	48	160,000	60	200	3.3×10^6	2 @ 40	
1250	72	4800	90	6	6.7×10^4	2 @ 7.5	124
1500	10 @ 253.7 nm	3000 @ 253.7 nm	—	—	3×10^5	0.1 @ 3000 A/W	125
3000	82	110,000	72	93	1.3×10^6	24 @ 85	126
1000	25	8200	60	20	3.3×10^5	10 @ 40	127
1250	33	1300	250	10	4×10^4	0.5 @ 10	128
1250	45	2000	160	7	4.4×10^4	0.5 @ 10	129
1250	28	1400	100	5	5×10^4	0.3 @ 5	
1250	40	20,000	200	100	5×10^5	30 @ 150	130
1500	45	3600	250	20	8×10^4	6 @ 30	131

PRELIMINARY SELECTION GUIDES
For Photomultiplier Tubes by Spectral Response (cont'd)

Spectral Response[a]	Nominal Tube Diameter Inches	Number of Stages	Viewing Configuration[b]	Cage Structure[c]	RCA Type No.●	Outline, Basing Diagram	MAXIMUM RATINGS: Supply Voltage (E) V	MAXIMUM RATINGS: Average Anode Current mA
132	3/4	10	H	I	C70042R	4	2100	0.5
	1	12	H	I	C31026	10	2200	0.5
	1-1/2	10	H	C	C7151W	18	1500	0.5
133	3/4	10	H	I	C70042J	4	1800	0.5
136	1-1/8	9	S	C	C31028	17	1250	0.5
137	2	11	H	I	C31000K	37	2000	0.1
138	1-1/2	10	H	C	C7151Y	24	1500	0.5

[a] See bar chart of Spectral response on page 156.
[b] Viewing configurations: H, head on; S, side on; and DW, dormer window.
[c] Cage structures: C, circular cage; I, in line; and V, venetian blind.
[d] With blue light source. Tungsten light source at color temperature of 2870°K. Corning C.S. No. 5-58, 1/2 stock thickness.

● Type numbers with prefix C are developmental types. Each of these C numbers identifies a particular laboratory tube design but the number and the identifying data are subject to change. No obligations are assumed as to future manufacture unless otherwise arranged.

PRELIMINARY SELECTION GUIDES
For Photomultiplier Tubes by Diameter

Nominal Tube Diameter Inches	Spectral Response[a]	Number of Stages	Viewing Configuration[b]	Cage Structure[c]	RCA Type No.●	Outline, Basing Diagram	MAXIMUM RATINGS: Supply Voltage (E) V	MAXIMUM RATINGS: Average Anode Current mA
1/2	102 (S-4)	9	S	C	8571	1	1250	0.02
	104 (S-5)	9	S	C	C70129H	2	1250	0.02
	123	9	S	C	C70129G	3	1250	0.02
3/4	101 (S-1)	10	H	I	C70102B	4	1500	0.01
	107 (S-11)	6	H	I	7764	5	1500	0.5
		10	H	I	4460	4	1500	0.5
		10	H	I	7767	4	1500	0.5
		10	H	I	C70102E	4	1500	0.5
		12	H	I	C31005B	6	2000	0.5

TYPICAL CHARACTERISTICS AT THE SPECIFIED SUPPLY VOLTAGE AND 22° C

Supply Voltage V	Sensitivity				Current Amplification (Approx.)	Anode Dark Current nA@ Anode Luminous Sensitivity A/lm	Spectral Response*
	Radiant		Luminous				
	Cathode mA/W	Anode A/W	Cathode uA/lm	Anode A/lm			
1500	44	5500	200	25	1.25×10^5	2 @ 30	
1800	43	26,000	250	150	6×10^5	40 @ 50	132
1250	40	10,000	200	50	2.5×10^5	1 @ 20	
1800	71	56,000	60	47	8×10^5	0.2 @ 7	133
1000	54	175,000	65	200	3.1×10^6	0.8 @ 20	136
1500	35	21,000	330	200	6×10^5	6 @ 100	137
1250	40	2400	200	12	6×10^4	3 @ 10	138

TYPICAL CHARACTERISTICS AT THE SPECIFIED SUPPLY VOLTAGE AND 22° C

Supply Voltage V	Sensitivity				Current Amplification (Approx.)	Anode Dark Current nA@ Anode Luminous Sensitivity A/lm	Nominal Tube Diameter Inches
	Radiant		Luminous				
	Cathode mA/W	Anode A/W	Cathode uA/lm	Anode A/lm			
1000	34	73,000	35	75	2.1×10^6	2 @ 20	
1000	44	44,000	35	35	1×10^6	20 @ 20	1/2
1000	31	21,000	30	20	6.7×10^5	8 @ 15	
1250	2.8	310	30	3.3	1.1×10^5	800 @ 4	
1200	48	480	60	0.6	1×10^4	2 @ 0.3	
1250	48	6000	60	7.5	1.25×10^5	6 @ 7.5	3/4
1250	48	12,800	60	16	2.7×10^5	4 @ 7.5	
1250	56	8800	70	11	1.6×10^5	1.4 @ 7.5	
1500	56	120,000	70	155	2.2×10^6	100 @ 100	

PRELIMINARY SELECTION GUIDES
For Photomultiplier Tubes by Diameter (cont'd)

Nominal Tube Diameter Inches	Spectral Response[a]	Number of Stages	Viewing Configuration[b]	Cage Structure[c]	RCA Type No.●	Outline, Basing Diagram	MAXIMUM RATINGS: Supply Voltage (E) V	MAXIMUM RATINGS: Average Anode Current mA
3/4 (Cont'd)	110 (S-20)	10	H	I	8644	4	2100	0.5
		10	H	I	8645	8	1800	0.1
	114	10	H	I	C70042D	4	2100	0.5
	115	10	H	I	4516	4	1800	0.5
		10	H	I	C70102M	4	1800	0.5
	121	12	H	I	C31005	6	2500	0.5
	124	10	H	I	C70102N	4	1500	0.5
	125	12	H	I	C70128	7	1800	0.5
	131	10	H	I	C70042K	4	2100	0.5
	132	10	H	I	C70042R	4	2100	0.5
	133	10	H	I	C70042J	4	1800	0.5
1	115	10	H	C	C31016A	9	1500	0.02
		10	H	C	C31016B	9	1500	0.02
	132	12	H	I	C31026	10	2200	0.5
1-1/8	101 (S-1)	9	S	C	C31004A	11	1500	0.01
	102 (S-4)	9	S	C	1P21	11	1250	0.1
		9	S	C	931A	11	1250	1.0
		9	S	C	4471	11	1250	1.0
		9	S	C	4472	11	1250	1.0
		9	S	C	4473	11	1250	0.1
		9	S	C	6328	12	1250	0.1
		9	S	C	6472	13	1250	0.1
		9	S	C	7117	12	1250	0.1
		9	S	C	C7075J	11	1250	0.1
	103	9	S	C	1P28/V1	11	1250	0.5
		9	S	C	1P28A/V1	11	1250	0.5
	104 (S-5)	9	S	C	1P28	11	1250	0.5
		9	S	C	1P28A	11	1250	0.5
	105 (S-8)	9	S	C	1P22	11	1250	1.0
	109 (S-19)	9	S	C	7200	14	1250	0.5
	123	9	S	C	C31022	15	1250	0.1

TYPICAL CHARACTERISTICS AT THE SPECIFIED SUPPLY VOLTAGE AND 22° C

Supply Voltage V	Sensitivity				Current Amplification (Approx.)	Anode Dark Current nA@ Anode Luminous Sensitivity A/lm	Nominal Tube Diameter Inches
	Radiant		Luminous				
	Cathode mA/W	Anode A/W	Cathode uA/lm	Anode A/lm			
1500	64	5100	150	12	8×10^4	3 @ 30	
1500	64	5100	150	12	8×10^4	3 @ 30	
1500	60	4300	140	10	7.1×10^4	6 @ 30	
1500	71	56,000	60	47	8×10^5	0.2 @ 7	
1500	79	32,000	67	27	4×10^5	0.2 @ 7	
2100	9.2 min. @ 253.7 nm	9200 min. @ 253.7 nm	—	—	1×10^6 min.	0.1 @ 3000 A/W	3/4
1250	72	4800	90	6	6.7×10^4	2 @ 7.5	(Cont'd)
1500	10 @ 253.7 nm	3000 @ 253.7 nm	—	—	3×10^5	0.1 @ 3000 A/W	
1500	45	3600	250	20	8×10^4	6 @ 30	
1500	44	5500	200	25	1.25×10^5	2 @ 30	
1800	71	56,000	60	47	8×10^5	0.2 @ 7	
1250	71	12,000	60	10	6×10^5	0.5 @ 7	
1250	79	15,000	67	13	1.9×10^5	0.5 @ 7	1
1800	43	26,000	250	150	6×10^5	40 @ 50	
1250	1.9	235	20	2.5	1.25×10^5	300 @ 2	
1000	40	120,000	40	120	3×10^6	1 @ 20	
1000	40	83,000	40	80	2×10^6	5 @ 20	
1000	40	100,000	40	100	2.5×10^6	5 @ 20	
1000	40	100,000	40	100	2.5×10^6	5 @ 20	
1000	40	160,000	40	160	4×10^6	1 @ 20	
1000	—	35,000	—	35	—	—	
1000	—	32,500	—	35	—	—	
1000	—	35,000	—	35	—	—	1-1/8
1000	40	83,000	40	80	2×10^6	5 @ 20	
1000	48	160,000	60	200	3.3×10^6	2 @ 40	
1000	48	160,000	60	200	3.3×10^6	2 @ 40	
1000	50	120,000	40	100	2.5×10^6	5 @ 20	
1000	50	250,000	40	200	5×10^6	5 @ 20	
1000	2.3	7500	3	10	3.3×10^6	6 @ 0.8	
1000	65	65,000	40	40	1×10^6	4 @ 20	
1000	48	160,000	60	200	3.3×10^6	2 @ 40	

PRELIMINARY SELECTION GUIDES
For Photomultiplier Tubes by Diameter (cont'd)

Nominal Tube Diameter Inches	Spectral Response[a]	Number of Stages	Viewing Configuration[b]	Cage Structure[c]	RCA Type No.[e]	Outline, Basing Diagram	MAXIMUM RATINGS: Supply Voltage (E) V	MAXIMUM RATINGS: Average Anode Current mA
1-1/8 (Cont'd)	128	9	S	C	C31025C	16	1500	0.1
	129	9	S	C	C31025B	16	1800	0.1
		9	S	C	C31025G	16	1800	0.1
	136	9	S	C	C31028	17	1250	0.5
1-1/2	101 (S-1)	10	H	C	7102	18	1500	0.01
		10	H	C	C70114D	19	1500	0.01
	107 (S-11)	10	H	C	2060	18	1250	0.75
		10	H	C	2067	20	1250	0.75
		10	H	C	4438	21	1250	0.75
		10	H	C	4439	21	1250	0.75
		10	H	C	4440	21	1250	0.75
		10	H	C	4441	19	1250	0.75
		10	H	C	4441A	19	1250	0.75
		10	H	C	4461	19	1500	1.0
		10	H	C	6199	18	1250	0.75
		10	H	C	C7151N	22	1600	0.5
		10	H	C	C70132B	20	1600	0.5
	110 (S-20)	10	H	C	C70114C	19	1800	1.0
	111	10	DW	C	4526	23	2000	0.1
	112	10	H	C	C70114E	19	1800	1.0
	115	10	H	C	4517	18	1800	0.5
		10	H	C	C70114F	19	1800	0.5
		10	H	C	C7151Q	22	1800	0.5
		10	H	C	C70132A	20	1800	0.5
	117	10	H	C	C70114J	19	1800	0.5
	127	10	H	C	C7151U	24	1250	0.75
	132	10	H	C	C7151W	18	1500	0.5
	138	10	H	C	C7151Y	24	1500	0.5
2	101 (S-1)	12	H	I	C70007A	25	2000	0.01
	106 (S-10)	10	H	C	6217	26	1250	0.75
	107 (S-11)	10	H	C	2020	27	1500	2.0
		10	H	C	2061	28	1500	2.0
		10	H	C	2062	28	1250	0.75

TYPICAL CHARACTERISTICS AT THE SPECIFIED SUPPLY VOLTAGE AND 22° C							
Supply Voltage V	Sensitivity				Current Amplification (Approx.)	Anode Dark Current nA@ Anode Luminous Sensitivity A/lm	Nominal Tube Diameter Inches
	Radiant		Luminous				
	Cathode mA/W	Anode A/W	Cathode uA/lm	Anode A/lm			
1250	33	1300	250	10	4×10^4	0.5 @ 10	
1250	45	2000	160	7	4.4×10^4	0.5 @ 10	1-1/8
1250	28	1400	100	5	5×10^4	0.3 @ 5	(Cont'd)
1000	54	175,000	65	200	3.1×10^6	0.8 @ 20	
1250	2.8	660	30	7	2.3×10^5	1900 @ 4	
1250	2.8	420	30	4.5	1.5×10^5	1700 @ 4	
1000	36	36,000	45	45	1×10^6	4.5 @ 20	
1000	60	16,000	74	20	2.7×10^5	2.6 @ 20	
1000	36	22,000	45	27	6×10^5	16 @ 20	
1000	36	22,000	45	27	6×10^5	16 @ 20	
1000	36	22,000	45	27	6×10^5	16 @ 20	
1000	36	22,000	45	27	6×10^5	16 @ 20	
1000	36	22,000	45	27	6×10^5	16 @ 20	
1250	48	8000	60	10	1.7×10^5	5 @ 10	
1000	36	36,000	45	45	1×10^6	4.5 @ 20	1-1/2
1500	70	56,000	85	70	8.1×10^5	0.8 @ 20	
1500	70	56,000	85	70	8.1×10^5	0.8 @ 20	
1500	77	11,000	180	25	1.4×10^5	4 @ 10	
1250	89	4400	300	15	5×10^4	2 @ 20	
1500	77	11,000	180	25	1.4×10^5	4 @ 10	
1500	79	56,000	67	47	7×10^5	0.2 @ 7	
1500	79	39,000	67	33	5×10^5	0.3 @ 7	
1500	79	39,000	67	33	5×10^5	0.3 @ 7	
1500	79	65,000	67	55	8.2×10^5	0.4 @ 6.7	
1500	79	39,000	67	33	5×10^5	0.3 @ 7	
1000	24	8200	60	20	3.3×10^5	10 @ 40	
1250	40	10,000	200	50	2.5×10^5	1 @ 20	
1250	40	2400	200	12	6×10^4	3 @ 10	
1250	2.8	940	30	10	3.3×10^5	400 @ 4	
1000	20	50,000	40	100	2.5×10^6	200 @ 20	
1250	40	4800	50	6	1.2×10^5	4 @ 20	2
1250	64	—	80	—	—	—	
1000	61	96,000	76	120	1.6×10^6	6 @ 20	

PRELIMINARY SELECTION GUIDES
For Photomultiplier Tubes by Diameter (cont'd)

Nominal Tube Diameter Inches	Spectral Response[a]	Number of Stages	Viewing Configuration[b]	Cage Structure[c]	RCA Type No. •	Outline, Basing Diagram	MAXIMUM RATINGS: Supply Voltage (E) V	MAXIMUM RATINGS: Average Anode Current mA
2 (Cont'd)	107 (S-11) (Cont'd)	10	H	V	2063	29	2000	2.0
		10	H	C	5819	26	1250	0.75
		10	H	C	6342A	30	1500	2.0
		10	H	C	6655A	30	1250	0.75
		10	H	I	7746	31	2500	2.0
		10	H	V	8053	29	2000	2.0
		12	H	I	7850	25	2600	2.0
		14	H	I	6810A	32	2400	2.0
		14	H	I	7264	32	2400	2.0
	108 (S-13)	10	H	C	6903	30	1250	0.75
	110 (S-20)	10	H	V	4463	29	2500	1.0
		10	H	I	7326	33	2400	1.0
		12	H	I	4459	25	2800	1.0
		14	H	I	7265	32	3000	1.0
	113	12	H	I	C31000A	34	3000	1.0
		12	H	I	C31000B	34	3000	1.0
	114	10	H	V	C70109E	29	2500	1.0
		14	H	I	C7268	32	3000	1.0
	115	10	H	C	4518	30	2000	0.5
		10	H	V	4523	29	2500	0.5
	116	12	H	I	8575	34	3000	0.2
		12	H	I	8850	34	3000	0.2
		12	H	I	8851	34	3000	0.2
	119	12	H	I	C31000E	34	2500	1.0
		12	H	I	C31000F	34	2500	1.0
	120	10	H	V	8664	35	2000	2.0
		10	H	V	8664/V1	35	2000	2.0
	126	5	H	I	C31024	36	6000	0.5
	130	10	H	C	C7164R	30	1500	0.5
	137	11	H	I	C31000K	37	2000	0.1
3	107 (S-11)	10	H	V	2064B	38	2000	2.0
		10	H	V	8054	38	2000	2.0
	110 (S-20)	10	H	V	4464	38	2500	1.0

TYPICAL CHARACTERISTICS AT THE SPECIFIED SUPPLY VOLTAGE AND 22° C							
Supply Voltage V	Sensitivity				Current Amplification (Approx.)	Anode Dark Current nA@ Anode Luminous Sensitivity A/lm	Nominal Tube Diameter Inches
	Radiant		Luminous				
	Cathode mA/W	Anode A/W	Cathode uA/lm	Anode A/lm			
1500	56	—	70	—	—	—	
1000	40	80,000	50	100	2×10^6	6 @ 20	
1250	64	25,000	80	31	3.9×10^5	4 @ 20	
1000	61	96,000	76	120	1.6×10^6	6 @ 20	
1500	56	100,000	70	130	1.8×10^6	16 @ 20	
1500	56	34,000	70	42	6×10^5	4 @ 9	
1800	56	510,000	70	640	9.1×10^6	64 @ 160	
2000	56	3,000,000	70	3800	5.4×10^7	1000 @ 2000	
2000	56	3,400,000	70	4200	6.1×10^7	1000 @ 2000	
1000	48	72,000	60	90	1.5×10^6	10 @ 20	
2000	68	11,000	160	25	1.6×10^5	4.8 @ 12	
1800	64	38,000	150	88	5.9×10^5	3 @ 20	
2300	64	430,000	150	1000	6.6×10^6	30 @ 300	
2400	64	3,000,000	150	7200	4.8×10^7	50 @ 1000	
2000	77	270,000	200	700	3.5×10^6	5 @ 200	2
2000	77	270,000	200	700	3.5×10^6	5 @ 200	(Cont'd)
1500	68	3400	160	8	5×10^4	0.2 @ 6	
2400	64	2,200,000	150	5200	3.4×10^7	50 @ 1000	
1500	79	39,000	67	33	5×10^5	0.24 @ 7	
1500	71	32,000	60	27	4.5×10^5	0.5 @ 13	
2000	97	970,000	85	850	1×10^7	1 @ 200	
2000	97	710,000	85	620	7.3×10^6	0.6 @ 200	
2000	97	710,000	85	620	7.3×10^6	0.6 @ 200	
1500	45	18,000	250	100	4×10^5	10 @ 30	
1500	45	18,000	250	100	4×10^5	10 @ 30	
1500	69	18,000	67	17	2.6×10^5	1 @ 7.5	
1500	69	18,000	67	17	2.6×10^5	1 @ 7.5	
3000	82	110,000	72	93	1.3×10^6	24 @ 85	
1250	40	20,000	200	100	5×10^5	30 @ 150	
1500	35	21,000	330	200	6×10^5	6 @ 100	
1500	64	—	80	—	—	—	
1500	64	35,000	80	43	5.4×10^5	4 @ 9	3
2000	68	11,000	160	25	1.6×10^5	4.8 @ 12	

PRELIMINARY SELECTION GUIDES
For Photomultiplier Tubes by Diameter (cont'd)

Nominal Tube Diameter Inches	Spectral Response[a]	Number of Stages	Viewing Configuration[b]	Cage Structure[c]	RCA Type No. •	Outline, Basing Diagram	MAXIMUM RATINGS: Supply Voltage (E) V	MAXIMUM RATINGS: Average Anode Current mA
3 (Cont'd)	112	14	S	I	C70045C	39	6000	1.0
	115	10	H	V	4524	38	2500	0.5
	117	14	S	I	C70045D	39	6000	1.0
	122	10	H	V	4521	40	2000	0.5
5	107 (S-11)	10	H	V	2065	41	2000	2.0
		10	H	V	8055	41	2000	2.0
	110 (S-20)	10	H	V	4465	41	2500	1.0
	115	10	H	V	4525	41	2500	0.5
		10	H	V	C31027	42	2000	0.5
		12	H	V	C31029	43	2500	0.5
	118	14	H	I	4522	44	3000	0.5
		14	H	I	C70133B	44	3000	0.5

[a] See bar chart of Spectral response on page 156.
[b] Viewing configurations: H, head on; S, side on; and DW, dormer window.
[c] Cage structures: C, circular cage; I, in line; and V, venetian blind.
[d] With *blue light source. Tungsten light source* at color temperature of 2870°K. Corning C.S. No. 5-58, 1/2 stock thickness.

• Type numbers with prefix C are developmental types. Each of these C numbers identifies a particular laboratory tube design but the number and the identifying data are subject to change. No obligations are assumed as to future manufacture unless otherwise arranged.

PRELIMINARY SELECTION GUIDES
Ruggedized Photomultiplier Tubes by Size

Nominal Tube Diameter Inches	Spectral Response[a]	Viewing Configuration[b]	Cage Structure[c]	RCA Type Number	Military Specification[d]
1/2	S-4 (102)	S	C	8571	—
	S-5 (104)	S	C	C70129H	—
3/4	S-1 (101)	H	I	C70102B	MIL-E-5272C

TYPICAL CHARACTERISTICS AT THE SPECIFIED SUPPLY VOLTAGE AND 22° C

Supply Voltage V	Sensitivity[1] Radiant Cathode mA/W	Radiant Anode A/W	Luminous Cathode uA/lm	Luminous Anode A/lm	Current Amplification (Approx.)	Anode Dark Current nA@ Anode Luminous Sensitivity A/lm	Nominal Tube Diameter Inches
5000	60	—	140	—	5×10^6	500 @ 1000	
1500	71	32,000	60	27	4.5×10^5	1 @ 13	3
5000	72	—	—	—	1×10^7	1000 @ 10,000	(Cont'd)
1500	87	19,000	83	18	2.2×10^5	2 @ 7.5	
1500	88	—	110	—	—	—	
1500	88	35,000	110	44	4×10^5	4 @ 9	
2000	68	11,000	160	25	1.6×10^5	4.8 @ 12	
1500	80	32,000	67	27	4×10^5	1.5 @ 13	5
1500	88	13,000	77	11.5	1.5×10^5	2 @ 0.9 A/incident lm[d]	
1750	88	130,000	77	11.5	1.5×10^6	20 @ 9 A/incident lm[d]	
2000	88	2,600,000	77	2300	3×10^7	60 @ 2000	
2000	88	2,600,000	77	2300	3×10^7	60 @ 2000	

Quality Conformance Inspection[f]	ENVIRONMENTAL TESTING[e] Shock	Vibration[g]	Acceleration	Temperature Cycling	Nominal Tube Diameter Inches
Design	30 g 11 ms	20 g 5-2000 Hz 1-1/2 hrs	15 g 5 min	−45 +75°C 8 hrs	1/2
Design	30 g 11 ms	20 g 5-2000 Hz 1-1/2 hrs	15 g 5 min	−45 +75°C 8 hrs	
100%	30 g 11 ms	20 g 20-2000 Hz 15 min			3/4
Design	30 g 11 ms	20 g 20-2000 Hz 6 hrs	100 g 1 min		

PRELIMINARY SELECTION GUIDES
Ruggedized Photomultiplier Tubes by Size (cont'd)

Nominal Tube Diameter Inches	Spectral Response[a]	Viewing Configuration[b]	Cage Structure[c]	RCA Type Number	Military Specification[d]
3/4 (Cont'd)	S-11 (107)	H	I	4460	MIL-E-5272C
	S-11 (107)	H	I	C70102E	MIL-E-5272C
	115	H	I	C70102M	MIL-E-5272C
	124	H	I	C70102N	MIL-E-5272C
1	115	H	C	C31016A	MIL-STD 810 B
	115	H	C	C31016B	MIL-STD 810 B
1-1/2	S-11 (107)	H	C	4441A	MIL-E-5272C
	S-11 (107)	H	C	4461	MIL-E-5272C
	S-11 (107)	H	C	C7151N	MIL-E-5272C
	115	H	C	C7151Q	MIL-E-5272C
	S-20 (110)	H	C	C70114C	MIL-E-5272C
	S-1 (101)	H	C	C70114D	MIL-E-5272C

Quality Conformance Inspection[f]	ENVIRONMENTAL TESTING[e] Shock	Vibration[g]	Acceleration	Temperature Cycling	Nominal Tube Diameter Inches
100%	30 g 11 ms	20 g 20-2000 Hz 15 min			
Design		20 g 20-2000 Hz 6 hrs	100 g 1 min		
100%	30 g 11 ms	20 g 20-2000 Hz 15 min			
Design	30 g 11 ms	20 g 20-2000 Hz 6 hrs	100 g 1 min		3/4
100%	30 g 11 ms	20 g 20-2000 Hz 15 min			(Cont'd)
Design	30 g 11 ms	20 g 20-2000 Hz 6 hrs	100 g 1 min		
100%	30 g 11 ms	20 g 20-2000 Hz 15 min			
Design	30 g 11 ms	20 g 20-2000 Hz 6 hrs	100 g 1 min		
Design	75 g 11 ms	20.7 g (rms) 50-2000 Hz 1-1/2 hrs	100 g		
Design	75 g 11 ms	20.7 g (rms) 50-2000 Hz 1-1/2 hrs	100 g		1
100%	30 g 11 ms	20 g 20-2000 Hz 15 min			
Design		20 g 20-2000 Hz 6 hrs	100 g 1 min		
100%	30 g 11 ms	20 g 20-2000 Hz 15 min			
Design		20 g 20-2000 Hz 6 hrs	100 g 1 min		
100%		20 g 20-2000 Hz 15 min			1-1/2
Design	30 g 11 ms	20 g 20-2000 Hz 6 hrs	100 g 1 min		
Design	30 g 11 ms	20 g 20-2000 Hz 6 hrs	100 g 1 min		
Design	30 g 11 ms	20 g 20-2000 Hz 6 hrs	100 g 1 min		
100%	30 g 11 ms	20 g 20-2000 Hz 15 min			
Design	30 g 11 ms	20 g 20-2000 Hz 6 hrs	100 g 1 min		

PRELIMINARY SELECTION GUIDES
Ruggedized Photomultiplier Tubes by Size (cont'd)

Nominal Tube Diameter Inches	Spectral Response[a]	Viewing Configuration[b]	Cage Structure[c]	RCA Type Number	Military Specification[d]
1-1/2 (Cont'd)	112	H	C	C70114E	MIL-E-5272C
	115	H	C	C70114F	MIL-E-5272C
	115	H	C	C70132A	MIL-E-5272C
	117	H	C	C70114J	MIL-E-5272C
	S-11 (107)	H	C	C70132B	MIL-E-5272C
2	120	H	V	8664	—
	120	H	V	8664/V1	—

[a] See bar chart of spectral response on page 156.
[b] Viewing configurations: H, head on; and S, side on.
[c] Cage structures: C, circular cage; I, in line; and V, venetian blind.
[d] Military Specifications:
MIL-E-5272C, 13 April 1959, Amendment 1, 5 January 1960;
MIL-STD-810B, 15 June 1967
[e] For detailed information on environmental testing, request a technical data sheet on the specific type.
[f] Quality Conformance Inspection: 100%, every tube tested; sample, some tubes tested from each lot; and Design, initial tubes only are tested.
[g] Vibration: Cycling ranges from minimum; to maximum to minimum; time is total time for vibration in three axes (equal time for each axis).

Quality Conformance Inspection[f]	ENVIRONMENTAL TESTING[e] Shock	Vibration[g]	Acceleration	Temperature Cycling	Nominal Tube Diameter inches
Design	30 g 11 ms	20 g 20-2000 Hz 6 hrs	100 g 1 min		
Design	30 g 11 ms	20 g 20-2000 Hz 6 hrs	100 g 1 min		
Design	30 g 11 ms	20 g 20-2000 Hz 6 hrs	100 g 1 min		1-1/2 (Cont'd)
Design	30 g 11 ms	20 g 20-2000 Hz 6 hrs	100 g 1 min		
100%		20 g 20-2000 Hz 15 min			
Design	30 g 11 ms	20 g 20-2000 Hz 6 hrs	100 g 1 min		
Sample	150 g 11 ms 1500 g 50 ms	60 g 48-3000 Hz 15 min			
Design		60 g 48-3000 Hz 6 hr	150 g 6 min		2
Sample	150 g 11 ms 1500 g 50 ms	60 g 48-3000 Hz 15 min			
Design		60 g 48-3000 Hz 6 hr	150 g 6 hr		

SPECTRAL RESPONSE AND RELATED PHOTOCATHODE CHARACTERISTICS

SPECTRAL RESPONSE				TYPICAL DATA			
RCA Code No.	EIA Designation	Cathode Material	Window Material	k lm/W	S μA/lm	σ mA/W	Approx. QE %
101	S-1	Ag-O-Cs	Lime or Borosil.	94	30	2.8	0.4
102	S-4	Cs-Sb	Lime or Borosil.	1036	40	40	12.4
103	—	Cs-Sb	UV Glass	800	60	48	13.2
104	S-5	Cs-Sb	UV Glass	1253	40	50	18.2
105	S-8	Cs-Bi	Lime or Borosil.	754	3	2.3	0.8
106	S-10	Ag-Bi-O-Cs	Lime or Borosil.	508	40	20	5.5
107	S-11	Cs-Sb	Lime or Borosil.	803	70	56	15.7
108	S-13	Cs-Sb	Fused Silica	794	60	48	13.5
109	S-19	Cs-Sb	Fused Silica	1593	40	65	24.4
110	S-20	Na-K-Cs-Sb	Lime or Borosil.	429	150	64	18.8
111	—	Na-K-Cs-Sb	Lime or Borosil.	295	300	89	20.8
112	—	Na-K-Cs-Sb	UV Glass	428	180	77	22.7
113	—	Na-K-Cs-Sb	Pyrex	385	200	77	23.9
114	—	Na-K-Cs-Sb	Fused Silica	428	140	60	17.7
115	—	K-Cs-Sb	Lime or Borosil.	1190	67	79	24.5
116	—	K-Cs-Sb	Pyrex	1140	85	97	31.2
117	—	K-Cs-Sb	UV Glass	1190	67	79	24.4
118	—	K-Cs-Sb	UV Glass	1140	77	88	27.2
119	—	Na-K-Cs-Sb	Pyrex	180	250	45	9.7
120	—	K-Cs-Sb	UV-grade Sapphire	1030	60	71	22
121	—	Cs-Te	Fused Silica	—	—	11.6	7.2

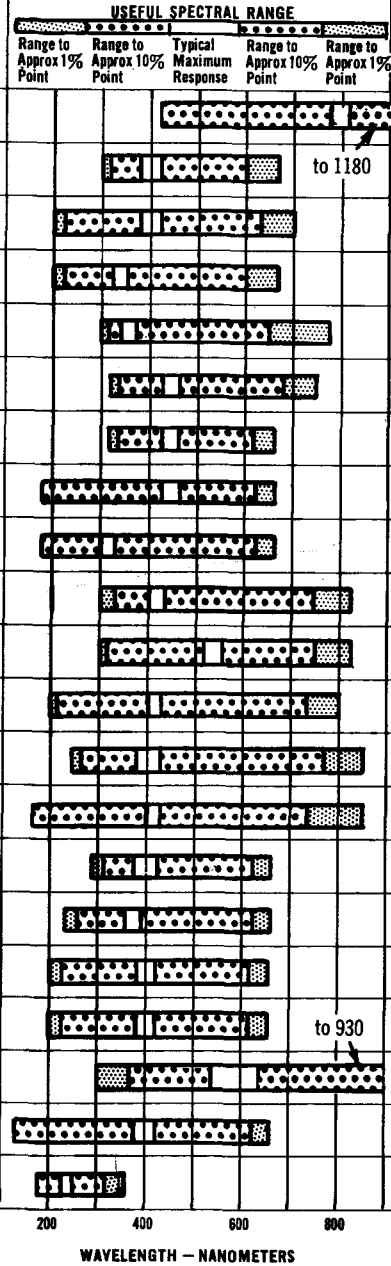

SPECTRAL RESPONSE				USEFUL SPECTRAL RANGE					TYPICAL DATA			
CA Code No.	EIA Designation	Cathode Material	Window Material	Range to Approx 1% Point	Range to Approx 10% Point	Typical Maximum Response	Range to Approx 10% Point	Range to Approx 1% Point	k lm/W	S μA/lm	σ mA/W	Approx. QE %
122	—	K-Cs-Sb	Aluminum Oxide						1040	83	87	26.9
123	—	Cs-Sb	UV-grade Sapphire						800	60	48	13.2
124	—	Cs-Sb	UV Glass						803	90	72	21.2
125	—	Cs-Te	Lithium Fluoride						—	—	11.5	6.1
126	—	K-Cs-Sb	Lime or Borosil.						1140	72	82	27.4
127	—	Ag-Bi-O-Cs	UV Glass					to 910	410	60	25	6.2
128	—	Ga-As	UV Glass						133	250	33	7
129	—	Ga-As-P	UV Glass						280	200	56	17
130	—	Na-K-Cs-Sb	Lime or Borosil.						203	200	40	9
131	—	Na-K-Cs-Sb	Lime or Borosil.					to 930	180	250	45	9.7
132	—	Na-K-Cs-Sb	Lime or Borosil.						221	200	44	10.4
133	—	K-Cs-Sb	Fused Silica					to 910	1190	60	71	22
134	—	Ga-As	UV-grade Sapphire						148	250	37	10.2
135	—	Ga-As-P	UV-grade Sapphire						303	200	61	16.8
136	—	K-Cs-Sb	Lime						837	65	54	16.7
137	—	Ga-As	Lime or Borosil.						105	330	35	7.9
138	—	Na-K-Cs-Sb	UV Glass						201	200	40	9

200 400 600 800

WAVELENGTH — NANOMETERS

k = Conversion Factor
S = Luminous Sensitivity

σ = Radiant Sensitivity at Wavelength of Maximum Response
QE = Quantum Efficiency at Wavelength of Maximum Response

ELECTRON MULTIPLIER STRUCTURES

Electron multiplier structures are identical to those used in photomultiplier tubes. Electron multipliers are intended for use in vacuum systems in the detection and measurement of electrons, ions and other charged particles, as well as X-radiation and vacuum ultraviolet radiation. The maximum average anode current (30 second average) for all structures listed in the chart below is 10 microamperes.

- For Particle and Radiation Detection
- For Use in a Vacuum System of 10^{-5} Torr, or Lower
- Broad Selection of Mechanical and Electrical Characteristics
- Various Types Feature an Integral Voltage Divider
- High Stability Copper-Beryllium Dynodes

RCA Dev. Type No.	RCA Photomultiplier Tube With Similar Dynode Structure	Cage Structure (CuBe Dynodes)	Number of Dynodes	Outer Structure	Radiation Opening Inches	TYPICAL VALUES: Voltage, Anode to Dynode No. 1, Volts (equal volts per stage)	TYPICAL VALUES: Current Amplification at Typical Conditions
C7075D	931A	Circular Cage	10	Flexible leads, sealed in bulb	.31 × .94	2000 to 3000	1×10^{7}
C7187J	6810A	In-Line	14	Glass stem, (20) flexible leads (B20-102 base supplied)	.375 ± .010 × .375 ± .010	3000 to 4000	1 to 10×10^{6}
C7187K	6810A	In-Line	14	Flange, glass stem, (20) flexible leads (B20-102 base supplied)	.375 ± .010 × .375 ± .010	3000 to 4000	1 to 10×10^{6}
C31017	8664	Venetian Blind	14	Stacked ceramic and Kovar construction, ring terminals, Flange mounting, shipped with sealed flange	.900 × .730	3000 to 4000	1 to 10×10^{6}
C31017A	8664	Venetian Blind	10	Same as C31017 above	.900 × .730	2500 to 3500	1 to 10×10^{5}
C31017B	8664	Venetian Blind	10	Stacked ceramic and non-magnetic material construction, ring terminals, flange mounting	.900 × .730	2500 to 3500	1 to 10×10^{7}

RCA Dev. Type No.	RCA Photomultiplier Tube With Similar Dynode Structure	Cage Structure (CuBe Dynodes)	Number of Dynodes	Outer Structure	Radiation Opening Inches	TYPICAL VALUES	
						Voltage, Anode to Dynode No. 1, Volts (equal volts per stage)	Current Amplification at Typical Conditions
C31017C	8664	Venetian Blind	10	Stacked ceramic and Kovar construction, ring terminals, flange mounting	.900 × .730	2500 to 3500	1 to 10 × 10^5
C31019	4460	In-Line	14	Kovar flange, glass stem, (16) flexible leads, shipped in plastic bag	.250 ± .005 D.	3900 to 4500	5 × 10^5
C31019A	4460	In-Line	14	Glass stem, (16) flexible leads, unsealed in bulb	.250 ± .005 D.	3900 to 4500	5 × 10^5
C31019B	4460	In-Line	14	Support brackets, integral divider, (3) flexible leads, shipped in plastic bag	.250 ± .005 D.	3900 to 4500	5 × 10^5
C31019C	4460	In-Line	14	Integral divider, shipped in plastic bag	.250 ± .005 D.	3000 to 3500	1 × 10^5
C31021	4460	In-Line	12	Kovar flange, glass stem, (14) flexible leads, shipped in plastic bag	.250 ± .005 D.	3400 to 4000	2.5 × 10^5
C31021A	4460	In-Line	12	Glass stem, (14) flexible leads, shipped unsealed in bulb	.250 ± .005 D.	3400 to 4000	2.5 × 10^5
C70102F	4460	In-Line	10	Glass stem, (14) flexible leads, shipped sealed in bulb	.250 ± .005 D.	3000 to 3500	1 × 10^5
C70102N	4460	In-Line	10	Kovar flange, glass stem, (12) flexible leads, shipped in plastic bag	.250 ± .005 D.	3000 to 3500	1 × 10^5

ELECTRON MULTIPLIER STRUCTURES (cont'd)

RCA Dev. Type No.	RCA Photomultiplier Tube With Similar Dynode Structure	Cage Structure (CuBe Dynodes)	Number of Dynodes	Outer Structure	Radiation Opening Inches	TYPICAL VALUES	
						Voltage, Anode to Dynode No. 1, Volts (equal volts per stage)	Current Amplification at Typical Conditions
C70102K	4460	In-Line	10	Glass stem, (14) flexible leads, shipped unsealed in bulb	.250 ± .005 D.	3000 to 3500	1 to 5 × 10^5
C70120E	8053	Venetian Blind	14	(16) rod terminals, shipped in plastic bag	.800 ± .010 D.	3000 to 4000	1 to 10 × 10^6
C70129D	8571	Circular Cage	10	Glass stem, (12) flexible leads, shipped unsealed in bulb	.06 × .375	2000 to 3000	1 × 10^5
C70131	7850	In-Line	12	(13) tab terminals, shipped in plastic bag	.375 ± .005 D.	3000 to 4000	2.5 × 10^5

Outlines

THIS section shows the dimensional outlines for RCA photomultipliers. See the Preliminary Selection Guides in the **Technical Data Section** for outlines and basing reference numbers.

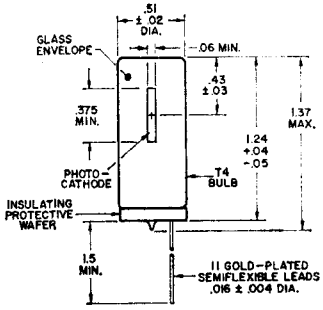

-1-

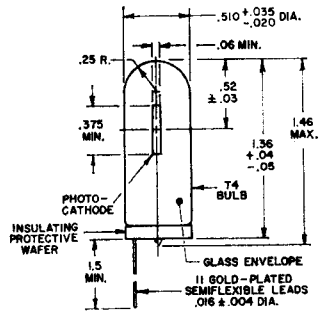

-2-

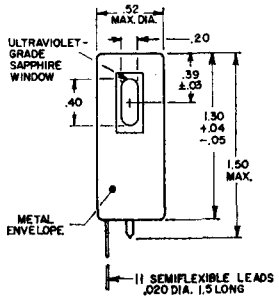

-3-

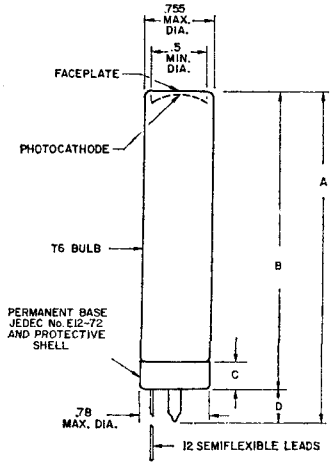

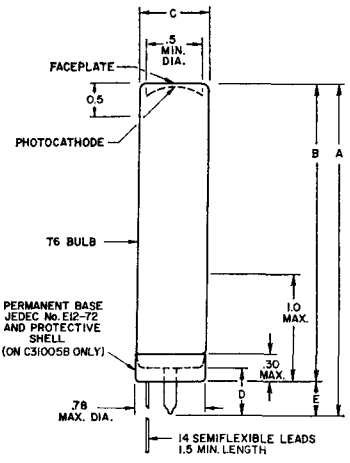

4460 C70102B C70102E C70102M C70102N	4516 7767 C70042J	8644 C70042D C70042K C70042R
A-3.38 Max.	3.94 Max.	3.8 Max.
B-2.94 $+.06$ $-.12$	3.50 $+.06$ $-.12$	3.26 $\pm$ 0.15
C-0.30 Max.	0.30 Max.	0.28 Max.
D-0.38 Max.	0.38 Max.	0.30 Max.

C31005	C31005B
A-3.7 Max.	3.94 Max.
B-3.26 $+.06$ $-.12$	3.50 $+.06$ $-.12$
C-0.87 Max. Dia.	0.755 Max. Dia.
D-0.5 Max.	—
E —	0.38 Max.

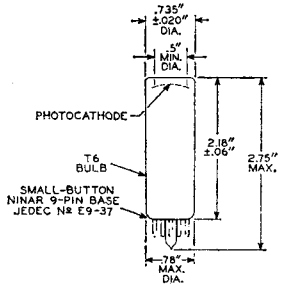

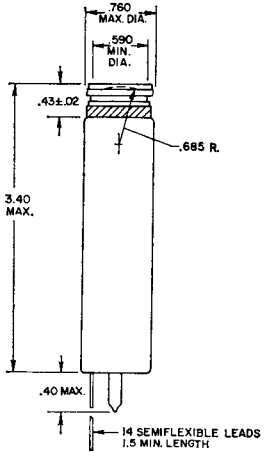

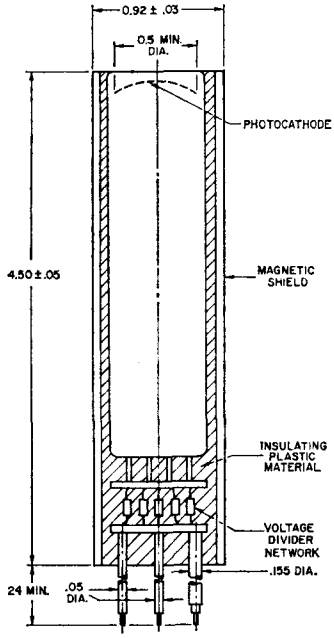

- 8 -

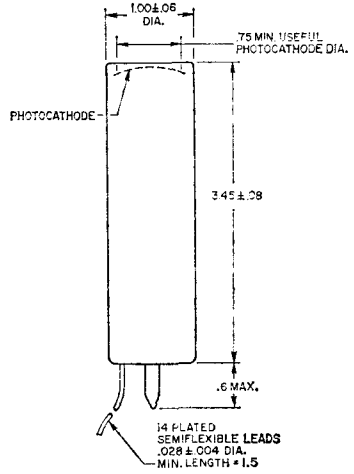

- 10 -

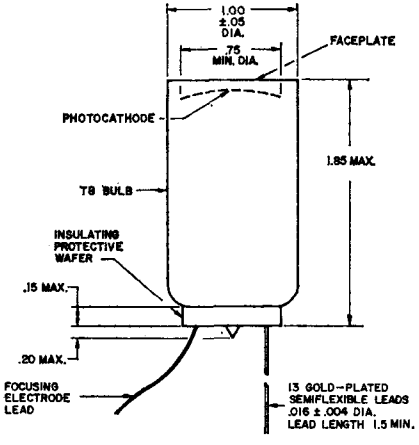

- 9 -

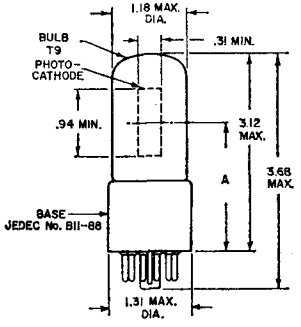

1P21 1P22 1P28 931A 4471 4472 4473 C31004 1P28A	 1P28/V1 1P28/V1 C7075J
A — 1.94 ± 0.09	1.99 ± 0.09

- 11 -

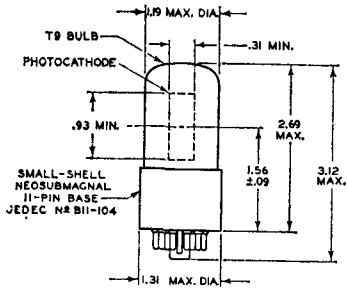

- 12 -

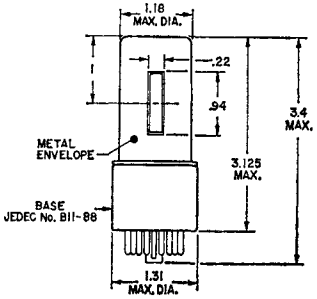

- 15 -

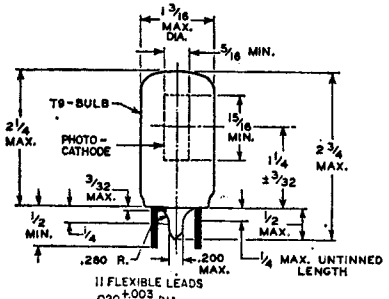

- 13 -

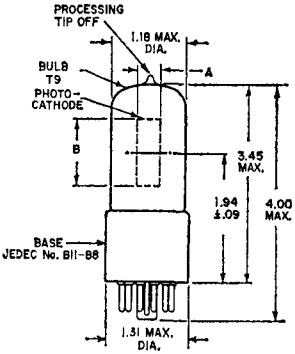

C31025B C31025G	C31025C
A-0.31 Min. B-0.94 Min	0.2 Min. 0.6 Min

- 16 -

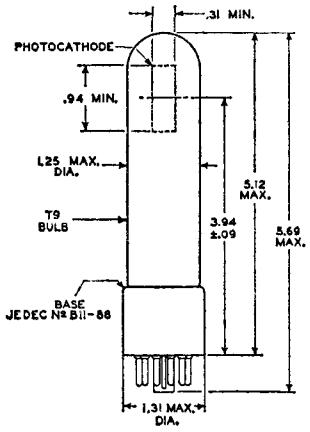

- 14 -

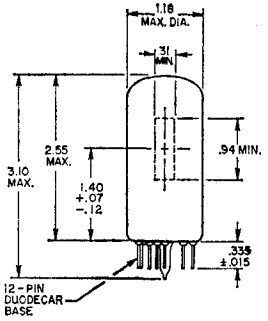

- 17 -

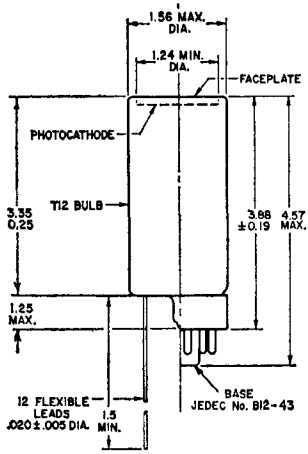
1.56 MAX. DIA.
1.24 MIN. DIA.
FACEPLATE
PHOTOCATHODE
T12 BULB
3.35 0.25
3.88 ±0.19
4.57 MAX.
1.25 MAX.
12 FLEXIBLE LEADS .020±.005 DIA.
1.5 MIN.
BASE JEDEC No. B12-43

- 18 -

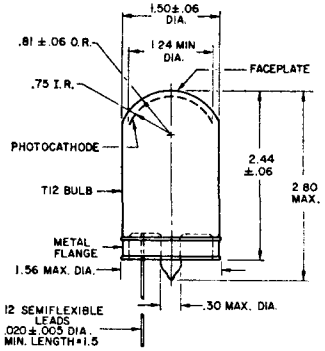
1.50±.06 DIA.
.81 ±.06 O.R.
1.24 MIN. DIA.
FACEPLATE
.75 I.R.
PHOTOCATHODE
T12 BULB
2.44 ±.06
2.80 MAX.
METAL FLANGE
1.56 MAX. DIA.
.30 MAX. DIA.
12 SEMIFLEXIBLE LEADS .020±.005 DIA. MIN. LENGTH=1.5

- 20 -

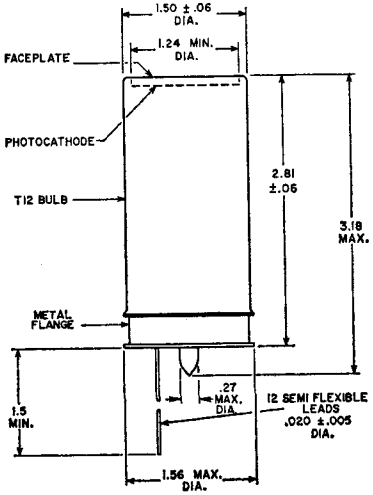
1.50 ±.06 DIA.
1.24 MIN. DIA.
FACEPLATE
PHOTOCATHODE
T12 BULB
2.81 ±.06
3.18 MAX.
METAL FLANGE
1.5 MIN.
.27 MAX. DIA.
12 SEMI FLEXIBLE LEADS .020 ±.005 DIA.
1.56 MAX. DIA.

- 19 -

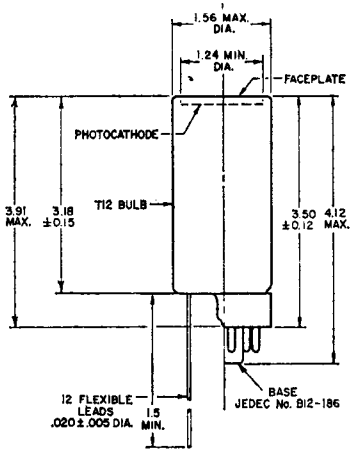
1.56 MAX. DIA.
1.24 MIN. DIA.
FACEPLATE
PHOTOCATHODE
3.91 MAX.
3.18 ±0.15
T12 BULB
3.50 ±0.12
4.12 MAX.
12 FLEXIBLE LEADS .020±.005 DIA.
1.5 MIN.
BASE JEDEC No. B12-186

- 21 -

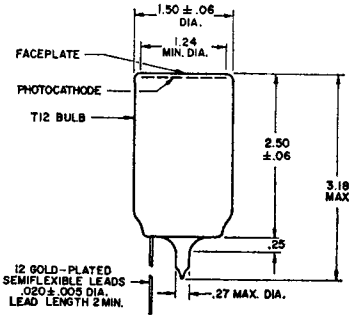
1.50 ±.06 DIA.
1.24 MIN. DIA.
FACEPLATE
PHOTOCATHODE
T12 BULB
2.50 ±.06
3.18 MAX
.25
12 GOLD-PLATED SEMIFLEXIBLE LEADS .020±.005 DIA. LEAD LENGTH 2 MIN.
.27 MAX. DIA.

- 22 -

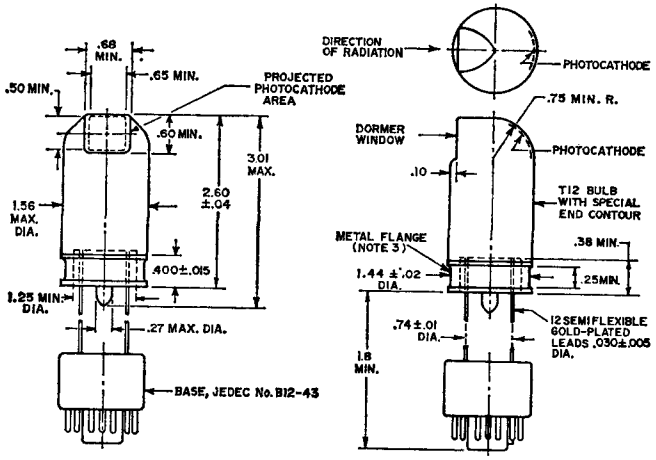
.68 MIN.
.65 MIN.
.50 MIN.
PROJECTED PHOTOCATHODE AREA
.60 MIN.
3.01 MAX.
2.60 ±.04
1.56 MAX. DIA.
.400±.015
1.25 MIN. DIA.
.27 MAX. DIA.
BASE, JEDEC No. B12-43
DIRECTION OF RADIATION
PHOTOCATHODE
.75 MIN. R.
DORMER WINDOW
PHOTOCATHODE
.10
T12 BULB WITH SPECIAL END CONTOUR
METAL FLANGE (NOTE 3)
.38 MIN.
1.44 ±.02 DIA.
.25MIN.
.74±.01 DIA.
12 SEMIFLEXIBLE GOLD-PLATED LEADS .030±.005 DIA.
1.8 MIN.

- 23 -

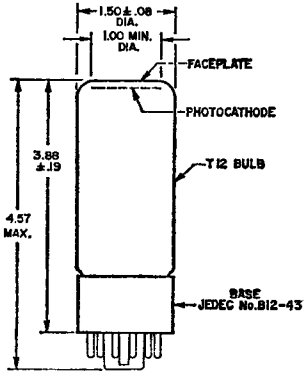
1.50±.08 DIA.
1.00 MIN. DIA.
FACEPLATE
PHOTOCATHODE
3.88 ±.19
T12 BULB
4.57 MAX.
BASE JEDEC No.B12-43

- 24 -

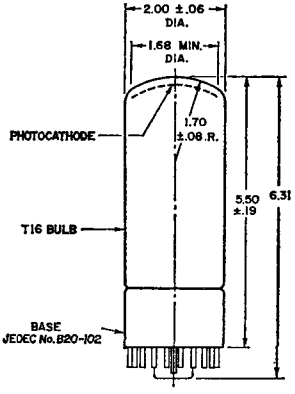
2.00 ±.06 DIA.
1.68 MIN. DIA.
1.70 ±.08 R.
PHOTOCATHODE
T16 BULB
5.50 ±.19
6.31
BASE JEDEC No.B20-102

- 25 -

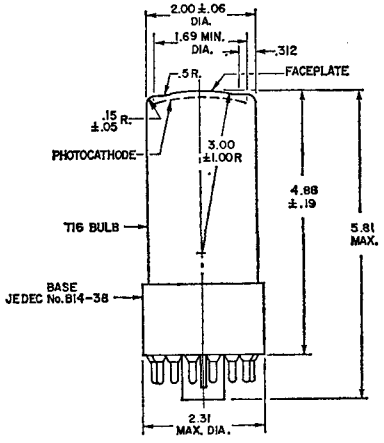
2.00 ±.06
DIA.
1.69 MIN.
DIA.
.312
.5R.
FACEPLATE
.15 R.
±.05
PHOTOCATHODE
3.00
±1.00R
4.88
±.19
5.81
MAX.
T16 BULB
BASE
JEDEC No. B14-38
2.31
MAX. DIA.

- 26 -

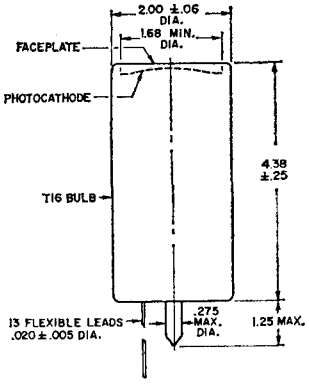
2.00 ±.06
DIA.
1.68 MIN.
DIA.
FACEPLATE
PHOTOCATHODE
4.38
±.25
T16 BULB
13 FLEXIBLE LEADS
.020 ± .005 DIA.
.275
MAX.
DIA.
1.25 MAX.

- 28 -

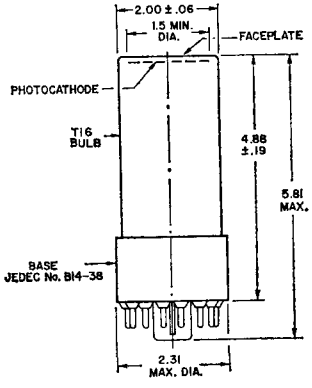
2.00 ± .06
1.5 MIN.
DIA.
FACEPLATE
PHOTOCATHODE
T16
BULB
4.88
±.19
5.81
MAX.
BASE
JEDEC No. B14-38
2.31
MAX. DIA.

- 27 -

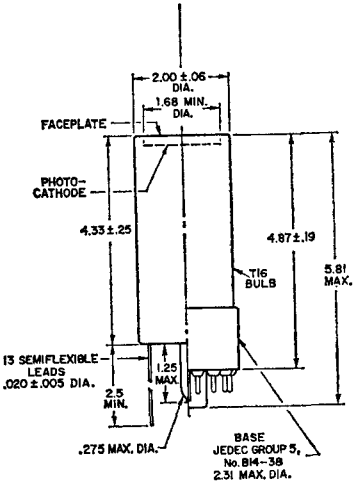
2.00 ±.06
DIA.
1.68 MIN.
DIA.
FACEPLATE
PHOTO-
CATHODE
4.33±.25
4.87±.19
T16
BULB
5.81
MAX.
13 SEMIFLEXIBLE
LEADS
.020 ±.005 DIA.
1.25
MAX.
2.5
MIN.
.275 MAX. DIA.
BASE
JEDEC GROUP 5,
No. B14-38
2.31 MAX. DIA.

- 29 -

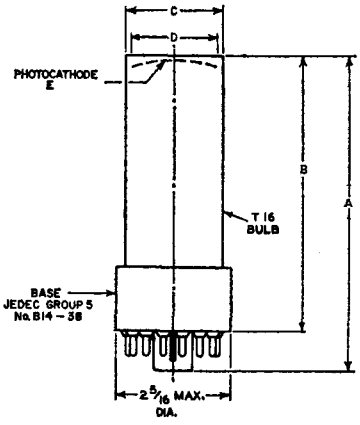

C7164R	6342A, 6655A, 4518	6903
A-5.2 Max.	5.81 Max.	6-9/16 Max.
B-4.25 ± 0.19	4.87 ± 0.19	5-5/8 ± 3/16
C-2.00 ± 0.06 Dia.	2.00 ± 0.06 Dia.	2 ± 5/32 Dia.
D-1.68 Min. Dia.	1.68 Min. Dia.	1-5/8 Min. Dia.
E-Curved	Curved	Flat

- 30 -

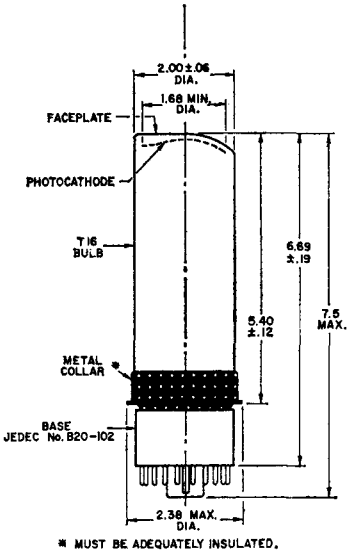

* MUST BE ADEQUATELY INSULATED.

- 32 -

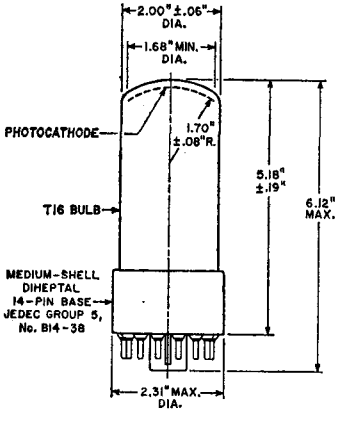

- 31 -

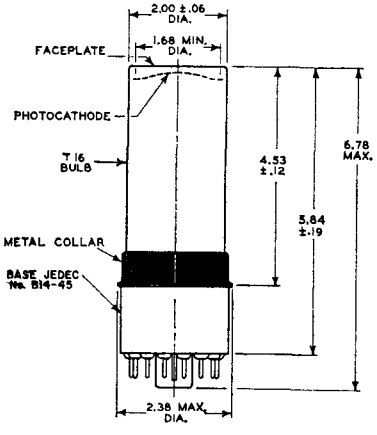

- 33 -

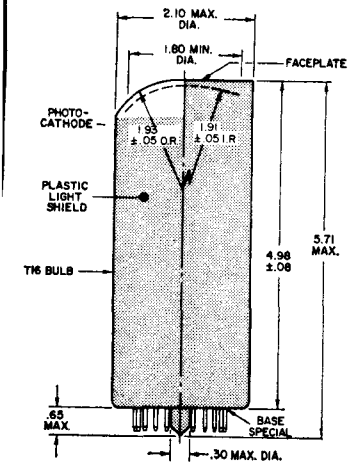
2.10 MAX. DIA.
1.80 MIN. DIA.
FACEPLATE
PHOTO-CATHODE
1.93 ±.05 O.R.
1.91 ±.05 I.R.
PLASTIC LIGHT SHIELD
T16 BULB
4.98 ±.08
5.71 MAX.
.65 MAX.
BASE SPECIAL
.30 MAX. DIA.

- 34 -

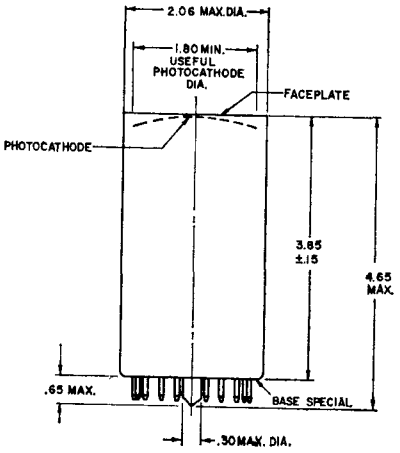
2.06 MAX. DIA.
1.80 MIN. USEFUL PHOTOCATHODE DIA.
FACEPLATE
PHOTOCATHODE
3.85 ±.15
4.65 MAX.
.65 MAX.
BASE SPECIAL
.30 MAX. DIA.

- 36 -

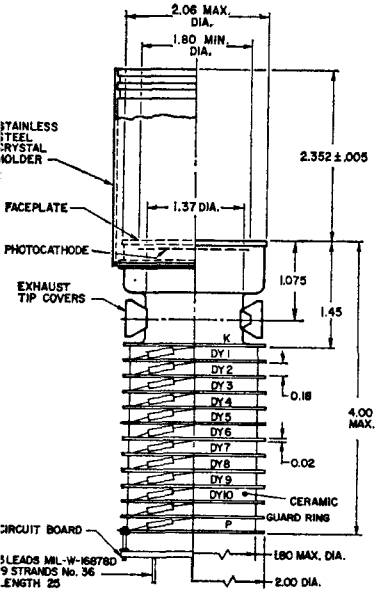
2.06 MAX. DIA.
1.80 MIN. DIA.
STAINLESS STEEL CRYSTAL HOLDER
2.352 ±.005
FACEPLATE
1.37 DIA.
PHOTOCATHODE
EXHAUST TIP COVERS
1.075
1.45
K
DY 1
DY 2
DY 3
DY 4
DY 5
DY 6
DY 7
DY 8
DY 9
DY10
P
0.18
0.02
4.00 MAX.
CERAMIC
GUARD RING
CIRCUIT BOARD
LEADS MIL-W-16878D
9 STRANDS No. 36
LENGTH 25
.180 MAX. DIA.
2.00 DIA.

- 35 -

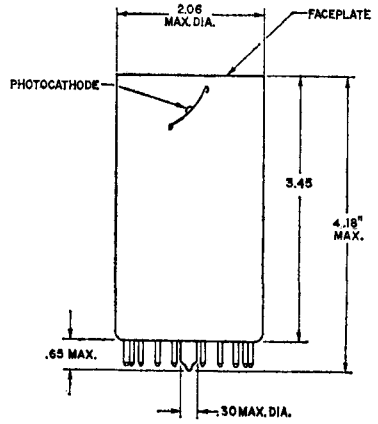
2.06 MAX. DIA.
FACEPLATE
PHOTOCATHODE
3.45
4.18" MAX.
.65 MAX.
.30 MAX. DIA.

- 37 -

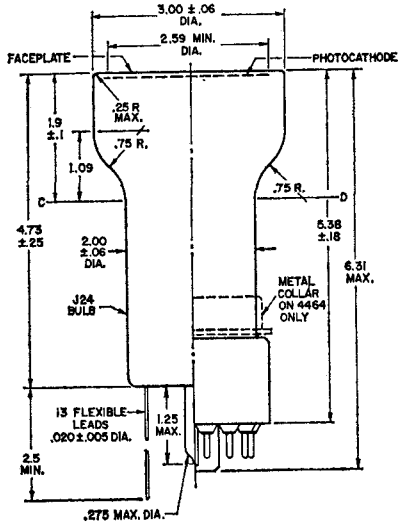
3.00 ± .06 DIA.
2.59 MIN. DIA.
FACEPLATE
PHOTOCATHODE
.25 R MAX.
.75 R.
1.9 ±.1
1.09
C
D
.75 R.
4.73 ±.25
2.00 ±.06 DIA.
5.38 ±.18
6.31 MAX.
METAL COLLAR ON 4464 ONLY
J24 BULB
13 FLEXIBLE LEADS .020±.005 DIA.
1.25 MAX.
2.5 MIN.
.275 MAX. DIA.

- 38 -

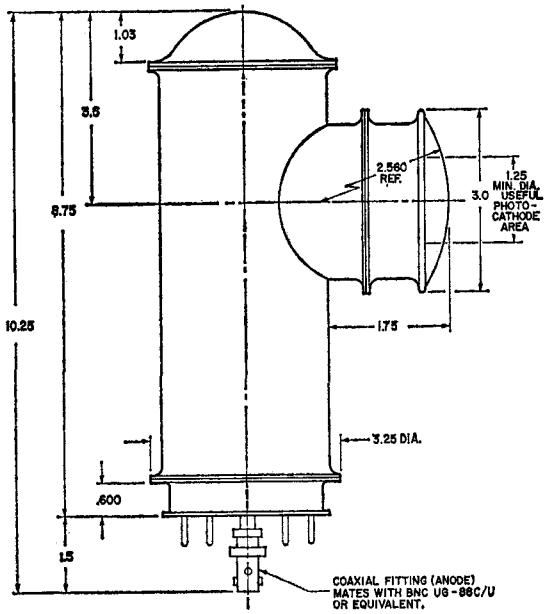
1.03
3.6
8.75
10.25
2.560 REF.
3.0
1.25 MIN. DIA. USEFUL PHOTO-CATHODE AREA
1.75
3.25 DIA.
.600
1.5
COAXIAL FITTING (ANODE) MATES WITH BNC UG-88C/U OR EQUIVALENT.

- 39 -

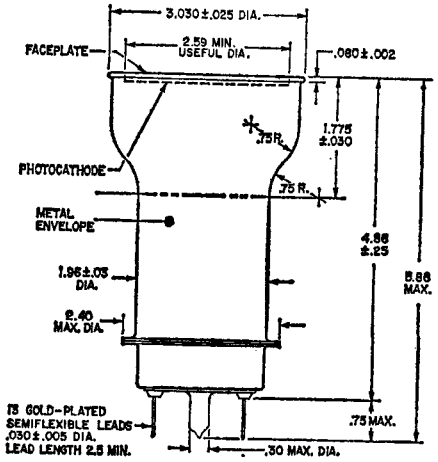
3.030±.025 DIA.
2.59 MIN. USEFUL DIA.
FACEPLATE
.080±.002
.75R.
1.775 ±.030
PHOTOCATHODE
.75 R.
METAL ENVELOPE
4.86 ±.25
5.86 MAX.
1.96±.03 DIA.
2.40 MAX. DIA.
13 GOLD-PLATED SEMIFLEXIBLE LEADS .030±.005 DIA. LEAD LENGTH 2.5 MIN.
.75 MAX.
.30 MAX. DIA.

- 40 -

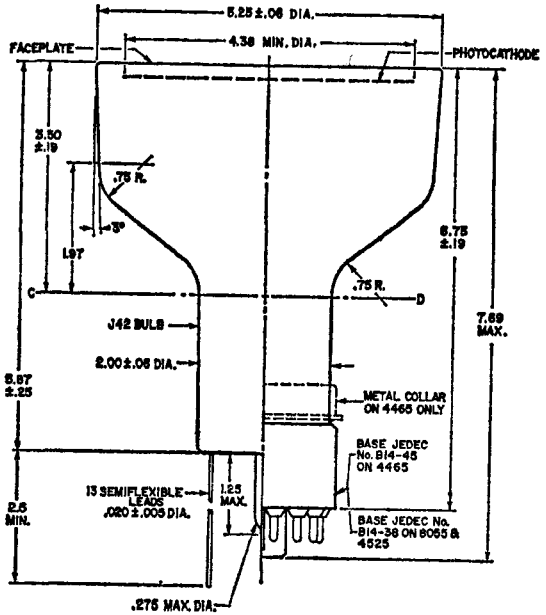
5.25±.06 DIA.
4.38 MIN. DIA.
FACEPLATE
PHOTOCATHODE
3.50 ±.19
.75 R.
3°
1.97
6.75 ±.19
C
.75 R.
D
J42 BULB
7.69 MAX.
2.00±.06 DIA.
5.87 ±.25
METAL COLLAR ON 4465 ONLY
BASE JEDEC No. B14-45 ON 4465
13 SEMIFLEXIBLE LEADS .020±.005 DIA.
1.25 MAX.
2.5 MIN.
BASE JEDEC No. B14-38 ON 8055 & 4525
.275 MAX. DIA.

- 41 -

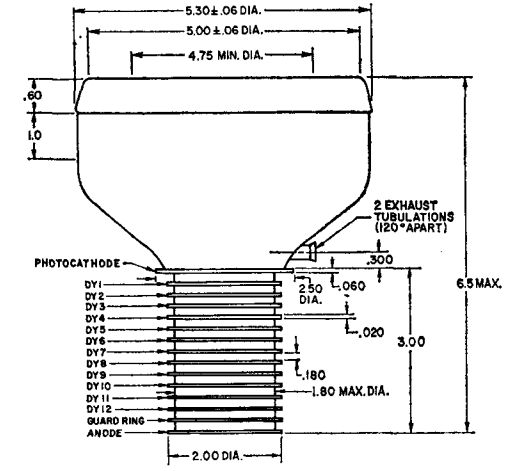
5.30±.06 DIA.
5.00±.06 DIA.
4.75 MIN. DIA.
.60
1.0
2 EXHAUST TUBULATIONS (120° APART)
.300
PHOTOCATHODE
DY1
DY2
DY3
DY4
DY5
DY6
DY7
DY8
DY9
DY10
DY11
DY12
GUARD RING
ANODE
2.50 DIA.
.060
.020
.180
1.80 MAX. DIA.
6.5 MAX.
3.00
2.00 DIA.

- 42 -

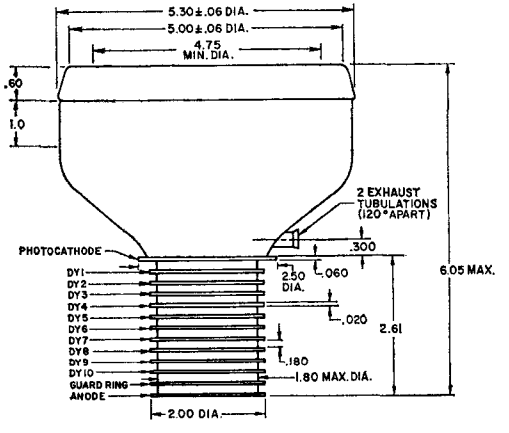
5.30±.06 DIA.
5.00±.06 DIA.
4.75 MIN. DIA.
.60
1.0
2 EXHAUST TUBULATIONS (120° APART)
.300
PHOTOCATHODE
DY1
DY2
DY3
DY4
DY5
DY6
DY7
DY8
DY9
DY10
GUARD RING
ANODE
2.50 DIA.
.060
.020
.180
1.80 MAX. DIA.
6.05 MAX.
2.61
2.00 DIA.

- 43 -

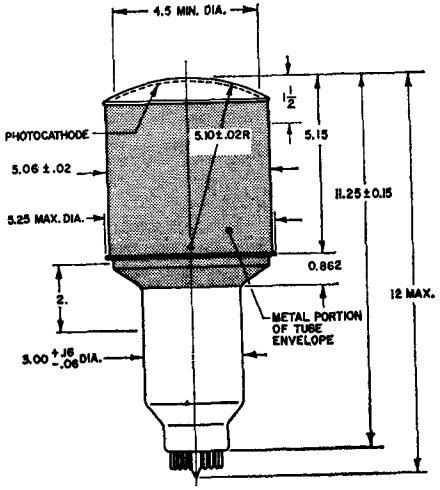
4.5 MIN. DIA.
1/2
PHOTOCATHODE
5.10±.02R
5.15
5.06 ± .02
11.25±0.15
5.25 MAX. DIA.
0.862
12 MAX.
2.
METAL PORTION OF TUBE ENVELOPE
3.00 +.16 -.06 DIA.

Basing Diagrams

This section shows the basic diagrams for RCA photomultipliers. See the Preliminary Selection Guides in the **Technical Data Section** for outline and basing reference numbers. Temporary bases are given at end of this section.

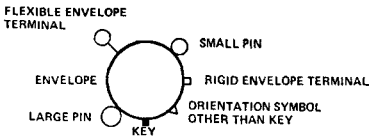

Key to Terminal Connections on Basing Diagrams.

8571 C70129G* C70129H*

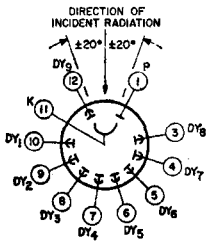

-1- -2- -3-

4460 4516 7767 C70042J° C70102E° C70102M° C70102N°

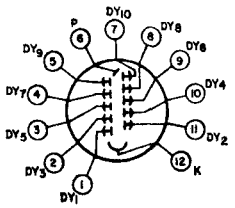

-4-

8644° C70042D° C70042K° C70042R°

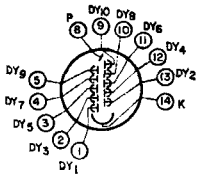

-4-

C70102B°

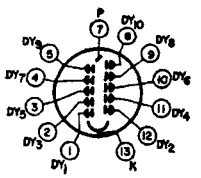

-4-

* Supplied with temporary base A.

° Supplied with temporary base B.

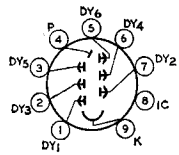

- 5 -

C31005B+

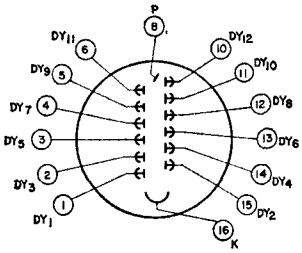

- 6 -

C31005+ C70128+

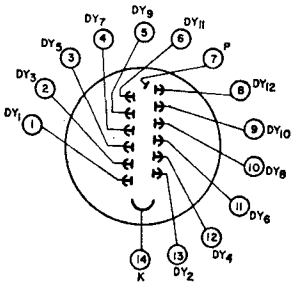

- 6 - - 7 -

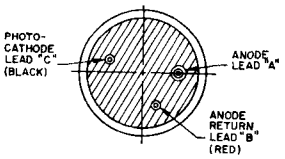

- 8 -

+ Supplied with temporary base C.

C31016A●

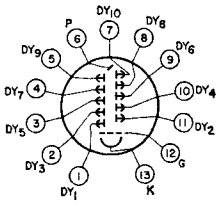

- 9 -

C31016B●

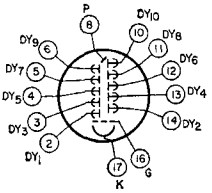

- 9 -

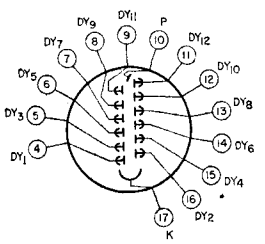

- 10 -

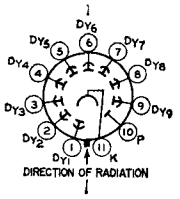

- 11 - - 12 -

● Supplied with temporary base D.

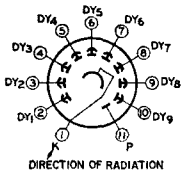

- 13 -

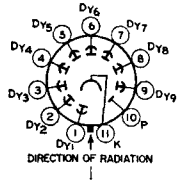

- 14 - - 15 - - 16 -

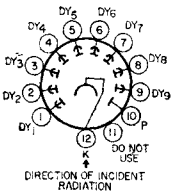

- 17 -

4517 6199 7102 C7151W

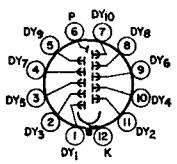

- 18 -

° Supplied with temporary base B.

2060°

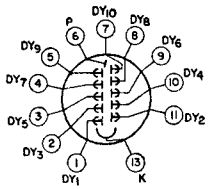

- 18 -

4441 4441A 4461A

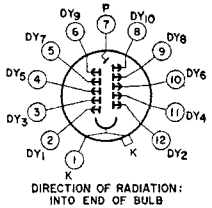

- 19 -

C70114C° C70114E°

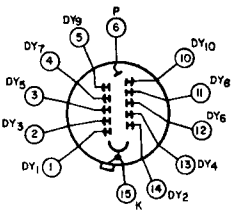

- 19 -

C70114D° C70114F° C70114J° C70132B°

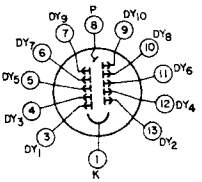

- 19 - - 20 -

2067° C70132A°

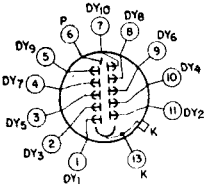

- 20 -

C7151Q°

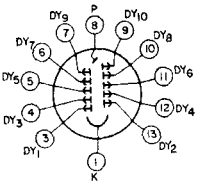

- 22 -

4438 4439°

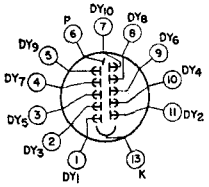

- 21 -

4526°

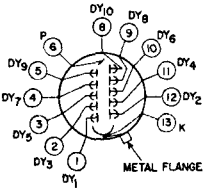

- 23 -

4440

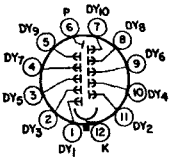

- 21 -

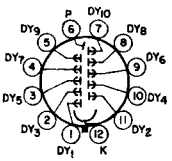

- 24 -

C7151N°

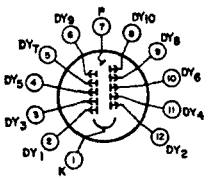

- 22 -

° Supplied with temporary base B.

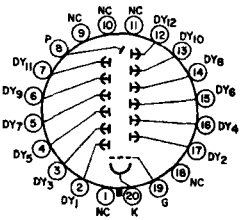

- 25 -

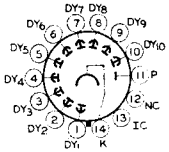

- 26 -

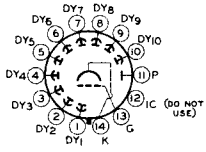

- 27 -

2061‡ 2062‡

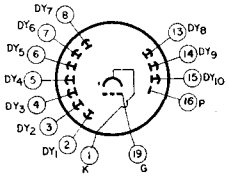

- 28 -

2063‡

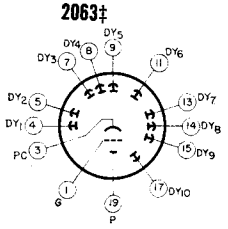

- 29 -

4463 4523 8053
C70109E

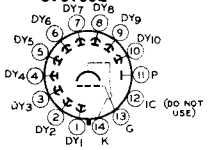

- 29 -

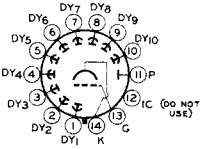

- 30 -

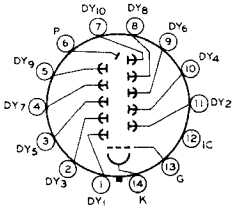

- 31 -

6810A 7264

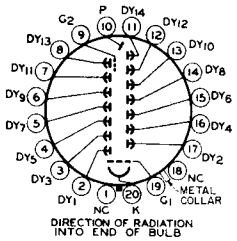

- 32 -

‡ Supplied with temporary base E.

7265 C7268

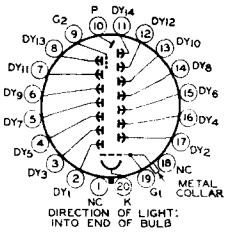

- 32 -

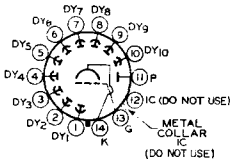

- 33 -

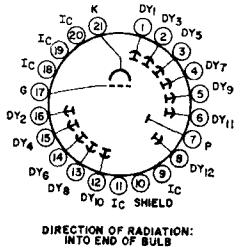

- 34 -

Flanges provide electrode connections

- 35 -

‡ Supplied with temporary base E.

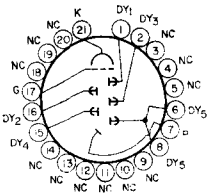

- 36 -

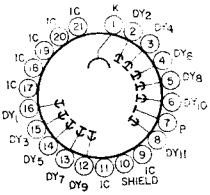

- 37 -

4464 4524 8054

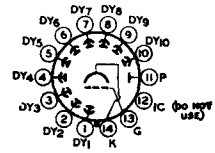

- 38 -

2064B‡

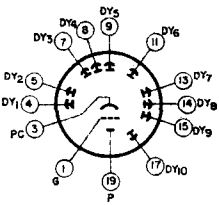

- 38 -

Request technical data sheet for electrode connection information

- 39 -

4521‡

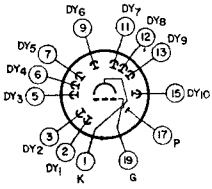

- 40 -

4525 8055

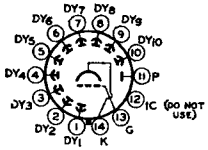

- 41 -

4465

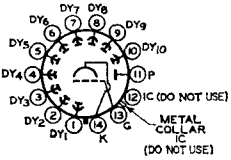

- 41 -

‡ Supplied with temporary base E.

2065‡

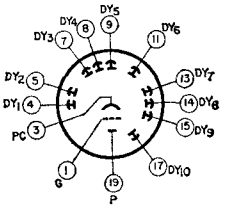

- 41 -

Flanges provide electrode connections

- 42 - - 43 -

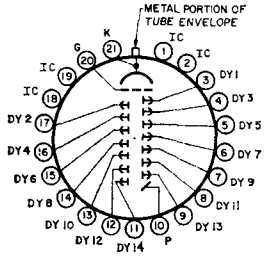

- 44 -

DY — Dynode
G — Grid
IC — Internal connection (do not use)
NC — No connection
P — Anode
K — Photocathode

TEMPORARY BASES

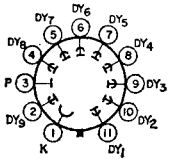

- A -

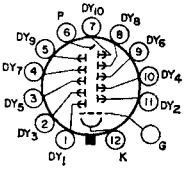

- D -

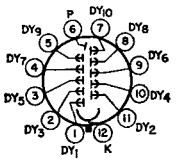

- B -

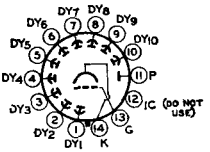

- E -

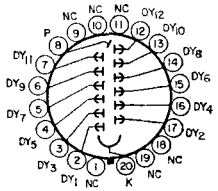

- C -

DY — Dynode
G — Grid
IC — Internal connection (do not use)
NC — No connection
P — Anode
K — Photocathode

Index

Absorption spectroscopy 100
Acceptor level 8
Afterpulsing 47
Anodes 24, 25
Atmosphere 36

Band gap 7
Bandwidth, noise 68
Basing 27
Bialkali photocathode 10, 11
Black-body radiation 119
Box-and-grid multiplier structure 23

Cathodes
  bialkali 10, 11
  ERMA 10, 11
  multialkali 11
  opaque 10, 19
  semitransparent 10, 19
  trialkali 11
Cerenkov radiation 77, 86
Charge integration 93
Collection efficiency 20
Compression, signal 110
Conduction band 7
Conversion
  of units 112
Counting 46, 51
  interpretation 89
  photon 95
Current control 55
Current protection 110
Current rating
  anode current 32
  cathode current 31

Dark current 19, 40
  equivalent anode dark current input (EADCI) 42
  reduction 43
Dark noise 44, 45, 66
Data, classes of 30
Densiometry 99
Detection
  digital method 94
  low-light level 93
  photon counting 95
Doping 9
Dynamic compression 110
Dynode 5, 6
  box-and-grid 21, 23

EADCI 43
Electric field, exterior 34
Electron affinity 7
Electron multipliers 21, 26
  time response 26
Energy band 7, 8
Energy sources 128
ENI 43
Environment 35
  atmospheric 36
  shock 35
  temperature 32
  vibration 35
Equivalent Noise Input (ENI) 43
Extended Red Multi-Alkali (ERMA) photocathode 11, 12
Eye characteristics 112

Fatigue 49, 50
Fermi level 7
Fluctuations 56, 64
Flying leads 27
Flying-spot scanning 90
  CRO 91
  objective lens 92
  photomultiplier 92
Forbidden band 7

Gas ionization 66

Hysteresis 51

Integration, charge 93

Lamps 120
Laplace equation 19, 24
Lasers 121
-range finder 89
Life expectancy 52
Light detection 93
photon counting 95
Light feedback 67
Light sources 121
Linearity 53
Logarithmic photometry 99

Magnetic field 34, 36
Matching
calculations 130
-factor 132
source-detector 127
Multiplier analysis 24
Multipliers
contribution to noise 61
for scintillators 82
structures 22, 23

Negative electron affinity 8
Noise
-and bandwidth 68
dark 66
gas ionization 66
group I and II sources 66
multiplier contributions 60
photocathode contributions 57
photon 56
statistics for dynodes 61

Output-current control 55

Parameters, design 30
Peak-to-valley ratio 46
Photocathode 6, 19
contribution to noise 57
opaque 10
reflection at- 54
ruggedized 26
semitransparent 10
sensitivity 9, 38
spectral response 39
transit-time difference 25
Photoemission 5
time lag 16
Photometry 97
color-balancing 98
densiometry 99
logarithmic 99
units 113
Photomultiplier 5, 19, 37
applications 77
characteristics 82
current protection 110
data 37
design 19
-for photometry 97
-for photon counting 96
-for Raman spectroscopy 102
-for scanner 92
sensitivity 37
testing 126
Photon noise 56
Power supply 110
high-voltage 110
stability 111
Pulse counting 46, 106
Pulse height
distribution 63
resolution 46

Quantum efficiency 40

Radiant energy 119
sources 120
Radiation
black-body 119
sources 120
Raman spectroscopy 101
Ratings 30
anode current 32
cathode current 31
temperature 32
voltage 30
Reflected light 54
Regenerative effects 41
Ruggedization 26

Scintillation
counter 77, 80
materials 80, 83
mechanism 79
processes 78
spectrometer 84
Secondary emission 5, 13, 61
statistics, effect of 16
time lag 16
Sensitivity 9, 37
blue 38
integral radiant 38
loss 50
luminous 38
radiant 38
Shock 35
Signal compression 110
Source-detector matching 127, 129
Spacial uniformity 55
Spectral response 10, 39, 127
Spectrometry 100
absorption 100
Raman 101

Spectroscopy
energy 84
time 87
Stability 49, 51
Statistical fluctuations 56

Temperature rating 32
Time-domain reflectometry (TDR) 25
Time lag 16
in photoemission 16
in secondary emission 16
Time response 19, 26, 48
electron-multiplier 26
Time spectroscopy 87
Time stability test 52
Transit time 25
-spread 49

Uniformity, spacial 55

Valence band 7
Venetian-blind multiplier structure 22
Vibration 35
Video amplifier 93
Voltage divider 103
tapered 109
-for pulsed operation 106
-resistors 104
voltage ratio 104
wiring 107
Voltage rating 30

Wiring techniques 107

LIST OF MAJOR CONTRIBUTORS TO THE RCA PHOTOMULTIPLIER MANUAL

Ralph W. Engstrom
Fred A. Helvy
Harold R. Krall
Thomas T. Lewis
W. Dean Lindley
Ramon U. Martinelli
Robert M. Matheson
Anthony G. Nekut
Dennis E. Persyk
Ronald M. Shaffer
Albert H. Sommer

Other RCA Technical Manuals

● **RCA POWER CIRCUITS**—SP-51—(8" x 5¼")—448 pages. Contains design information for a broad range of power circuits using RCA silicon transistors, rectifiers, and thyristors (SCR's, triacs, and diacs). Gives design criteria and procedures for applications involving rectification, supply filtering, power conversion and regulation, ac line-voltage controls, rf power amplifiers, and control and low frequency amplifiers. Shows design examples and practical circuits. Price $2.00.*†

● **RCA TRANSISTOR, THYSISTOR & DIODE MANUAL**—SC-14 (8" x 5¼")—656 pages. Contains up-to-date definitive data on over 700 semiconductor devices including tunnel diodes, silicon controlled rectifiers, varactor diodes, conventional rectifiers, and many classes of transistors. Features easy-to-understand text chapters, as well as tabular data on RCA discontinued transistors. Contains 38 practical circuits, complete with parts lists, highlighting semiconductor- device applications. Price $2.50.*†

● **RCA HIGH-SPEED, HIGH-VOLTAGE, HIGH-CURRENT POWER TRANSISTORS**—PM-80 (8" x 5¼")—96 pages. Provides a basic understanding of the theory and application of the RCA line of medium-frequency power transistors. Covers physical theory, structures, geometries, packaging, critical application-limiting factors, and the operation and requirements of power transistors in amplifier, switching, and control applications. Typical circuits illustrate the use of transistors in series voltage regulators, linear amplifiers, switching regulators, and inverters and converters, and the application of complementary transistor pairs. Selection charts are included to facilitate choice of the optimum type of power transistor for a variety of military, industrial, and commercial applications. Price $2.00.*†

● **RCA SOLID-STATE HOBBY CIRCUITS MANUAL**—HM-91 (8⅜" x 5⅜")—368 pages. Contains complete construction information on 62 circuits of general interest to all experimenters. Circuits use diodes, transistors, SCR's, triacs, MOS transistors, integrated circuits, and light and heat detectors. Circuit operation is described in detail; construction layouts, photographs, schematic diagrams, and parts lists are given; and full-size drilling or printed-circuit templates are included for most circuits to simplify construction. Price $1.95.*†

● **RCA SILICON CONTROLLED RECTIFIER EXPERIMENTER'S MANUAL**—KM-71 (8⅜" x 5⅜")—136 pages. Contains 24 practical and interesting control circuits that can be built with a complement of active devices available in kit form. Includes photographs, schematic diagrams, and descriptive writeups. Also includes brief descriptions of solid-state components used (rectifiers, transistors, SCR's) and short section on troubleshooting. Price 95 cents.*†

● **RCA RECEIVING TUBE MANUAL**—RC-27 (8" x 5¼")—672 pages. Contains technical data on more than 1400 receiving tubes for home-entertainment use. Includes six easy-to-read text chapters that provide basic information on electron-tube operation, ratings and characteristics, and applications. Also features a detailed application guide for receiving tubes; quick-reference charts for replacement and discontinued RCA receiving tubes, black-and-white and color picture tubes, and voltage-reference tubes; and a Circuits section that includes schematic diagrams, descriptive writeups, and complete parts lists for 36 practical electron-tube circuits for a wide variety of applications. Price $2.00.*†

● **RCA TRANSMITTING TUBES**—TT-5 (8⅜" x 5⅜")—320 pages. Gives data on over 180 power tubes having plate-input ratings up to 4 kW and on associated rectifier tubes. Provides basic information on generic types, parts and materials, installation and application, and interpretation of data. Contains circuit diagrams for transmitting and industrial applications. Features lie-flat binding. Price $1.00*†

● **RADIOTRON° DESIGNER'S HANDBOOK**—4th Edition (8¾" x 5½")—1500 pages. Comprehensive reference covering the design of radio and audio circuits and equipment. Written for the design engineer, student, and experimenters. Contains 1000 illustrations, 2500 references, and cross-referenced index of 7000 entries. Edited by F. Langford-Smith. Price $7.00.*†

● **RCA PHOTOMULTIPLIER MANUAL**—PT-61 (8¼" x 5¼")—192 pages. The construction, operation, and application of photomultipliers are detailed in this well-illustrated manual. Discussions of photoemission, secondary emission, and the design of multiplier structures are followed by a description of photomultiplier performance characteristics. An analysis of statistical fluctuation and noise effects then leads into a section on applications of photomultipliers. Photometric and radiant units, radiant energy sources, spectral response, and source-detector matching are set forth. An extensive tabulation of technical data includes a selection guide for over one hundred RCA photomultiplier tubes, with a special section on ruggedized types. Outlines, basing diagrams, and circuit information are furnished. A complete index adds to the convenience of this manual. Price $2.50.*†

● **RCA ELECTRO-OPTICS HANDBOOK**—EOH-10 (8½" x 5½")—154 pages. Data from the many technical areas involved in electro-optics are compiled and unified in this manual. The presentation is convenient, featuring more than one hundred tables, charts, and graphs. A coherent system of symbols and definitions is listed, and data on radiometry, blackbody radiation, and photometry are presented. Information on radiant sources, lasers, atmospheric transmittance, and detection, resolution, and recognition are included. Treatments of detector characteristics, image and camera tubes, and optics are followed by a section on electro-optics systems analysis. References and an extensive index add to the usefulness of this unique handbook. Price $2.50.*†

● **RCA LINEAR INTEGRATED CIRCUITS**—IC-42 (8¼" x 5⅜")—416 pages. Explains the basic principles involved in the fabrication, design, and application of linear integrated circuits. Includes a discussion of the basic silicon monolithic fabrication process, analyses of the building-block elements used in linear integrated circuits, explanations of the operation and applications of RCA linear integrated circuits, and detailed ratings and characteristics data and package information for RCA linear integrated circuits. Price $2.50.*†

° Trade Mark Reg. U.S. Pat. Off.
* Prices shown apply in U.S.A. and are subject to change without notice.
† Optional price.

RCA TYPICAL PHOTOCATHODE SPECTRAL RESPONSE CHARACTERISTICS (cont'd)

Spectral Response	Cathode Material	Window Material	Transmission Type	Opaque Type	Sensitivity μA/lm	Sensitivity mA/W @ λ max.	Quantum Efficiency % @ λ max.	Dark Emission at 22° C fA/cm²* (1 fA = 1 x 10^{-15} A)
117	K-Cs-Sb	UV Glass	×	—	67	79	24.4	0.02
118	K-Cs-Sb	UV Glass	×	—	77	88	27.2	0.02
119	Na-K-Cs-Sb	Pyrex	×	—	250	45	9.7	—
120	K-Cs-Sb	UV-grade Sapphire	×	—	60	71	22	—
121	Cs-Te	Fused Silica	×	—	—	11.6	7.2	—
122	K-Cs-Sb	Aluminum Oxide	×	—	83	87	26.9	—
123	Cs-Sb	UV-grade Sapphire	—	×	60	48	13.2	—
124	Cs-Sb	UV Glass	×	—	90	72	21.2	—
125	Cs-Te	Lithium Fluoride	×	—	—	11.5	6.1	—
126	K-Cs-Sb	Lime or Borosil.	×	—	72	82	27.4	—
127	Ag-Bi-O-Cs	UV Glass	×	—	50	34	8.4	—
128	Ga-As	UV Glass	—	×	200	35	7.9	0.1
129	Ga-As-P	UV Glass	—	×	200	61	16.8	0.01
130	Na-K-Cs-Sb	Lime or Borosil.	×	—	200	40	9	—
131	Na-K-Cs-Sb	Lime or Borosil.	×	—	250	45	9.7	—
132	Na-K-Cs-Sb	Lime or Borosil.	×	—	200	44	10.4	—
133	K-Cs-Sb	Fused Silica	×	—	60	71	22	—
134	Ga-As	UV-grade Sapphire	—	×	200	35	7.9	—
135	Ga-As-P	UV-grade Sapphire	—	×	200	61	16.8	0.01

RCA TYPICAL PHOTOCATHODE SPECTRAL RESPONSE CHARACTERISTICS

The Chart of RCA typical photocathode spectral response characteristics given on the inside front and back covers of this Manual contains curves representing many of the photomultiplier-tube spectral response characteristics currently available from RCA. These curves do not show RCA's complete capability and, fo clarity reasons, only the most com mon are illustrated.

The table below summarizes th typical characteristics of the photo cathodes indicated on the spectra response chart.

Spectral Response	Cathode Material	Window Material	Trans-mission Type	Opaque Type	Sensi-tivity μA/lm	Sensi-tivity mA/W @ λ max.	Quantum Efficiency % @ λ max.	Dark Emission at 22° C fA/cm²* (1 fA = 1 x 10^{-15} A)
101 (S-1)	Ag-O-Cs	Lime or Borosil.	×	×	30	2.8	0.43	900
102 (S-4)	Cs-Sb	Lime or Borosil.	—	×	40	40	12.4	0.2
103	Cs-Sb	UV Glass	—	×	60	48	13.2	0.3
104 (S-5)	Cs-Sb	UV Glass	—	×	40	50	18.2	0.3
105 (S-8)	Cs-Bi	Lime or Borosil.	—	×	3	2.3	0.78	0.13
106 (S-10)	Ag-Bi-O-Cs	Lime or Borosil.	×	—	40	20	5.5	70
107 (S-11)	Cs-Sb	Lime or Borosil.	×	—	70	56	15.7	3
108 (S-13)	Cs-Sb	Fused Silica	×	—	60	48	13.5	4
109 (S-19)	Cs-Sb	Fused Silica	—	×	40	65	24.4	0.3
110 (S-20)	Na-K-Cs-Sb	Lime or Borosil.	×	—	150	64	18.8	0.4
111	Na-K-Cs-Sb	Lime or Borosil.	—	Note 1	300	89	20.8	0.4
112	Na-K-Cs-Sb	UV Glass	×	—	180	77	22.7	0.4
113	Na-K-Cs-Sb	Pyrex	×	—	200	77	23.9	0.4
114	Na-K-Cs-Sb	Fused Silica	×	—	140	60	17.7	0.4
115	K-Cs-Sb	Lime or Borosil.	×	—	67	79	24.5	0.02
116	K-Cs-Sb	Pyrex	×	—	85	97	31.2	0.02

Chart Continued on Preceding Page.

* Based on Dark Current Measured in Typical PMT's.
Note 1: Reflective Substrate